Gebruik van functionele beeldvorming en optogenetica
voor de exploratie van doelwitten voor diepe hersenstimulatie
bij de ziekte van Parkinson en epilepsie

Use of Functional Neuroimaging and Optogenetics
to Explore Deep Brain Stimulation Targets
for the Treatment of Parkinson's Disease and Epilepsy

Nathalie Van Den Berge

Promotoren: prof. dr. R. Van Holen, prof. dr. C. Vanhove, prof. dr. R. Raedt
Proefschrift ingediend tot het behalen van de graad van
Doctor in de Ingenieurswetenschappen: Biomedische Ingenieurstechnieken

Vakgroep Elektronica en Informatiesystemen
Voorzitter: prof. dr. ir. R. Van de Walle
Faculteit Ingenieurswetenschappen en Architectuur
Academiejaar 2015 - 2016

UNIVERSITEIT
GENT

ISBN 978-90-8578-899-7
NUR 954
Wettelijk depot: D/2016/10.500/31

Department of Electronics and Information Systems
Faculty of Engineering and Architecture
Ghent University

MEDISIP - INFINITY
IBiTech – iMinds
Campus UZ, Block B
De Pintelaan 185
9000 Ghent
Belgium

Promotors:
Prof. dr. Roel Van Holen
Prof. dr. Christian Vanhove
Prof. dr. Robrecht Raedt

Board of examiners:
Prof. dr. ir. Rik Van de Walle, Ghent University, chairman
Prof. dr. ir. Emmeric Tanghe, Ghent University, secretary
Prof. dr. Alfred Meurs, Ghent University
Dr. Jean Delbeke, Ghent University
Prof. dr. Georgios Keliris, Antwerp University
Prof. dr. Yen-Yu Ian Shih, University of North Carolina

This work was funded by iMinds-Medical IT and by a grant of The Research Foundation - Flanders (FWO).

Acknowledgements

"If you find a path with no obstacles, it probably doesn't lead anywhere" Frank A. Clark

About four years ago I decided to switch career lines to Biomedical Engineering. It was certainly not easy and I could not have achieved the work presented in this dissertation without the guidance, support and collaboration of others. Therefore, I would like to express my gratitude to everybody in this section.

First of all, I would like to thank my promotors **prof. dr. Roel Van Holen**, **prof. dr. Christian Vanhove** and **prof. dr. Robrecht Raedt**. **Roel**, thank you for believing in my potential as a researcher and giving me the opportunity and guidance to find my way in Biomedical Engineering. Thank you for giving me many chances to attend international conferences, your career advice, and shaping me into the researcher I am today. **Chris**, thank you for your everlasting patience, support and enthusiasm. I really enjoyed working at the INFINITY lab and feel very lucky to have you as my supervisor. **Robrecht**, your contributions and ideas considering the neurology aspect of this dissertation were indispensable. Your feedback helped me a lot to take my research to a higher level. Additionally I would like to thank **prof. dr. Stefaan Vandenberghe**, **prof. dr. Paul Boon** and **prof. dr. Kristl Vonck** for their feedback and supporting my research projects.

Second, I would like to thank all my colleagues at **MEDISIP** for their great work and their continuous support: **Carmen**, **Inge**, **Karen**, **Shandra**, **Willeke**, **Lara**, **Radek** and **Scharon**, for the many meet-ups and encouraging and sweet words. I wish you the best with your further career and I'm sure we will keep in touch. **Inge** and **Carmen,** for helping me put things in perspective in difficult moments; I am looking forward to our summer trip! **Pieter VM**, **Gregor** and **Vincent,** for the memorable conference trips, party moments, advice and contribution to my research. **Benedicte** and **Scharon**, for your enthusiasm, patience and your incredible help performing experiments. I wish you both the best of luck with your new family member. **Karel**, **Pieter M** and **Bert,** for the friendly chats, the technical support and CT reconstruction. I wish you all the best with MOLECUBES. **Saskia** and **Inge**, for the great administrative support. Furthermore, I thank **Thibault**, **Stijn**, **Ester**, **Kim** and **Jens** for reinforcing the MEDISIP team. I wish you the best of luck with your research.

Then, I would like to thank all my colleagues from **LCEN3**: **Lisa**, **Lars**, **Wouter**, **Mathieu**, **Annelies**, **Leen**, **Ine B**, **Ine D**, **Sofie D**, **Sofie C** and **Bregt**, for always being there to help when experiments did not go so smooth, for your motivating words and inviting me to all your after-work events.

Next, I would also like to thank everyone from the **Shihlab** at the University of North Carolina. Special thanks to my supervisor **prof. Ian Shih**, for making a research stay in your lab possible, for sharing your knowledge and experience on preclinical MR imaging and giving me the opportunity to go to ISMRM with the lab. Being part of your lab for five months was a great experience that I will never forget. **Dan**, for being such a great colleague, helping me out with

the interpretation of our data and improving my research skills. I had a great time working with you. **Heather**, for sharing tears and laughs and all the great party moments. **Manasmita** and **Esteban**, for helping me out when I really needed it. **Lindsay**, **SungHo**, **Martin** and **Alex** for reinforcing the Shihlab. I could not have wished for a better research stay abroad and hope that our paths will cross again.

Furthermore, I would also like to thank the researchers from **Antwerp University**: **Prof. Annemie Van Der Linden**, **Prof. Marleen Verhoye** and **Prof. Georgios Keliris**, for giving me the opportunity to present my work and collaborate with your lab. **Rukun**, for sharing your experience on optogenetics and fMRI with me. I wish you the best with your research.

I would especially like to thank **my parents**, **grandfather** and **sister** for giving me all the opportunities I can think of. Thank you for the many dinners out when I needed a break from work, and for your continuous support in all my travels and studies abroad.

Finally I would like to thank my friends for all the great moments next to my research: **Simon** and **Steffen**, for the many party nights in Ghent and rides back home, **Blomme** for the many "Spijkertjes" and being a great friend for many years. **Tom**, **Jolien**, **Joke**, **Thierry**, **Annelies**, **Jan**, **Nike**, **Bram**, **Marlies** and **Lukas** for the many dinners and apero times, for sharing tears and laughs, and for being always there for me. **Liesbeth**, **Jenny**, **Gert**, **Tine** and **Gregory**, thanks for being coconut crazy and for the memorable moments we had together. I feel very lucky to have you all as my friends. And finally **Jesper**, for your incredible support during these last few months, coping with my crazy ideas ;) and all your help moving to Denmark. I'm looking forward to all the adventures ahead of us!

And all others which I'm not forgetting here but simply omitting due to a lack of space: thank you!

Nathalie
April 2016
Gent

Samenvatting

Diepe hersenstimulatie (DHS) is een neurochirurgische behandeling voor verscheidene neurologische and psychiatrische aandoeningen, waarbij een electrode stereotactisch in een bepaalde hersenstructuur wordt ingebracht. Op die manier kunnen (hoog-frequente) elektrische impulsen worden doorgegeven aan de hersenstructuur via een elders in het lichaam geplaatste stimulator. DHS van de *subthalame nucleus* (STN) en DHS van de *anterieure nucleus van de thalamus* (ANT) zijn reeds FDA-goedgekeurd (Eng: Food and Drug Administration) voor de behandeling van respectievelijk, de ziekte van Parkinson en epilepsie. Klinisch onderzoek heeft reeds aangetoond dat DHS een effectieve alternatieve therapie is voor de onderdrukking van tremor of epilepstische aanvallen in patienten waarbij de verzorging op basis van medicatie onvoldoende blijkt te werken. Ondanks het bewezen succes van STN- en ANT-DHS als een alternatieve behandelingsmethode, zijn er nog steeds patienten die niet reageren op DHS-therapie en/of bijwerkingen ondervinden. Bovendien is er slechts weinig geweten omtrent de onderliggende (therapeutische) werkingsmechanismen van DHS. Bijkomend onderzoek naar DHS van alternatieve potentiële hersenstructuren en de werkingsmechanismen van DHS is dus nodig om de effectiviteit van de behandeling te maximaliseren. Onderzoek in patienten is gelimiteerd omwille van ethische overwegingen, moeilijke rekrutering van patienten en de heterogeniteit binnen een groep patienten. Dierenproeven kunnen onder uiterst gecontroleerde experimentele condities doorgaan, en zijn bijgevolg onmisbaar in de studie naar de effecten van DHS en de zoektocht naar nieuwe potentiele DHS-structuren.

In voorgaand dierenonderzoek werden voornamelijk electrofysiologische metingen gehanteerd, om het effect van DHS op neurale netwerken te bestuderen. Dergelijke metingen werden typisch uitgevoerd in vooraf gedefinieerde hersenstructuren die men belangrijk acht binnen het onderzoek. Echter, op deze manier wordt de identificatie van minder gekende maar mogelijks relevante DHS-structuren belemmerd. Deze limitatie kan omzeild worden door het gebruik van functionele beeldvormingstechnieken zoals fMRI (Eng: functional Magnetic Resonance Imaging) en PET (Eng: Positron Emission Tomography), die de visualizatie van het effect van DHS in het gehele brein toelaten. In dit proefschrift focussen we op de studie van nieuwe hersenstructuren binnen experimenteel DHS-onderzoek voor de behandeling van de ziekte van Parkinson en epilepsie. We definieren drie specifieke doelen

1. De *Substantia Nigra pars reticulata* (SNr) en de *Globus Pallidus externa* (GPe) zijn twee potentiele hersenstructuren die momenteel onderzocht worden voor DHS-therapie van Parkinson patienten. Extra onderzoek is nodig om na te gaan hoe deze structuren functioneel geconnecteerd zijn met andere regio's. Ons doel is om de functionele connectiviteit van deze kernen in kaart te brengen aan de hand van DHS en simultane fMRI metingen.
2. Het toedienen van elektrische pulsen in een diepe hersenstructuur gebeurt echter niet specifiek. Naburig hersenweefsel ondervindt namelijk ook invloed van de elektrische stimulatie. Optogenetica is een zeer nieuwe techniek die gebruik maakt van licht ipv. electriciteit om hersencellen uiterst selectief te manipuleren. fMRI laat ons, net zoals bij DHS, toe om de effecten van optogenetische stimulatie te visualiseren. Het tweede doel is dan ook om de functionele connectiviteit van de GPe meer gedetailleerd te onderzoeken mbv. optogenetica en simultane fMRI metingen.
3. DHS in de hippocampus, ook hippocampale DHS genoemd, wordt momenteel onderzocht als therapie voor de behandeling van temporal kwab epilepsie. Voorgaand onderzoek in diermodellen heeft een gedaalde perfusie in het limbisch systeem van de hersenen aangetoond tengevolge van hippocampale DHS. Het derde doel van deze thesis is tweeledig: (1) onderzoek naar het effect van hippocampale DHS op het glucose metabolisme in de hersenen, en (2) de visualisatie van het hersennetwerk dat gemoduleerd wordt door hippocampale DHS.

Om deze onderzoeksdoelen te verwezenlijken, hebben we vier afzonderlijke preklinische beeldvormingsstudies uitgevoerd; toegelicht in deel II en III van dit proefschrift. Deel I van deze thesis geeft meer achtergrondinformatie rond DHS, de ziekte van Parkinson, epilepsie, de gebruikte functionele beeldvormingstechnieken en optogenetica.

Deel I – Achtergrondinformatie

Hoofdstuk 1 start met een beschrijving van DHS therapie. Vervolgens, lichten we de ziekte van Parkinson toe, nl. de basisbeginselen, het hersennetwerk dat aangetast is, en toepassingen van DHS-therapie bij Parkinson patienten. Tenslotte wordt epilepsie op een gelijkaardige manier uitgelegd, nl. basisbeginselen, het hersennetwerk dat aangetast is, en toepassingen van DHS-therapie bij epilepsie patienten.

Om onze onderzoeksdoelstellingen te bereiken, hebben we gebruik gemaakt van een combinatie van functionele beeldvormingstechnieken (fMRI en PET) en neuromodulatietechnieken (DHS en optogenetica). De basisprincipes en huidige DHS-gerelateerde applicaties van fMRI, PET en optogenetica worden toegelicht in **hoofdstuk 2** van dit proefstuk. De functionele beeldvorming laat toe om op een niet-invasieve manier *in vivo* metabole- of bloedstroom-parameters, welke gekoppeld zijn aan hersenactiviteit, van de volledige hersenen te visualizeren. Het gebruik van deze technieken is bijgevolg cruciaal om meer te weten te komen over hoe de hersenen functioneren in gezonde en zieke toestand, alsook hoe een therapie, zoals bijvoorbeeld DHS, de hersenfunctie kan beinvloeden. In dit proefschrift hebben we voornamelijk fMRI gebruikt om de modulatiepatronen van DHS of optogenetica in kaart te brengen. fMRI metingen opgenomen tijdens elektrische stimulatie of optogenetische stimulatie benoemen we verder als "DHS-fMRI"

en “opto-fMRI” respectievelijk. Bovendien hebben we in 1 studie PET gebruikt om het effect van DHS op het glucoseverbruik in de hersenen te analyseren,
Elektrische stimulatie wordt gekenmerkt door diffuse “off-target” effecten omdat de toegediende stroom ook steevast naburig hersenweefsel beinvloedt. Met DHS-fMRI kunnen we dus geen gedetailleerde respons op de neuromodulatie van een bepaalde hersenstructuur waarnemen. Het gebruik van opto-fMRI zou deze limitatie grotendeels kunnen omzeilen. Optogenetica is immers een nieuwe techniek binnen de neurowetenschappen die revolutionair beschouwd wordt owv. zijn voordien ongeziene cellulaire, spatiele en temporele specificiteit.

Deel II – Parkinson: Twee DHS-structuren

In deel II van dit proefstuk beschrijven we twee preklinische beeldvormingsstudies waarbij we de connectiviteit van twee potentiele DHS-structuren in kaart brachten, die relevant zijn voor de behandeling van de ziekte van Parkinson.

Hoofdstuk 3: Visualisatie van de functionele connectiviteit van twee “striatal” outputkernen, mbv. simultane “DHS-fMRI” metingen.

Bij de ziekte van Parkinson zijn de basale kernen (ook: basale ganglia) van de hersenen aangetast. De basale ganglia bevatten twee belangrijke kernen die de output van het striatum reguleren, namelijk de substantia nigra pars reticulata (SNr) en de globus pallidus externa (GPe). Onderzoek naar de verbindingen, tussen deze kernen en met andere hersenstructuren, is noodzakelijk om de impact van een therapie zoals DHS op de werking van de basale ganglia te begrijpen. Elektrische stimulatie van de SNr en GPe kent reeds enkele successen als DHS-therapie bij Parkinson (en ook andere aandoeningen). Desalnietemin, is er weinig bekend hoe deze therapie de netwerken in het brein beinvloedt, voornamelijk het effect van verschillende stimulatie frequencies op netwerkmodulatie. Om deze reden willen we met deze preklinische studie de connectiviteit van de SNr en GPe in de normale rathersenen in kaart brengen mbv. simultane DHS-fMRI metingen; dit onder verchillende DHS-frequenties gaande van 20-400Hz.
Onze analyse heeft mogelijks nieuwe modulatiepatronen binnen de basale ganglia kenbaar gemaakt, namelijk de modulatie van de prefrontale cortex door GPe-DHS en de bilaterale modulatie van het striatum door SNr- en GPe-DHS. Bovendien bleek de aard van deze modulaties gecorreleerd te zijn aan de frequentie waarmee de kernen gestimuleerd werden. De ipsilaterale netwerkenverbindingen toonden namelijk een verhoogde functionele connectiviteit tov. de contralaterale hersenhelft bij hogere frequenties. Dit effect verdween onmiddelijk na het stoppen van de elektrische stimulatie.

Hoofdstuk 4: Visualisatie van de functionele connectiviteit van de Globus Pallidus externa in normale en Parkinson ratten, mbv. simultane “opto-fMRI” metingen.

DHS heeft echter zijn tekortkomingen. De toegediende elektrische pulsen bereiken namelijk niet enkel de specifieke zenuwcellen waarop wordt gemikt, maar beïnvloeden ook naburig hersenweefsel. Dit zorgt voor diffuse “off-target” effecten, dewelke aan de basis van de therapeutische effecten en/of neveneffecten kunnen liggen. De toepassing van de nieuwe neuromodulatietechniek, optogenetica, in preklinisch DHS-onderzoek laat toe om hersencellen veel selectiever te manipuleren. Bij optogenetische stimulatie gebruikt men licht in plaats van elektriciteit voor het aansturen van zenuwcellen die voor dit doel genetisch gemodificeerd werden tot lichtgevoelige cellen. Maar, er is weinig bekend in hoeverre optogenetica de effecten van elektrische stimulatie kan weerspiegelen. Daarom doelden wij in deze studie op het in kaart

brengen van het modulatiepatroon van optogenetische stimulatie van de GPe in gezonde en Parkinson dieren, mbv. fMRI.
In tegenstelling tot de voorgaande DHS-fMRI experimenten, resulteerden de opto-fMRI experimenten enkel in ipsilaterale modulatie. Met optogenetische stimulatie van de GPe was er geen effect in de prefrontale cortex. Onze resultaten benadrukken de verhoogde selectiviteit van optogenetica tov. elektrische stimulatie om neuronen te manipuleren. Bovendien waren de modulatiepatronen zeer verschillend tussen de normale en Parkinson ratten (e.g., sterkere positieve modulatie in de GPe). Dit toont aan dat de "zieke" basale kernen anders communiceren dan de "gezonde" ten gevolge van het afsterven van de dopamine-producerende zenuwcellen. Verder onderzoek is nodig naar het verband tussen onze bevindingen en een therapeutisch effect in Parkinson ratten om zo de potentiele rol van GPe-neuronen in DHS-therapie te achterhalen.

Part III – Epilepsie: Hippocampale DHS

In deel III van dit proefstuk beschrijven we twee preklinische beeldvormingsstudies waarbij we het effect van hippocampale DHS in de hersenen van normale ratten onderzochten.

Hoofdstuk 5: Onderzoek van het effect van hippocampale DHS op het glucoseverbruik in de hersenen, mbv. FDG-PET

Uit de resultaten van voorgaand SPECT (Eng: Single Photon Emission Computed Tomography)- onderzoek bleek dat hippocampale DHS lokaal hypoperfusie (i.e. verminderde bloeddoorstroming) veroorzaakte in beide hippocampi. Bovendien bleek de aard van de hypoperfusie gecorreleerd te zijn met de stimulatie parameters. Om uit te sluiten dat dergelijke hypoperfusie niet veroorzaakt werd door DHS-geinduceerde vasoconstrictie (i.e. vernauwen van de bloedvaten), is er bijkomend onderzoek nodig. Omdat fluorodeoxyglucose-PET (FDG-PET) een directe maat van het glucoseverbruik voorziet, hebben we een FDG-PET-studie uitgevoerd in een gelijkaardige experimentele setting als gebruikt in de SPECT-studie. In die studie was de hippocampus het doelwit, omdat er een aanzienlijke hoeveelheid bewijs voorhanden is dat aantoont dat de hippocampus een belangrijke rol heeft in de aanvalsinitiatie in temporale kwab epilepsie.
Onze analyse wijst op DHS-geinduceerde lokale verminderingen in het cerebraal glucoseverbruik ter hoogte van beide hippocampi en bijkomende hersenregio's binnen het limbisch systeem. Deze bevindingen ondersteunen de voorgaande SPECT-studie en suggereren een functioneel inhiberend effect van DHS.

Hoofdstuk 6: Onderzoek naar het effect van hippocampale DHS op neurale netwerken, mbv. DHS-fMRI

Met deze studie wilden we het effect van hippocampale DHS op cerebrale netwerken in kaart brengen mbv "DHS-fMRI".
Statische analyse van de opgenomen fMRI data toonde positieve modulatie tijdens DHS in beide hippocampi en bijkomende hersenstructuren van het limbisch systeem. Dit was te verwachten, aangezien de hippocampus een belangrijke component is binnen het limbisch netwerk. Deze "activatie" staat in contrast met de waargenomen DHS-geinduceerde dalingen in het cerebral glucoseverbruik. Dit contrast kan te wijten zijn aan het verschil in stimulatieduur binnen beide experimentele protocol; in de PET-studie werd er immers 60 minuten continu gestimuleerd, terwijl in de fMRI-studie slechts blokken van 20 seconden DHS toegediend werden. Dit verschil was noodzakelijk gezien het onderliggende verschil in temporele resolutie

tussen beide modaliteiten. Wanneer we beide bevindingen samen beschouwen, zou dit kunnen wijzen op (1) een initieel acuut "activerend" effect van DHS op hersenregio's die geconnecteerd zijn met de gestimuleerde structuur; en mogelijks op (2) een "inhiberend" effect van DHS op langere termijn effect dat gepaard gaat met een verminderd glucoseverbruik. Dit laatste kan mogelijks verklaard worden door homeostatische neerregulatie mechanismen die plaatsvinden ten gevolgde van de 1-uur-durende toelevering van elektrische pulsen. Bovendien benadrukken deze studies de toegevoegde waarde van multi-modale beeldvorming binnen het onderzoek naar DHS en neurologische aandoeningen.

Part IV – Conclusies en toekomstmogelijkheden

We hebben drie specifieke doelen binnen experimenteel DHS-onderzoek verwezenlijkt. Ten eerste, hebben we mogelijks nieuwe verbindingen, binnen het netwerk gemoduleerd door SNr- en GPe-DHS, kenbaar gemaakt. Ten tweede, hebben we de toegevoegde waarde van "opto-fMRI" aangetoond om de onderliggende mechanismen van DHS en neurologische aandoeningen nauwkeuriger te onderzoeken. Ten derde, hebben we het effect van hippocampale DHS op het glucoseverbruik in de hersenen gevisualizeerd. Hiermee valideren we een voorgaande SPECT-studie. Beide studies wijzen op een onderliggend functioneel inhiberend effect van DHS. Bovendien, waren we in staat om het effect van hippocampale DHS op neurale netwerken te visualiseren met fMRI.

Een belangrijke bijdrage van dit werk, is de aanzienlijke vooruitgang die we geboekt hebben in de ontwikkeling en toepassing van preklinische fMRI procedures om de effecten van DHS en optogenetica te bestuderen. Voor zover we weten, zijn dit de eerste preklinische "DHS-fMRI" experimenten om de SNr, GPe en hippocampus *in vivo* te onderzoeken, en de eerste "opto-fMRI" studie van de GPe in gezonde en Parkinson ratten. De kennis en praktische ervaring die we vergaard hebben doorheen de uitvoering van deze experimenten zal toekomstig dierenonderzoek, naar de onderliggende mechanismen van neurologische aandoeningen en DHS-therapie, mbv "DHS-fMRI" en "opto-fMRI" vergemakkelijken. We zouden immers "opto-fMRI" gebruiken in toekomstig epilepsie-onderzoek, om bijvoorbeeld de rol van een specifieke neuronengroep in aanvalsinitiatie/propagatie of aanvalsonderdrukking te onderzoeken.

Dit onderzoek werd uitgevoerd in de onderzoeksgroep MEDISIP (Eng: MEDical Image and Signal Processing) en het INFINITY lab (Eng: in vivo small animal imaging lab), beide van de vakgroep ELIS van de faculteit ingenieurswetenschappen van de Universiteit van Gent (UGent). Dit onderzoek werd uitgevoerd in samenwerking met het Shihlab van het BRIC (Eng: Biomedical Research Imaging Center) aan de Universiteit van North Carolina (UNC), LCEN3 (Eng: Laboratory for Clinical and Experimental Neurophysiology, Neurobiology and Neuropsychiatry) van de faculteit biomedische wetenschappen van de UGent. De experimenten beschreven in deel II van dit proefstuk werden uitgevoerd in het Shihlab (UNC). Het voorgestelde werk resulteerde in 4 A1-tijdschrifpublicaties 1 ingediend en 1 in voorbereiding), 2 A1-tijdschriftpublicaties als co-auteur (1 ingediend en 1 in voorbereiding) en 13 bijdrages op internationale conferenties. De referenties van deze publicaties zijn in het hoofdstuk "list of publications" opgesomd.

Summary

Deep brain stimulation (DBS) is a neurosurgical therapy for multiple neurological and psychiatric disorders. In DBS, an electrode is stereotactically implanted in a specific region of the brain and (usually) high frequency electrical stimulation is delivered using a subcutaneous pacemaker-like stimulator. Currently, DBS is FDA (Food and Drug Administration) approved in the *subthalamic nucleus* and the *anterior thalamic nucleus* for Parkinson's disease (PD) and epilepsy, respectively. It has been shown that DBS is an effective therapy to suppress tremor in PD or seizures in epilepsy, when pharmacological treatment becomes inadequate or symptoms become intolerable.

Despite the rapidly growing use of DBS as a possible treatment, the mechanisms underlying the effects of DBS are poorly understood, representing a major challenge to refinement for enhanced efficacy and reduced side-effects. Research is necessary to explore whether other brain structures might have therapeutic potential as well. However, research in patients is restricted because of ethical reasons, difficult patient recruitment and the large variation among patients. Thus, in order to better understand the effects of DBS and to search for potential new DBS targets, animal research becomes indispensable because it offers highly controlled experimental conditions. Previous animal studies of DBS-relevant circuitry largely relied on electrophysiological recordings at predefined brain areas with assumed relevance to DBS therapy. Due to their inherent regional biases, such experimental techniques prevent the identification of less recognized (non-canonical) brain structures that might be suitable DBS targets. Therefore, we wanted to overcome this limitation by using functional neuroimaging techniques, such as functional Magnetic Resonance Imaging (fMRI) and Positron Emission Tomography (PET), which allow to visualize and to analyze the whole brain during DBS. In this work, we will focus on two neurological disorders, namely PD and epilepsy. The three major research goals of this thesis are:

1. The *Substantia Nigra pars reticulata* (SNr) and the *Globus Pallidus externa* (GPe) are currently being explored as potential non-canonical DBS targets for PD. However, more research is necessary to explore how these striatal output nuclei are interconnected to other brain regions. Our aim is to use fMRI to visualize other brain areas that are functionally interconnected to these potential DBS targets.

2. Optogenetics, or stimulation using light, is a state-of-the-art neuromodulation technique that has been proposed as a more selective alternative to electrical stimulation (DBS). Our aim is to combine optogenetics and fMRI, to investigate how other brain regions respond to optogenetic stimulation of the GPe.

3. *Hippocampal DBS* has been proposed as an effective treatment for refractory temporal lobe epilepsy. Previous animal research has shown that electrical stimulation of the hippocampus results in reduced perfusion of several region of the limbic system. Our third aim is twofold: 1) to investigate whether hippocampal DBS also results in a reduced glucose metabolism using PET, and 2) to visualize the brain network modulated during hippocampal DBS using fMRI.

In order to meet our research goals, we performed four preclinical neuroimaging studies, explained in part II and III of this thesis. In order to fully understand our preclinical investigations, some background information on DBS, PD, epilepsy, the functional neuroimaging techniques used and optogenetics is provided in the first part of this thesis.

Part I - Background

In **chapter 1** of this dissertation we first describe DBS therapy more in detail. Second, we explain the basic principles of PD pathology, the brain circuitry affected by PD pathology and the state-of-the-art of DBS as a treatment in drug resistant PD. Finally, we discuss the basic principles of epilepsy, the brain circuitry affected by epilepsy and the state-of-the-art of DBS as a treatment in drug resistant epilepsy.
In order to meet our research goals we used a combination of functional imaging techniques, DBS and optogenetics. The basic principles and current DBS-applications of fMRI, PET and optogenetics are explained in **chapter 2** of this thesis. Functional imaging techniques allow non-invasive *in vivo* visualization of the brain's metabolism, blood flow or blood volume, which are assumed to reflect neural activity. Therefore, these techniques are crucial for gaining insight in the brain circuitry and its function, and how the brain circuitry is affected by neurological disorders and treatments such as DBS. In this dissertation we used mainly functional Magnetic Resonance Imaging (fMRI), which is a well-established research tool to investigate alterations in brain circuitry, induced by an external stimulus such as DBS or optogenetics. Additionally, we used the nuclear imaging technique Positron Emission Tomography (PET) in order to evaluate how DBS affects the glucose metabolism.
Because DBS can recruit connected brain areas through both ortho- and antidromic signal propagation across fibers, functional circuit mapping using DBS-fMRI cannot readily distinguish between up- and downstream circuit elements. The use of optogenetics should provide a more precise means for functional imaging-based circuit mapping. Optogenetics is a new revolutionary technique in the field of neuroscience that provides a means to control cell behavior by using light with unprecedented cellular, spatial and temporal specificity.

Part II - Parkinson's Disease: Two DBS targets

In part II of this dissertation we describe the two preclinical imaging studies we performed in order to explore how potential DBS targets, relevant for the treatment of Parkinson's disease, are interconnected, using DBS-fMRI (chapter 3) and opto-fMRI (chapter 4).

Chapter 3: Functional Circuit Mapping of Striatal Output Nuclei using Simultaneous DBS-fMRI

Parkinson's disease is associated with dysfunction within the basal ganglia. The identification of functional circuit or network connections among the basal ganglia's two major striatal output nuclei, i.e. substantia nigra pars reticulata (SNr) and external globus pallidus (GPe), is necessary to elucidate basal ganglia function in the healthy brain, PD brain and treatment strategies such as DBS. DBS-therapy, targeting the SNr or GPe, has already demonstrated some therapeutic potential. However, very little is known about how this treatment influences neural circuitry, particularly at different stimulation frequencies. Therefore, this preclinical study aimed to map the network-level connectivity of the SNr and GPe in the healthy rat brain, using simultaneous DBS and fMRI, also called "DBS-fMRI", at different frequencies ranging from 20Hz-400Hz.

Remarkably, statistical analysis revealed potentially new findings related to basal ganglia circuitry, in particular activation of the prefrontal cortex by GPe-DBS and local signal changes in the striatum by SNr- and GPe-DBS, in a frequency-dependent manner. Additionally, functional connectivity was generally enhanced in the hemisphere ipsilateral to SNr or GPe stimulation in a frequency-dependent manner, and readily reversed following cessation of stimulation.

Chapter 4: Functional Circuit Mapping of the Globus Pallidus externa in the healthy and PD brain using Opto-fMRI

DBS broadly modulates neural circuits and networks, which may be important for its diverse therapeutic as well as side-effects. It is therefore highly interesting to gain insight in the functional contribution of a certain group of neurons to DBS-therapy. Preclinical DBS studies allow for the experimental introduction of optogenetic tools, which provide superior neural circuit stimulation specificity compared to electrical DBS. Specifically, in addition to modulation of neuronal populations proximal to the electrode, electrical DBS can also recruit undesirable neighboring fibers of passage. In contrast, optogenetic stimulation is generally confined to only the cells that express light-sensitive proteins and their efferent outputs. Furthermore, the presence of an optic fiber introduces less artifact in the MR image, as opposed to a metal DBS-electrode. Because of this added specificity for neural modulation, optogenetic tools have been employed to inform potential circuit mechanisms of DBS therapy in preclinical models. However, little is known regarding the extent to which optogenetic stimulation mirrors the circuit-level responses achieved with electrical DBS. Therefore, in the present study, we aimed to evaluate the circuit modulation profile achieved by selective stimulation of GPe neurons, in a healthy and PD rat model, using opto-fMRI.
As opposed to electrical stimulation of the GPe (chapter 3), fMRI responses were observed only ipsilaterally using optogenetic stimulation of the GPe, and we were unable to achieve detectable circuit modulation in the prefrontal cortex, confirming the selectivity of the optogenetics technology. Electrical stimulation of the GPe likely affects passing fibers as well as input- and output projections from/to the prefrontal cortex, whereas optogenetic stimulation is mostly restricted to output projections. In PD rats, we observed larger positive responses as opposed to healthy rats, suggesting GPe circuit remodeling following dopamine loss. Correlation of these findings to motor improvement in these rats could reveal the therapeutic role of the GPe neurons in DBS.

Part III - Epilepsy: Hippocampal DBS

In part III of this dissertation we describe two preclinical imaging studies we performed to investigate DBS of the hippocampus, an experimental DBS target that is relevant for the treatment of epilepsy, by investigating how hippocampal DBS affects the brain's glucose metabolism (chapter 5), and the brain circuitry (chapter 6).

Chapter 5: Investigation of the Glucose Metabolism during Hippocampal DBS using FDG-PET

A previous Single Photon Emission Computed Tomography (SPECT)-study revealed DBS-induced hypoperfusion in both hippocampi. Moreover, a clear distinction in spatial extent and intensity of hypoperfusion was observed between stimulation parameters. Extra research is necessary to confirm that this hypoperfusion is caused by actual DBS-induced decreases in the brain's metabolism, as opposed to pure DBS-induced vasoconstriction. In order to have a direct

measure of the glucose metabolism, we therefore performed an fluorodeoxyglucose-PET (FDG-PET) study in the same experimental set-up as used in the SPECT-study previously performed in our lab. In that study, the hippocampus was chosen as DBS target, because there is considerable evidence that the hippocampal formation is involved in seizure initiation in refractory temporal lobe epilepsy

Complementary to the earlier SPECT-study, we observed significant decreases in the glucose metabolism in the ipsi- and contralateral hippocampus, as well as in other areas of the limbic network. These findings suggest an underlying functional inhibition mechanism of hippocampal DBS. The net effects of DBS in a certain target structure vary depending on the composition of the inhibitory and excitatory axon terminals.

Chapter 6: Functional Circuit Mapping of the Hippocampus using Simultaneous DBS-fMRI

In this study, we aimed to map the brain network modulated by acute hippocampal DBS using fMRI.

Statistical analysis of the fMRI data revealed positive signal modulation in the hippocampus and other structures of the limbic network during DBS. This is not surprising, since the hippocampus is a key structure within the limbic system and therefore connects to several areas of the limbic system. In contradiction to the DBS induced metabolic signal drop in the limbic system, our DBS-fMRI study demonstrates DBS-induced activation of the limbic system. This may be attributed to the difference in length of stimulation in both experimental protocols, i.e. 60min of continuous DBS (PET-study) vs. blocks of 20s of DBS (fMRI-study). This difference in stimulation duration was necessary considering that PET and fMRI are characterized by a different temporal resolution. Taken together, these studies suggest that DBS leads to an initial (order of seconds) activation of the brain network related to the target; and probably leads to a metabolic decrease over time due to homeostatic downscaling mechanisms that occur in reaction to 60min of continuous electrical stimulation. Moreover, these studies highlight the importance of multi-modal imaging in the investigation of DBS and neurological disorders.

Part IV- Conclusions and future perspectives

Three major research goals have been achieved. First, we identified pathways that are less well known using DBS-fMRI of the SNr and GPe. Second, we employed opto-fMRI for selective modulation of GPe neurons alone, and hereby demonstrated the potential of opto-fMRI, to unravel DBS- and pathology-mechanisms in a far more selective manner than with the use of electrical stimulation. Third, we demonstrated that hippocampal DBS causes hypometabolism in the limic system, hereby further validating a previous SPECT-study showing bilateral hypoperfusion in the hippocampus during hippocampal DBS. Both studies indicate DBS-induced decreases in the brain's metabolism, suggesting underlying functional inhibition mechanisms of DBS. Additionally, we were able to visualize the brain network modulated by hippocampal DBS using fMRI.

Our considerable progress in the development and application of fMRI procedures to study the effects of DBS and optogenetics in rats, tackling several of the major technical hurdles, can be seen as one of the major contributions of this research. To our knowledge, these are the first preclinical DBS-fMRI studies to investigate the SNr, GPe and hippocampus *in vivo*, and the first opto-fMRI study of the GPe in healthy and Parkinsonian rats. The knowledge and experience obtained throughout these studies, enables further preclinical investigation using DBS- and opto-fMRI to explore neurological disorders and DBS-therapy. More specifically, we

want to apply opto-fMRI in future research to investigate the role of a specific group of neurons in seizure initiation/propagation or seizure suppression in rodent models of epilepsy.

This research was performed at the research group MEDISIP (MEDical Image and Signal Processing) and the INFINITY lab (in vivo small animal imaging lab), both part from the ELIS department of the faculty of engineering at Ghent University, in collaboration with Shihlab at the Biomedical Research Imaging Center from the University of North Carolina (UNC), LCEN3 (Laboratory for Clinical and Experimental Neurophysiology, Neurobiology and Neuropsychiatry) of the faculty of biomedical sciences at Ghent University. The experiments described in part II of this thesis were all performed at Shihlab (UNC). The work presented in this dissertation resulted in 4 A1 journal papers as a first author (1 submitted and 1 in preparation), 2 A1 journal publications as a co-author (1 submitted and 1 in preparation), and 13 contributions at international conferences.

Table of contents

IV Conclusions

List of Abbreviations

AAV	adeno-associated virus
AD	afterdischarge
Ag	silver
Au	gold
ANOVA	analysis of variance
ANT	anterior nucleus of the thalamus
AP	anteroposterior
ATP	adenosine triphosphate
BSL	biosafety level
BOLD	blood oxygenation level dependent
C	carbon
CA	cornus ammonis
CBV	cerebral blood volume
CBF	cerebral blood flow
CE	european conformity
ChAT	choline acetyltransferase
ChR2	channelrhodopsin-2
$CMRO_2$	cerebral metabolic rate of oxygen
CNR	contrast-to-noise
CNS	central nervous system
CT	computed tomography
DBS	deep brain stimulation
DHS	diepe hersenstimulation
DPSS	diode-pumped solid-state
DMV	dorsal motor nucleus of the vagus nerve
DV	dorsoventral
EEG	electroencephalography
$EtCO_2$	end tidal CO_2
EPI	echo planar imaging
EYFP	enhanced yellow fluorescent protein

FA	flip angle
fcMRI	functional connectivity magnetic resonance imaging
FDA	food and drug administration
FDG	fluorodeoxyglucose
fMRI	functional magnetic resonance imaging
FOV	field of view
FWHM	full width half maximum
GABA	gamma-aminobutyric acid
GE	gradient echo
GLM	general linear model
GP	globus pallidus
GPe	globus pallidus externa
GPi	globus pallidus interna
Hb	hemoglobin
hDBS	hippocampal deep brain stimulation
HFS	high frequency stimulation
HK	hexokinase
HMPAO	hexamethylpropyleneamineoxime
HRF	hemodynamic response function
hSyn	human Synapsin
ICA	independent component analysis
iEEG	intracranial electroencephalopgraphy
ILAE	International League Against Epilepsy
ILBD	incidental Lewy body disease
LED	light emission diode
lTLE	lateral temporal lobe epilepsy
LV	lentivirus
MFB	medial forebrain bundle
ML	mediolateral
MLEM	maximum likelihood expectation maximization
MION	monocrystalline iron oxide
MRI	magnetic resonance imaging
mTLE	mesial temporal lobe epilepsy
NAc	nucleus accumbens
NMR	nuclear magnetic resonance imaging
NphR	halorhodopsin
OHDA	hydroxydopamine
PD	parkinson’s disease

PD	proton density
PET	positron emission tomography
PFC	prefrontal cortex
PNS	peripheral nervous system
PtIr	platinum iridium
RARE	Rapid acquisition with relaxation enhancement
rCBF	regional cerebral blood flow
RF	radio-frequency
RNS	responsive neurostimulation
ROI	region of interest
SE	status epilepticus
SE	spin echo
SEM	standard error of the mean
SN	substantia nigra
SNc	substantia nigra pars compacta
SNr	substantia nigra pars reticulata
SNR	signal-to-noise
SPECT	single photon emission tomography
SpO2	oxygen saturation
SS	stainless steel
STN	subthalamic nucleus
TE	echo time
TH	tyrosine hydroxylase
TLE	temporal lobe epilepsy
TR	repetition time
TTL	transistor-transistor logic
VA	ventral anterior nucleus
vGAT	GABA vesicular transporter
VL	ventrolateral nucleus
VNS	vagus Nerve Stimulation
VTA	ventral tegmental area
W	Tungsten

Introduction

The work presented in this dissertation uses functional imaging techniques and optogenetics to investigate the mechanism of deep brain stimulation (DBS) in Parkinson's disease and epilepsy. The rationale behind this investigation, research goals and outline of the thesis are described in this introductory chapter.

Rationale

In DBS, electrical pulses are delivered to specific brain targets by means of stereotactically implanted deep brain electrodes (Fig. 0.1). In contrast to resective surgery, DBS is an adjustable and reversible therapy. DBS has become the preferred surgical treatment for advanced Parkinson's disease (PD) and is a promising therapy for other neurological and psychiatric disorders, such as other movement disorders (Birdno et al., 2008; Benabid 2003), refractory epilepsy (Fischer et al., 2010; Boon et al., 2009; Vonck et al., 2013) and obsessive-compulsive disorder (Nuttin et al., 1999; Abelson et al., 2005).

Figure 0.1: Illustration of an implanted Deep Brain Stimulation system in humans. A multi-contact DBS-electrode is implanted in a deep brain structure, fixed to the skull and connected to a subcutaneously implanted pulse generator. (Figure adopted from http://www.wired.com).

Already in ancient times, electrical stimulation was used to treat neurological disorders such as migraine, by placing certain electricity-producing fish on the head. In the early 19th century, scientists started to use electrical stimulation to understand brain function and for therapeutic purposes. But it was not until the 1950s that scientists observed that stimulation of certain brain structures, suppressed abnormal electrical activity in the brain during surgery. Consequently, DBS was born and has led to positive results for the treatment of PD, resulting worldwide in over 30000 patients with movement disorders that are presently being treated with DBS. Currently DBS-therapy is FDA (Food and Drug Administration) approved for the subthalamic nucleus and anterior nucleus of the thalamus, for the treatment of PD and epilepsy patients, respectively. Despite the rapidly growing use of DBS as a treatment, to (partially) suppress tremor in refractory PD or epileptic seizures in refractory epilepsy, the working mechanisms

underlying the therapeutic effects of DBS are poorly understood, limiting clinical efficacy. Therefore, further research is necessary to reduce the amount of non-responders to this invasive and expensive treatment by exploring new possible DBS targets.
Research in patients is restricted because of ethical reasons, difficult patient recruitment and the large variation among patients. Thus, in order to better understand the effects of DBS and to search for potential new DBS targets, animal research becomes indispensable because it offers highly controlled experimental conditions.

Medical imaging is a tool to visualize the body's anatomy and physiology in a non-invasive way (i.e. without opening the body), and enables diagnosis and prognosis of several pathologies, including the evaluation of the effects of therapy. Medical imaging that focuses on visualizing the brain and its physiology is called neuroimaging. Neuroimaging techniques are crucial for understanding the relationships between specific areas of the brain and their function; helping to locate the areas of the brain that are affected by neurological or psychiatric disorders; and developing new or improving existent treatments for these disorders. Similar to medical imaging, neuroimaging techniques fall into two broad categories: structural and functional neuroimaging techniques. Structural neuroimaging investigates the structure of the brain and can be used for the diagnosis of anatomical abnormalities, such as tumor or injury. Examples of structural imaging techniques are: Computed Tomography (CT) and Magnetic Resonance Imaging (MRI). However, in many diseases, functional changes appear well before any structural modifications. In such case, functional neuroimaging can be used because it can reveal the activity in certain brain regions by detecting changes in metabolism, blood flow, blood volume or biochemical composition. Functional neuroimaging is commonly used for research in brain function of the healthy and diseased brain, and to evaluate the effect of treatments such as DBS. Examples of functional imaging techniques are: functional Magnetic Resonance Imaging (fMRI) and Positron Emission Tomography (PET). Examples of different imaging modalities are shown in Fig. 0.2.

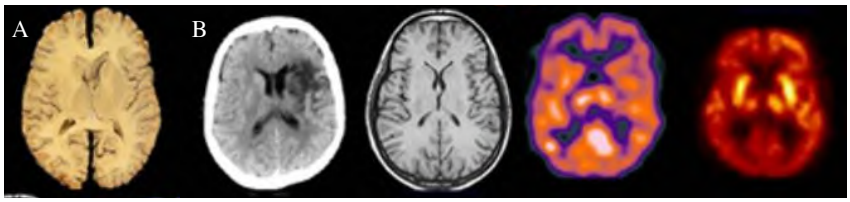

Figure 0.2: Examples of different imaging modalities: (A) Real axial slice of the human brain; (B) axial slice of the human brain acquired with different imaging modalities from left to right: X-ray, MRI, SPECT and PET. (Figure modified from http://www.unige.ch/cyberdocuments/).

As the brain processes information, blood flows to the responsible areas to provide the required oxygen and glucose. However, the oxygen consumption is much less compared to the bloodflow increase and glucose consumption, leading to a net increase in the amount of oxygen present in the blood and tissue, which forms the basis of the fMRI-signal. A more detailed explanation of the fMRI-signal is provided in paragraph 2.1 of this thesis. Basically, fMRI is a series of MR-images acquired sequentially for a period of time to investigate how the blood flow changes over that period of time. PET is a nuclear imaging technique that requires the injection of a radioactive labeled molecule or tracer that participates in the subject's metabolism, and distributes accordingly. Besides the metabolism other functional processes such as blood flow and receptor density can be visualized using PET, depending on the tracer that is used. The most widely used PET tracer is fluorodeoxyglucose (FDG), a glucose analog where one of the hydroxyl groups is replaced by the 18F radionuclide. The body metabolizes FDG in the same way as endogenous glucose, except that once phosphorylated glucose continues along the glycolytic pathway for energy production, whereas FDG cannot enter

glycolysis and becomes effectively trapped intracellularly where it accumulates. And thus, FDG PET can be used to visualize changes in the glucose metabolism of the brain. As opposed to PET, fMRI makes use of endogenous contrast or non-radioactive exogenous contrast agents to visualize brain function. Our MR and PET scanner are depicted in Fig. 0.3A and B respectively.

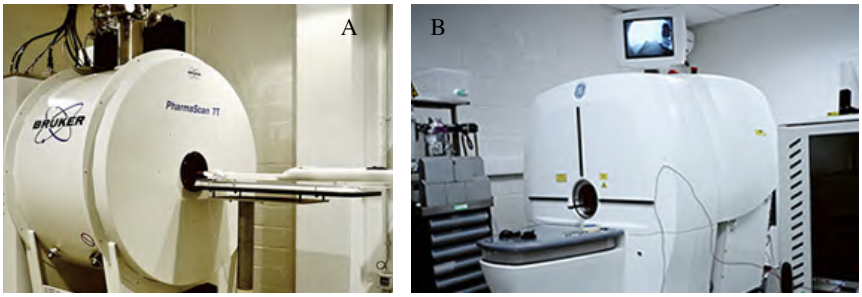

Figure 0.3: Medical scanners in our lab: (A) 7 Tesla small animal MRI from Bruker; (B) PET/CT system from TriFoil Imaging.

One of the advantages of using functional neuroimaging techniques, such as fMRI and PET, is that the effect throughout the entire brain can be captured. In contrast, cellular or electrophysiology studies measure at predefined regions of interest, and therefore important findings in unexpected brain structures might be "missed", introducing regional bias in the results. This is especially important in the investigation of DBS as a treatment for PD or epilepsy, since it is well known that PD and epilepsy are "network-diseases", affecting the entire brain. For example, in the case of epilepsy, this means that the seizure proneness, of a certain brain structure, is influenced by activity in other brain structures that are connected to that specific brain structure. The network as a whole is thus responsible for the clinical and electrophysiological characteristics associated with seizures. In conclusion, PD, epilepsy and DBS are characterized by modulating entire brain networks, and functional neuroimaging techniques are ideal tools to evaluate the mechanisms of DBS in network diseases such as PD and epilepsy.

Additionally, we employed optogenetics with fMRI readout, also referred to as "opto-fMRI", for a more detailed investigation of brain circuitry. Optogenetics is a new state-of-the-art technology that enables changes in cell behavior on a millisecond timescale, simply by using light. This technique has much higher temporal, spatial and cellular specificity compared to pharmacological and electrical stimulation treatments, and therefore is revolutionary in the field of neuroscience. In short, a gene, that encodes a light-sensitive protein, is attached to a promoter that allows transfecting a specific group of neurons. This viral vector is then introduced into a brain structure of interest. But only those promoter-specific neurons (or non-neuron cells) will express the light-sensitive protein in their cell membrane. Finally, an optic fiber is implanted just above the targeted structure, so light can be brought into the brain, onto the transfected area (Fig. 0.4).

In 2010, optogenetics was awarded "Method of the Year" by the scientific journal Nature Methods. Since then, optogenetics has been used successfully to control more complex functions in the mammalian brain, such as cognitive function, reward behavior, to restore vision or to investigate DBS therapy.

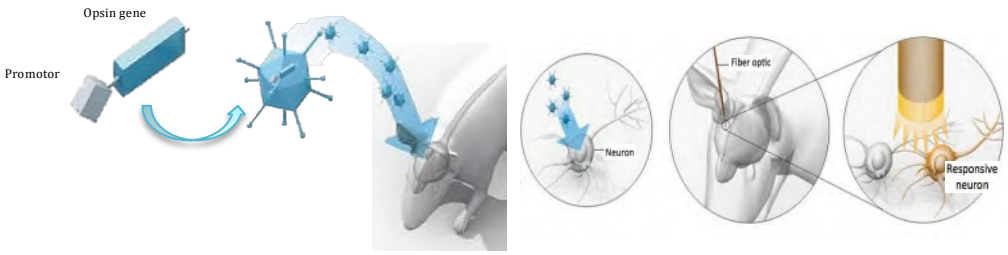

Figure 0.4: Basic principles of optogenetics. In optogenetics, neuroscientists insert opsin genes into brain cells with the aid of engineerd viruses. They can then trigger neural activity on demand with flashes of light and observe the effects on experimental animals' behavior. (Figure modified from http://www.nature.com/scientificamerican/journal/v303/n5/box/)

Recently, fMRI and optogenetics have been combined, to examine the whole-brain effect of a light stimulus in the brain. Before, neural circuitry has been examined using electrical stimulation of small groups of cells whilst simultaneously performing fMRI. However, electrical stimulation does not only affect the targeted cells, but also passing fibers, causing off-target effects that potentially confound the fMRI signal. Combined optogenetics and fMRI would largely avoid this problem, since only the neurons, where the promotor of the introduced gene package is activated, are responsive to light.

Research goals

Our research ultimately aims at refinement of DBS therapy in order to reduce the amount of non-responders to this expensive and invasive treatment. In order to contribute to this objective we aimed to explore several experimental DBS targets. The three major research goals of this thesis are:

1. The *Substantia Nigra pars reticulate* (SNr) and the *Globus Pallidus externa* (GPe) are currently being explored as potential non-canonical DBS targets for PD. However, more research is necessary to explore how these striatal output nuclei are interconnected to other brain regions. Our aim is to use fMRI to visualize other brain areas that are functionally interconnected to these potential DBS targets.

2. Optogenetics, or stimulation using light, is a state-of-the-art neuromodulation technique that has been proposed as a more selective alternative to electrical stimulation (DBS). Our aim is to combine optogenetics and fMRI, to investigate how other brain regions respond to optogenetic stimulation of the GPe.

3. *Hippocampal DBS* has been proposed as an effective treatment for refractory temporal lobe epilepsy. Previous animal research has shown that electrical stimulation of the hippocampus results in reduced perfusion of several region of the limbic system. Our third aim is twofold: 1) to investigate wheter hippocampal DBS also results in a reduced glucose metabolism using PET, and 2) to visualize the brain network modulated during hippocampal DBS using fMRI.

Outline

This dissertation is divided into four parts: (1) background information on DBS, PD; epilepsy; the functional neuroimaging modalities used and optogenetics; detailed explanation of our preclinical imaging experiments related to (2) PD and (3) epilepsy; and (4) final conclusions and future perspectives.

In **part I** of this dissertation, we provide some background information on DBS, PD, epilepsy, fMRI, PET and optogenetics. In **chapter 1**, we first explain the general principles of DBS and provide a short history of the development of DBS. Second, we elaborate on PD, including the basic principles of the pathology, the brain network affected by PD, and the state-of-the-art of DBS as a treatment for PD. Finally, we explain epilepsy more in detail, including the basic principles, the brain network involved in epilepsy, and the state-of-the-art of DBS as a treatment for epilepsy. **Chapter 2** focuses on the methods used in this research. First, we describe fMRI, including MRI and fMRI basics, and its application in the investigation of DBS, PD and epilepsy. Second, we explain the basic principles of PET imaging and its applications in the investigation of DBS, PD and epilepsy. Finally, we elaborate on optogenetics and its current applications.

Part II and III provide detailed information on the preclinical imaging experiments performed in this dissertation, including a rationale, materials and methods used, results, interpretation of the results and limitations of the experiments. In **part II**, our goal was to map the brain network modulated by striatal output nuclei using DBS-fMRI (**chapter 3**) and opto-fMRI (**chapter 4**), and to validate the presumed higher selectivity of opto-fMRI. Since the striatal output nuclei are involved in motion generation/suppression, these are considered potential DBS targets for the clinical treatment of PD. In **part III**, we used DBS-PET (**chapter 5**) and DBS-fMRI (**chapter 6**) to evaluate changes in the glucose metabolism and network activation, respectively; induced by electrical stimulation of the hippocampus.

Finally, in **part IV**, general conclusions are made and possible future research is discussed.

List of publications

List of publications

[1] Van Den Berge N, Keereman V, Vanhove C, Van Nieuwenhuyse B, van Mierlo P, Raedt R, Vonck K, Boon P, Van Holen R (2015) Hippocampal deep brain stimulation reduces glucose utilization in the healthy rat brain. Molecular Imaging & Biology, 17: 373-383

[2] Van Den Berge N, Vanhove C, Descamps B, Dauwe I, van Mierlo P, Vonck K, Keereman V, Raedt R, Boon P, Van Holen R (2015) Functional MRI during hippocampal Deep Brain Stimulation in the Healthy Rat Brain. Plos One. DOI: 10.1371/journal.pone.0133245.

[3] Albaugh D*, Van Den Berge N*, Stuber G, Vanhove C, Van Holen R, Shih YY (2015) Functional circuit mapping of striatal output nuclei using simultaneous DBS fMRI. Manuscript submitted. *Shared first author.

[4] Van Den Berge N*, Albaugh D*, Stuber G, Vanhove C, Van Holen R, Shih, YY (2015) Mapping the Neural Circuitry Modulated by Optogenetic Stimulation of the External Globus Pallidus in the Healthy and Parkinsonian Rat using fMRI. Manuscript in preparation. *Shared first author.

[5] Albaugh D, Salzwedel A, Van Den Berge N, Stuber G, Wei G, Shih YY (2015) Functional MRI of the Neural Circuitry Modulated by Deep Brain Stimulation of the Rat Nucleus Accumbens. Manuscript submitted.

[6] Das M, Oyarzabal E, Decot H, Shah N, Montgomery SA, Filnov NA, Van Den Berge N, Lee SH, Shih YY (2016) High Performance Micro-Magnetic Resonance Angiography and Functional Brain Mapping with an Optimized Preparation of Carboxymethyl Dextran-Coated Iron Oxide Nanoparticles. Manuscript in preparation.

List of conference contributions

[1] Van Den Berge N, Keereman V, van Mierlo P, Vanhove C, Van Holen R (2013) Reproducibility of the visualization of the rat somatosensory network using Independent Component Analysis in whole-brain fMRI. Abstract presented at the 30th Annual Scientific Meeting of the European Society for Magnetic Resonance in Medicine and Biology, Toulouse, France.

[2] Van Den Berge N, Keereman V, Vanhove C, Van Nieuwenhuyse B, van Mierlo P, Raedt R, Vonck K, Boon P, Van Holen R (2014) PET functional imaging of deep brain stimulation in the healthy rat brain. Klinische Neurophysiologie, 45(1). Abstract presented at the 30th International Congress of Clinical Neurophysiology, Berlin, Germany.

[3] Van Den Berge N, Keereman V, Vanhove C, Van Nieuwenhuyse B, van Mierlo P, Raedt R, Vonck K, Boon P, Van Holen R (2014) Statistical group-analysis of PET data reveals whole-brain effect of hippocampal deep brain stimulation. Abstract presented at the World Molecular Imaging Congress 2014, Seoul, South-Korea.

[4] Gutierrez Diaz S, Vanhove C, Descamps B, Van Den Berge N, Van Holen R (2014). Small animal radiation therapy using probabilistic tissue classification of multiple MR images. Abstract presented at the World Molecular Imaging Congress 2014, Seoul, South-Korea.

[5] Van Den Berge N, Dauwe I, van Mierlo P, Vonck K, Raedt R, Boon P, Vanhove C, Van Holen R (2014) FMRI of hippocampal deep brain stimulation in the rodent brain. Abstract presented at the 4th Biennal Conference on Resting State / Brain Connectivity, Boston, US.

[6] Suigzdaite R, Descamps B, Van Den Berge N, Wu G, van Mierlo P, Fias W, Raedt R, Marinazzo D (2014) Lesion to left hippocampus changes functional connectivity according to changes in structure. Abstract presented at the 4th Biennal Conference on Resting State / Brain Connectivity, Boston, US.

[7] Gutierrez Diaz S, Van Holen R, Descamps B, Van Den Berge N, Vanhove C (2014). Pseudo-CT generation from multiple MR images for small animal irradiation. Abstract presented at the 17th International Conference on Medical Image Computing and Computed Assisted Interventions, Boston, US.

[8] Van Den Berge N, Dauwe I, Vanhove C, van Mierlo P, Raedt R, Vonck K, Boon P, Van Holen R (2014) Simultaneous DBS and fMRI in the rodent brain. Abstract presented at the 5th Belgian Brain Congress, Ghent, Belgium.

[9] Van Den Berge, N., Dauwe, I., Vanhove C., Descamps, B., van Mierlo, P., Vonck, K., Raedt, R., Boon, P., Van Holen, R. (2015) Simultaneous deep brain stimulation and functional MRI of the healthy rat brain. Brain Stimulation, 8(2), pp. 351-352. DOI: 10.1016/j.brs.2015.01.135 Abstract presented at the 1st International Brain Stimulation Conference, Singapore.

[10] Van Den Berge N, Vanhove C, Descamps B, Dauwe I, van Mierlo P, Raedt R, Vonck K, Boon P, Van Holen R (2015) Longitudinal simultaneous DBS fMRI in the rodent brain. Abstract presented at the 15th European Congress on Clinical Neurophysiology, Brno, Czech Republic.

[11] Suigzdaite R, Descamps B, Van Den Berge N, Wu G, van Mierlo P, Fias W, Raedt R, Marinazzo D (2015) Lesion to Hippocampus changes resting state functional connectivity in rat brain reflecting structural damage. Abstract presented at the Second Belgian Neuroinformatics Congress, Leuven, Belgium.

[12] Van Den Berge N*, Albaugh D*, Vanhove C, Van Holen R, Shih YY (2015) Deep brain stimulation of the rodent SNr: a clinical target for neocortical epilepsy. Abstract presented at the 69th Annual Meeting of the American Epilepsy Society, Philadelphia, US. *Shared first author.

[13] Albaugh D*, Van Den Berge N*, Salzwedel A, Wei G, Stuber G, Shih YY (2016) Deciphering the Functional Connectome of the External Globus Pallidus with Electrical and Optogenetic Deep Brain Stimulation-fMRI. Abstract to be presented at the 24th Annual Meeting of International Society for Magnetic Resonance in Medicine, Singapore. *Shared first author.

Part I

Background

Chapter 1

DBS in Parkinson's Disease and Epilepsy

1.1 Deep Brain Stimulation

1.1.1 General principles

Deep brain stimulation (DBS) is a neuromodulation therapy that has been used successfully in the treatment of several neurological disorders, such as advanced Parksinon's disease (McIntyre, 2004; Benabid et al., 1991) and refractory epilsepsy (Fischer et al., 2010; Boon et al., 2009; Vonck et al., 2013), and neuropsychiatric disorders, such as obsessive-compulsive disorder, depression and addiction (Kringelbach et al., 2007; Wichmann and DeLong, 2006; Goodman and Alterman, 2012; Lozano and Lipsman, 2013). With DBS, electrical pulses are delivered to specific parts of the brain (via a subclavicular or paraumbilical implanted pulse generator, intracranial electrodes and a subcutaneous lead), in order to interfere with the neural activity of the target site. An example of the DBS-unit is shown in the introductory chapter (Fig. 0.1). Especially in movement disorders, such as PD, DBS has become a fixed value in the treatment protocol of PD patients (Benabid et al., 1991). Also in the therapy of refractory epilepsy, when anti-epileptic drugs do not (longer) offer a solution, DBS may be a valid alternative by targeting key structures for seizure onset (e.g. hippocampus) or seizure propagation (e.g. thalamus) (Sprengers et al., 2014). Compared to the previously used lesion-based neurosurgical tools, DBS is advantageous because of its reversibility (stimulation can be turned off) and capacity to modulate stimulation parameters (active contacts, voltage, frequency, pulse width) (Benabid et al., 1991; Kuncel and Grill, 2004). The latter trait is particularly important for optimizing the therapeutic benefits of DBS while reducing stimulation-related side-effects (McIntyre et al., 2004). The Food and Drug Administration (FDA) approved anterior nucleus of the thalamus (ANT)-DBS of Medtronic in 2002 (SANTE-study), and approved responsive neurostimulation therapy, the NeuroPace® RNS® System, for epilepsy in 2013 (fda.gov). Thus, it is clear that DBS is an effective treatment for PD and epilepsy. However, there are still a lot of non-responders to this expensive and invasive therapy. Therefore, the potential of DBS in other targets, as a clinical treatment for PD, epilepsy, and also for other neurological or psychiatric disorders are highly fascinating, but also highly challenging. There are still many unresolved technical, ethical and regulatory problems concerning the identification of the targets and DBS-parameters for each disease, the selection of the patients and the evaluation of the results within and across patient groups.

1.1.2 Short history

The use of electrical stimulation to treat neurological disorders can be tracked back to ancient times (Rossi, 2003) when certain electricity-producing fish were placed on the cranial surface as a remedy for headache and other applications such as for the treatment of seizures, depression, and pain (Kellaway, 1946; Schwalb and Hamani, 2008). In the early 19th century, scientists started to use electrical brain stimulation to understand the functioning of the brain and to treat neurological and psychiatric disorders (Aldini, 1804; Boling et al., 2002; Parent, 2004). At that time, Aldini reported that electrical stimulation on the exposed human cerebral cortex of recently decapitated prisoners caused horrible facial expressions. After various animal experiments Bartholow was the first to perform electrical stimulation of the cerebral cortex in awake humans (Bartholow, 1874), demonstrating the electrical excitability of the cortex. But it wasn't until the 1950s that electrical brain stimulation was used during stereotactic surgery as a way to identify and delineate functional brain tissue (Hassler and Riechert, 1955; Penfield, 1950). Scientists observed during surgery that stimulation of certain brain structures suppressed abnormal electrical activity in the brain. Consequently, DBS was born. Over the last 30 years DBS-therapy has led to positive results for the treatment of PD, essential tremor, and dystonia (Groiss et al., 2009; Benabid et al., 1991; Coubes et al., 2002; Ruge et al., 2011). Worldwide, more than 30000 patients with movement disorders are currently treated with DBS. DBS does not provide a cure, but it alleviates the symptoms and improves the quality of life of the patient, by decreasing the dose and the side effects of medication. The Food and Drug Administration (FDA) approved DBS for therapeutic treatment for essential tremor in 1997, for PD in 2002, and for dystonia in 2003 (fda.gov). Additionally, DBS has been evaluated as a treatment for epilepsy (Cooper et al., 1973), Tourette's syndrome (Vandewalle et al., 1999), depression (Mayberg et al., 2005), obsessive–compulsive disorder (Nuttin et al., 1999), cluster headaches (Franzini et al., 2003), eating disorders (Kumar et al., 2015; Lacan et al., 2008), and memory enhancement (Hamani et al., 2008), in more recent years. Fig. 1.1 shows a timeline indicating the different applications for DBS.

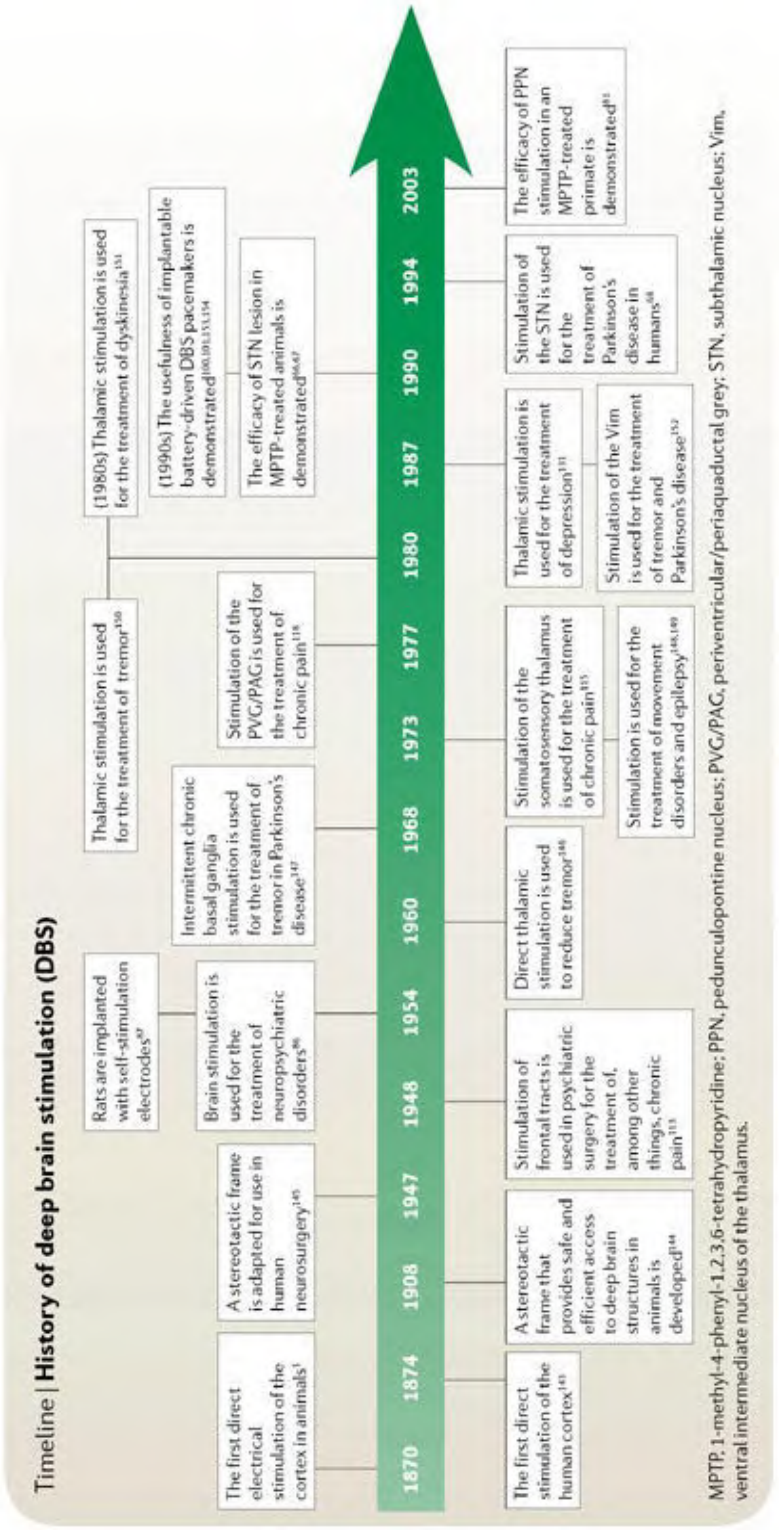

Figure 1.1: Timeline indicating the history of deep brain stimulation (Figure adopted from Kringelbach et al., 2007).

1.2 Parkinson's disease

In the following paragraphs we provide some background information on Parkinson's disease (PD), in order to fully understand why we want to examine brain circuitry modulated by DBS of the Substantia Nigra pars reticulate (SNr) and Globus Pallidus externa (GPe).

1.2.1 General principles

1.2.1.1 Symptomatic PD: dopamine loss

PD is a degenerative and progressive disorder of the central nervous system (CNS). The main symptoms of PD are tremor at rest, slow movements, stiffness and balance problems (Weiner & Lang, 1989). Therefore, PD is classified as a motor system disorders. The PD-symptoms are caused by the loss of dopamine-producing cells in the substantia nigra pars compacta. Nerve cells in the substantia nigra pars compacta produce the neurotransmitter dopamine, which is critical for normal movement (Savitt et al., 2006). Loss of dopamine-based inhibition ultimately leads to pathological spontaneous low-frequency oscillation, causing PD deficits. When PD progresses to other nuclei of the basal ganglia and to the nerves that control the muscles, also other neurotransmitters get thrown out of balance. The basal ganglia are made up of many complex, interconnected neuronal systems. The neuropathology of PD is thus regulated by a number of different neurotransmitters in addition to dopamine, such as GABA, glutamate, serotonin… For example, high levels of glutamate also appear in PD, probably due to intrinsic homeostatic control mechanisms that occur in the Parkinsonian brain to compensate for the lack of dopamine (Bezard et al., 2011).

The main PD symptoms, such as tremor at rest, arise when 80 percent of dopamine is lost (Weiner & Lang, 1989). In addition to these primary symptoms, PD patients can also suffer from depression, dementia, speech issues, constipation and REM-sleep disorder (Marsden, 1984). About 10 million people worldwide are living with PD, from which 4% are diagnosed before the age of 50. Men are 1.5 times more likely to develop PD, compared to women. The table below lists and provides a brief description of typical motor and non-motor symptoms of PD patients.

Table 1.1: Common motor- and non-motor symptoms in Parkinson's disease

Motor symptoms	**Non-motor symptoms**
Tremor (involuntary trembling of the of the hands and sometimes the legs, neck, face, or jaw at rest; it typically stops upon voluntary movement of the part and is intensified by stimuli such as cold, fatigue, and strong emotions)	Sleep disorders (REM behavior disorder, vivid dreams, daytime drowsiness, sleep fragmentation, rest- less legs syndrome)
Bradykinesia (slow movement)	Gastrointestinal disorders (gastroparesis, constipation)
Dystonia (abnormal muscle contraction)	Depression
Dyskinesia (impaired voluntary movement that produces repetitive involuntary twisting movements and abnormal posturing of the neck, trunk, face, and extremities)	Cognitive impairment (dementia, tip-of-the tongue (word finding) phenomenon)
Rigidity (muscle stiffness, decreased arm swing)	Sensory symptoms (impaired sense of smell and/or taste, pain in shoulder and/or back)
Postural instability (falls, freezing of gait)	Psychosis/hallucinations
Hypomimia (reduction in the expressiveness of the face, marked by diminished movement of the facial muscles and speech problems)	

Currently, there is no cure for PD. Therefore, treatments aim at reducing symptoms, and creating a more active lifestyle, to improve the patient's quality of life. The earliest treatment for PD involved lesioning of the subthalamic nucleus (STN) or Globus Pallidus interna (GPi) (Groiss et al., 2009). The post-operative difficulties and morbidity, together with the prospects of a potentially beneficial pharmacological treatment in the 1970's, led to an almost complete abandonment of the surgical treatment for this disorder. Pharmacological treatment involves replacing or mimicking the lost dopamine (or other neurotransmitters). Initially, levodopa therapy demonstrated to successfully compensate for dopamine depletion in PD. However, as PD progresses, patients eventually develop resistance to dopaminergic drugs, and in many cases develop levodopa-induced dyskinesias and motor fluctuations, and even psychosis (Rascol et al., 2003). Inefficient pharmacological treatment and surgical approaches to treat all PD patients paved the way for novel approaches such as DBS to complement the existing therapies, more specifically using high frequency stimulation (HFS) (Benabid et al., 2005; Lozano and Hamani, 2004).

DBS does not reverse or stop the progressive loss of dopamine-producing cells, but it is hypothesized that DBS overrides the "pathological" low-frequency oscillatory activity with "normal" periodic high-frequency oscillations, as observed in healthy subjects (Grill and Snyder, 2004; Hashimoto et al., 2003; McIntyre et al., 2004; Montgomery and Baker, 2000). The basal ganglia are made up of a complex group of coupled neuronal systems that each spontaneously oscillate. It is well known that coupled oscillators tend to synchronize. In PD, it is hypothesized that dopamine depletion causes a pathological low-frequency synchronization of the basal ganglia (i.e. a group coupled neuronal systems). Furthermore, disruption of the pathological low-frequency oscillation by DBS in the basal ganglia is associated with improvement of motor symptoms and normal firing of motor neurons. However, how the electrical stimulation and the pathological and normal oscillatory activity interact remains to be elucidated. Unfortunately, as the loss of dopamine-producing cells progresses, the increased abnormal oscillatory activity will eventually overwhelm the capacity of DBS to override them. The clinical care of a PD patient costs about 2500 euros per year, and therapeutic surgery can cost up to 100000 euros per patient (Parkinson's Disease Foundation.org, 2016).

1.2.1.2 Presymptomatic PD: the prion hypothesis

Recently, it has been hypothesized that PD initiates in the periphery years before the first symptoms occur, after which it extends to the CNS via the vagus nerve (Greggio et al., 2012). As the disease progresses, the severity of lesions in the areas affected and the amount of areas affected increases, causing presymptomatic problems related to those areas. This hypothesis might explain why PD patients frequently have a wide range of non-motor symptoms (such as constipation or REM-sleep disorder), related to dysfunction of the peripheral nervous system (PNS), which often precede the primary motor symptoms of PD. Finally, the pathogenic cells work their way up in a prion-like fashion, causing degeneration of dopamine-producing nerve cells in the substantia nigra.

Besides the loss of dopamine, PD is characterized by the presence of pathogenic cells or intraneuronal inclusions containing misfolded proteins, namely aggregated alpha synuclein (αsyn). The formation and self-propagation of misfolded proteins, such as αsyn aggregates, is called a prion-like process. The build-up of aggregations induces oxidative stress and inflammation and causes a prion-like cell-to-cell spreading of disease throughout the enteric wall, resulting in the construction of Lewy-bodies (Natale et al., 2011a; Natale et al., 2011b).

Lewy pathology is found throughout the PNS in both clinically diagnosed PD patients (Beach et al., 2010) as well as cases of clinically asymptomatic incidental Lewy body disease (ILBD) (Bloch et al., 2006; Dickson et al., 2008; Parkkinen et al., 2005). These findings are highly interesting as these ILBD-subjects are thought to represent presymptomatic PD at the earliest stage, eventually developing PD (Dickson et al., 2008; Minguez-Castellanos, 2007). Furthermore, a few studies have shown that PD patients had pathological alpha-synuclein inclusions in the gut 0.4 - 20 years prior to PD diagnosis (average 7 years) (Borghammer et al., 2016; Hilton et al, 2014; Ito et al, 2014; Shannon et al, 2012). In addition, more than half of these patients had Lewy pathology, and it was seen up to 20 years prior to diagnosis (Borghammer et al., under review).

Braak and colleagues assessed the distribution of αsyn aggregates in the brains of 110 αsyn-positive subjects, from which 41 were clinically diagnosed with PD, leading to the development of their widely accepted model of PD progression. According to Braak's model, PD starts in the lower brainstem in the dorsal motor nucleus of the vagus nerve (DMV), and in the anterior olfactory structures. The disease then ascends rostrally from the DMV through susceptible regions of the medulla, pontine tegmentum, midbrain, and basal forebrain, eventually reaching the cerebral cortex (Fig. 1.2). This is a non-random, progressive process, with specific nuclei and neuronal types resulting in the development of Lewy pathology (i.e. abnormal aggregates of protein that develop inside nerve cells) in a stereotypic pattern. This development of Lewy-bodies contributes to the PD pathogenesis. As the pathology advances upwards from the brainstem, both the severity of the lesions and the PD symptoms increase (Braak and Braak, 2000; Braak et al., 2006; Sulzer and Surmeier, 2013).

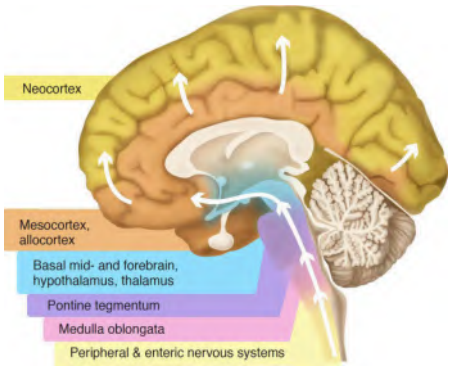

Figure 1.2: Staging of Lewy pathology according to the Braak model. Schematic summarizing the progression of Parkinson's disease as proposed by Braak and colleagues (Figure adopted from Braak et al., 2003).

Moreover, the formation and accumulation of misfolded protein aggregates have become increasingly important in the investigation of the pathogenesis of several neurodegenerative diseases, including Alzheimer's and PD (Recasens and Dehay, 2014). These recent findings that PD might initiate in the gut and progresses in a prion-like fashion has important implication for early therapeutic intervention (Frost et al., 2010; Guest et al., 2011). Since there is currently no therapy available to slow down or stop the progression of PD, the potential therapeutic perspectives on therapies targeting the mechanism responsible for cell-to-cell spreading of the pathology are highly exciting and fascinating. Although this hypothesis seems promising, we should be careful in the acceptation of a prion-based PD progression, particularly in all cases of PD. The mechanisms contributing to PD progression may be as variable as the pathology itself (Visanji et al., 2013). Preclinical and clinical research is necessary to validate this hypothesis. Additionally, functional imaging of the gut of PD patients could provide a biomarker for presymptomatic PD (Gjerloff et al., 2015).

1.2.2 The brain network involved in PD

1.2.2.1 The basal ganglia

The basal ganglia are a set of subcortical nuclei that are primarily responsible for motor control. All these nuclei have similar functions and work together to control body movement based on the "brake hypothesis". For instance, in order to sit still, all movements need to be stopped, except for those maintaining an upright posture. In order to move, postural reflexes are stopped, and brakes on voluntary movement are released. This involves a highly complex chain of decisions. Consequently, small disruptions in the basal ganglia network can throw the whole system out of balance, causing motion deficits (Chakravarthy et al., 2010; Albin et al., 1989; Rothwell, 2011).

The cortex, thalamus, and the basal ganglia are the key components in the basal ganglia circuitry. The schematic of the basal ganglia circuitry is presented in Fig. 1.3. The major nuclei of the basal ganglia are the caudate nucleus, putamen, globus pallidus, nucleus accumbens, subthalamic nucleus and substantia nigra. Yet, the relationships between them are incompletely understood. Firstly, there is the caudate nucleus and the putamen (also called the dorsal striatum), receiving most of their input from the cerebral cortex and providing the main input to the basal ganglia. Secondly, there is the globus pallidus (GP) which has an outer and an inner part, namely the globus pallidus externa (GPe) and the globus pallidus interna (GPi), both receiving input from the dorsal striatum, and both projecting to the subthalamic nucleus (STN), a third nuclei from the basal ganglia. Fourthly, there is the nucleus accumbens (NAc) (also called ventral striatum) that receives its input from frontal cortex and limbic areas, and is therefore more involved in depression and addiction than in movement disorders. Finally, there are the substantia nigra (SN), which can be divided in two parts, namely the SN pars compacta (SNc) and the SN pars reticulata (SNr):

- The SNc mostly contains dopaminergic neurons and is reciprocally interconnected with the dorsal striatum.
- The SNr mostly contains GABAergic neurons and also receives input from the dorsal striatum, but conveys the signals from the basal ganglia to other brain structures for the control of head and eye movements.

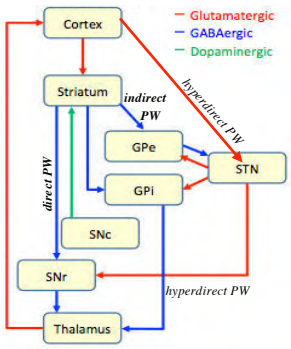

Figure 1.3: Schematic of the basal ganglia circuitry showing excitatory glutamatergic pathways as red, inhibitory GABAergic pathways as blue, and modulatory dopaminergic pathways as green. (Abbreviations: **GPe**: globus pallidus externa; **GPi**: globus pallidus interna; **STN**: subthalamic nucleus; **SNc**: substantia nigra pars compacta; **SNr**: substantia nigra pars reticulata).

1.2.2.2 The striatum

In PD, the loss of dopamine-producing cells in the SNc results in reduced levels of dopamine in the striatum due to reciprocal connections between both structures. The striatum is the major input structure of the basal ganglia and therefore represents a critical node within the brain's action-selection circuitry. Dysregulation of these striatal circuits can manifest in several neurological and neuropsychiatric diseases, including PD. PD deficits can be largely explained by the effects of dopamine loss on the two striatal output pathways, namely the direct (striatum - SNr) and indirect pathway (striatum - GPe).

- In the direct pathway, excitatory projections from the cortex provide striatal input, after which GABA-ergic neurons project to the "SNr/GPi-complex", causing a reduced inhibition of the thalamus, resulting in the excitation of the motor cortex by the thalamus. Finally, the cortex projects its own excitatory outputs via the corticospinal tract to the muscle fibers.
- In the indirect pathway, cortical cells project excitatory inputs to the striatum, which in turn projects its GABA-ergic axons to the GPe, causing a reduced inhibition of the STN. The STN then projects glutamatergic inputs to the "SNr/GPe-complex", causing inhibition of the thalamus, eventually resulting in reduced muscle activity.

Both pathways are indicated in Fig. 1.3. The body is able to maintain balance between excitation and inhibition of motion through opposing mechanisms of the direct and indirect pathway, but how exactly remains to be elucidated. In healthy subjects, dopamine increases the excitatory effect of the direct pathway on muscle activity (causing movement) and decreases the inhibitory effect of the indirect pathway on muscle activity (preventing full inhibition of movement). When there is not enough dopamine in the striatum to transmit messages to the basal ganglia, this causes dysfunction of the delicate and complex basal ganglia circuitry, consequently causing motion disruption or tremor. For example, dopamine depletion could cause overstimulation of the STN, which causes excitation of the GPi, resulting in interruption or disruption of normal motion. On the other hand, when the GPi is overstimulated, it has an over-inhibitory effect on the thalamus (VA/VL), resulting in tremor (Albin et al., 1989; DeLong, 1990). Fig. 1.4 displays this rewiring (i.e. alterations in communication) of the basal ganglia as a consequence of the reduced levels of dopamine in the striatum, caused by the degeneration of dopamine-producing cells in the SNc of PD subjects.

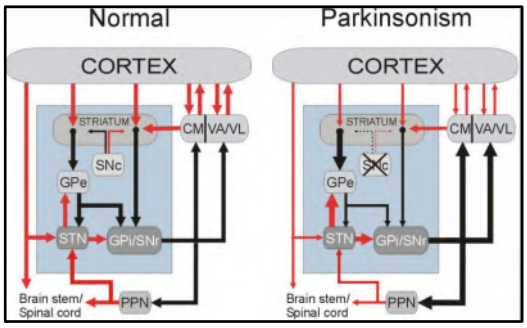

Figure 1.4: Rewiring of the basal ganglia in Parkinson's disease. Thick lines indicate increased output, and thin arrows indicate decreased output patterns present in PD. Black lines indicate inhibitory actions, and lines in red indicate excitatory actions. Note that, with loss of SNc function, the cascade of effects causes decreased thalamic (i.e. ventral anterior/ventral lateral nuclei) function, which leads to loss of motor control. (Figure adopted from Galvan et al., 2015).

1.2.3 DBS as a treatment for PD

1.2.3.1 Clinical efficacy

The discovery of electrical stimulation as a potential treatment for PD happened during the surgical procedures that were performed before the use of DBS. During those operations, electrical probes were used as a tool to guide the surgeon to the correct place, by receiving electrical signals from the passing areas. Surgeons were surprised to observe that PD symptoms were sometimes alleviated by the weak signals administered by the sensing probes. The areas that had the greatest effect, namely STN and GPi, became the most common DBS targets for PD (Follet et al., 2010). Now PD patients can be treated by the less invasive and reversible electrical stimulation, as opposed to the irreversible lesioning approaches. Especially patients in the late stages of PD, who often experience unstable "on-off" responses to the medication, can be treated with DBS. Already more than 30000 PD patients have been treated with HFS and this number is increasing every day (Lozano and Hamini, 2004). About 80% of those patients has experienced a complete or significant reduction in their tremor and/or other motor disabilities, lasting at least several years (Cigna Health Care, 2005). And most PD patients are able to reduce the dosage and thus the side effects of their medication (Oluigbo et al., 2012). DBS is proven to be an effective treatment in particular in patients with a history of good responses to levodopa therapy, but where the response becomes less and less as the disease progresses. In those patients, DBS therapy usually results in less "on-off" fluctuations with longer "on" periods and less dyskinesias. It also has proven to be effective for tremor when drugs did not help. Unfortunately, as PD progresses, the pathology will eventually overwhelm the capacity of DBS, and patients who previously did not respond to levodopa therapy will likely not benefit from DBS (Benabid et al., 2005; Lozano & Mahant, 2004).

1.2.3.2 DBS targets

High frequency STN-DBS and GPi-DBS have been shown to be the most effective locations for application of DBS. High frequency STN-DBS improves motor function by at least 60% and greatly improves the patient's quality of life (Benabid et al., 2005; Lozano and Mahant, 2004). Although, the STN seems to be the preferred target for DBS, only one small randomized trial has compared STN- to GPi-DBS, finding no difference between both therapies in the reduction of PD motor symptoms. In addition, the reported maximal clinical improvement of GPi-DBS (67%) is not significantly different than that reported for STN-DBS (71%). While reductions in levodopa dosages are required with STN-DBS (to avoid inducing dyskinesia), GPi-DBS may directly suppress dyskinesia precluding the need to reduce medication. There are also significantly more reports of behavioral changes reported for STN stimulation (Vitek, 2002). Yet in order to draw conclusions about the optimal DBS-target, there is a need for well-designed clinical trials with randomized and standardized assessments that evaluate motor, nonmotor and adverse effects, and lead locations.

However, neither STN-DBS nor GPi-DBS provides a satisfactory control of non-dopaminergic deficits, such as walk, balance and cognitive deficits, which are frequent and debilitating symptoms in advanced PD patients. Therefore, new potential DBS-targets are currently being explored to overcome the current DBS limitations (Castrioto and Moro, 2013; Vitek et al., 2012). Note that the SNc, where the dopamine depletion is initiated, has usually deteriorated far too much to be considered as a DBS-target by the time DBS treatment is considered for a patient, because about 80% of the dopaminergic cells in the SNc already died before any PD

symptoms appear. Instead, DBS targets brain structures involved in the basal ganglia-thalamocortical circuit that still have all their neurons intact (such as the STN and GPi) that make connections with other parts of the motor loop. In this dissertation, we will explore the GPe and SNr as non-canonical DBS-targets for PD.

1.2.4 Rodent models of PD

Experiments in humans, with the purpose of unraveling DBS mechanisms and optimizing DBS therapy, are difficult and restricted due to ethical problems, and the necessity of large and homogeneous patient groups. Therefore, studies in animal models of PD are indispensable. These models are designed according to our considerations about the etiology of PD.

In this dissertation, we employed the most commonly used 6-hydroxydopamine (6-OHDA) model to evaluate the brain circuitry in PD rats. When injecting the neurotoxin 6-OHDA in the brain it induces the degeneration of dopaminergic and noradrenergic neurons (Ungerstedt 1968; Luthman et al. 1989). Typically 6-OHDA is injected unilaterally (hemiparkinsonian model), leaving the unlesioned contralateral side as an internal control. This way, it is easier to evaluate the lesion within a single subject and intrasubject variability, i.e. using behavioral testing (Grealish et al. 2010). The degree of dopamine depletion induced by 6-OHDA is dependent on the site of injection (Agid et al. 1973; Przedborski et al. 1995; Przedborski and Tieu 2006). When injected into the medial forebrain bundle, like we did in our experiments, 6-OHDA produces a complete and rapid lesion in the nigrostriatal pathway (Sauer and Oertel 1994; Przedborski et al. 1995). Like many other neurotoxin models of PD, the main disadvantage of the 6-OHDA model is the acute neurodegeneration, following the intracerebral injection, therefore excluding progressive age-dependent effects of PD. Additionally, Lewy bodies, another neuropathological hallmark in PD, are not present in this model.

1.3 Epilepsy

In this paragraph we provide some background information on epilepsy, in order to fully understand why hippocampal DBS is currently under investigation as and experimental therapy for epilepsy.

1.3.1 General principles

1.3.1.1 Epilepsy

Epilepsy is a chronic neurological disorder, characterized by an enduring predisposition to generate epileptic seizures. An epileptic seizure is caused by abnormal, hypersynchronous and/or excessive electrical activity in the brain (Seino, 2006). Clinically, an epileptic seizure manifests as a sudden and transient abnormal event, affecting autonomic, motor and sensory functions, memory, cognition, consciousness, emotions and behavior (Engel, 2006). Seizures affect at least one of those functions depending on the location of the seizure onset zone in the brain, patterns of propagation, age, confounding pathologic processes, medications, sleep, alcohol, stress and other factors, (Fischer et al., 2005).

The occurrence of a single seizure does not make a person have epilepsy. According to the International League Against Epilepsy (ILAE) a person can be diagnosed with epilepsy under any of the following conditions: (1) at least two unprovoked (or reflex) seizures occurring >24 h apart; (2) one unprovoked (or reflex) seizure and a probability of further seizures similar to the general recurrence risk (at least 60%) after two unprovoked seizures, occurring over the next 10 years; (3) diagnosis of an epilepsy syndrome (Fischer et al., 2014).

About 0.5-1% of the population worldwide is diagnosed with epilepsy, making it the second most common chronic neurological disorder after cerebrovascular disorders (Banerjee, 2009; Forsgren et al., 2005; Hauser et al., 1996). Age-related incidence of epilepsy shows two peaks. The first peak occurs early in life and represents epilepsy due to genetic defect, a pre- or perinatal brain injury o a (congenital) brain malformation. The second peak occurs during late adulthood and represents symptomatic epilepsies secondary to a traumatic event such as febrile status epilepticus (SE), stroke, head injury, brain infection, brain tumor etc. In some cases the cause of epilepsy is unclear (Hauser et al., 1996). Unlike in PD, the incidence rate of epilepsy is not gender related.

Epilepsy should not be understood as a single disorder, but rather as a group of syndromes with divergent symptoms but all involving recurrent, abnormal, hypersynchronous and/or excessive electrical activity in the brain. Next we give a short overview of the different epileptic seizure types and epilepsy syndromes.

1.3.1.2 Seizures

Epileptic seizures can be divided into two main categories depending on their onset, namely focal epileptic seizures that are partial in onset, limited to one hemisphere, and generalized epileptic seizures with a generalized onset over both hemispheres (Berg et al., 2010). Focal or partial seizures originate from one hemisphere and can be subclassified as simple or complex, based on the effect of the seizure on the consciousness. Simple partial seizures affect normal sensory, motor, autonomic, cognitive or emotional functioning, without losing consciousness.

In contrast, complex partial seizures are always associated with loss of consciousness. Both simple and complex partial seizures may gradually develop into secondary generalized seizures when the epileptic activity spreads to the contralateral hemisphere.

Generalized seizures seem to initiate in all parts of the brain simultaneously, due to rapid spreading after onset, making it impossible to identify the onset zone in many cases. Generalized seizures are categorized, based on their clinical symptom, into tonic-clonic seizures (also known as the "grand mal seizure"), clonic seizures, tonic seizures, absence seizures (also known as the "petit mal seizure"), myoclonic and atonic seizures (drop attacks). Generalized seizures are usually accompanied by loss of consciousness from onset to the late phase of recovery. Typically, a tonic-clonic seizure is preceded by an aura, followed by muscles contractions (tonic phase) and clonic jerking of the lower and/or upper limbs (clonic phase) (Zifkin and Dravet, 2008). In the case a patient experiences a partial or generalized seizure that lasts several minutes or longer, a state of continuous seizure activity, called a status epilepticus, occurs (Seino et al., 2006).

1.3.1.3 Syndromes

Epilepsy syndromes are categorized based on their ethiology, namely genetic cause, known structural or metabolic cause associated with the risk for developing epilepsy, and unknown cause (Berg et al., 2010).

1.3.1.4 Temporal lobe epilepsy

Temporal Lobe Epilepsy (TLE) is one of the most common types of epilepsy and one of the most difficult to treat effectively with anti-epileptic drugs (Engel, 2001; Panayiotopoulos, 2007). About one third of all epilepsy patients suffer from TLE and more than 30% of those TLE patients are medically intractable (de Lanerolle and Lee, 2005; Duncan and Sagar, 1987). Additionally, in about 75% of the TLE patients, seizures are poorly controlled, making TLE the most drug resistant type of epilepsy (Spencer, 2002). This provides motivation for further research to develop alternative treatments, such as DBS, to treat drug resistant epilepsy.

TLE is characterized by complex-partial seizures, with or without secondary generalization. Prior to the onset of these complex-partial seizures, a previous acute brain insult occurred in the patient's life, such as febrile seizures, trauma, or a status epilepticus, causing initial neural damage. Months or years later, TLE develops, during which cellular and molecular changes occur, eventually leading to the manifestation of spontaneous recurrent seizures (Arzimanoglou et al., 2002).

TLE is subdivided into mesial TLE (mTLE), characterized by seizure generation from the mesial temporal lobe, and lateral TLE (lTLE), characterized by seizure generation from the lateral temporal lobe. mTLE is the most common epilepsy in adults, and is therefore well documented due to the large series of patient data available, as opposed to the far less documented lTLE. Therefore, in this dissertation, we refer to mTLE when we name TLE.

1.3.2 The brain network involved in TLE

1.3.2.1 The limbic system

The underlying cause of TLE remains to be elucidated but electro-encephalography and neuroimaging studies suggest that the limbic system, and more specifically the hippocampus, plays an important role in the process of developing TLE (King et al., 1995; Mathern et al., 1995; Spencer and Spencer, 1994). The limbic system, also called "the emotional brain", is a complex set of brain structures that lies on both sides of the thalamus, right under the cerebrum.

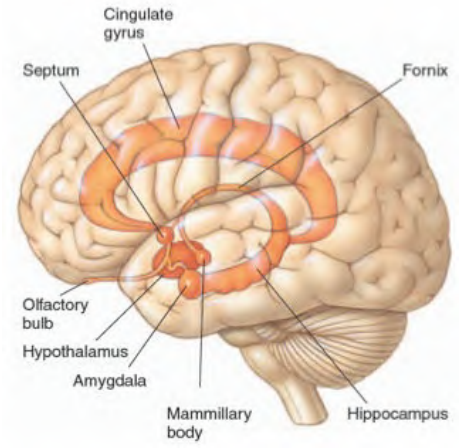

Figure 1.5: Schematic representation of the limbic system. (Figure adopted from http://mikeclaffey.com/psyc170/).

Besides emotion, it is also involved in cognitive processes, such as the formation of memories. Structures of the limbic system include the hippocampus, hypothalamus, thalamic nuclei, amygdala, mammillary bodies, septum, fornix, cingulate gyrus, olfactory bulb, limbic cortex, and other brain structures nearby. The main structures are depicted in Fig. 1.5.

In particular, the hippocampus seems to be important in the development of TLE. The information flow and pathophysiology in TLE of this important structure are explained in the next two paragraphs.

1.3.2.2 The hippocampus: information flow

The hippocampus can easily be identified by its characteristic shape and unique macroscopic and microscopic structure. In essence, the hippocampus is a cortical wrapping of the archaeocortex. It evolved from a simple cortical plate in amphibians to a complex structure in mammals, tightly connected to the neocortical regions (El-Falougy and Benuska, 2006). The hippocampus itself consists of two "banana-shaped" structures, defining the hippocampal formation. The hippocampal formation consists of the dentate gyrus (containing granule cells), the subiculum, the Cornu Ammonis (CA) fields CA1, CA2, CA3 and CA4. Each hippocampal substructure has its own structural and functional properties.

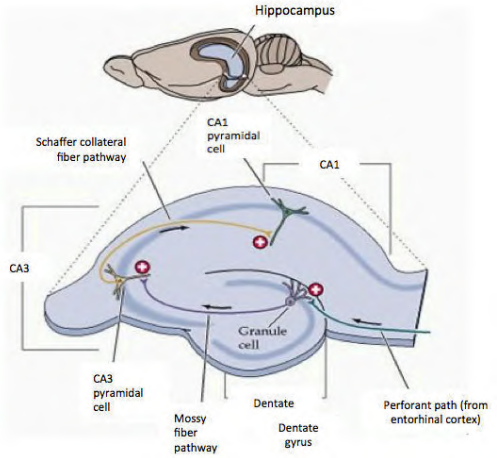

Figure 1.6: Schematic representation the main information flow through the rodent hippocampal formation. (Figure modified from Hyde and Strowbridge, 2012).

Information flow through the hippocampus occurs in a well-established unidirectional manner (see Fig. 1.6), following a closed loop that originates in the entorhinal cortex. The main input to the hippocampus originates from the pyramidal cells of the entorhinal cortex and enters the hippocampus via the perforant path targeting the dentate gyrus. Next, the information flow proceeds from the dentate gyrus to CA3 along the mossy fiber pathway. These CA3 cells are connected to the ipsi- and contralateral CA1, called the Schaffer collateral fiber pathway, and eventually target the subiculum.

1.3.2.3 The hippocampus: pathophysiology

In the last decades, the (patho)physiology of the limbic system and the hippocampus in particular has been extensively studied. Histological evaluation of human epileptic hippocampal tissue suggests that the hippocampus plays an important role in the process of epileptogenesis (King et al., 1995; Spencer and Spencer, 1994), featured by neuronal cell loss (Lewis, 2005) and granule cell dispersion (Fahrner et al., 2007), gliosis (Blumcke et al., 2002), synaptic plasticity under the form of mossy fiber sprouting (Parent et al., 1999), neurogenesis (Parent, 2002), inflammation (Vezzani et al., 2002), and molecular reorganization in cellular membranes and extracellular matrix (Avanzini and Franceschetti, 2003) in the limbic system.
Moreover, neuroimaging of TLE patients indicates that 70% of those TLE patients displays hippocampal sclerosis (deLanerolle and Lee, 2005) and surgical removal of the sclerotic hippocampus leads to seizure-freedom in 70% of the TLE-cases (Spencer, 2002). In rodents, hippocampal sclerosis is characterized by the selective loss of neurons in the CA3 mainly (Ben-Ari and Cossart, 2000). As a response to this selective cell loss, the axons of the granule cells need to target structures that they normally do not innervate. This process is called mossy fiber sprouting (Mathern et al., 1996) and is a presumed mechanism of increased excitability of the hippocampal circuit (Brandt et al., 2003; Spencer and Spencer, 1994; Zhang et al., 2002). Despite the large amount of available data and formed hypotheses, it remains to be elucidated how these pathophysiological changes in the hippocampus contribute to, or are the consequence of, the epileptogenesis.

1.3.3 DBS as a treatment for TLE

Epilepsy patients are always treated with anti-epileptic drugs first. For the one third of epilepsy patients that is medically refractory, alternative treatment options such as epilepsy surgery (Spencer, 2002), gamma knife surgery (Romanelli and Anschel, 2006), ketogenic diet (Huffman and Kossoff, 2006) and neurostimulation such as DBS can be used.

Since its success in PD and other movement disorders, the number of neurological diseases being investigated for DBS as a therapeutic strategy is growing steadily. Also for refractory epilepsy, treating unsuitable resective surgery candidates with neurostimulation may be more successful.
Since 1988, Vagus Nerve Stimulation (VNS) has provided an alternative treatment option for unsuitable resective surgery candidates (Van Roost et al., 2007). VNS consists of the implantation of a helical stimulation electrode, attached around the left vagus nerve in the neck area. By means of a subclavicular pulse generator, the vagus nerve is intermittently stimulated (Ben-Menachem, 2002). VNS-treatment was approved as a therapy for epilepsy in 1997, and since then over 70000 patients worldwide have undergone VNS treatment (Magdaleno-Madrigal et al., 2014). However, about 30% of the patients treated with VNS do not experience any improvement (Handforth et al., 1998). DBS might provide a better alternative treatment option, since direct electrical stimulation of brain structures may exert stronger seizure suppressing effects, as opposed to VNS, which influences brain structures in an indirect manner. An additional benefit, of direct stimulation of brain targets involved in the seizure, is that possible systemic side-effects are avoided, as opposed to the typically systemic administration of anti-epilepstic drugs. Additionally, DBS not only allows for a reversible alternative but also features the adjustment of stimulation parameters, enabling a more patient-specific therapy compared to resective surgery.

1.3.3.1 Clinical efficacy

Two key long-term multi-center clinical trials have lead to the establishment of DBS as a treatment for refractory epilepsy, namely stimulation of the anterior nucleus of the thalamus (SANTE) and responsive focal stimulation (NeuroPace), respectively (Heck et al., 2014; Fisher et al., 2010).

The SANTE study - The SANTE trial showed that high frequency (145Hz) stimulation in a structure responsible for seizure propagation (i.e. the anterior nuclei of the thalamus (ANT)) in patients with focal epilepsy resulted in a >50% reduction in seizure rate by two years (Fisher et al., 2010). This SANTE trial demonstrated safety and efficacy of ANT-DBS, resulting in FDA approval for ANT-DBS in 2009, and CE marking in 2010.

The Neuropace study - In the second trial, responsive neurostimulation (RNS) was used to stimulate the seizure onset zone whenever a seizure is detected by the system (NeuroPace®RNS®). In this study, the median seizure reduction was 53% after two years (Heck et al., 2014). Showing clinical efficacy, the NeuroPace®RNS® system was approved for the treatment of adults with partial onset seizures whom have not been controlled with two or more antiepileptic drugs in 2013. Despite these positive results with responsive focal neurostimulation, it remains to be elucidated whether RNS stimulation is more effective than ANT-DBS.

1.3.3.2 Hippocampal DBS

As mentioned before, a seizure often initiates in the hippocampus in TLE patients (Sprengers et al., 2014; Spencer, 2002). Currently, hippocampal DBS is being explored as an experimental DBS-therapy for the treatment of refractory TLE. Over the past fifteen years, several centers have explored the efficacy of scheduled hippocampal DBS as a treatment for refractory epilepsy, demonstrating promising results. Table 1.2 lists the outcome of small open label and small randomized controlled trials of hippocampal DBS as a treatment for refractory epilepsy. So far, hippocampal high frequency DBS has been applied in approximately 43 patients worldwide (Vonck et al., 2013; Boon et al., 2007; Osorio et al., 2005; Tellez-Zenteno et al., 2006; Velasco et al., 2007; Velasco et al., 2000b), and 70% of those patients experience a clear reduction in seizure frequency. Results vary from a moderate 15% seizure reduction (Tellez-Zenteno et al., 2006) up to promising >50% seizure reduction, and even seizure freedom in 50% of some patient series (Velasco et al., 2007). These studies typically show reductions of seizure frequency of 40% acutely, and 50–69% after several years, with the maximal effect seen typically 1–2 years after implantation. Seizure intensity might also be reduced.
Boon et al. treated thirteen refractory TLE patients with long-term DBS (i.e. > 3 years), with 90% of patients experiencing reduction in seizures (Vonck et al., 2013; Boon et al., 2007). Two of those 13 patients eventually underwent an amygdalo-hippocampectomy (i.e. removal of the hippocampus or amygdala).

Table 1.2: Outcome of open label and small randomized controlled trials of hippocampal DBS as a treatment for refractory epilepsy.

Clinical trial	DBS parameters (frequency (Hz), pulse width (μs), amplitude (A,V))	Seizure rate reduction			
		>90%	50-90%	30-50%	<30%
Velasco et al., 2007	130Hz, 450μs, 0.3A	4/9	5/9	-	-
Vonck et al., 2013; Boon et al., 2007	130Hz, 0.1-0.2V	6/11	2/11	1/11	2/11
Cuckiert et al., 2014	130Hz, 300μs, 0.5-1-3.5V	2/9	5/9	-	2/9
Boex et al., 2011	130Hz, 450μs, 0.5-2V	2/8	4/8	-	2/8
McLachlan et al., 2010	185Hz, 90μs, 1.8-4.5V	-	-	2/2	-
Tellez-Zenteno et al., 2006	190Hz, 90μs, 1.8-4.5V	-	-	2/4	2/4

Although these results seem promising, the high responder rate should be interpreted with caution. The value of hippocampal DBS is difficult to assess in these open label studies with a limited amount of patients, where stimulation parameters were tailored to achieve optimal seizure control in the individual patient during daily clinical practice. A recent Cochrane analysis on all small, randomized, controlled trials that conducted DBS, demonstrated that hippocampal DBS, next to ANT-DBS and responsive focal DBS, seems to be a valid option to reduce seizure frequency in refractory epilepsy (Sprengers et al. 2014). Additionally, improved efficacy with longer treatment duration has been observed after long-term treatment with hippocampal DBS, similar to the open label phase of the SANTE and NeuroPace trial (Heck et al., 2014; Vonck et al., 2013; Fisher et al., 2010). In this work, we will further explore the hippocampus as alternative DBS target for epilepsy.

The hippocampus is a key-component in normal cognitive functioning and is mainly responsible for the formation of new memories, spatial navigation and conversion of short-term to long-term memory (El-Falougy and Benuska, 2006). Thus, damage to the hippcocampus (i.e. due to apoxia or encephalitis) leads to disorientation and difficulties in memory formation and retrieval (Alvarez et al., 1995; Scoville and Milner, 1957). Because of the inhibition-like effect of DBS on the stimulated target structures, it is likely that hDBS may lead to memory impairment. Therefore, every implanted patient should undergo thorough post-surgical testing. Conversely, the previously discussed open label randomized trials on hippocampal DBS did not report effects on memory and learning (Tellez-Zenteno et al., 2006; Velasco et al., 2007; Boon et al., 2007; Boex et al., 2011; Cukiert et al., 2014). Moreover, studies have demonstrated an overall improvement in the emotional state (Miatton et al., 2011), and enhanced short-term memory (Luna-Munguia et al., 2012). In conclusion, the implantation of DBS hardware and the stimulation itself is considered safe, with limited risks and insignificant cognitive impairment. However, extra research is necessary, involving larger patient groups with long-term follow-up, in order to identify complications that might be overlooked in pilot-trials with limited sample sizes.

1.3.4 Rodent models of epilepsy

Although DBS as a treatment for epilepsy is promising, the working mechanism of action and optimal settings of DBS remain to be elucidated. Experiments in humans are difficult and restricted due to ethical problems and the necessity of large and homogeneous patient groups. Studies in animal models for epilepsy are therefore indispensable, not only to understand the therapeutic mechanisms underlying DBS and optimize DBS therapy, but also to unravel the pathogenesis of TLE.

When modeling human epileptic seizures and epilepsy, three categories of *in vivo* animal models can be distinguished, namely genetic models, acute seizure models (that do not necessarily indicate the presence of an epileptic condition) and chronic models (associated with spontaneous recurrent seizures) (Engel et al., 2006). No animal model can faithfully mimic all complex features of a seizure or syndrome. Thus, each animal model focuses on certain key components of seizures and syndromes. For example, post-status epilepticus models are mostly used to investigate the pathogenesis of TLE. These models are characterized by a latent period during which the epilepsy develops (similar to TLE), resulting in spontaneous seizures and lesions such as mossy fiber sprouting. Post-status epilepticus models can be achieved by chemically (i.e. kainic acid or pilocarpine) or electrically (i.e. kindling) inducing epilepsy. The chemical kainic acid and pilocarpine model better mimic the pathophysiology of epilepsy. Unfortunately, spontaneous motor seizures do not or are less likely to develop in kindling models.

Chapter 2

Functional Neuroimaging and Optogenetics

2.1 Functional Magnetic Resonance Imaging

Functional Magnetic Resonance Imaging (fMRI) is a functional neuroimaging technique that measures the activity of the brain by detecting related changes in blood flow. fMRI makes use of endogenous contrast (the blood oxygenation level dependent contrast) or non-radioactive exogenous contrast agents (the cerebral blood volume contrast) to visualize brain function. Basically, fMRI is a series of MR-images acquired sequentially for a period of time to investigate how the blood oxygen level changes over that period of time. In this paragraph, we explain the general principles of MRI and fMRI, after which we elaborate on fMRI contrasts and its applications in DBS. Additionally, we describe a pilot experiment where we evaluated different MRI compatible electrode materials.

2.1.1 Magnetic Resonance Imaging

2.1.1.1 Basic principles

MRI is based on the principle of proton nuclear magnetic resonance (NMR). The MR scanner (Fig. 2.1) consists of a set of embedded coils: one coil that generates the main magnetic field, three "gradient coils" that produce variations in the magnetic field in the X, Y, and Z directions for localization of the source of the MR-signal, and one or two "RF coils" for transmitting and receiving radio-frequency (RF) pulses.

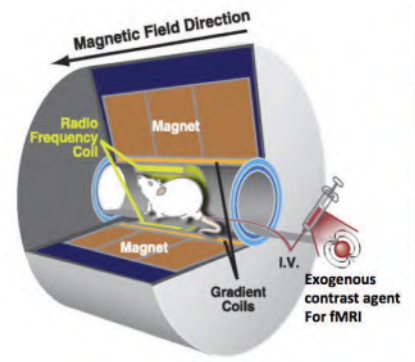

Figure 2.1: Schematic representation of a small animal magnetic resonance imaging (MRI) showing the basic principles of this technique. In case of a functional MRI, an exogenous contrast agent is injected to visualize cerebral blood volume changes over time. (Figure modified from http://physrev.physiology.org/).

About 70 percent of the human body consists of water. The hydrogen atoms, or protons, of this water molecules act as very small magnets, which are randomly orientated under normal circumstances. However, when the body is placed into the strong magnetic field of the MR scanner, these protons are aligned with the magnetic field of the MR scanner, i.e. the polarized state. This magnetization alignment can be briefly disturbed by applying a RF pulse produced by the RF transmitter coil, i.e. the depolarized state. When the RF pulses are then turned off, the protons realign themselves or decay back to their polarized state. This decay or relaxation process creates a changing magnetic flux density, causing the protons to re-emit an RF signal. Finally, the receiver coil picks up this emitted RF-signal and this information can be used to create an MR image. Note that MRI detects not only water protons. And different relaxation or ontrast is formed based on specific proton bindings in different molecules. Since proton binding is different for different tissues, tissues align and decay at different rates, resulting in images with excellent endogenous contrasts between different tissues (Fig. 2.3). In order to distinguish the signals from different locations in the brain (or body), spatial encoding is obtained by applying 3 different magnetic field gradients (smaller magnetic fields) across the patient in the X-, Y- and Z-direction. These gradient coils enable the correlation of the RF-signals to a given location in the brain (or body). The fourier transform of the recorded signals results in a data matrix that is called k-space. In order to reconstruct the MR-image out of the k-space data an inverse fourier transform is applied (Scherzinger and Hendee, 1985).

2.1.1.2 Relaxation processes: T1, T2 and T2*

This RF-signal is a combination of two different relaxation processes that occur immediately after the application of the RF pulse by the transmitter coil: the T1 or spin-lattice relaxation and the T2 or spin-spin relaxation. The T1 relaxation occurs because the protons decay back to a stable state due to energy loss caused by interactions with the surroundings. The T1 relaxation is characterized by the T1 time constant, which is the value of T1 when 63% of the longitudinal magnetization is recovered (Fig. 2.2C). The T2 or transverse relaxation occurs due to the dephasing of the proton spins caused by spin-spin interactions. The T2 relaxation is characterized by the T2 time constant, which is the value of T2 when 63% of the transverse magnetization has decayed (Fig. 2.2D). T2 relaxation happens long before the complete recovery of the longitudinal magnetization. Typically, T1 relaxation has a time constant of 832ms and 1331ms for white and gray matter, respectively, in a 3T scanner. Whereas, T2 relaxation typically has a time constant of 79.6ms and 110ms for white and gray matter, respectively.

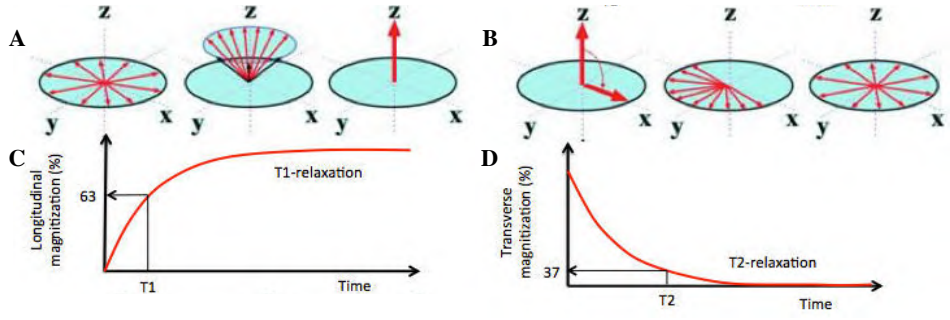

Figure 2.2: Schematic of relaxation processes: (A) Schematic of the longitudinal decay. (B) Schematic of the longitudinal recovery induced by the transverse magnetization. The time constant for this recovery is T1 and is dependent on the strength of the external magnetic field, and the internal motion of the molecules. (C) Schematic of the T2 or transverse relaxation. (C) Schematic of the loss of transverse magnetization due to the dephasing of spins (D) Schematic of the T2 time constant, which is more or less independent from the external magnetic field. (Figure modified from Rorden and Morgan, 2016)

In reality, local variations in the magnetic field cause the transverse magnetization to decay much faster than predicted by spin-spin interactions alone. This faster "effective" transverse relaxation is called T2* and results mainly from inhomogeneities in the main magnetic field due to field distortions induced by the tissue or other materials placed inside the magnet, or by magnet defects (Chavhan et al., 2009).

Depending on the MR sequence parameters, we can choose for the image to be T1, T2, T2* or proton density (PD) weighted (Fig. 2.3). For example T1-weighting (water appears black) is usually used to investigate structural abnormalities, and T2-weighting (water appears white) is usually used to investigate lesions, since most lesions associate with a higher water content. The realization of these weighted images depends on the acquisition sequence (e.g. spin echo SE, gradient echo GE, etc.) and their corresponding sequence parameters chosen, such as repetition time TR, echo time TE, flip angle FA. Here, we provide a brief description of these parameters and how to achieve T1, T2, and T2* weighted images.

Generally, the T1- or T2-effect on image contrast is determined by the combination of the echo time TE and the repetition time TR; with TE being the time between the 90° RF pulse and MR signal detection, and TR being the time between 2 excitations pulses (i.e. time between two 90° RF pulses). With short TR values (500ms) and short TE values (<30ms), the resulting image contrast will be T1-weighted; and the longer the TR values, the smaller the T1 effect on the tissue contrast. With a long TE (>80ms) and long TR (1500ms), the image contrast will be T2-weighted. And, a long TR (1500ms) with a short TE (<30ms) will result in a PD-weighted MR image.

A spin echo (SE) is generated by two RF-pulses, whereas a gradient echo (GE) is generated by one RF pulse in conjunction with a gradient reversal. The most important difference between both sequences is that SE (but not GE) reverses static field inhomogeneities due to the rephasing of spins induced by the second (180°) RF pulse. In contrast, the gradient reversal of GE refocuses only those spins that have been dephased by action of the gradient itself. More specifically, phase shifts resulting from magnetic field inhomogeneities, static tissue susceptibility gradients, or chemical shifts are not cancelled at the center of the GE as they are in SE sequences. This means that image contrast using GE sequence is obtained by T2*effects

and not pure T2 relaxation, as opposed to SE. Additionally, since with GE only one RF-pulse is applied, the echo can be recorded much more quickly in a GE sequence. Therefore, the TE is generally shorter for GE sequences than for SE sequences. When GE sequences are used with a narrow flip angle (i.e. the amount of rotation of the net magnetization during application of the RF pulse), shorter values of repetition time TR may also be used. The combination of short TR and short TE values allows for very rapid signal acquisition. For these reasons GE-based MR sequences with a relatively short TE are used to accentuate local variations in the magnetic field and therefore provide T2*-weighted images. Such sequences aid the detection of hemorrhage and form the basis of functional MRI (Chavhan et al., 2009).

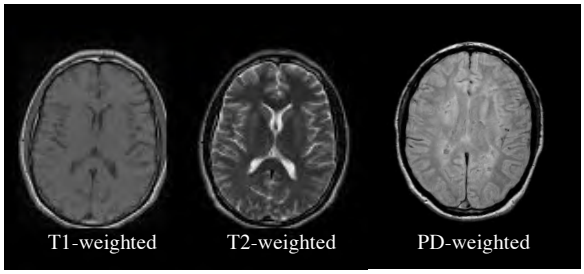

Figure 2.3: Representative example of an axial slice through the human brain from a T1-weighted, T2-weighted and proton density (PD)-weighted MR image.

2.1.2 Functional Magnetic Resonance Imaging

In contrast to structural MRI that is used to acquire anatomical images of the brain, fMRI can be used to reveal information about brain function. fMRI has been used extensively to locate brain structures that are activated by a physical sensation or stimulus. fMRI provides indirect information about neuronal activity by measuring the changes in metabolic requirements, which are related to the neuronal activity. For example, with an increased neuronal activity, the neurons use more energy, and it is the subsequent hemodynamic changes in response to the energy need that are measured with fMRI. However, the exact relation between the neuronal activity increases and corresponding metabolic and hemodynamic changes are incompletely understood. The most commonly used fMRI contrast is the blood oxygenation level dependent (BOLD) contrast, which is based on the level of deoxyhemoglobin in the vascular system of the brain (Huettel et al., 2009a). This basis of BOLD fMRI was discovered in the early 1990s by Seiji Ogawa (Bell Laboratories, New Jersey, USA). Ogawa discovered that oxygen-poor hemoglobin was affected differently by a magnetic field than oxygen-rich hemoglobin. Ogawa realized that changes in neural activity in a brain structure cause changes in the oxygen content in that structure, and that this change in oxygen content induces local changes in the magnetic field and therefore can be used as a endogenous contrast agent to map images of brain activity on a normal MRI scan (Bandettini, 2012). Figure 2.4 illustrates how the use of fMRI to investigate brain function in the healthy and pathological brain has been rocketed since then. The widespread and successful application of fMRI to human brain imaging has been the result of the fact that it is a non-invasive technique, without the need for (radioactive) exogenous contrast agents. The next section will explain the physiological basis and measurement of BOLD fMRI more in detail.

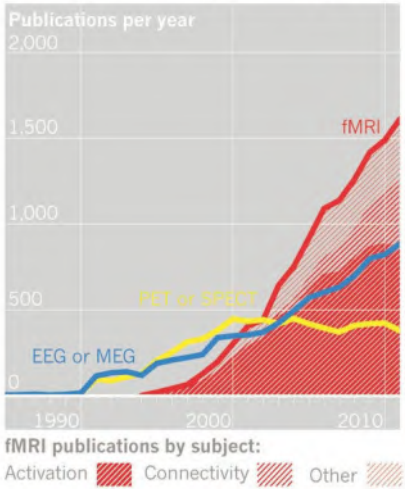

Figure 2.4: The rise of fMRI. Use of fMRI has rocketed and now more and more studies are looking at connectivity between areas. fMRI, functional magnetic resonance imaging; PET, positron emission tomography; SPECT, single-photon emission computed tomography; EEG, electroencephalography; MEG, magnetoencephalography. (Figure adopted from ISI Web of Knowledge.)

2.1.3 The BOLD contrast

2.1.3.1 Principles

All neurons in the brain consume oxygen. The hemoglobin molecules (i.e. the molecules that carry oxygen) in the blood provide the neurons continuously with new oxygen. Logically, an increase of neuronal activity increases also the demand of oxygen. This leads to an increased concentration of oxygenated (i.e. oxygen-rich) blood in the capillaries surrounding the active brain area. These local increases in blood flow can be mapped using fMRI as a change in raw image intensity (Huettel et al., 2009a; Kim et al., 2006), because oxygen-rich and oxygen-poor blood are characterized by different magnetic susceptibility. These differences in magnetic susceptibility induce small magnetic field distortions, and reflect in the relaxation process of the protons in the area with changing brain activity.

FMRI measurements are based on the concentration of oxygen-poor blood deoxyhemoglobin (deoxy-Hb) in the vascular bed of the brain (Huettel et al., 2009a; Kim et al., 2006). Deoxy-Hb has paramagnetic properties, and therefore can act as an endogenous contrast, because it affects the transverse relaxation, namely an increase in deoxy-Hb decreases the MR-signal using T2∗-weighted imaging. More specifically, the T2∗ time constant becomes shorter in areas with high deoxy-Hb concentration and longer in areas with low deoxy-Hb concentration. In the active brain area the intensity of a voxel in the fMRI image is brighter (longer T2∗) (Huettel et al., 2009a; Shmuel, 2010). These changes in fMRI signal are not directly related to neuronal activity, but reflect the energy requirements involved with processing of neuronal activity (Huettel et al., 2009b). In fact, more oxygen will be supplied than is actually consumed during neuronal activation (Huettel et al., 2009a). Therefore, the local concentration of oxy-Hb will be increased in the capillaries supporting the activated brain tissue and in the downstream veins, thus resulting in a decreased concentration of deoxy-Hb. This process is illustrated in Fig. 2.5. As a result, the local signal intensity of the T2*-weighted images will be increased. Thus, an fMRI scan indirectly measures brain activity by measuring the change in blood levels (specifically hemoglobin as it deoxygenates), resulting in an image of the brain with brighter or darker areas where blood is oxygenated or deoxygenated, respectively. This very small change of intensity can however not be readily detected and special signal processing techniques are needed to reveal the active brain areas. Also, this effect can only be measured at higher field strengths (i.e. 1.5T or higher).

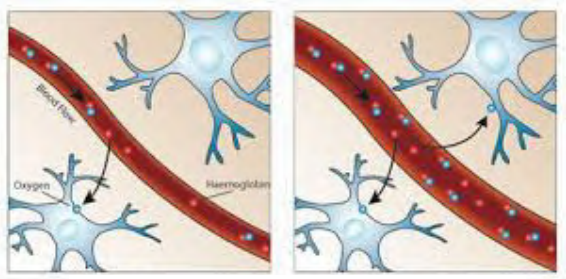

Figure 2.5: Summary of the generation of the BOLD signal. (A) shows the ratio oxy- and deoxyhemoglobin during rest. (B) When neurons in the surrounding tissue are activated, more oxyhemoglobin is provided by the vascular system resulting in a decreased concentration of deoxyhemoglobin. (Figure adapted from Oxford fMRIB).

2.1.3.2 The hemodynamic response function

In a typical fMRI experiment the goal is to map patterns of neuronal activation in the subject's brain while he or she performs specific tasks. However, fMRI does not measure the neuronal activity itself. Instead, the BOLD response to activation is dependent on the concentration change of deoxyhemoglobin, which in turn is dependent on the cerebral blood flow (CBF), the cerebral blood volume (CBV), and the cerebral metabolic rate of oxygen ($CMRO_2$) (Kim et al., 2006; Shmuel, 2010; Huettel et al., 2009a). The relation between these effects are captured by a theoretical model, called the hemodynamic response function (HRF) (Fig. 2.6) (Kornak et al., 2011; Lindauer et al., 2010; Deichmann et al., 2010, Huettel et al., 2009a; Buxton et al., 2004).

This model shows that the signal decreases directly after neuronal activation, i.e. the initial dip. This is caused by an increased $CMRO_2$, and thus an increase of deoxy-Hb concentration. To correct for the oxygen consumption, CBF is increased after 1 or 2 seconds. An increase in oxygen due to an increased CBF causes a decreased deoxy-Hb concentration. This results in a total increase of the fMRI signal with a maximal response about 5s after neuronal activation. After, the fMRI signal drops below baseline, also called the post-stimulus undershoot (PSU). Initially it was assumed that the PSU was caused by a delayed vascular compliance: i.e. CBV is increased in response to neural activation and because the inflow of blood is initially larger than the outflow. CBF appears to decrease more rapidly than CBV, causing a greater concentration of deoxy-Hb in previously active brain structures, consequently leading to the PSU (Buxton et al., 1998). However, more recent fMRI studies conclude that the PSU rather reflects a sustained increase in $CMRO_2$ (Van Zijl et al., 2013).

This model is a theoretical description of the expected mechanism of the BOLD response. In practice the shape of the HRF depends on stimulus conditions and varies between subjects, and even between brain regions (Handwerker et al., 2004; Aguirre et al., 1998; Siero et al., 2011; Rosa et al., 2010).

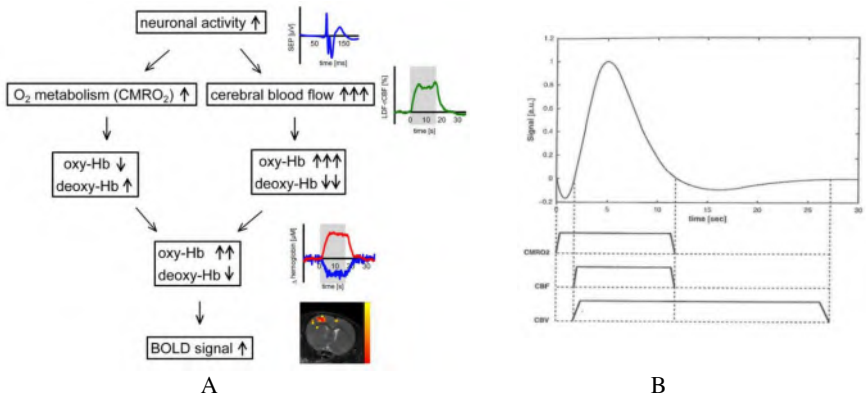

A B

Figure 2.6: (A) Graphical representation of the BOLD contrast, as a response to a stimulus to the brain. The increased neuronal activity requires a higher cerebral blood flow to the active regions, leading to an induced change in the ratio of oxygenated hemoglobin to deoxygenated hemoglobin, which in turn leads to an increased MR signal, the so-called HRF (B) (Figure adopted from Deichmann et al., 2010).

2.1.3.3 The negative BOLD signal

Also negative responses have frequently been observed (Shih et al., 2009; Schridde et al., 2008; Smith et al., 2004; Shmuel et al., 2006), but the nature of these negative BOLD responses remain to be elucidated. However, three theoretical mechanisms have been proposed to account for the fMRI signal decreases: (1) active neuronal inhibition; (2) vascular steal; and (3) depleted local oxygen levels (Wade et al., 2002).

- In case of active neuronal inhibition functional activity could be reduced below the baseline level in certain brain structures in response to particular stimuli, and therefore, are supplied with less oxygenated blood, showing a reduced BOLD signal during the stimulus period (Shmuel et al., 2002).
- Vascular steal occurs because only a limited amount of oxygenated blood is available at once to increase blood flow. Some of it could be diverted to active areas, thus draining from neighboring areas, thereby reducing the BOLD signal in those areas.
- It is possible that areas showing a negative fMRI signal actually have an increased level of neuronal activity, together with local oxygen depletion, during the stimulus period. In this interpretation, the fMRI signal is an extended version of the so-called “initial dip” (see previous paragraph) (Schridde et al., 2008).

The active suppression hypothesis is supported by many showing that some cortical regions can exhibit a negative BOLD response linked to activation in the opposite hemisphere (Tootell et al., 1998, Shmuel et al., 2002) where the effect of passive hemodynamic blood flow changes must be negligible (Shmuel et al., 2002). Future EEG-fMRI measurements are necessary to validate that reduced neuronal activity actually corresponds to a decrease in the fMRI signal, and consequently, caution needs to be taken when interpreting a negative fMRI signal (Shih et al., 20011).

2.1.3.4 Spatial and temporal resolution

The sequence parameters used in BOLD fMRI acquisitions affect the intensity of the fMRI signal, and the spatial and temporal resolution of the fMRI data (Huettel et al., 2009a). The most influential parameters are the magnetic field strength, TR, TE, and the type of imaging technique involved. Most commonly, fMRI data are acquired with an echo planar imaging (EPI) sequence (Deichmann et al., 2010; Huettel et al., 2009c), which is an efficient way of T2*-weighted scanning in which images are typically acquired with a TR of 0.5 to 3s.

In an ideal situation, signal changes are only related to the changes in deoxy-Hb in the capillaries closest to the site of neuronal activation. However, also larger and more distant vessels can contribute to the MR signal. Therefore, the maximal possible spatial resolution is affected by the anatomy of the vasculature in relation to the neuronal activity (Huettel et al., 2009a). But in general, the spatial resolution is determined by the voxel size. The chosen voxel size is a trade-off between a good spatial resolution (which requires a small voxel size) and a good signal-to-noise ratio (which requires a large voxel size). A good spatial resolution is necessary to eliminate partial volume effects, which means that multiple tissue types may contribute to the fMRI signal of a given voxel. Although the voxel size cannot be infinitely small, the spatial resolution of fMRI is much better than that of PET. Therefore, fMRI is a good technique to visualize activity from multiple sources and deep brain structures, such as mesial temporal structures or basal ganglia nuclei.

The temporal resolution is determined by the chosen TR and the number of phase encoding steps (i.e. phase matrix size) (Huettel et al., 2009a; Kim et al., 2006): a shorter TR and a smaller phase matrix will in principle increase the temporal resolution. But choosing a shorter TR will decrease the number of slices that can be acquired, thus affecting the axial field-of-view and/or axial spatial resolution. FMRI data can be acquired in a very short time; therefore a very high temporal resolution is possible in principle. However, the temporal resolution is limited by a lagged hemodynamic response (5.5s, Fig 2.6) to neuronal activity (1-100ms) and a finite signal-to-noise ratio. Therefore EPI datasets are usually acquired with a TR of 5s in a clinical setting and 1-2s in a preclinical setting.

2.1.4 The CBV contrast

2.1.4.1 Principles

Recently, an exogenous contrast agent, monocrystalline iron oxide particle (MION), has been introduced for fMRI, which has been shown to increase the functional sensitivity and signal-to-noise (SNR) ratio compared with the traditional BOLD technique. This is demonstrated in Fig. 2.7, where a comparison is made between BOLD fMRI and CBV fMRI during electrical stimulation of the rat forepaw (Shih et al., 2011).

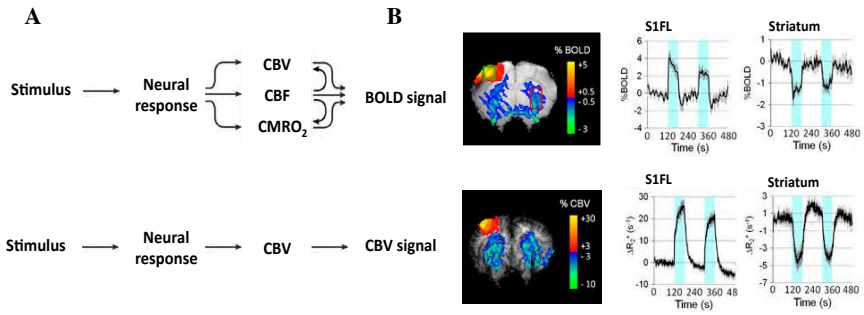

Figure 2.7: Comparison of BOLD and CBV fMRI (A) Schematic illustration of the relation between a stimulus and the BOLD or CBV signal. (B) Comparison of the spatial and temporal response to noxious rat forepaw stimulation using BOLD and CBV fMRI (Shih et al., 2011), demonstrates the enhanced specificity and SNR of CBV fMRI. Note, the CBV signal changes are inverted for the ease of comparison. In reality, the CBV signal is opposite in sign to the BOLD signal.

The CBV contrast mechanism is illustrated in Fig. 2.8. The MION is injected intravenously, and the presence of the blood-brain barrier prevents the contrast agent molecules from entering brain tissue. A few minutes after the injection of MION a constant concentration of the contrast agent, or a steady state, is obtained in a resting state (i.e. no stimulus is applied). This steady state is proportional to the local CBV. Stimulus-induced CBV changes can then be translated to MR signal changes in a T2*-weighted sequence, because the injection of a paramagnetic substance (such as MION) decreases the transverse relaxation rate of the MR signal, similar to the BOLD mechanism where paramagnetic deoxy-Hb causes a shorter T2*. An increase in the local CBV, associated with a local increase in neural activity, will therefore cause a drop in the fMRI signal. Note, the CBV-weighted signal, which reduces with activation, is opposite to the BOLD signal, which increases with functional activation.

In summary, there are two effects that contribute to the observed fMRI signal in experiments employing iron oxide contrast agent: the superparamagnetic effect of the contrast agent; and the BOLD effect resulting from the susceptibility difference between oxygenated and deoxygenated hemoglobin. Because both effects are opposite in sign, sufficiently high doses of contrast agent are needed in order for the susceptibility effect of the contrast agent to override the BOLD effect. In this way, the fMRI signal becomes insensitive to BOLD changes and primarily reflects CBV changes. Importantly, paramagnetic deoxy-Hb shortens blood relaxation times at higher field strengths, meaning the BOLD effect increases with higher field strengths. Consequently, higher MION doses are required at higher field strengths in order for the susceptibility effect of the contrast agent to overwhelm the increased BOLD effect (Lu et al., 2007).

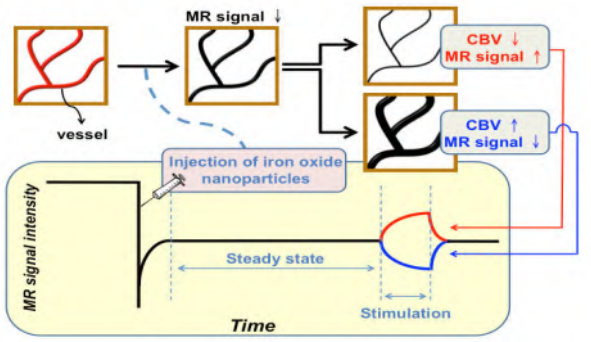

Figure 2.8: Schematic illustration of the CBV contrast principles. (Figure adopted from Shihlab).

2.1.4.2 Advantages

The main advantages of CBV fMRI over BOLD fMRI are an enhanced signal-to-noise ratio, specificity, and sensitivity. We shortly review them below.

Usually, BOLD fMRI needs to be performed at higher field strengths in order to detect changes, without averaging results from a very large number of animals. However, higher field strengths tend to cause more image distortion or signal dropout. Therefore, when using BOLD fMRI a trade-off has to be made between a reduced image quality (reduced SNR) or a reduced sensitivity, as a consequence of using short gradient echo times or spin echo methods to improve SNR. In contrast, when performing MION-based fMRI, the dose of exogenous contrast agent can be adjusted to optimize blood magnetization for any given echo time or imaging strategy. This means that CBV fMRI enables the reduction of image artifacts without compromising functional sensitivity. In theory, the highest sensitivity should occur at short echo times and high doses of agent. Additionally, a high dose of contrast agent also acts to overwhelm the opposing high-field BOLD effects, to an extent that the contribution of BOLD effect in the fMRI signal becomes negligible. Combining high-dosage of the contrast agent and short echo times, fivefold increases in SNR of the CBV signal have been observed at 1.5T, compared to the BOLD signal. Moreover, Mandeville et al. showed that the contrast-to-noise ratio (CNR) of MION-based fMRI in rats is 5.7 and 1.5 times that of BOLD at 2T and 4.7T, respectively (Mandeville et al., 1998).
Because the BOLD effect increases with higher field strengths, CBV fMRI has a better signal advantage over BOLD fMRI when it is performed at lower field strengths, as the CBV signal is less influenced by the BOLD signal (which is opposite to the CBV signal) at lower field strengths. Yet, even at very high field strength of 9.4 T, MION-based CBV method was still shown to provide a better sensitivity compared to BOLD fMRl (Zhao et al., 2006).

Besides improved SNR and sensitivity, another important advantages of MION-based fMRI is that its specificity is greater than conventional BOLD fMRI. The injection of a paramagnetic agent allows to measure solely CBV changes associated with functional activation, as opposed to the BOLD contrast, which is a resultant from complex interactions between CBV, CBF and $CMRO_2$ as a response to increased neural activity (Fig. 2.7A). CBF changes have no effect, since the concentration of paramagnetic agent is essentially the same in the arterial and venous circulation, so increased flow does not affect susceptibility. The imaging contrast is thus only sensitive to the concentration of paramagnetic agent in the imaging voxel. Additionally, the CBV contrast is not dependent on the anatomy of the brain vessels (size and orientation), since a steady state concentration of the contrast, proportional to the local CBV, provides a baseline independent from the vasculature anatomy. Consequently, CBV-weighted imaging offers enhanced sensitivity and specificity in fMRI studies, partially due to the reduced contributions from large vessels. Spatial specificity of MlON-based CBV fMRI in cats, undergoing selective stimulation of the columnar structures of the visual cortex, has demonstrated that CBV fMRl can distinguish two brain regions as close as 1.4 mm apart (Zhao et al. 2005).

In conclusion, there is existing evidence that CBV fMRI enhances functional sensitivity and uniformity of functional sensitivity, and diminishes large vessel artifacts. Therefore, MION-based CBV fMRI is suggested as the preferred method for functional brain mapping in animal models. If suitable contrast agents obtain human approval, CBV fMRI could be promising for clinical functional activation studies in human subjects.

2.1.5 DBS-fMRI applications

2.1.5.1 Evoked fMRI

To investigate a specific brain function, usually a task or a stimulus is presented to the subject that triggers the phenomena one wants to investigate (Aguirre, 2006; Huettel et al., 2009b). These studies are called paradigm-driven or evoked fMRI experiments. The most popular design is a block-design, in which stimuli are presented in repeated blocks, typically in the order of tens of seconds. The analysis of evoked fMRI experiments is based on the difference in fMRI signal between activation and baseline conditions. This contrast is typically formulated within the general linear model (GLM) framework, which is a model-driven approach to detect the brain regions that are significantly correlated with the stimulus paradigm (Fig. 2.9). Note that fMRI analysis provides qualitative information, as opposed to PET, which allows more quantitative estimates (e.g., receptor density, arterial blood sampling).

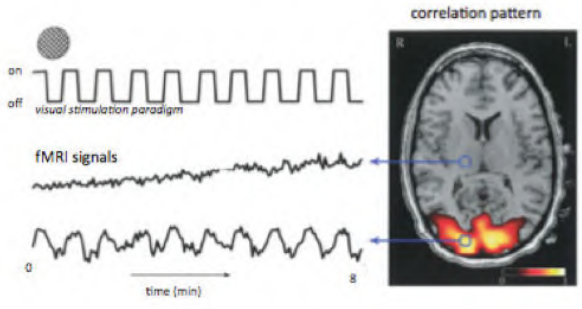

Figure 2.9: Example of a paradigm-driven fMRI experiment using a visual stimulus. A flickering checker board was presented to a subject in blocks of 20s. The stimulus caused an increase in the fMRI signal of a voxel in the visual cortex. The result of the GLM analysis is a correlation pattern projected onto an anatomical MRI indicating which voxels were significantly correlated to the stimulus (Figure modified from van Houdt, 2013).

Within the preclinical investigation of DBS, evoked fMRI plays an important role, since it allows the evaluation of brain regions modulated by DBS via direct comparison of activity-induced regional hemodynamic responses to applied stimulation. Notably, fMRI paradigms can be rapidly repeated several times in a single scanning session to evaluate for example frequency-dependent effects of DBS. Considering that a hallmark of therapeutic DBS is strong sensitivity to stimulation frequency, this represents a major strength of fMRI.

2.1.5.2 Functional connectivity MRI

In contrast to evoked fMRI, functional connectivity fMRI (fcMRI) is a technique where the subject does not have to perform a specific task, such that spontaneous brain activity can be investigated (Biswal et al., 1997). The subject is asked to relax and lie still with eyes closed, without thinking of something in particular (Cole et al., 2010). fcMRI measures low frequency spontaneous fluctuations in activity-related hemodynamic signals and employs data-driven analysis strategies (Cole et al., 2010), such as cross-correlational analysis, spatial independent component analysis (ICA) (Beckmann et al., 2004; Damoiseaux et al., 2006; Valente et al., 2010), and other network methods to measure signal coherence (connectivity) between regions of interest (Fox et al, 2007). fcMRI has been used effectively to identify candidate circuit function changes during brain stimulation (Figee et al., 2013).

In this dissertation, both evoked fMRI and fcMRI were used. Evoked fMRI was used to identify brain regions that correlate directly to the applied DBS-paradigm. Additionally, we used fcMRI to determine direct and indirect DBS-dependent changes in circuit connectivity by comparing fcMRI data before and during DBS. Overall, preclinical DBS-fMRI seems to be a promising tool for functional circuit mapping in the healthy and diseased brain. Yet, the complexities that come with this technique prevent extensive *in vivo* use. The main limitations include the presence of the metal artifact in the images and the use of anesthetics that might suppress neural activity. A careful experimental set-up is crucial for successful implementation of DBS-fMRI (Younce et al., 2014).

2.1.5.3 Patient studies

DBS-fMRI studies in patients are limited due to safety constraints. The presence of intracerebral metal makes MRI a potentially dangerous technique in patients with implanted DBS units, i.e. risk of electrode-heating (Tagliati et al., 2009; Baker et al., 2005; Jech et al., 2003; Finelli et al., 2002). Feasibility studies in phantoms reported severe potential hazards for patients but that under certain conditions, safe MR imaging examinations during active DBS was feasible (Georgi et al., 2004). Another phantom study observed false-positive activation on fMRI during DBS (Liu et al., 2008).

An fMRI study in PD patients, implanted with bilateral STN-DBS, demonstrated widespread modulatory effects on all the major components of the motor cortico-striato-thalamo-cortical loop. Interestingly, the authors showed that stronger direct pathway connectivity correlated to reduced PD deficits (Kahan et al., 2014). This finding is highly concordant with models of basal ganglia (dys)function in PD, that propose that dopamine depletion results in an underactive direct pathway, and an overactive indirect pathway, resulting in thalamic inhibition (Albin et al., 1989; DeLong, 1990).

Another fMRI study of PD patients that are being treated with DBS, also demonstrated widespread activation of the sensorimotor cortex and basal ganglia (Arantes et al., 2006). Note that DBS was turned off in both studies during scanning and that fMRI was performed during rest or a motor task. An illustration of DBS artifacts on fMRI images from human subjects is shown in Fig. 2.10.

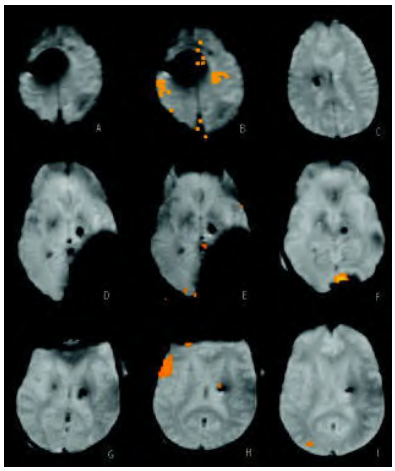

Figure 2.10: DBS artifacts: (A) Patient 1 EPI. Artifact in vertex due to DBS component; (B) Patient 1 fMRI. Artifact disturbs detection of SMA and SM1; (C) Patient 1 EPI. Electrode location with punctate loss of signal; (D) Patient 2 EPI. Artifact in occipital pole; (E) Patient 2 fMRI. Artifact precludes detection of temporoccipital activation; (F) Patient 2 fMRI after connector repositioning. Reduction in the occipital artifact; (G) Patient 3 EPI. Frontal artifact due to air; (H) Patient 3 fMRI. A region of artifact is seen close to the frontal activation; (I) Patient 3 fMRI. Days later without artifact. (Figure adopted from Arantes et al., 2006).

There is one study of Philips et al. that performed fMRI in 5 patients during active STN-DBS, after extensive phantom safety testing of DBS lead systems. The authors showed activation in the ipsilateral basal ganglia in all subjects and additional activation in the ipsilateral thalamus, STN and/or substantia nigra depending on the DBS-electrode location (Philips et al., 2006).

2.1.6 Evaluation of MR-compatible electrode materials

The presence of a metallic DBS-electrode in the MR scanner, can introduce large artifacts in the MR images, ranging from signal loss or pile-up, failure of fat suppression, to geometric distortion (Hargreaves et al., 2011). The use of MR-compatible materials, careful parameter and pulse sequence selection can avoid or reduce artifacts. Therefore, before the start of our preclinical fMRI experiments we performed a pilot experiment (phantom study and *in vivo*) to evaluate different materials and acquisition parameters. Note, this trial is a comparative study of a selection of materials, meaning other alternative electrode materials and designs were not included in this study.

2.1.6.1 Phantom study

We investigated 6 potential electrode materials on their MR-compatibility, bio-compatibility, workability and conductivity: stainless steel (SS), tungsten (W), platinum iridium (PtIr), gold (Au), silver (Ag) and carbon (C). The properties of these materials are listed in Table 2.1. The selection of these materials was based on literature: tungsten (Chao et al., 2014; Martinez-Santiesteban et al., 2007); platinum iridium (Hung et al., 2010; Jupp et al., 2006); gold (Dunn et al., 2009; Jupp et al., 2006); silver (Nyenhuis and Duan, 2009; Bosetti et al. 2002); carbon (Dunn et al., 2009; Jupp et al., 2006). This shows that the need for MR-compatible electrodes is not new, however, results are contradictory. For example Jupp et al. found that "Gold electrodes did not induce any change in signal intensity in T2-weighted images" (Jupp et al., 2006), while Dunn et al. stated that "Gold wires were rejected as they showed significant susceptibility artifacts in the 9.4T MRI" (Dunn et al., 2009). Differences in the electrode design and imaging parameters used might explain discrepancies between studies. Therefore, we performed our own pilot experiment to validate MR-compatible electrode materials in our own experimental set-up. In addition to MR-compatibility we also examined the conductivity, workability and bio-compatibility of each material.

Table 2.1: Material properties

Material	bare diam [μm]	coated diam [μm]	Manufacturer	Reference
Ag	76	140	Science products	
Au	76	140	Science products	Jupp et al. (2006)
C	unknown	200	Self-made	Jupp et al. (2006); Dunn et al. (2009)
PtIr	76	140	A–M Systems	Jupp et al. (2006); Martinez Santiesteban et al. (2007)
SS		125		
W	76	114	Science products	Martinez Santiesteban et al. (2007); Chao et al. (2014)

MR-compatibility - For each material we constructed twisted bipolar electrodes with a total lead length around 3cm and placed them a plastic tube filled with agarose gel, which resembles brain tissue. Note, leads were left open-ended and were not connected to a stimulator in the phatom-study. T1- and T2-weighted MR-images were acquired of the phantoms using a 7T MR scanner

(Pharmascan Bruker, Ettlingen, Germany). The MR-compatibility of a material depends on different properties. Most importantly, the material has to be MR-safe, and thus not ferromagnetic, and the diagnostic information of a taken scan should not be affected. Each material introduced inside the scanner influences the magnetic field of the scanner. A paramagnetic material will appear larger on the image compared to its real size, which could lead to misinterpretation of the result. For each material tested *in vitro* the artifact size was determined both on the CT and MR images. CT was used as a reference because it makes no use of magnetic fields and thus results in less metal artifact compared to MRI.

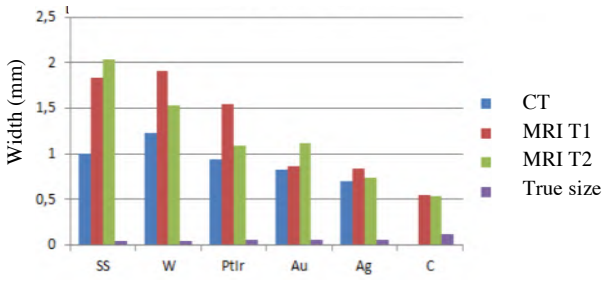

Figure 2.11: Comparison of the size of the electrode artifact on CT and MR-images (T1 and T2) and the actual electrode size.

Fig. 2.11 compares the size of the different electrode artifacts with CT and MR, and the actual electrode size, for the 6 different materials. Carbon (C) scored highest on MR-compatibility. However, we were unable to twist two wires without breaking the material. We can conclude that Ag and Au appear to be the most MR-compatible materials using a twisted bipolar electrode design.

Conductivity - As the electrode is used for stimulation, the conductivity of the material is also important. Therefore, the wires of each electrode need to be twisted and the electrode is electrolytically cleaned to assure optimal signal conductivity. The impedance was measured using an impedance meter (IMP-2, Bak electronics, Sanford Florida, USA).

Table 2.2: Impedance measurements of silver (Ag), stainless steel (SS), Platinum Iridium (PtIr), tungsten (W) and gold (Au).

Material	Impedance
Ag	34 kΩ
SS	45 kΩ
PtIr	50 – 100 kΩ
W	50 – 100 kΩ
Au	110 kΩ

The results of the impedance measurements are listed in Table 2.2. The impedance needs to be adequately low so the required current can be delivered. On the other hand, if the impedance is too low an incorrect current will be delivered. The first impedance measurements of PtIr and W resulted in relative high values, but after electrolytic cleaning of the electrodes, all tested materials resulted in comparable impedance around 50kΩ. Gold has the highest impedance, i.e. 110kΩ, and Ag the lowest, i.e. 34kΩ. The maximum impedance allowed for successful stimulation depends on the compliance voltage of the stimulator, in this case 48V. Thus, when a stimulation current of 500μA needs to be applied, a maximal impedance of 240kΩ is allowed.

Workability - It is crucial for a good DBS-electrode design that the material is nor too flexible, nor too brittle. The electrode cannot be too flexible, so it doesn't bend when "hitting" the cortex, and cannot be too brittle so it doesn't break during fabrication, more specifically during the twisting of the wires. This is especially important when twisting four wires to make quadripolar electrodes with a bipolar stimulation and a bipolar registration.
During fabrication of the bipolar electrodes for the phantom study, it appeared that some of the materials were less appropriate to make electrodes. We found that Au was too flexible (i.e. a bipolar electrode would bend upon "hitting" the dura), W on the brittle side (i.e. more difficult to make a quadri-polar electrode), and it was impossible to make electrodes of C, since the wires break immediately during twisting. We concluded that Ag, PtIr and SS are the most workable materials for our purposes. Note, multi-stranded wires (Guo et al. 2015) might render carbon electrode fabrication feasible but were not included due to the rather complex fabrication procedure.

Biocompatibility - As the electrodes would be chronically implanted, bio-compatibility is an important factor to take into account. It is well known silver is too toxic for use in longitudinal studies. Chronic exposure to silver causes a permanent blue-gray discoloration and/or irritation of the skin and/or eyes. Additionally, silver intoxication may cause damage to the liver, kidneys, intestinal tract, respiratory system and blood cells (Drake and Hazelwood, 2005). However, considering the good MR-compatibility, conductivity and workability of silver, we performed an *in vivo* test in order to check whether we could use silver in acute studies. Unfortunately this was not the case, since the animal died already 3 days after implantation, so we had to exclude silver as a suitable DBS-electrode material, even for acute studies. We found no evidence of the other materials to be bio-incompatible. Fig. 2.12 shows the head cap after post-mortem removal. The white residue at the site of the electrode, which was not seen in the previously used head caps, might be a sign of silver intoxication.

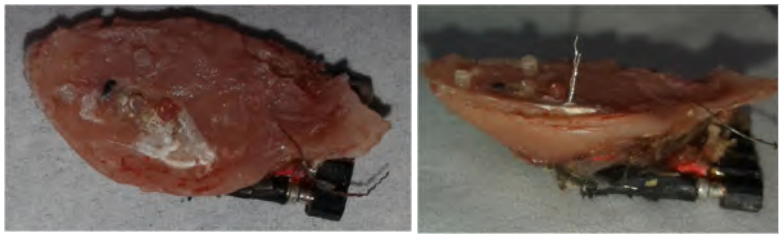

Fig. 2.12: Cap with silver electrode after post-mortem removal of the head cap. The white residue might indicate silver intoxication.

2.1.6.2 *In vivo* study

Both PtIr and W had acceptable phantom results, based on their MR-compatibility, biocompatibility, workability and conductivity, and therefore were tested *in vivo* in two rats (male, Sprague-Dawley, 200-250g). In the *in vivo* set-up the electrode leads were connected to a ground and a stimulator. Note, this evaluation focuses on image quality, meaning we did not check for potential heating effects and electrical induction at the level of the electrodes, caused by MR gradrient switching.
We evaluated the electrode artifacts on both the structural and functional MR images. For the structural MR images, T2 weighted anatomical images were obtained using a Turbo RARE sequence with TR = 6345ms, TE = 37ms, slice thickness = 0.6mm, matrix size = 276x320, FOV

= 3x3.5cm^2. Functional MR acquisitions were performed using a multi-slice single-shot gradient echo echo-planar imaging sequence (GE-EPI). Twelve interleaved slices were acquired with TE = 20ms, slice thickness = 1mm, matrix size = 80x80, FOV = 2.5x2.5cm^2 and voxel size = 0.312x0.312x1mm^3.

An axial slice of the acquired T2 images, at the height of the electrode, is shown in Fig. 2.13. PtIr (0.28mm) appears slightly larger on MR images compared to W (0.23mm). We can conclude that both W and PtIr can be used as electrode material for stimulation or registration within the MR-scanner, as we were able to visualize the global effect of DBS on the oxidative metabolism by detecting responses in brain structures local and downstream from the site of stimulation, with both materials (Fig. 2.14).

In this work, both materials were used. PtIr was used when a quadri-polar electrode (i.e. bipolar stimulation plus bipolar registration) was required, since tungsten appeared to be far less workable (breaking or splitting) when using four wires. However, tungsten was used when a bipolar electrode was sufficient. A bipolar electrode was used during DBS-fMRI experiments in PD, while a quadripolar electrode was used during DBS-fMRI experiments in epilepsy because this also requires simultaneous registration of the encephalogram to verify that no seizures occurred during the experiments.

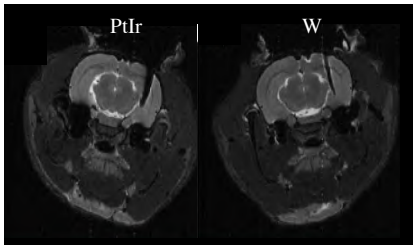

Figure 2.13: Electrode artifact on a T2 anatomical MR-image, axial slice at height of the electrode. Left: PtIr, Right: W.

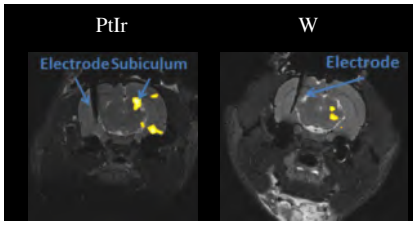

Figure 2.14: DBS-induced BOLD response in axial slice at height of the electrode (GLM, $p < 0.001$). Left: PtIr, Right: W.

2.2 Positron Emission Tomography

2.2.1 Basic principles

Positron emission tomography (PET) - together with single photon emission tomography (SPECT) - is a functional nuclear imaging technique. These nuclear imaging techniques are based on the tracer principle, proposed by George de Hevesy in 1911 (de Hevesy, 1948), and require the injection of a radioactive labeled molecule or tracer, into the human body, that participates in the subject's metabolism and distributes accordingly. A molecule can be turned into a radioactive tracer by linking a radionuclide to it, or by replacing one or more atoms in that molecule by a radionuclide. In case of PET, the radionuclides that are used are positron emitters. These positrons are very unstable particles and move typically ±1mm into our body, after which they annihilate with an electron, producing two gamma photons that will travel into opposite directions and that have an energy of 511 keV. These two gamma photons are picked up by the detector ring and readout-electronics of the PET scanner, resulting into the detection of a line of response. A line of response is characterized by a position and an angle, and many lines of response can be accumulated into a so-called sinogram. This acquired sinogram can be used to reconstruct a three-dimensional image, visualizing the distribution of the radioactive tracer into the body. The basics of PET imaging are illustrated in Fig. 2.15.

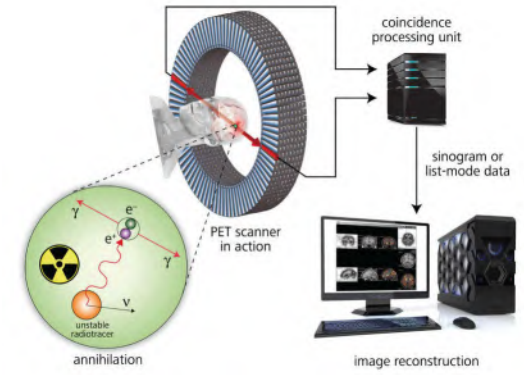

Figure 2.15: The basic principles of PET: positron annihilation forming two back-to-back gamma-rays with an energy of 511 keV, detected by the detector ring of the PET scanner. This information can be reconstructed resulting in a brain image showing the affected structures. (Figure adopted from Espinosa et al., 2009).

Nowadays, a spatial resolution of 4-5mm and 1-2mm can be achieved using a clinical and preclinical PET system, respectively. The spatial resolution is dependent on a combination of many factors, such as the detector size, acollinearity, positron range, penetration into the detector ring, imperfect decoding in the PET camera, geometry of the subject, and sampling error or statistical noise (Moses, 2011). A detailed review of the hardware of the PET system, the reconstruction techniques and these confounding mechanisms is out of the scope of this dissertation.

2.2.2 Radioactive glucose

The most commonly used radionuclide for PET is ^{18}F and has a half-life of 109.8min. ^{18}F is produced using a cyclotron by the irradiation of enriched water with protons. A very well known PET tracer is fluorodeoxyglucose (^{18}F-FDG), a radioactive glucose analog, where the hydroxyl group at the 2-position is replaced by ^{18}F (Fig. 2.16).

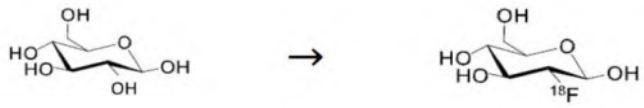

Figure 2.16: Chemical coupling of ^{18}F to the glucose molecule, replacing the OH-group at the 2-position. This results in a radioactive glucose analogue ^{18}F-FDG. (Figure adopted from Grull and Robillard, 2006).

The brain uses glucose as its main source of energy and increased neural activity requires more glucose. Since the uptake of FDG by the different tissues into our body is analogue to that of endogenous glucose and the mammalian brain uses glucose as its main source of energy, FDG-PET can be used to visualize changes in the glucose metabolism of the brain due to disease progression or due to the effects of a therapy.

Once the ^{18}F-FDG is produced, it is intravenously injected into the patient's bloodstream. The blood-brain-barrier is semi-permeable, and small and highly soluble molecules such as FDG are able to pass it. ^{18}F-FDG targets the Glut-1 transporters of the cell, which are groups of membrane proteins that are responsible for the transport of glucose from the blood stream into the cells. In the cell, both endogenous glucose and ^{18}F-FDG are then phosphorylated by the enzyme hexokinase II (HK II), rendering glucose-6-phosphate and ^{18}F-FDG-6-phosphate (^{18}F-FDG-6-PO4) respectively. From this step on, the metabolism differs for both molecules: glycolysis continues for the glucose-6-phosphate molecule, resulting in the production of ATP (adenosine triphosphate) by the cell's mitochondria. In contrast, ^{18}F-FDG-6-PO4 cannot be further metabolized, because it lacks the hydroxyl group at the 2-position. The radioactive phosphorylated FDG molecule is now trapped in the cell, resulting in an imaging signal at that specific cell (Fig. 2.17). The biodistribution of the ^{18}F-FDG reaches a steady state condition in the brain about 30-45min after injection, enabling visualization of the glucose metabolism in a qualitative way (Games and Gambhir, 2012; Choi and Gruetter, 2012).

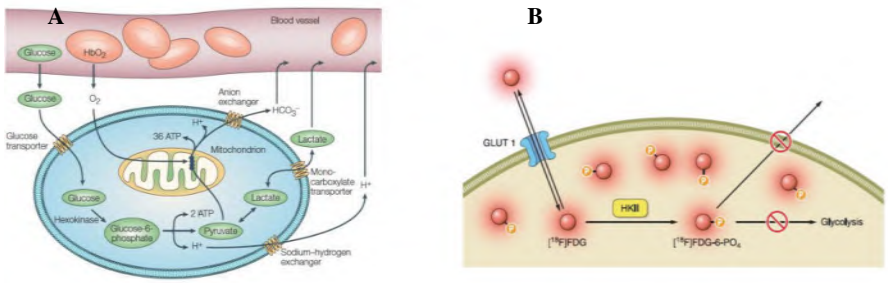

Figure 2.17: Metabolism process for glucose and ^{18}F-FDG: (A) Glucose is taken up from the blood stream to the cell with the help of glut proteins. It is then phosphorylated and further metabolized in order to produce ATP and thus energy for the cell (glycolysis). (B) ^{18}F-FDG undergoes the same first two steps (glut transport and phosphorylation by hexokinase), but is then trapped in the cell because it lacks the hydroxyl group at the 2-position for further metabolic progress. (Figure adopted from Games and Gambhir, 2012).

FDG-PET is widely used in clinical practice to visualize the glucose metabolism for diagnosis, assessment of disease severity, and evaluation of novel medical and (surgical) therapy in oncology and neurology.

2.2.3 Micro-PET

Since the advance in the wide range of small animal models of human disease in the mid 90's, PET has extended to small animal imaging (micro-PET). Considering the size difference between humans and rodents (75kg versus 200g), it is clear that a better spatial resolution is needed in order to obtain useful images. Whilst clinical PET systems are characterized by spatial resolutions in the order of 4 to 5mm, small animal PET has already reached values around 0.7-2mm (Boss et al, 2010; Palmowski et al., 2013; Kuntner and Stout, 2014). Over the past years, the spatial resolution of PET has been improved by the use of smaller scintillator crystals and spatial localization has been improved due to the combination of PET with CT. This improved spatial resolution can be achieved by decreasing the size of the scintillator detectors (Chatziioannou et al., 2001; Yang et al., 2004). On the downside, smaller scintillation crystals means less counts per crystal and thus a decreasing SNR (Kuntner and Stout, 2014). Not only the size of the crystals is important for the resulting sensitivity of the scanner, but also the type of material used, its packing fraction and the way in which the material covers the detector ring. Keeping in mind that a trade-off between sensitivity and spatial resolution has to be made, small animal PET has usually a lower sensitivity in comparison with clinical PET (±6% vs. ±9%), although this can be increased by enlarging the axial field of view (FOV) and decreasing the bore diameter (Kuntner and Stout, 2014; Saha et al., 2010). Moreover, new innovative micro-PET systems have become available with improved sensitivity up to 16% (SOFIEBiosciences).

The most extensive application of micro-PET imaging in small animal models is in the area of oncology (tumor detection and follow-up). Micro-PET is able to monitor molecular and cellular processes *in vivo*, and because repeated imaging of the same animals is possible, quantitative information about migration and expansion of tumours can be acquired over time.

A challenge specific for small animal imaging, is the need for animal immobilization during imaging. This can be accomplished by restraining devices, which unfortunately alter the metabolic rate of the animal and thus confound the result. The same holds for the use of anaesthetics, which show confounding effects on cardiovascular, respiratory and central nervous system. More recently, preclinical PET studies have been performed with tracer uptake in conscious condition by means of a carefully attached tail vein catheter.

2.2.4 DBS-PET applications

Over the past twenty years, PET imaging has been used in the domain of deep brain stimulation to investigate DBS-induced changes in the glucose metabolism nearby the electrode as well as in more distant brain regions (Klein et al., 2011). One of the main advantages of PET imaging in comparison to functional Magnetic Resonance Imaging (fMRI) for the investigation of DBS, is that the acquired images are not influenced by the presence of intracerebral metal as opposed to fMRI images. Even though fMRI studies make use of MR-compatible DBS-electrodes, the fMRI image will always be confounded by an artifact around the DBS-electrode (Lai et al., 2014). Moreover, with DBS-PET there are no risk for heating effects and electrical induction at the level of the electrodes, caused by gradient switching of RF pulses.
To investigate the effect of DBS on the glucose metabolism of the brain, the PET scan is usually run twice, namely, once at the baseline condition (i.e. no DBS) and once at the experimental condition (i.e with DBS). The difference between both conditions can then be determined,

resulting in the visualization of the brain structure(s) that are affected by the experimental condition.

2.2.4.1 Patient studies

Several DBS-related PET studies have been conducted in PD patients (Kalbe et al., 2009; Arai et al., 2008; Hilker et al., 2008; Karimi et al., 2008; Asanuma et al., 2006; Trost et al., 2006; Goerendt et al., 2006; Hershey et al., 2003; Thobois et al., 2002). However, the outcomes have not always been identical, probably due to methodological differences. STN-DBS has demonstrated correction of abnormal PD-related metabolic activity for motor networks, but not for cognitive networks (Eckert et al., 2007). More specifically, STN-DBS has shown reduced metabolism in the GPi and caudal midbrain (Trost et al., 2006); and appropriate recruitment of motor areas and widespread nonspecific reductions of compensatory or competing cortical activity (Grafton et al., 2006). Moreover, Haslinger et al. demonstrated that the STN-DBS-frequency was correlated to rCBF changes around the STN, and that frequency increases were correlated to motor cortex activity decreases (Haslinger et al., 2005).

In the field of epilepsy, FDG PET can be used to help identify the seizure onset zone. Ideally, PET imaging could be used to compare the cerebral metabolism during a seizure (i.e. ictal PET) with the subject's basal metabolism (i.e. interictal PET). However, ictal PET-scans usually reflect a mix of interictal, ictal and post-ictal metabolic activity because the ictal state is usually shorter than the FDG-uptake period of 30-45min. Therefore, the use of ictal PET is limited and only used in patients with frequent extratemporal seizures (Nooraine et al., 2013; Meltzer et al., 2000). More commonly, interictal PET is used in the presurgical evaluation of refractory TLE-patients, mainly to lateralize the epileptogenic focus, which presents as unilateral temporal hypometabolism. The observed focal interictal glucose hypometabolism is usually associated with the seizure focus. It is particularly useful in patients with a normal brain CT or MR scan or multi-focal MR scan. Yet, the hypometabolic area is typically larger than the ictal focus, reflecting the altered neuronal function in the ictal focus and possibly extending to the areas of first ictal spread. The mechanism explaining the hypometabolism in ictal areas is not yet fully understood. According to existing hypotheses the hypometabolism might reflect a protective inhibitory effect induced by repeated seizures on the brain or the underlying dysfunctional cortex (i.e. dysplasic areas, tubers…) (Kumar et al., 2012).
In contrast to PET, ictal SPECT is feasible and allows to assess the cerebral blood flow changes in the ictal state because the tracer reaches a steady state within 1 minute and the distribution remains almost unaltered until after the seizure. Interictal PET and ictal SPECT offer similar diagnostic sensitivity (Bouilleret et al., 2002; Hwang et al., 2001; Ho et al., 1995; Spencer, 1994) and serve as complementary tools in patients with inconclusive lateralization on ictal video-EEG monitoring and MR imaging (Siclari et al., 2013; Kim and Mountz, 2011; Won et al., 1999).

2.3 Optogenetics

Optogenetics is a new state-of-the-art technology that allows cell-type specific manipulation of neural circuits with unprecedented cellular, spatial and temporal specificity. For a better understanding of this complex and challenging technology, we will explain how optogenetics was discovered, its basic principles, and readout methods to investigate its effects. In addition, we will list some challenges and applications of the technique.

2.3.1 Short history

Optogenetics is a recent technique that was pioneered by Karl Deisseroth at Stanford University in early 2000. Optogenetics technology uses light to control neurons, which have been genetically modified to become responsive to light. The initial idea to control cell behavior using light can be traced back to the 1970s. Scientists realized that in order to understand how the brain works, there is a need for selective cell manipulation without affecting surrounding cells. However, this was highly challenging with the available techniques at that time, since microelectrodes could not differentiate between different cells within the targeted brain structure. Francis Crick was the first to bring up the idea of using light instead of electricity for selective manipulation (Crick, 1979). The first actual experiment that used light to activate neurons, was carried out by Fork, and later Yuste, in 1971. They demonstrated activation of neurons within intact tissue using laser light. However, this was not done in a genetically targeted manner. The earliest reported method, which used light to control genetically sensitized neurons, was performed by Miesenböck and Zemelman in 2002. They employed photoreceptors from the fruit fly for controlling neural activity in cultured mouse neurons (Zemelman et al., 2002). But although this was a breakthrough and a proof that light could be used to control neurons, the effectiveness of light in stimulating neurons was limited, and their protocol was hard to translate to other biological systems, preventing other neuroscientist from implementing this technique.

The real breakthrough of optogenetics came in 2005, when Deisseroth's laboratory published the first paper, showing the successful implementation of a microbial opsin, called channelrhodopsin-2 (ChR2), to activate mammalian neurons with blue light. ChR2 is a single-component light-activated ion channel from unicellular algae. Deisseroth's group figured out how to get these opsins safely into mammalian neurons in order to make these neurons responsive to light (Deisseroth et al., 2006 and Zhang et al., 2006). Since then, research using optogenetics technology has rocketed and hundreds of papers have been published, investigating several neurological and neuropsychiatric disorders (Gradinaru et al., 2009; Covington et al., 2010; Alilain et al., 2008; Kravitz et al., 2010, Witten et al., 2010; Busskamp et al., 2010; Tye et al., 2011). For instance, Kravitz et al. targeted two basal ganglia pathways in mice responsible for movement. By selective control of those pathways, they were able to induce or stop movement of the mice using only light. When they performed the same experiment in Parkinsonian mice, they found that activating the pathway that stimulates movement reestablishes normal movement in Parkinsonian mice (Kravitz et al., 2011). These experiments indicate great potential of optogenetics as a research tool to develop new and refine existing therapies, and to understand diseased brain functioning.

2.3.2 Optogenetics versus electrical stimulation

The use of optogenetics in neuroscience research has become extremely popular, mainly due to its increased specificity and speed compared to previous methods. It is far more specific than electrical stimulation and much faster than pharmacological intervention. In order to understand how the brain works, specific cells need to be controlled with a millisecond-scale precision in living tissue. In the past, fast control of neuronal activity was achieved with microelectrodes, *in vitro*, as well as *in vivo* in both animals and humans. However, the brain is complex and a single brain structure can contain many different types of neurons, through which microelectrodes cannot differentiate. Electrical stimulation therefore causes unwanted off-target effects in the surrounding tissue. In contrast, flashing light onto a brain area solely affects the cells that you have specifically targeted to express a light-sensitive protein. This means that researchers can now selectively trace the function of a certain group of neurons that is blent within other groups of neurons in the targeted brain structure, without confounding effects of those other neuron groups (Histed et al., 2009; Llewellyn et al., 2010).

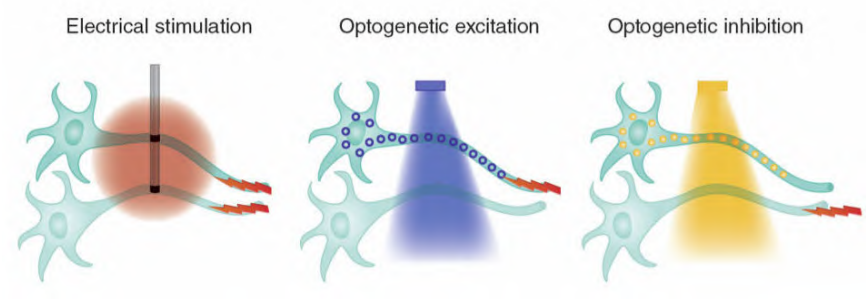

Figure 2.18: Targeted excitation (as with a blue light–activated channelrhodopsin) or inhibition (as with a yellow light– activated halorhodopsin), conferring cellular specificity and even projection specificity not feasible with electrodes while maintaining high temporal (action-potential scale) precision. (Figure modified from Deisseroth, 2011).

Because of its high temporal and spatial resolution, optical stimulation of cells is superior to classical activation by microelectrodes. This high temporal and spatial resolution that defines optogenetics can be achieved by using a combination of optics and genetics. Additionally the neuron group of interest can be excited or inhibited, depending on the light-sensitive protein and light that is used. Depending on the opsin used, a specific color of light enables excitation or inhibition of a specific group of neurons or non-neuronal cells (Fig. 2.18).

2.3.3 Basic principles

In order to control cell behavior with light, two questions need to be answered: (1) how to achieve selective *in vivo* control over a specific group of neurons? (2) how to measure the effects of such selective neuromodulation with a similar precision? In order to achieve this, a combination of techniques from genetics and optics is used.

The entire process of optogenetics includes five steps: (1) creation of a gene construct; (2) insertion of the gene construct into a virus; (3) insertion of the virus deep into organisms as complex as mammals; (4) insertion of the optical fiber (or optrode, i.e. optical fiber plus electrode) and fiber-optic cable; (5) administration of light with a specific wavelength to the cells of interest, which causes the ion channels of those specific neurons to open (Yizhar et al.,

2011). Each of the steps are visualized in Fig. 2.19. The genes for light-activated ion channels are introduced to a population of cells by a human engineered virus. The cells that express these light-sensitive channels depends on the promoter region of the inserted DNA sequence. Cells which contain a promoter that can recognize the promoter sequence will express these channels while cells that lack a promoter specific for the sequence will not. Once the genes have been inserted, it can take 1-3 weeks for them to be fully expressed. An optic fiber is surgically inserted near the brain area of interest and attached to the top of the skull. After, a fiber-optic cable is connected to the optic fiber, so light can be sent to control the neurons.

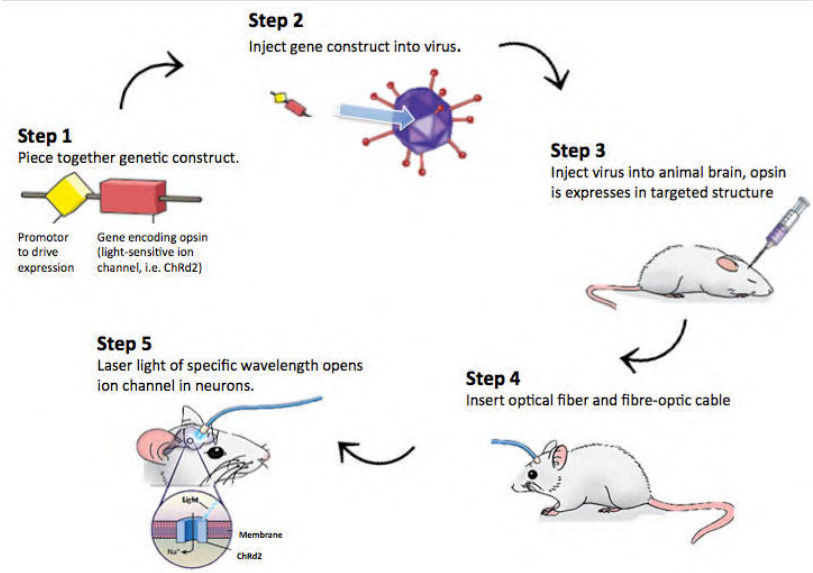

Figure 2.19: Five steps to optogenetics: (1) creation of a gene construct; (2) insertion of the gene construct into a virus; (3) insertion of the virus deep into the mammalian brain; (4) insertion of the optical fiber; (5) administration of light with a specific wavelength to the cells of interest. (Figure modified from Yizhar et al., 2011).

Optogenetics makes use of optogenetic actuators, such as microbial rhodopsins, for spatially-precise neuronal control; and temporally-precise readouts (Yizhar et al., 2011). Both are explained in the next paragraphs.

2.3.4 Microbial rhodopsins

The major optical stimulation approach is the activation of light-sensitive proteins (such as rhodopsins) using light, which then excite the cells that express the opsin in their membrane. The discovery of ChR2 from the unicellar alga (i.e. Chlamydomonas reinhardtii) was the starting point for the optogenetic approach by enabling the activation of mammalian cells using blue light (λmax 470nm) (Nagel et al., 2003; Zhang et al., 2008). More recently, the discovery of halorhodopsin (NpHR) from the archea Natronomonas pharaonis, enables inhibition of neural activity with yellow light (λmax 580nm) (Matsuno-Yagi and Mukohata, 1977; Lanyi and Oesterhelt, 1982). The light-sensitive ion channels, called ChR2, activate the cells with blue light by depolarization, whereas the light-driven ion pumps, called NpHR, inactivate the cells with yellow light by hyperpolarization of the cells (Fig. 2.20). Together, these proteins form an ideal pair for the activation and inhibition of neural cells (at two different wavelengths). Because ChR2 and NpHR and their variants can be easily expressed in neural cells or used to form transgenic animals, these microbial rhodopsins have now become very popular tools within neurobiological research.

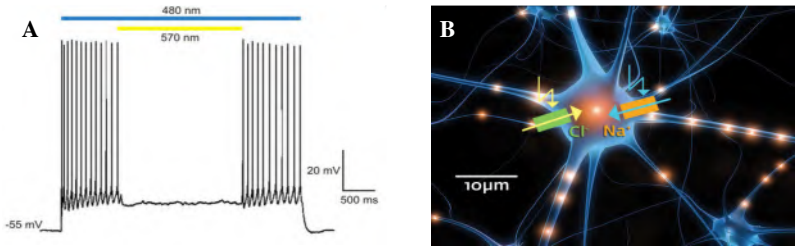

Figure 2.20: (A) Schematic representation of the action of channelrhodopsin2 and halorhodopsin on neural cells. (B) Triggering of spikes by channelrhodopsin-2 (blue light) and their repression by halorhodopsin (yellow light) in cultivated hippocampal cells (© MPI of Biophysics).

Yet a major limit to the utility of optogenetic inhibition using NpHR is the limited addressable quantity of neural tissue. Very recently, next-generation inhibitory opsins have become available such as the chloride-conducting channelrhodopsins iC++ and ArchT3.0. Currently, iC++ and ArchT3.0 have successfully inhibited volumes of approximately one cubic millimeter. ArchT is a light-driven proton pumps found in archaebacteria that provides silencing via a hyperpolarizing current in response to 566 nm light. A comparison study performed by Deisseroth's lab has shown that archeorhodopsins seem to perform slightly better than the best available halorhodopsin mutant. In particular ArchT3.0 (an enhanced version of ArchT) generates about twice as much photocurrent and a exhibits slightly faster kinetics than NpHR3.0. In addition, it was demonstrated that brief episodes of NpHR3.0 activation tend to increase the probability of spiking in response to a stream of presynaptic action potentials, while Arch activation did not (Mattis et al., 2012).

2.3.5 Readout methods

As important as establishing optogenetic control of neural activity is, is the monitoring of the effects of the manipulated cellular activity. The monitoring method chosen depends on the experimental goals. The most common readout methods include behavioral testing, electrophysiological recordings, calcium imaging, and more recently also fMRI. They are shortly reviewed below.

2.3.5.1 Behavioral testing

The development of lightweight and flexible fiber-optic neural interfaces enabled the assessment of complex behaviors in freely moving mammals, including worms, flies, fish and mammals (Adamantidis et al., 2007; Aravanis et al., 2007; Gradinaru et al., 2009; Witten et al., 2010; Tye et al., 2011).

2.3.5.2 Electrophysiological recordings

In contrast to electrical stimulation, optogenetic stimulation allows simultaneous electrical recording of neural activity without confounding artifacts associated with electrical stimulation. The extracellular unit recordings are easily integrated within the optogenetics technology. The integration of the optical fiber and electrode into a single component is called "optrode" (Gradinaru et al., 2009). Alternative to the regular fusion approach of the optical fiber and the microelectrode, coaxial integrated multi-electrode devices (Zhang et al., 2009a, Zhang et al., 2009b), or silicon probes are used (Royer et al., 2010).

2.3.5.3 Calcium imaging

The combination of using simultaneous calcium imaging and optogenetic stimulation enables cell-type-specific readout of cell-type-specific control (by optogenetic stimulation) (Zhang et al., 2010; Airan et al., 2009; Dreosti et al., 2009; Dreosti and Lagnado, 2011, Lundby et al., 2010; Tian et al., 2009). Calcium imaging allows to optically probe intracellular calcium, by using calcium indicators, which are fluorescent molecules that respond to the binding of calcium ions by changing their fluorescence properties. *In vivo* calcium imaging can be achieved by using mini epi-fluorescent microscopes that are equipped with microendoscopes, or two-photon microscopy in the freely moving or fixed rodent respectively.

2.3.5.4 Functional Magnetic Resonance Imaging

In 2010, Lee and colleagues combined optogenetics with fMRI for the first time, and called it 'opto-fMRI'. They used the technique to validate that increased activity in local excitatory neurons causes an increase in the local BOLD signal, and showed that opto-fMRI could be used to visualize the effects of precise optogenetic manipulations throughout the entire brain (Lee et al., 2010; Leopold, 2010; Desai et al., 2011; Li et al., 2011). Using opto-fMRI, Lee et al. provided the first direct evidence that the fMRI signal is in fact closely related to neural activity, as opposed to simply correlated with (Lee et al., 2010). Lee et al. also stated in that paper that "unidirectional stimulation of downstream structures, eliminating the antidromic drive from which electrical stimulation suffers, also shows a distinct and robust BOLD response enabling macro-circuit mapping of the brain" (Lee et al., 2010). Therefore, the most significant value of opto-fMRI will be as a research tool for mapping the global effect of defined cells throughout the entire brain, and potentially identifying disease-related or therapy-related circuit modulations, in a very specific way. This degree of specificity was not feasible earlier with the use of microelectrodes. With optogenetics specific local cells can be directly accessed using global fMRI signal mapping. Or alternatively, when targeting specific axons, the effect of specific distant cells can be assessed. Thus, downstream activation of other circuits or brain structures is a resultant from the output of the targeted cells only, and not due to off-target effects from which electrical stimulation suffers.

2.3.6 Challenges

As with any new technology, many improvements are necessary in each step of the optogenetics protocol, i.e. transfections methods, opsins and light source. These technical challenges are shortly reviewed below.

2.3.6.1 Transfection methods

Transfection methods are focused on the construction of vectors and promoters for cell specific expression of the microbial rhodopsins. There is enormous variety of constructs, which have to be tested by time consuming screening, presenting a major challenge. As carriers for gene transfer one can chose between different viruses or transgenic animal models. The virus approach is quick and efficient, whereas the construction of transgenic animals (rodents, fruitflies, zebrafish and C. elegans) are time consuming but have been proven to be ideal for a variety of different experiments in basic research. Most commonly, viral transduction is

preferred to introduce the promoter-opsin construct. However, there's only a limited, small amount of genetic info that can be packaged in viral vectors, although some can contain more than others (e.g. lentivirus (LV) can store more than adeno-associated virus (AAV)) (Yizhar et al., 2011).

2.3.6.2 Opsins

LV and AAV are particularly useful for optogenetics because they are characterized by a high multiplicity or opsin expression level so they are able to provide the high number of opsin genes that are required to ensure robust *in vivo* optogenetic responses. On average, LVs yield a lower expression and diffusion rate, and higher immunogenic potential, compared to AAVs (Yizhar et al., 2011). Besides the opsin expression level, a good light sensitivity is necessary for effective *in vivo* experiments. Despite the well-established use of ChR2 and NpHR, their transmittance is rather low. Some mutations can cause longer channel-opening times, ranging from seconds to minutes, resulting in an improved light sensitivity.

Additionally, transgenic rodent models were developed for applications that require inhibition of neural activity. For example, by using the Cre/loxP system, limitations imposed by the weakness of a promoter can be circumvented (Kuhlman and Huang, 2008, Zhang et al., 2008, Atasoy et al., 2008; Sohal et al., 2009).

Finally, an important group of neurons are the fast-spiking inhibitory interneurons (i.e. parvalbumin neurons), which are responsible for the interneuronal communication and are involved in complex cognitive processes (Freund, 2003). It has to be noted that ChR2-based activation of these fast-spiking neurons is not accurate at frequencies higher than 40Hz. ChETA-based (i.e. a channelrhodopsin mutated with E123) activation has demonstrated very accurate spike detection up to 200Hz in vitro. Moreover, the most recent opsin providing ultra-fast optogenetic control is chronos, which is developed by Boyden's lab. Chronos is a blue- and green-light drivable channelrhodopsin with kinetics faster than any previous channelrhodopsin and it appears to work better *in vivo* than ChETA (Klapoetke et al., 2014).

2.3.6.3 Light source

Arrays of micro light pipes are sufficient for light stimulation of cortical brain structures or within the brain if only a submillimeter scale is needed. For subcortical optogenetic stimulation of tiny brain structures, a high spatial resolution in the micrometer range is required. This can be achieved by using light emission diodes (LED´s) or lasers due to their inherent higher transmittance (Yizhar et al., 2011).

2.3.7 Applications

Optogenetics has demonstrated great potential for basic research, because it allows for neuronal excitation and silencing with high spatial and temporal precision in a reversible manner, using just light. Additionally, the microbial rhodopsins appear harmless in the mammalian brain. This paragraph provides a short overview about its most important current preclinical applications and its clinical potential.

2.3.7.1 Preclinical applications

Brain network mapping - Optogenetics provides new opportunities to analyze neural circuitry, since it has the ability to investigate functionally connected, but anatomically downstream brain structures to the targeted brain structure (Petreanu et al., 2009). Simultaneous recording of electrical activity of neurons in anatomically distant areas during light stimulation of neurons in a targeted area would reveal whether the recorded neurons are functionally connected downstream to the stimulated neurons, or whether they share the same neural circuit. For example, Douglas et al. demonstrated that stimulation of a single neuron can trigger the downstream circuit responsible for escape behavior in zebrafish (Douglas et al., 2008). Zhang and Oertner demonstrated that optogenetics can induce long-term potentiation of orthodromic connections in the hippocampal CA1 area. Additionally, results are obtained on the movement of whisker of rodents, on the olfactory system where light replaces the ligands, and on the movement of animals after light stimulation of the motor cortex (Tye and Deisseroth, 2012, Huber et al., 2008, Nagel et al., 2005). Together, these studies have shown the potential of optogenetics to examine *in vivo* neural circuitry. Moreover, the use of opto-fMRI has shown great potential for global brain mapping of precise optogenetic manipulations (Lee et al., 2010; Leopold, 2010; Desai et al., 2011; Li et al., 2011).

Deep brain stimulation - Preclinical DBS studies allow for the experimental introduction of optogenetic tools, which provide superior neural circuit stimulation specificity compared to electrical stimulation (Fiala et al., 2010; Yizhar et al., 2011). The geometry of DBS-electrodes allows a precision of about one millimeter only. Consequently, electrical DBS also recruits nonreciprocal afferent inputs (via antidromic signal propagation), as well as neighboring fibers of passage. In contrast, optogenetic stimulation generally only recruits the opsin-expressing cells and their efferent outputs. Because of this added specificity for neural modulation, optogenetic tools have been employed to inform potential circuit mechanisms of DBS therapy in preclinical models (Creed et al., 2015; Gradinaru et al, 2009).

2.3.7.2 Clinical applications

Optogenetics has potential for future direct clinical applications. In the future, gene therapy using optogenetics appears to be possible. The transduction of cells in the human retina to replace missing retinal enzymes via adeno-associated virus (AAV) has been performed successfully on the human eye to cure a rare eye disease called Lebers Congenital Amaurosis (Maguire et al, 2009). This means that when integrating microbial rhodopsins within AAV's that they could be used for gene therapy to treat retinal diseases or Parkinson's disease (Gradinaru et al., 2009) or epilepsy (Tønnesen et al., 2009). Additionally, Zhang et al. demonstrated that opsin expression in mammalian systems lasts up to one year (Zhang et al., 2006). However, for clinical purposes this has to be extended to longer timescales, and mammalian systems are different from human systems, so the foreign opsin proteins that seem harmless in animal studies, might harm humans. Finally, there are some ethical issues related to the direct control of human behavior.

There is also substantial interest and discussion related to the future use of optogenetics as an alternative treatment for DBS (LaLumiere, 2011). The rationale for this discussion relates to the presumptive ability of optogenetic stimulation to achieve therapeutic efficacy with a reduced side-effect profile from 'off-target' circuit recruitment. The enhanced specificity of optogenetics

allows to distinguish between different substructures. For example, within the investigation of TLE, with electrical stimulation one can only distinguish between the dorsal and ventral hippocampus at the most. In contrast, with optogenetic stimulation one can distinguish between the different hippocampal substructures, and between the different neuron groups within a substructure, consequently, resulting in a deeper understanding of the cause of TLE. With respect to PD similar arguments would hold. On the other end, it is widely hypothesized that DBS exerts its therapeutic effects via large-scale network modulation (van Westen et al., 2015; Deniau et al., 2010), little is known regarding the extent to which optogenetic stimulation mirrors the circuit-level responses achieved with electrical DBS.

In conclusion, optogenetics might not lead to immediate direct clinical implementations as a treatment. But, the use of optogenetics as a research tool to investigate healthy and diseased brain circuitry or to optimize existing treatment has demonstrated potential by many laboratories. Optogenetics offers great opportunities for basic neuroscience research, and is especially helpful in defining and describing the disruption of global circuit wiring of the brain in neurological disorders such as PD and epilepsy. Consequently the use of optogenetics as a research tool might have an important indirect clinical impact. Although optogenetics is not an answer to every neuroscience problem and should be used only after critical assessment of the research problem and consideration of other available research tools, optogenetics represents a powerful new technique within the available assortment of research strategies.

Part II

Parkinson's disease:
Circuit mapping of Two DBS targets

Chapter 3

Functional Circuit Mapping of Two Striatal Output Nuclei using DBS-fMRI

3.1 Introduction

The striatum represents the major input nucleus of the basal ganglia, critical for the processing and regulation of motor, cognitive, and limbic functions. Striatal output pathways within the basal ganglia are classified as "direct" or "indirect", based on neurochemical phenotype and axonal projection patterns. More specifically, direct pathway striatal neurons express the D1 dopamine receptor and project to the substantia nigra pars reticulata (SNr) and/or internal globus pallidus (GPi), whereas indirect pathway striatal neurons express the D2 dopamine receptor and innervate the external globus pallidus (GPe). Both the direct and indirect pathways ultimately converge upon thalamocortical relays, either through direct innervation (SNr/GPi), or polysynaptic routes (GPe). According to long-upheld models of the basal ganglia, these pathways are functionally antagonistic; the direct pathway recruits thalamocortical circuits and the indirect pathway suppresses them (Albin et al., 1989; DeLong, 1990).

In recent years, this relatively simplistic framework of direct/indirect pathway function has come under increasing scrutiny (Calabresi et al., 2014; Cui et al., 2013; Friend and Kravitz, 2014; Gittis et al., 2014; Goldberg et al., 2013; Jahfari et al., 2011; Tecuapetla et al., 2014). Although evidence continues to support the notion of functional antagonism between these pathways (Freeze et al., 2013; Kravitz et al., 2010; Schmidt et al., 2013), additional anatomical and functional studies have identified unanticipated circuit connectivity in both the SNr and GPe (among other basal ganglia nuclei). Recent examples in the GPe include the identification of a pallidocortical projection that entirely bypasses thalamic relays to modulate frontal cortex (Chen et al., 2015; Saunders et al., 2015), as well as pallidostriatal innervation by so-called "arkypallidal" GPe neurons (Abdi et al., 2015; Mallet et al., 2012). The SNr, generally conceptualized as an inhibitory nucleus, contains a subset of glutamatergic neurons recently mapped to innervate and excite the reticular thalamus, a higher-order non-relay region (Dunn et al., 2009). The functional roles of these novel circuit elements are likely complex and not easily predicted.

Functional Magnetic Resonance Imaging (fMRI) is a powerful tool to study neural circuit modulation on a global scale. When combined with neural stimulation approaches such as Deep Brain Stimulation (DBS), fMRI allows for the relatively unbiased identification of brain areas functionally interconnected with the stimulation target (Ross et al., 2016; Van Den Berge et al., 2015; Younce et al., 2014; Albaugh and Shih, 2014; Lai et al., 2014; Shih et al., 2013a; Knight et al., 2013; Lee et al., 2010; Canals et al., 2009; Dunn et al., 2009; Shyu et al., 2004). In addition to identifying putatively connected areas, DBS-fMRI may also shed light on the directionality of these circuit relationships (based on whether the hemodynamic change is positive or negative). Importantly, both the recruitment of select circuits, as well as the directionality of their fMRI responses, may be strongly contingent upon stimulation frequency. For example, low frequency (10Hz) electrical stimulation of the ventrolateral thalamus in pigs generated a positive blood-oxygen-level-dependent (BOLD) response in the motor cortex, whereas high frequency (130Hz) stimulation evoked a negative BOLD response in the same region. Thus, in varying stimulation parameters, DBS-fMRI can shed light on the tuning properties of functionally connected circuits.

The SNr and GPe represent the major striatal output nuclei of the rat direct and indirect pathways, respectively. In addition, both structures are currently being explored as potential non-canonical DBS targets for diverse neurological disorders (e.g. Parkinson's disease, Huntington's disease, epilepsy) (Chastan et al., 2009; Ligot et al., 2011; Piedimonte et al., 2013; Shi et al., 2006; Sutton et al., 2013; Temel et al., 2006; Velisek et al., 2002; Vitek et al., 2012; Weiss et al., 2013; Wille et al., 2011). However, more research is necessary to explore functional circuitry of these striatal output nuclei (Calabresi et al., 2014; Cui et al., 2013; Friend and Kravitz, 2014; Gittis et al., 2014; Tecuapetla et al., 2014). Therefore, in the present study, we employed simultaneous DBS-fMRI in the healthy rat to map the functional circuit connectivity of the SNr and GPe. More specifically, we chose to perform fMRI with cerebral blood flow (CBV) measurements, instead of the most commonly used BOLD measurements. Previous CBV fMRI studies have demonstrated a higher signal-to-noise ratio than traditional BOLD fMRI imaging (Kim et al., 2013; Zhao et al., 2009; Silva et al., 2007; Keilholz et al., 2006; Wu et al., 2003). In addition, we acquired both stimulus-evoked fMRI and functional connectivity MRI (fcMRI) data. In this way, DBS-sensitive circuit activity and connectivity changes on a whole-brain scale can be visualized.

Evoked-fMRI revealed CBV modulation by SNr- or GPe-DBS in a diverse complement of both overlapping and distinct brain regions, including convergent and unexpected CBV decreases within striatum, and GPe-DBS-evoked positive modulation of frontal cortex. Functional connectivity was preferentially modulated in the hemisphere ipsilateral to SNr or GPe-DBS, and readily reversed following cessation of stimulation. Notably, both circuit and network modulation by DBS at both targets was sensitive to stimulation frequency.

3.2 Materials & Methods

3.2.1 Animals

Thirteen adult male Sprague-Dawley rats (300–500g body weight; Charles River Laboratories, Wilmington, MA, USA) were used in this study. All procedures were performed in accordance with the National Institutes of Health Guidelines for Animal Research (Guide for the Care and

Use of Laboratory Animals) and approved by the University of North Carolina Institutional Animal Care and Use Committee. Animals were housed under environmentally-controlled conditions (12h normal light/dark cycles, 20-23°C and 40-60% relative humidity), with food and water provided *ad libitum*.

3.2.2 Surgery

Rats were anesthetized using nosecone-supplied isoflurane (1.5-2%), and headfixed within a stereotaxic frame (Model 962, Kopf Instruments, Tujunga, CA, USA). Following head shaving and exposure of the skull, four small burr holes were drilled: three for the positioning of MR-compatible miniature brass screws (Item #94070A031, McMaster Carr, Atlanta, GA, USA) and one for the insertion of a bipolar DBS electrode. Each electrode was custom-made using two-channel tungsten microelectrodes (A-M Systems, WA, USA.), with a 50μm diameter (single lead), as previously described (Lai et al., 2015). These electrodes were fully insulated with polyimide except at the tips, and the leads were adhered for direct contact using a saturated sucrose solution. The *in vitro* impedance of these electrodes was previously measured as 18-22 kΩ (Lai et al., 2015).

Electrodes were implanted targeting either the right SNr (n=6) or GPe (n=7). Stereotactic implantation coordinates were generated using a standard rat brain atlas (Paxinos and Watson, 2007) and are described as follows, in reference to bregma (anteroposterior, AP; mediolateral, ML) and cortical surface (dorsoventral, DV): SNr (AP -5.5mm, ML +2.2mm, DV -7.7mm); GPe (AP -0.96mm, ML +2.8mm, DV -5.8mm). Following electrode implantation, the placement was sealed using dental acrylic and the wound site was further protected with surgical sutures. A post-surgical recovery period of at least 24 hours was given prior to fMRI acquisition for each subject.

3.2.3 Data acquisition

In preparation for fMRI procedures, rats were endotracheally intubated and mechanically ventilated using a small animal ventilator (CWE Inc., SAR-830/PA, Ardmore, PA). Anesthesia was initially maintained under constant isoflurane (1.5-2%) mixed with medical air. Tail vein catheterization was then performed for intravenous drug and contrast agent injections. Immediately following intubation and tail vein catheterization, animals were placed within a head-holder, and harnessed to a small animal cradle (both plastic and custom-made). The cradle was lined with a circulating water blanket connected to a temperature-adjustable water bath located outside the scanner room (Thermo Scientific, Waltham, MA). A rectal probe was used and core body temperature was maintained at 37±0.5°C. Mechanical ventilation volume and rate were adjusted to maintain $EtCO_2$ of 2.8-3.2% and SpO_2 above 96%, using capnometry (Surgivet, Smith Medical, Waukesha, WI) and pulse oximetry (MouseOx Plus, STARR Life Science Corp., Oakmont, PA). $EtCO_2$ values from the capnometry system were previously calibrated against invasive sampling of arterial blood gas, reflecting a pCO_2 level of 30–40 mm Hg (Shih et al., 2012; Shih et al., 2013b).

MR images were acquired on a 9.4T Bruker BioSpec system with a BGA-9S gradient insert (Bruker Corp., Billerica, MA). A homemade single-loop surface coil with an internal diameter of 1.6cm, placed directly over the head, was used as a transceiver. Toothpaste was applied within the open coil loop to minimize MR susceptibility artifacts at the air-tissue interface. The set-up of the coil and DBS electrode is shown in Fig. 3.1A.

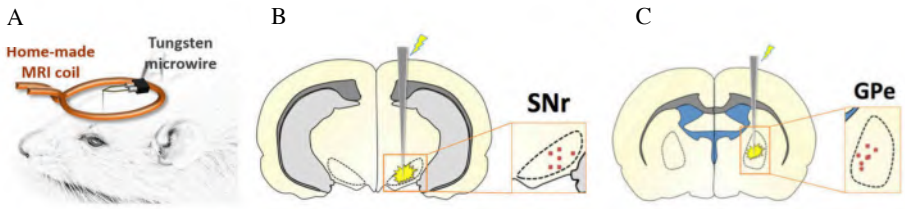

Figure 3.1: Experimetal set-up: (A) Schematic of experimental setup with homemade surface loop coil and tungsten microwire DBS electrode. (B) Electrode tip mapping to the SNr (n=6) and GPe (n=7) for all subjects. Tip placements were estimated using T_2-weighted anatomical scans, which we deemed satisfactory given the relatively large size (including anteroposterior distance) of our targets, as well as the minimal electrode artifact.

Magnetic field homogeneity was optimized first by global shim and followed by local first-order shims, and when necessary, local second-order shims using the FASTMAP protocol. For anatomical referencing, a T_2-weighted RARE pilot image was taken in the mid-sagittal plane to localize the anterior commissure; this structure is located at approximately 0.8mm posterior to the bregma and served as a reference for anteroposterior slice positioning in subsequent anatomical and functional scans. T_2-weighted anatomical images were obtained using a RARE sequence (scan parameters: TR = 2500ms, TE = 33ms, RARE factor = 8, slice thickness = 1mm, matrix size= 256x256, FOV= 2.56x2.56cm^2). Twelve axial slices were acquired, with the 5th slice from the anterior direction aligned with the anterior commissure (as acquired in the previous T_2-weighted pilot scan). The reduced electrode artifact (Fig. 3.2), together with standardized slice positioning, rendered these images sufficient to localize the electrode tip placement, as previously described (Lai et al., 2015; Lai et al., 2014). Electrode placement within the SNr or GPe was confirmed for each rat before including it to this study (Fig. 3.1B/C).

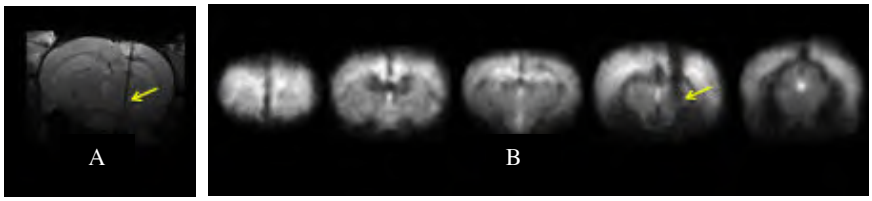

Figure 3.2: Representation of the electrode artifact on (A) an axial slice of an anatomical MR-image at height of the electrode (SNr), and on (B) five axial slices of a functional MR-image (SNr, same rat as in (A)). The electrode artifact is indicated with a yellow arrow.

Following setup processes and immediately prior to CBV fMRI scan acquisition, rats were administered a monocrystalline iron oxide contrast agent (MION; Feraheme; 30mg Fe/kg, i.v.). MION-based CBV measurements provide a well-established fMRI tool with a higher signal-to-noise ratio than traditional BOLD contrast imaging (Kim et al., 2013; Zhao et al., 2009; Silva et al., 2007; Keilholz et al., 2006; Wu et al., 2003). Subsequently, anesthesia was switched to dexmedetomidine (dexdomitor; 0.05mg/ml/hr, i.v.) cocktailed with the paralytic agent pancuronium bromide (0.5mg/ml/hr, i.v.). This cocktail was administered for the remaining scan duration, continuously supplemented by 0.5% isoflurane (Fukuda et al., 2013).

CBV fMRI scans were acquired using a multi-slice single-shot gradient echo echo-planar imaging sequence (GE-EPI) (scan parameters: TR= 1000ms, TE= 8.107ms, slice thickness= 1mm, matrix size= 80x80 (reconstructed to 128x128), FOV= 2.56x2.56cm^2 and voxel size = 0.312x0.312x1mm^3). Image slice geometry was imported from the previously acquired T_2-weighted anatomical image (12 slices).

3.2.4 Deep brain stimulation

Stimulation was applied in the same manner for all subjects, with bipolar and uniformly distributed unilateral stimulation of the SNr or GPe, with bipolar and uniformly distributed unilateral stimulation of the SNr or GPe. Each stimulation period consisted of a series of TTL-triggered biphasic, charge-balanced square-wave pulses with a pulse width of 500μs and a stimulation intensity of 300 μA. A 90 second block design paradigm was implemented, consisting of a 20 second baseline period (stimulation OFF) followed by 10 seconds of stimulation ON, and an additional 60 seconds of rest (stimulation OFF). An additional rest period of at least two minutes was given between each DBS scan to allow for neurovascular recovery. Stimulation frequencies were varied in a pseudo-randomized order (10, 40, 70, 130, 200 and 400 Hz), and each DBS frequency scan was repeated 5 times per rat for within-subject/session averaging (see section 3.2.5.1).

Immediately following evoked-fMRI scan acquisition, fcMRI scans were conducted in each subject. These scan series consisted of five, 5 minute scans during which either no stimulation or continuous DBS was applied (OFF and ON, respectively; ON consisted of stimulation of 300μA, 500μs pulse width, varied frequency). The fcMRI scans were conducted in succession without rest periods in the following order: OFF, ON (40Hz), OFF, ON (130Hz), OFF.

3.2.5 Data-analysis

3.2.5.1 Evoked fMRI

Preprocessing and image analysis was performed using SPM codes and custom-written Matlab (MathWorks Inc., Natick, MA) similar to our previous DBS-fMRI studies (Lai et al., 2015; Lai et al., 2014; Younce et al., 2014). First, evoked-fMRI data were grouped by subject and DBS frequency, and realigned to the first volume of a well-positioned subject using a least squares approach and a 6 parameter rigid body spatial transformation. Secondly, the datasets were skull-stripped using a semi-automatic threshold method with manual masking. Thirdly, the datasets were coregistered to an anatomical MRI rat atlas (Valdes-Hernandez et al., 2011). Finally, datasets were grand-averaged across subjects by stimulation frequency for generation of the mean response maps. Note that we used only 5 SNr-DBS subjects for the analysis of the evoked fMRI data and 6 SNr-DBS subjects for the analysis of the functional connectivity data. We decided to discard one subject in the SNr-DBS group due to poor image quality of the evoked fMRI datasets, probably caused by movement.

Functional response maps for averaged SNr- or GPe-DBS datasets (SNr: n=5, GPe: n=7) were generated using the general linear model (GLM), with reference to baseline (frames 1-20). Additionally, a hemodynamic delay of 5s was applied according to the ROI-based time-courses analysis results. A Bonferroni correction was applied to adjust for the multiple comparisons of fMRI maps by the number of brain voxels (corrected $p<0.05$ for positive and negative responses). All images were smoothed by applying a mean filter with a 3×3 kernel, and overlaid on an anatomical atlas for visualization (Valdes-Hernandez et al., 2011).
For temporal analysis of DBS-evoked CBV changes, 3-dimensional regions of interest (ROIs) were defined *a priori* according to anatomical structural boundaries (Paxinos and Watson, 2007; Valdes-Hernandez et al., 2011), and applied onto the coregistered data. The ROIs were chosen according to the anatomical areas showing statistically significant modulation in the functional response maps. Nineteen ROIs were identified for analysis, all ipsilateral to the DBS target

unless otherwise noted: cingulate cortex, dorsolateral striatum (ipsi- and contralateral), dorsomedial striatum (ipsi- and contralateral), GPe, infralimbic cortex, motor cortex, nucleus accumbens, orbitofrontal cortex, pedunculopontine tegmental nucleus, posterior hypothalamus, prelimbic cortex, SNr, somatosensory cortex, superior colliculus, ventral tegmental area, ventrolateral thalamus, and zona incerta. The baseline ΔR2* value was calculated as follows:

$$\text{Baseline } \Delta R2^* = -1/TE \ln (S_{prestim}/S_0),$$

where $S_{prestim}$ and S_0 are the MR signal intensities after and before Feraheme injection, respectively. The stimulus-evoked ΔR2* value (after Feraheme injection) was calculated as follows:

$$\Delta R2^* = -1/TE \ln (S_{stim}/S_{prestim}),$$

where S_{stim} and $S_{prestim}$ are the MR signal intensities during stimulation and before stimulation, respectively. CBV changes were calculated by dividing stimulus-evoked ΔR2* by baseline ΔR2* values. For each ROI, the CBV signal time-course was plotted across all 90 volumes (i.e. repetitions or time frames).

DBS-evoked changes in CBV amplitude were also compared across stimulation frequencies and ROIs. Stimulus-evoked CBV responses were averaged across the stimulation period (frames 21-30) for each DBS frequency and ROI. These data are presented as mean ± standard error of the mean (SEM). Statistical comparisons of DBS frequency effects on ΔCBV for each ROI were conducted using Graphpad Prism software (San Diego, CA). Two-tailed, one-way ANOVA tests were conducted, and when statistically significant ($p \leq 0.05$), Tukey post-hoc analyses were employed.

3.2.5.2 Functional connectivity MRI

Functional scans were preprocessed using the Analysis of Functional NeuroImages software suite (AFNI v2011-12-21-1014). The workflow included discarding the first 20 volumes (of each fcMRI-scan), slice-timing correction, motion correction, alignment to a pre-existing high-resolution T_2-weighted template, spatial smoothing (Gaussian kernel FWHM = 1.5mm), band-pass filtering (0.001– 0.5Hz), and regression of whole brain signal and the six motion parameters. The number of volumes discarded was increased from the traditional number (approximately 3-10) in order to ensure DBS-related changes from the initial stimulation were minimized. Furthermore, warping in the alignment procedure was limited to shifts and rotations to avoid unnecessary shearing and scaling of brain regions with signal drop-out associated with the DBS electrode.

Statistical fcMRI analysis was conducted using the temporal correlation method. Fisher-Z transformed correlation matrices were generated using the average functional time series extracted for each region-of-interest (ROI) in the template atlas. Ipsilateral and contralateral hemispheres ROIs were analyzed separately yielding correlation matrices detailing mean within and between hemisphere connectivity (SNr: n=6, GPe: n=7). Individual connections were further evaluated across animals using repeated measures ANOVA models and categorized based on direction of effect. For each significant pairwise connection (rANOVA $p<0.01$) a basic correlation analysis was carried using a tent function and the resulting sign was used to categorize connections as either enhanced (increased correlation) or suppressed (increased anti-

correlation). Pair-wise connections with weak modulation ($|\Delta_{Z\text{-}corr.}|<0.10$) were ignored. Finally, connections were grouped based on network classifications (sensorimotor, executive, limbic, and between network connections).

3.3 Results

3.3.1 Evoked fMRI

Both SNr- and GPe-DBS produced significant and frequency-dependent CBV responses in several brain structures both within and outside the basal ganglia circuit. Averaged response maps to 40 and 130Hz DBS are shown in Fig. 3.3A and Fig. 3.3B for SNr and GPe subjects, respectively. Four additional DBS-frequencies are displayed in Supplementary Fig. 3.2A/B for both groups. Supplementary Fig. 3.1 displays activation of 130Hz SNr-DBS on EPI. All supplementary figures mentioned in this chapter are included in paragraph 3.7 at the end of this chapter. In addition to generating functional response maps, CBV timecourses for each DBS target and stimulation frequency were calculated for anatomical 19 ROIs (Fig. 3.4 and Supplementary Fig. 3.3-4).

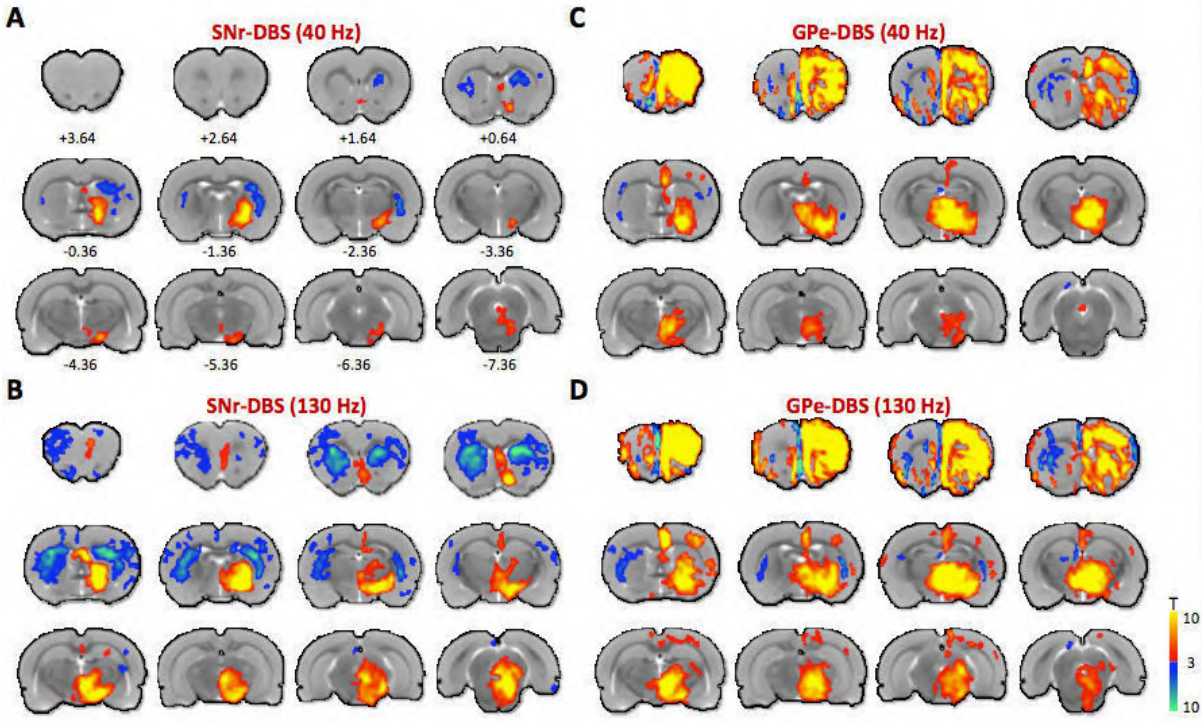

Figure 3.3: Functional activation maps of CBV modulation by SNr- and GPe-DBS. Two DBS stimulation frequencies are shown for each target: SNr- DBS at 40 or 130Hz (A and B, respectively), GPe-DBS at 40 or 130Hz (C and D, respectively). Notable observations include CBV decreases in the striatum at both targets, as well as large, ipsilateral frontal cortical modulation by GPe-DBS. At both targets, stimulation responses were largely ipsilateral and stronger at 130Hz compared to 40Hz. 12 slices were acquired in each scan, with numbers below slices denoting relative distance from bregma (in mm). Color bar denotes t score values obtained by GLM analyses, with a significance threshold of $p<0.05$. Functional activation maps for all additional tested frequencies are located in Supplementary Fig. 3.2.

10Hz DBS at either target produced no significantly modulated voxels, including within the electrode target region. In contrast, significant and extensive CBV modulation was noted at all other frequencies tested (40-400Hz). The spatial pattern of CBV modulation was qualitatively similar across stimulation frequencies, and in some respects also similar between SNr and GPe stimulation targets. For example, both GPe- and SNr-DBS resulted in CBV changes predominantly ipsilateral to the stimulation site, with the exception of the dorsal striatum, which was bilaterally modulated by DBS at either target. Dorsal striatal CBV changes were strongly positive in the ipsilateral hemisphere during GPe-DBS, yet vasoconstriction was observed concomitantly in the contralateral hemisphere (during GPe-DBS), and bilaterally during SNr-DBS. Also of note, a "double peak" of CBV modulation was a characteristic response to DBS in certain regions, including the ipsilateral somatosensory cortex (both DBS targets), and dorsal striatum (SNr-DBS) (see Fig. 3.4).

During GPe-DBS (40-400 Hz), robust CBV increases were observed in ipsilateral frontal and prefrontal cortices, including cingulate, motor, prelimbic, infralimbic, and orbitofrontal cortices. A wealth of subcortical areas also showed positive CBV responses, including the substantia nigra, nucleus accumbens, ventral tegmental area, zona incerta, and others (see Supplementary Fig. 7.4). Of all regions examined, peak CBV responses to GPe-DBS were strongest in orbitofrontal cortex, reaching nearly 30% CBV increases with 400 Hz stimulation.

SNr-DBS (40-400Hz) evoked positive CBV changes in multiple basal ganglia nuclei (GPe, substantia nigra striatum), as well as additional areas intimately tied to the basal ganglia (pedunculopontine tegmental nucleus, zona incerta, ventral tegmental area) (see Fig. 7.4 and Supplementary Fig. 7.3). Of all regions examined, the substantia nigra showed the largest CBV changes (nearly 30% CBV increases at 200 or 400 Hz DBS). In stark contrast to GPe-DBS, frontal and prefrontal cortical modulation by SNr-DBS was relatively sparse; functional activation maps revealed spatially restricted vasodilation (e.g., in cingulate cortex), as well as contralateral vasoconstriction in prefrontal cortex (most apparent at 130 Hz). However, a closer examination of this data by means of CBV traces revealed that many of these areas (e.g., motor, somatosensory, prelimbic cortices) were likely positively modulated by 200 Hz SNr-DBS, albeit with a long delay (and thus not detected with our functional activation maps). Also of note, the superior colliculus, which receives direct innervation from the SNr (Deniau et al., 2007; Kaneda et al., 2008), had little to no detectable CBV changes during SNr-DBS.

Lastly, to determine the frequency-dependency of DBS responses at both targets, the amplitude of CBV responses was quantified for a subset of ROIs: GPe, substantia nigra, dorsolateral striatum (ipsi- and contralateral, somatosensory cortex, posterior hypothalamus (SNr-DBS only), and prelimbic cortex (GPe-DBS only)) (Fig. 7.4). These amplitude measures correspond to the mean CBV changes during the stimulation epoch for each DBS frequency (see Methods); because of differences in the characteristic trace dynamics for each ROI (e.g., hemodynamic delays), the calculated values are best compared across frequencies but not across ROI's. A main effect of DBS frequency was found for each ROI analyzed ($p < 0.05$), and post-hoc testing revealed that 10Hz DBS drove CBV amplitude changes that often significantly differed from many other frequencies. However, as suggested by the CBV traces, the influence of stimulation frequency on CBV responses was inconsistent across ROIs. For example, CBV amplitudes for some ROIs scaled positively with DBS frequency (e.g., the GPe during SNr-DBS), whereas peak amplitudes occurred at frequencies below 400 Hz for other ROIs (e.g., prelimbic and somatosensory cortices during SNr-DBS).

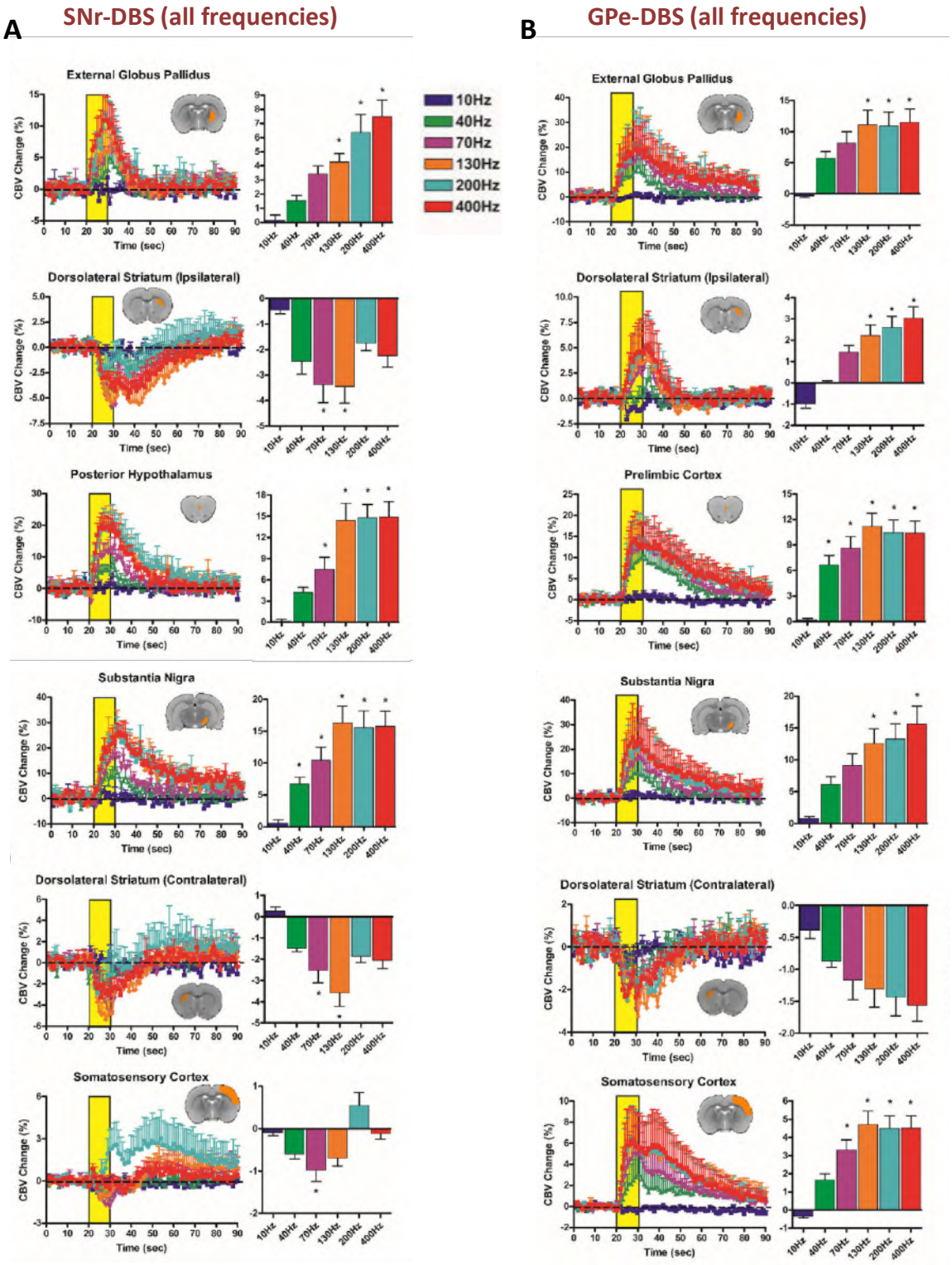

Figure 3.4: DBS evoked CBV changes at select, anatomically-defined regions of interest for (A) SNr-DBS and (B) GPe-DBS. CBV traces are shown for all frequencies, i.e. 10-400Hz. The yellow bar denotes the stimulation epoch. Note: a different Y-axis scale is used across ROIs. CBV traces are accompanied by bar graphs displaying percent changes in CBV amplitude changes during the stimulation period (mean ± SEM CBV values for the DBS stimulation period). Anatomically-defined ROIs are highlighted as figure inserts (single slice shown; note that many ROIs encompassed multiple slices). *$p \leq 0.05$ for 10Hz compared to all other frequencies (no other statistically significant comparisons). Additional ROIs (total=19) are located in Supplementary Fig. 3.3 (SNr-DBS) and 3.4 (GPe-DBS).

3.3.2 Functional connectivity MRI

Complementing our evoked-fMRI findings, fcMRI measurements revealed global and frequency-dependent modulation by DBS at both targets. Mean correlation matrices were generated for SNr (Fig. 3.5A) and GPe (Fig. 3.5B) subjects, for three rest and two stimulus conditions: rest1 (pre-DBS), Stim 40Hz, rest2 (in-between DBS), Stim 130Hz and rest3 (post-DBS). These cross-correlational matrices, displaying functional connectivity strength between 90 discrete brain regions (45 per hemisphere), revealed readily observable modulation during 130Hz DBS (compared to non-stimulation conditions), including both enhancements and losses of connectivity in the ipsilateral hemisphere. This modulation of fcMRI signals appeared readily reversible, as the post 130Hz stimulation "rest" scan (conducted immediately following the 130Hz DBS fcMRI scan), was qualitatively similar to prior non-stimulation scans. Functional connectivity modulation by 40Hz DBS was less apparent at both targets.

These observations were quantitatively confirmed by post-hoc testing (note that connections which were enhanced or suppressed during DBS were analyzed separately). These analyses revealed that functional connectivity was significantly altered during 130Hz DBS at both targets compared to either the 40Hz or resting conditions (see Fig. 3.6).

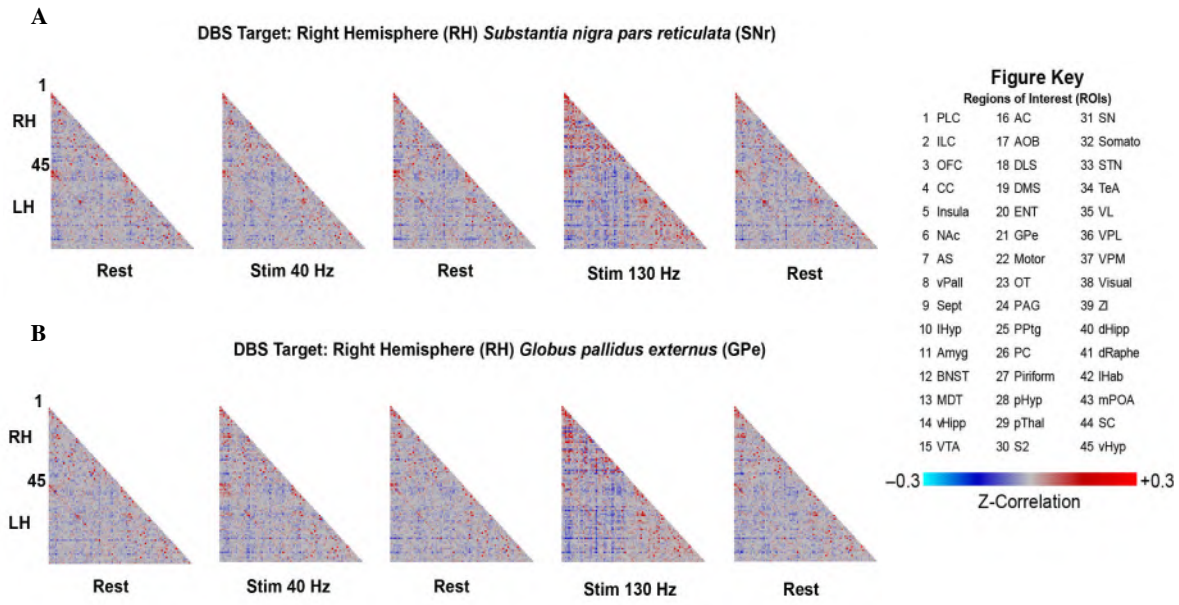

Figure 3.5: fcMRI Modulation by 40 and 130Hz (A) SNr-DBS and (B) GPe-DBS. Mean correlation matrices (*SNr: n=6; GPe: n=7*) for each rest and stimulus condition (rest1 (pre-DBS), Stim 40Hz, rest2 (in-between DBS), Stim 130Hz and rest3 (post-DBS)) using 45 regions-of-interest (ROIs, see Figure Key). Abbreviations: **PLC**: Prelimbic Cortex; **ILC**: Infralimbic Cortex; **OFC**: Orbitofrontal Cortex; **CC**: Cingulate Cortex; **Insula**: Insular Cortex; **NAc**: Nucleus Accumbens; **AS**; Anterior Striatum; **vPAll**: Ventral Pallidum; **Sept**: Septum; **lHyp**: Lateral Hypothalamus; **Amyg**: Amygdala; **BNST**: Bed Nucleus of the Stria Terminalis; **MDT**: Mediodorsal Thalamus; **vHipp**: Ventral Hippocampus; **VTA**: Ventral Tegmental Area; **AC**: Auditory Cortex; **AOB**: Accessory Olfactory Bulb; **DLS**: Dorsolateral Striatum; **DMS**: Dorsomedial Striatum; **ENT**: Entorhinal Cortex; **GPe**: External Globus Pallidus; **Motor**: Motor Cortex (Primary and Secondary); **OT**: Olfactory Tubercle; **PAG**: Periaqueductal Grey; **PPTg**: Pedunculopontine Tegmental Nucleus; **PC**: Parietal Cortex; **Piriform**: Piriform Cortex; **pHyp**: Posterior Hypothalamus; **pThal**: Posterior Thalamus; **S2**: Secondary Somatosensory Cortex; **SN**: Substantia Nigra; **Somato**: Primary Somatosensory Cortex; **STN**: Subthalamic Nucleus; **TeA:** Temporal Association Cortex; **VL**: Ventrolateral Thalamus; **VPL**: Ventral Posterolateral Thalamus; **Visual**: Visual Cortex (Primary and Secondary); **ZI**: Zona Incerta; **dHipp:** Dorsal Hippocampus; **dRaphe**: Dorsal Raphe Nucleus; **lHab**: Lateral Habenula; **mPOA**: Medial Preoptic Area; **SC**: Superior Colliculus; **vHyp**: Ventral Hypothalamus.

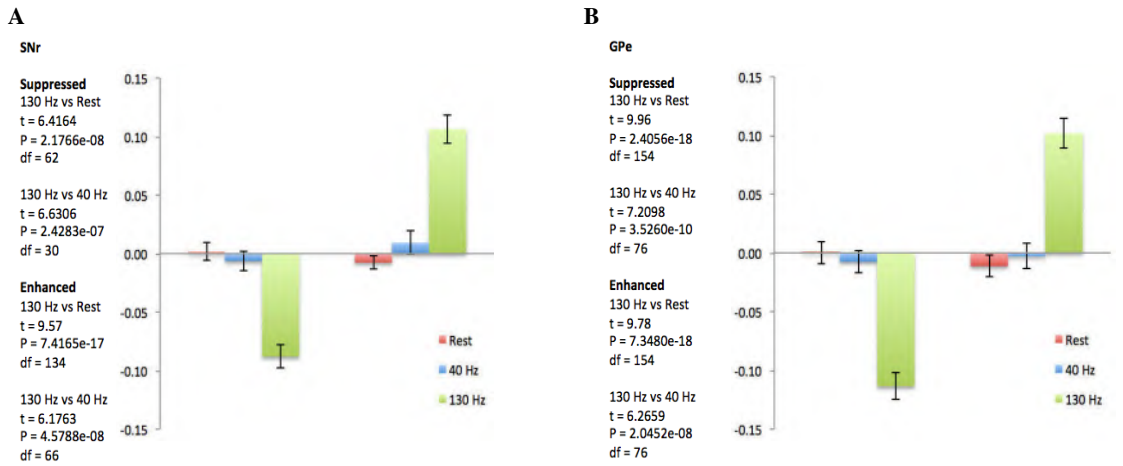

Figure 3.6: Statistical information concerning fcMRI modulation during rest, 40 and 130Hz for (A) SNr-DBS and (B) GPe-DBS. The graphs represent z- correlation mean and variance. Note, all ROIs with significant enhanced or suppressed connections were grouped, and the degrees of freedom (df) is dependent on the amount of connections within one group.

Next, individual fcMRI connections were measured (rANOVA, $p < 0.01$ uncorrected, ΔZ-Corr > 0.10) and visualized according to functional network groupings (Sensorimotor, Executive, Limbic, and Between network connections) and modulation direction (enhanced or suppressed) (see Supplementary Fig. 3.5A: SNr, Fig. Supplementary Fig. 3.5B: GPe). Note that Between network connections reflect connections that crossed functional category (e.g., between Sensorimotor and Limbic regions). Of connections meeting significance criteria, a larger proportion of enhancements were observed compared to suppressed connectivity (SNr: 21 enhanced, 8 suppressed; GPe: 23 enhanced, 14 suppressed). Most of these DBS-sensitive connections fell within the Between network category (SNr: 20; GPe, 25). Of the other networks examined, the Limbic network was the most highly represented by SNr-DBS (4 connections), whereas the Sensorimotor network had the strongest representation for GPe-DBS (6 connections).

3.4 Discussion

The present study was undertaken to map the functional circuit and network connectivity of the SNr and GPe, and to further evaluate the influence of stimulation frequency on the measured connectivity profiles. Although both regions have traditionally been classified as simple relay nuclei, our DBS results reveal extensive functional circuit and network interconnectivity, consistent with “extra-relay” processing power. Below, we highlight the major findings and limitations of this work.

3.4.1 Frequency-dependency

The usage of multiple stimulation frequencies in DBS-fMRI studies allows for the characterization of frequency tuning in neural circuits (Canals et al., 2008; Krautwald and Angenstein, 2012; Lai et al., 2014; Paek et al., 2015). 10Hz stimulation of either the SNr or GPe did not result in any detectable fMRI signal changes, while the stimulation frequency that evoked the largest CBV responses varied considerably by region. Perhaps the most compelling example of frequency selective circuit modulation in the present study occurred with 200Hz

SNr-DBS. At both lower and higher frequencies (40-130, 400Hz), prefrontal and frontal cortical regions (e.g., infralimbic, motor, cingulate cortices) responded to SNr-DBS with CBV increases that were modest and time-locked to the stimulation period. However, these brain regions responded to 200Hz stimulation with CBV increases that were much larger than at other frequencies, and peaked with a long delay (in certain case, after the cessation of stimulation). The reasoning behind such remarkably frequency selectivity in these responses, with highly unique temporal characteristics (in relation to the stimulation period), is an interesting area for future study.

The inclusion of very high stimulation frequencies in the present study (i.e., 130Hz and above) is also notable in the context of therapeutic DBS. Particularly as applied at basal ganglia targets, high frequency DBS has demonstrated therapeutic potential in neurological and neuropsychiatric diseases (DeLong and Wichmann, 2012; Goodman and Alterman, 2012). Both the SNr and GPe are being explored as potential non-canonical DBS targets for diverse neurological disorders (e.g., Parkinson's disease, Huntington's disease, epilepsy) (Chastan et al., 2009; Ligot et al., 2011; Piedimonte et al., 2013; Shi et al., 2006; Sutton et al., 2013; Temel et al., 2006; Velisek et al., 2002; Vitek et al., 2012; Weiss et al., 2013; Wille et al., 2011). Although we used a healthy rodent model, precluding behavioral tests of DBS efficacy, our evoked-fMRI results highlight strong parallels in circuit modulation by either moderate or high frequency stimulation of the SNr and GPe. The frequency sensitivity of symptom amelioration by SNr- or GPe-DBS would be interesting to study in the clinical setting, particularly in light of the possibility of prolonging the battery life of DBS pulse generators using lower frequency stimulation protocols.

3.4.2 Evoked fMRI

3.4.2.1 Striatal CBV modulation by SNr- and GPe-DBS

Both the SNr- and GPe are downstream targets of the striatum, receiving GABAergic input through the so-called direct and indirect pathways, respectively. Although striatal activity changes may thus be anticipated during either SNr- or GPe-DBS, our demonstration of striatal modulation by DBS at each target is of remarkable interest for several reasons. First, although the basal ganglia are frequently modeled as intrahemispheric systems, we observed pronounced bilaterality in striatal modulation by SNr- or GPe-DBS. Irrespective of whether this modulation occurs through feedforward thalamo-cortico-striatal loops, antidromic recruitment of striatal fibers, or other means, our results strongly suggest that presence of powerful bilateral connectivity within the basal ganglia systems. Of further interest is the directionality of this striatal hemodynamic response; prominent CBV decreases were noted within the dorsal striatum during DBS of either the SNr or GPe, and occurred across a wide range of stimulation frequencies (40Hz and higher). The extent and magnitude of these signals was greater at the SNr target compared to the GPe, and was also greater in the hemisphere contralateral to stimulation (although ipsilateral decreases were also observed with both DBS targets).

Although it may be intuitive to interpret our data as DBS-evoked neuronal inhibition, the situation appears to be particularly muddled in striatum, wherein dopaminergic neurotransmission has been hypothesized to induce vasoconstriction independent of direct activity changes within striatal neurons (Hsu et al., 2014) or regional metabolism (Shih, 2011). In addition, striatal CBV decreases have previously been shown with heightened local neuronal activity (Shih et al., 2014, Shih et al., 2009). In light of these complexities, further work will be

necessary to determine the underlying mechanism of striatal CBV decreases evoked during SNr- and GPe-DBS.

3.4.2.2 Frontal cortical CBV increases evoked by GPe-DBS

One major unexpected finding in this study was the robust modulation of frontal cortical areas (including prefrontal and motor cortices) by GPe-DBS. Historically, the GPe has been viewed primarily as a basal ganglia relay nucleus with only indirect control over cortical activity (Albin et al., 1989; DeLong, 1990). Very recently, however, two studies have identified a direct, ipsilateral projection from GPe to frontal cortex in mouse, rat, and monkey (Chen et al., 2015; Saunders et al., 2015). The GPe neurons that make up this projection are GABAergic and express the GABA vesicular transporter (vGAT), with a large subset additionally being cholinergic (expressing choline acetyltransferase (ChAT)). This pathway innervates all layers of cortex, targeting both pyramidal cells and interneurons. Unsurprisingly, selective optogenetic stimulation of this pathway results in mixed patterns of modulation among frontal cortical neurons, with both inhibition and enhanced firing rates observed *in vivo* (Saunders et al., 2015). As expected based on neurochemical makeup, selective stimulation of this projection is predominantly inhibitory for cortical neurons. However, given that this projection has been reported to biasedly innervate cortical interneurons, it is possible that distant inhibitory mechanisms result in enhanced cortical activity and vasodilatation. The robust modulation of frontal cortex by GPe-DBS observed in the present study may be the result of such pallido-cortical transmission, although the use of nonselective electrical stimulation precludes a definitive interpretation.

3.4.2.3 Comparison to canonical STN-DBS and GPi-DBS

High frequency DBS at the STN and GPi are widely used with great success for the symptomatic treatment of PD. However, the therapeutic mechanisms and how DBS at these ”classic” targets modulate neural circuitry are also still largely unknown. Therefore, prior to this study, an STN- and GPi-DBS-fMRI was performed by Lai et al. to map global brain responses to DBS at the STN and GPi of the rat. The authors demonstrated that STN- and GPi-DBS resulted in positive BOLD responses in multiple ipsilateral cortical brain structures, with peak responses observed at clinically relevant stimulation frequencies (i.e. 100-130Hz), indicating that both targets are functionally connected with the motor cortex at therapeutic stimulation frequencies. Additionally, negative BOLD responses were observed in contralateral cortical and striatal areas during GPi-DBS, but not during STN-DBS (Lai et al., 2013). When comparing the STN-and GPi-DBS data from Lai et al., to our SNr- and GPe-DBS data, we find that the responses to GPi-DBS resemble the responses to GPe-DBS. This is not surprisingly since the GPi and GPe are adjacent brain structures.

3.4.3 Functional connectivity MRI

Complementing our evoked-fMRI findings of modulation of the striatal output nuclei by SNr- and GPe-DBS, fcMRI measurements revealed robust enhancements in functional connectivity between many of the same regions. In general, we observed a trend of enhanced functional connectivity in the hemisphere ipsilateral to stimulation. Additionally, our data indicates that these connectivity shifts are frequency-dependent, being more apparent with 130Hz than 40Hz

stimulation of either DBS target. To our knowledge, this is the first example of DBS-induced frequency-dependent functional connectivity modulation.

3.4.4 Limitations

Our study includes several limitations that are generally characteristic of preclinical DBS-fMRI experiments. The usage of anesthesia, as is commonly employed in preclinical fMRI experiments (Haensel et al., 2015; Krautwald and Angenstein, 2012; Lai et al., 2014; Min et al., 2012), may alter the responsiveness of neural circuits to the effects of DBS. One possible means by which an anesthetic effect may be evident could be in the stimulation strength threshold for detectable fMRI responses. In pilot experiments, we were unable to reliably achieve evoked or functional connectivity fMRI responses with current amplitudes below 300μA (data not shown), and thus our experiments relied upon higher amplitudes than those generally used in preclinical DBS studies in awake rodents (typically 100-150μA) (Ewing et al., 2013; Hamani et al., 2014; Vassoler et al., 2008), although higher amplitudes have been reported for studies in both awake and anesthetized states (McCracken et al., 2007; van Dijk et al., 2013). We postulate that the relatively higher current amplitudes needed for DBS effects in the present study (i.e. 300μA) may have been necessitated by the usage of anesthesia in our model. This in turn increases the possibility of "off-target" stimulation effects, due to current spread outside the anatomical boundaries of the target regions. Future studies may rely upon conscious animal imaging to tackle these potential limitations (Ferris et al., 2006).
Second, the use of electrical stimulation for circuit mapping may be viewed as either a strength or weakness in the present study; it is highly translationally relevant in the context of clinical DBS therapy, yet comes with limitations of circuit recruitment specificity. As suggested above, electrical stimulation may be prone to off-target circuit recruitment, and may present another limitation to the present study. Electrical stimulation is capable of recruiting fibers of passage, and current may also spread beyond the anatomical boundaries of the target region; in either instance, "off-target" areas may be recruited by DBS. An additional, related point concerns the directionality of connectivity between the DBS target region and other modulated areas. Because DBS can recruit connected brain areas through both ortho- and antidromic signal propagation across fibers (Grill et al, 2008; Li et al., 2012) this approach to functional circuit mapping cannot readily distinguish between up- and downstream circuit elements. The use of opto- and/or pharmacogenetic tools should provide a more precise means for functional imaging-based circuit mapping (Lee et al., 2010; Michaelides et al., 2013), although at the likely expense of translational relevance in the context of therapeutic clinical DBS.

3.5 Conclusions

This study implemented a simultaneous DBS-fMRI approach to investigate the functional connectivity of the SNr and GPe, the two major striatal output nuclei. Through their roles in the basal ganglia loops, these regions have a diverse number of functional roles in cognition, motor control, and emotional processing. As demonstrated here and elsewhere, DBS-fMRI provides a global perspective of a brain region's functional connectivity profile, ultimately allowing for the identification and characterization of novel circuit connections. In the present work we identified, among other results, DBS-evoked negative fMRI signals in the bilateral striatum, as well as frequency-dependent, large-scale functional connectivity changes. Broadly, our work contributes to a growing literature demonstrating functional connectivity of the striatal outputs

outside of canonical thalamic relay connections. Further, the inclusion of high frequency stimulation in our DBS experiments facilitates a translational perspective on our connectivity maps, as high frequency DBS at the SNr or GPe has demonstrated therapeutic benefits in neurological disorders such as Parkinson's Disease.

3.6 Original contributions

The work presented in this chapter resulted in a number of international conference contributions (see [12-13] in list of conference contributions). The results of this study were submitted to the peer-reviewed A1 journal NeuroImage (see [3] in list of publications) (shared first author). Dan Albaugh and the author of this section both equally contributed to this study. Data-analysis of the functional connectivity data was performed in collaboration with Andrew Salzwesel.

3.7 Supplementary figures

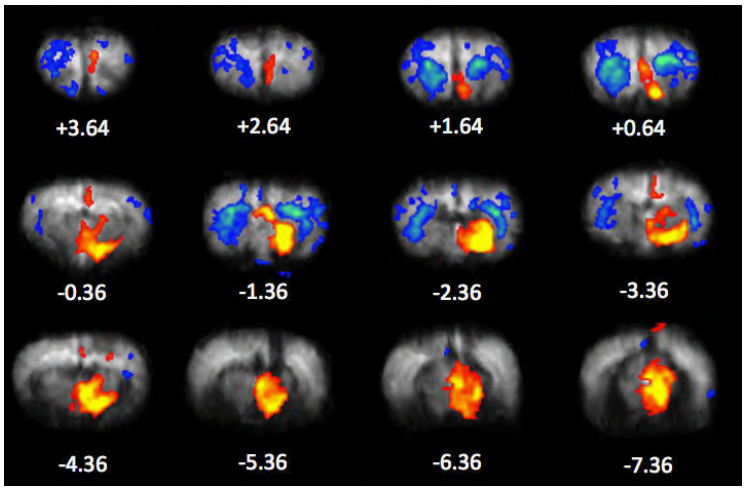

Supplementary Figure 3.1: Representative raw EPI images from averaged SNr-DBS scans (130Hz). Additional details regarding these images is located in the Fig. 3.3 caption.

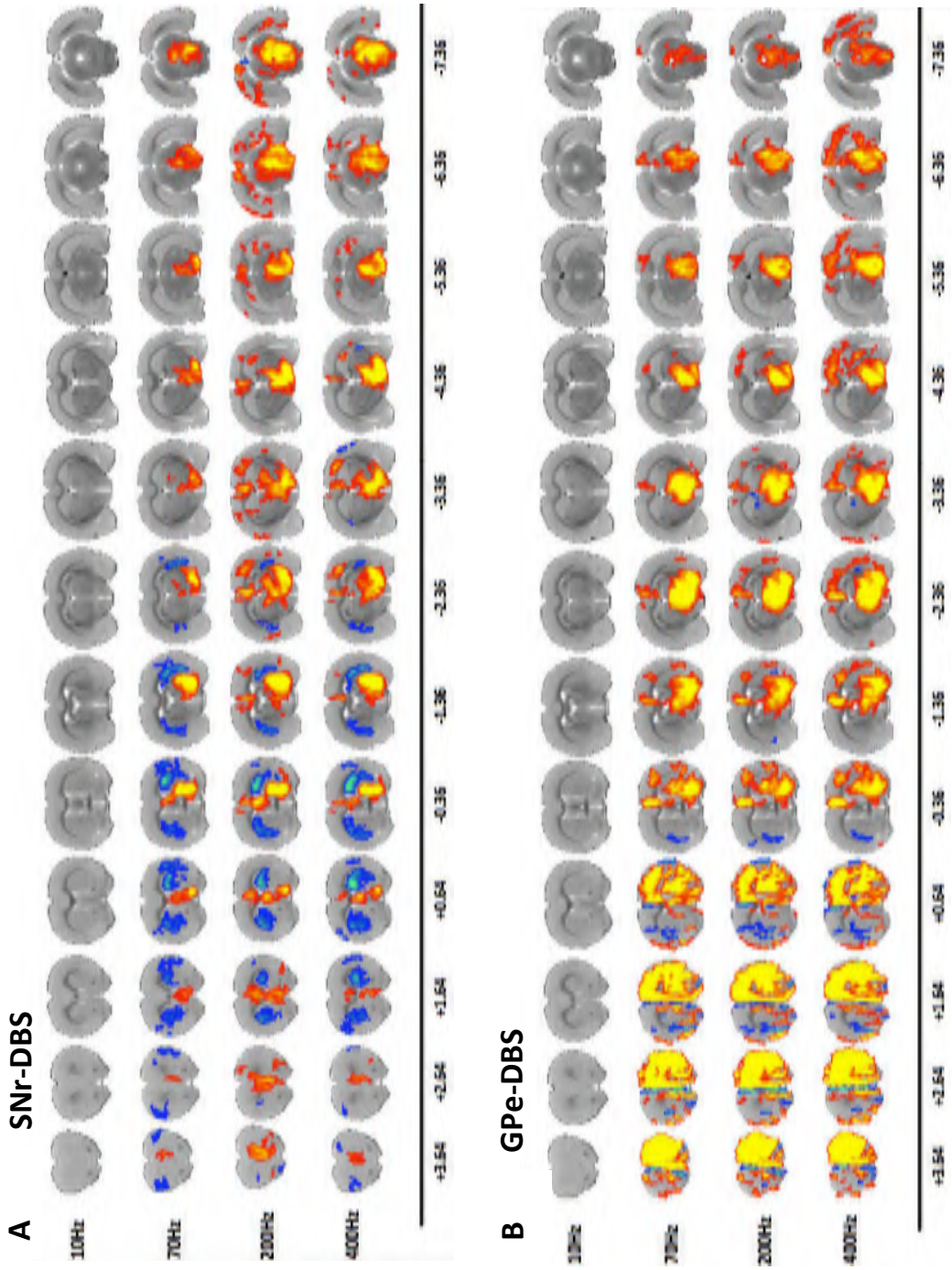

Supplementary Figure 3.2: Functional activation maps of CBV modulation by 10/70/200/400Hz of (A) SNr-DBS and (B) GPe-DBS. The maps represent a mean of 5 and 7 subjects, for SNr and GPe respectively. Coordinates (in mm) reflect approximate anteroposterior slice positioning relative to bregma.

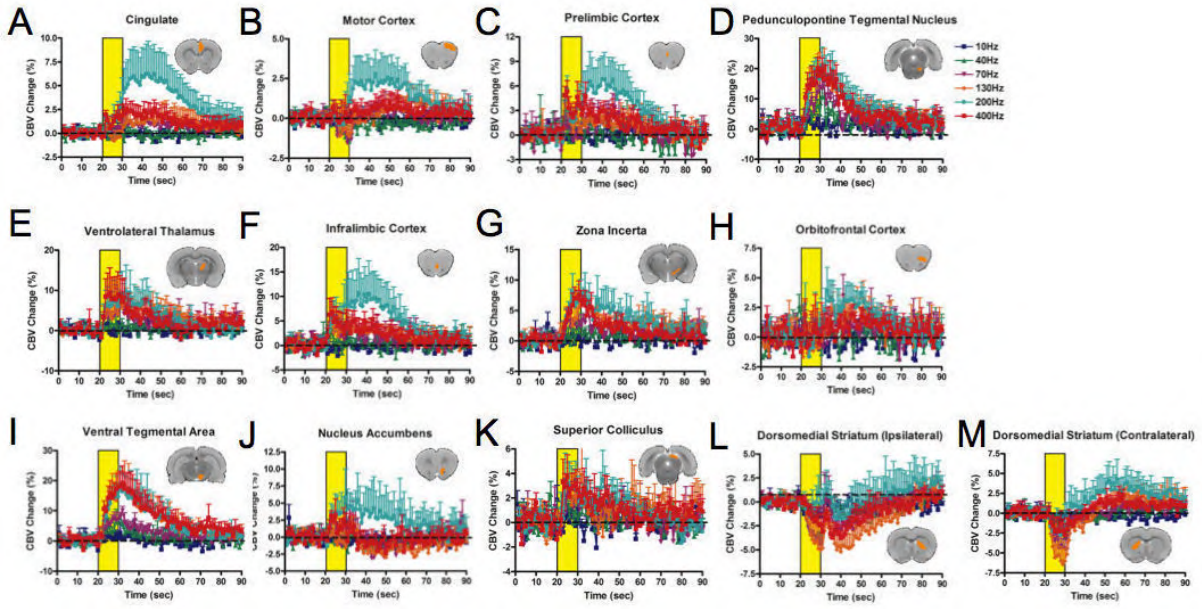

Supplementary Figure 3.3: SNr-DBS evoked CBV changes at select, anatomically-defined regions of interest for all frequencies (temporal trace CBV dynamics and percent change amplitudes measured during stimulation period). Continuation of Fig. 7.4 displaying additional ROIs: (A) Cingulate (B) Motor cortex (C) Prelimbic cortex (D) Pedunculopontine nucleus (E) Ventrolateral thalamus (F) Infralimbic cortex (G) Zona incerta (H) Orbitofrontal cortex (I) Ventral tegmental area (J) Nucleus accumbens (K) Superior colliculus (L) Ipsilateral dorsomedial striatum (M) Contralateral dorsomedial striatum.

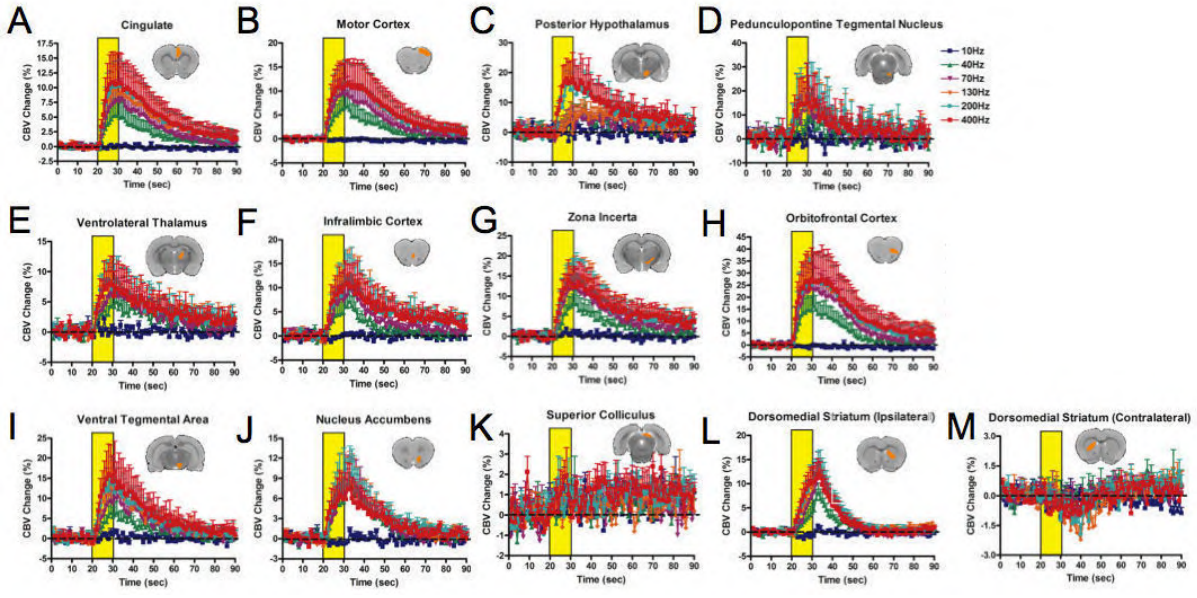

Supplementary Figure 3.4: GPe-DBS evoked CBV changes at select, anatomically-defined regions of interest for all frequencies (temporal trace CBV dynamics and percent change amplitudes measured during stimulation period). Continuation of Fig. 7.4 displaying additional ROIs: (A) Cingulate (B) Motor cortex (C) Posterior Hypothalamus (D) Pedunculopontine nucleus (E) Ventrolateral thalamus (F) Infralimbic cortex (G) Zona incerta (H) Orbitofrontal cortex (I) Ventral tegmental area (J) Nucleus accumbens (K) Superior colliculus (L) Ipsilateral dorsomedial striatum (M) Contralateral dorsomedial striatum.

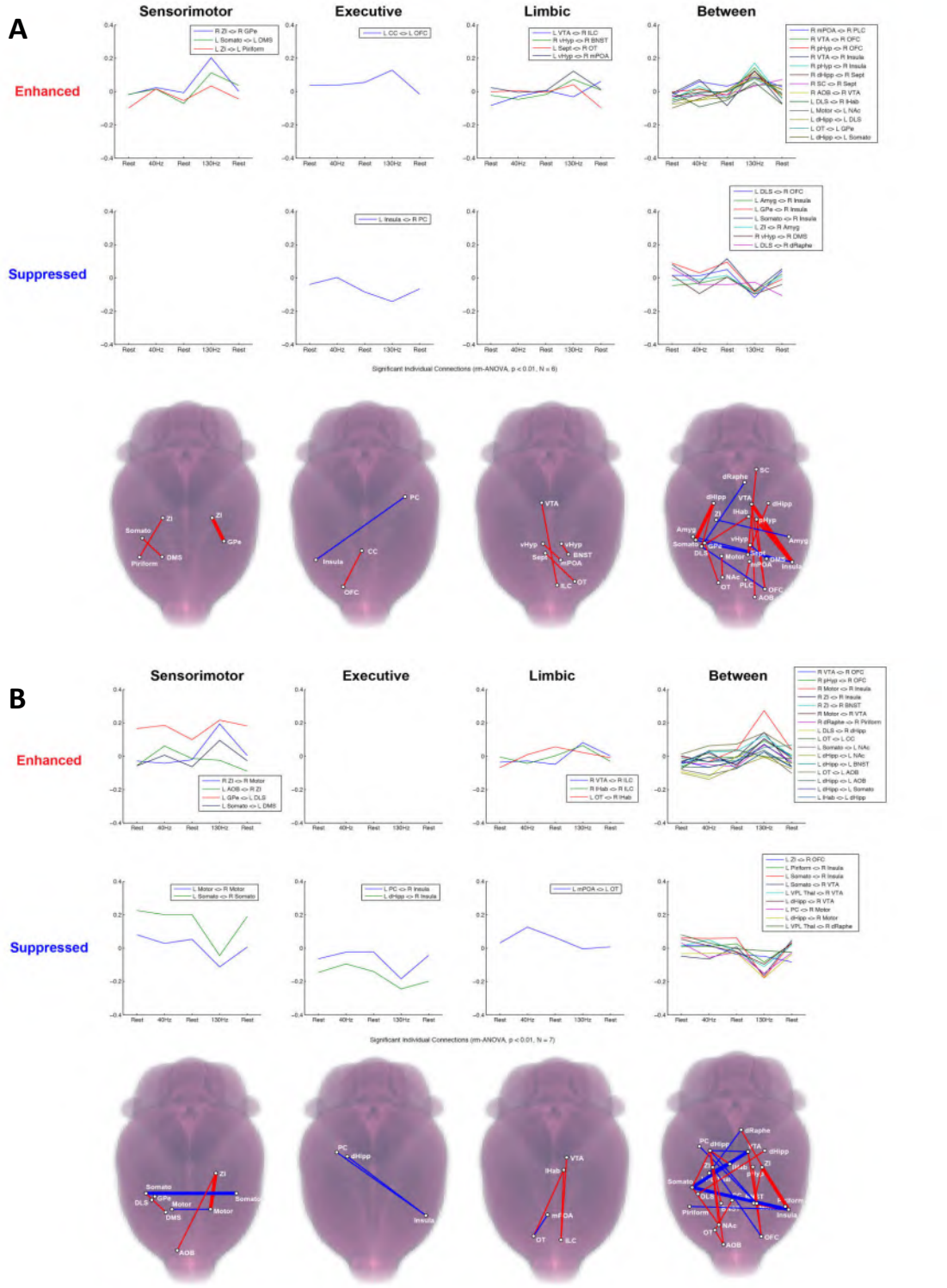

Supplementary Figure 3.5: Network-level visualization pair-wise fcMRI modulations during130Hz (A) SNr-DBS and (B) GPe-DBS. Significant (rANOVA, $p < 0.01$ uncorrected, ΔZ-Corr > 0.10) enhanced (red) or suppressed (blue) individual pair-wise connections grouped by canonical networks (Sensorimotor, Executive, Limbic, and Between Network Connections). Thick red lines represent ΔZ-Corr > 0.20.

Chapter 4

Functional Circuit Mapping of the Globus Pallidus externa using Simultaneous Opto-fMRI

4.1 Introduction

As explained in chapter 1, deep brain stimulation (DBS) is a widely accepted treatment for advanced Parkinson's disease (PD) (Okun et al., 2012; Bronstein et al., 2011). The subthalamic nucleus (STN) and the globus pallidus interna (GPi) are usually targeted in PD patients, because they appeared to work best in the previously used surgical treatment. Unlike the lesion-based approaches that earlier predominated surgical therapy, DBS is advantageous for its reversibility and the capacity to modulate stimulation parameters (active contacts, voltage, frequency, pulse width) (Benabid et al., 1991; Kuncel and Grill, 2004). The latter trait is particularly important for optimizing the therapeutic benefits of DBS while reducing stimulation-related side effects (McIntyre et al., 2004). Despite widespread clinical use, the therapeutic mechanisms of DBS are poorly understood. A better understanding of the neuronal networks modulated by DBS at new potential targets, is therefore required to improve treatment efficacy.

PD causes a progressive loss of inhibitory dopamine-producing cells within the basal ganglia, consequently inducing abnormalities in the spontaneous activity and sensorimotor responses of basal ganglia nuclei (Betchen and Kaplitt, 2003; Lozano et al., 2002; Marsden, 1984). This results in a rewiring of the basal ganglia in PD subjects (Lang and Lozano, 1998). Evidence exists that changes in striatal GABAergic microcircuits contribute to basal ganglia dysfunction in several movement disorders such as PD. These inhibitory interneurons could potentially be a therapeutic DBS target, since they are genetically and neurochemically distinct from striatal projection neurons (Gittis and Kreizer, 2012). Therefore, the Globus Pallidus externa (GPe), a GABAergic striatal output nuclei, is currently being explored as a potential non-canonical DBS target for PD (Angeli et al., 2005; Vitek et al., 2012). A contrasting effect on PD symptoms has been previously suggested depending on DBS being applied in GPi or GPe, with akinesia and gait being improved by GPe DBS even though with worsening of dyskinesia, while ventral GPi DBS improves dyskinesias but may worsen akinesia and gait (Angeli et al., 2005). Vitek et al. also showed that DBS of the GPe is associated with improvements in parkinsonian motor signs

Their data provided additional evidence that the GPe might be a potential therapeutic target for DBS in PD patients, and that DBS modulates GPe output in order to normalize the on-going pathologic neuronal activity within the basal ganglia. However, the mechanisms responsible for this therapeutic effect remain to be elucidated, and the beneficial effects of GPe-DBS need further investigation. Of particular clinical interest are the circuits modulated by GPe-DBS, as these may provide critical information about the underlying mechanisms for both therapeutic and off-target effects.

Whole-brain mapping of DBS-induced circuit modulation can be achieved using functional magnetic resonance imaging (fMRI). The key strengths to fMRI-based studies of DBS include the ability to detect dynamic changes in stimulus-evoked activity and connectivity, *in vivo*, across the whole brain with reasonably high spatiotemporal resolution. Previous attempts have used fMRI to study DBS effects in clinical populations (Figee et al., 2013; Jech et al., 2001), although its use is strongly limited by appropriate safety considerations (largely related to dangers associated with the introduction of DBS equipment to the MR environment) (Nazzaro et al., 2010; Tagliati et al., 2009; Chhabra et al., 2010). Animal models of DBS can be employed with simultaneous fMRI under more flexible experimental conditions, allowing for thorough mapping of DBS effects (Van Den Berge et al., 2015; Younce et al., 2014; Knight et al., 2013). Moreover, electrodes may be chosen with more MR-compatible materials (Lai et al., 2015), minimizing susceptibility artifacts that could otherwise preclude visualization of DBS effects in the area surrounding the electrode.

Preclinical DBS studies also allow for the experimental introduction of optogenetic tools, which provide superior neural circuit stimulation specificity compared to electrical DBS (Fiala et al., 2010; Yizhar et al., 2011). Specifically, in addition to modulation of neuronal populations proximal to the electrode, electrical DBS can also recruit nonreciprocal afferent inputs (via antidromic signal propagation), as well as neighboring fibers of passage. In contrast, optogenetic stimulation is generally confined to only the opsin-expressing cells and their efferent outputs. Because of this added specificity for neural modulation, optogenetic tools have been employed to inform potential circuit mechanisms of DBS therapy in preclinical models (Creed et al., 2015; Gradinaru et al., 2009). Additionally, when using simultaneous fMRI measurements, the artifact of the optic fiber is considerably smaller compared to the artifact of the metal DBS-electrode used in electrical stimulation, hereby increasing the quality of the MR images substantially.

There is also substantial interest and discussion related to the future use of optogenetic tools for refined, next-generation clinical DBS (LaLumiere, 2011; McDevitt et al., 2014; Williams et al., 2013). The rationale for this discussion relates to the presumptive ability of optogenetic stimulation to achieve therapeutic efficacy with a reduced side-effect profile from “off target” circuit recruitment. On the other hand, DBS is popularly suggested to exert its therapeutic effects via large-scale network modulation (van Westen et al., 2015; Deniau et al., 2010). However, little is known regarding the extent to which optogenetic stimulation mirrors the circuit-level responses achieved with electrical DBS.

Therefore, in the present study, we aimed to investigate the functional circuit response profile obtained by optogenetic stimulation of the GPe, measured with fMRI, in a healthy and PD rat model. The simultaneous employment of optogenetics and fMRI is further referred to as opto-fMRI, a technique that is currently being used to investigate DBS in preclinical studies (Detorakis et al., 2015; Creed et al., 2015; Gradinaru et al., 2009; Yizhar et al., 2011). For a rodent model of PD, we will use the unilateral 6-hydroxydopamine (6-OHDA) lesion model,

attractive due to its ease-of-use, robust motor deficits, and consistently demonstrated sensitivity to parkinsonian therapeutics, including DBS (So et al., 2012; McConnel et al., 2012; Iancu et al., 2005; Yuan et al., 2005). 6-OHDA is a hydroxylated analog of dopamine, and when injected into the medial forebrain bundle, 6-OHDA rapidly lesions the nigrostriatal pathway. Such lesioning induces degeneration of striatal terminals, consequently destructing dopaminergic-producing cells in the striatum (Tieu, 2011; Sarre et al., 2004).

Electrical stimulation of the GPe resulted in widespread modulation of evoked- and fcMRI signals (see chapter 3). Notable findings from our evoked-fMRI dataset include robust CBV increases of the ipsilateral prefrontal cortex, as well as bidirectional, stimulation frequency-dependent modulation of striatal CBV signals (negative at 10Hz, positive at 70Hz and above). fcMRI provided evidence of robust, frequency-dependent global network modulation by electrical GPe stimulation, with more robust network changes observed with 130Hz compared to 40Hz stimulation. Compared to electrical stimulation, optogenetic stimulation at 40Hz resulted in a more spatially restricted pattern of modulation, with prominent CBV increases locally within the GPe, and CBV decreases in the neighboring dorsal striatum. Surprisingly, in Parkinsonian rats, optogenetically-evoked striatal vasoconstriction downstream was substantially reduced. Moreover, a unique prefrontal negative CBV signal emerged during GPe stimulation in these subjects.

4.2 Materials & Methods

4.2.1 Animals

Twelve adult male Sprague-Dawley rats (300–500g body weight; Charles River Laboratories, Wilmington, MA, USA) were used in this study. All procedures were performed in accordance with the National Institutes of Health Guidelines for Animal Research (Guide for the Care and Use of Laboratory Animals) and approved by the University of North Carolina Institutional Animal Care and Use Committee. Animals were housed under environmentally-controlled conditions (12h normal light/dark cycles, 20-23°C and 40-60% relative humidity), with food and water provided *ad libitum*.

4.2.2 Optogenetic constructs

For optogenetic experiments (see paragraph 4.2.4), neuronal opsin expression was achieved using adeno-associated viral vectors (AAV, serotype 5), encoding either a humanized variant of ChannelRhodopsin-2 (hChR2; H134R) fused to an enhanced yellow fluorescent protein (EYFP), or EYFP alone. Both constructs were placed under the human Synapsin (hSyn) promoter to target GPe neurons. All viruses were obtained from the Vector Core at the University of North Carolina at Chapel Hill.

4.2.3 Surgery

For all surgical procedures, rats were endotracheally intubated and mechanically ventilated using a small animal ventilator (CWE Inc., SAR-830/PA, Ardmore, PA). Anesthesia was maintained under a constant flow of 2% isoflurane mixed with medical air, and physiological

parameters were continuously monitored and maintained within normal ranges using capnometry (Surgivet, Smith Medical, Waukesha, WI) and pulse oximetry (MouseOx Plus, STARR Life Science Corp., Oakmont, PA). Animals were head-fixed to a stereotactic frame (Kopf Instruments, Model 962, Tujunga, CA). Following head shaving and exposure of the skull, five small burr holes were drilled: four for the positioning of MR-compatible miniature brass screws (Item #94070A031, McMaster Carr, Atlanta, GA, USA), and one for the injection of the vector and the insertion of the custom-made optical fiber. In 5/12 rats an extra burr hole was drilled for the unilateral microinjection of 5µl of 6-OHDA (3µg/µl 6-OHDA dissolved in saline containing 0.02% ascorbic acid as antioxidants), targeting the medial forebrain bundle (MFB). Stereotactic injection coordinates were generated using a standard rat brain atlas (Paxinos&Watson, 2007), and are described as follows, in reference to bregma (anteroposterior, AP; mediolateral, ML) and cortical surface (dorsoventral, DV): AP -4.5mm, ML +1.4mm, DV -8mm). Injections were carried out at a rate of 0.5µl/min and a volume of 5µl was injected using a 10µl Hamilton microsyringe. The needle was left at the injected sites for 10min before being withdrawn. Degeneration of dopaminergic neurons takes place within 12h preceding a significant loss of striatal terminals, which occurs 2-3days later. Two weeks after injection the animals exhibited robust PD behavior. Already 2-3days after injection, all rats showed initial signs of PD, namely all rats turned to the right when lifting the animal up at its tail, due to the lesion in the right hemisphere, confirming successful hemiparkinsonism in all five rats.

For optogenetics, viral microinjections were targeted to the GPe, with the same stereotactic coordinates used for electrode implantations in the previous study (see chapter 7), namely AP -0.96mm, ML +2.8mm, DV -5.8mm (Paxinos&Watson, 2007). Injections were administered as 2µl volumes at a flow rate of 0.2µl/min, with a total infusion time of 10min. An additional 10 minutes was given for virus diffusion prior to slow retraction of the microsyringe needle. Chronically implantable optic fibers were placed 0.5mm above virus injection sites (see Fig. 4.1C). The optical fibers were custom-made according to the construction protocol for implantable optical fibers for long-term optogenetic manipulation of neural circuits, established by Sparta et al. (Sparta et al., 2012). At least three weeks were given before opto-fMRI experiments where undertaken, to allow for sufficient virus expression.

4.2.4 Optogenetic stimulation

For optogenetic stimulation of the GPe (n=10 for ChR2; n=2 for EYFP control), a 473nm wavelength diode-pumped solid-state (DPSS) laser (model BL473T8-200, Shanghai Laser & Optics Century, Shanghai, China) was connected via a coupler to a homemade patch cable terminating above the chronically implanted optic fibers. Wavelength-specific light output at the terminating end of the patch cable was calibrated to 20mW using a wattage meter. Optogenetic stimulation periods consisted of a series of TTL-triggered light pulses with a stimulation frequency of 10, 20 and 40Hz, and pulse duration of 10ms. A 100 seconds block design paradigm was implemented, consisting of 20 seconds of rest (stimulation OFF) followed by two 10 seconds stimulation periods (stimulation ON), with intervening and final rest periods of 30 seconds (i.e. 20sOFF-10sON-30sOFF-10sON-30sOFF) (see Fig. 4.1D).

A recent study has demonstrated hemodynamic changes following blue light laser stimulation (50% duty cycle) in naïve rat brain, possibly due to a laser heating artifact (Christie et al., 2012). To exclude the possibility of such an artifact as the source of the observed optogenetic

response, an identical stimulation paradigm was employed in two rats expressing an inert EYFP fluorophore in the GPe.

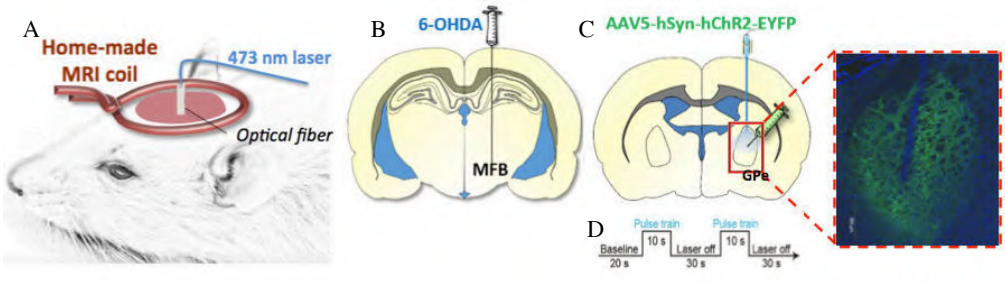

Figure 4.1: Experimental protocol: (A) Schematic of experimental imaging setup with homemade surface loop coil and optical fiber. (B) Schematic of 6-OHDA injection in the medial forebrain bundle (MFB). (C) Schematic of GPe-opto, representative confocal image illustrating ChR2 expression in the GPe (green). (D) Stimulation paradigm.

4.2.5 Data acquisition

The preparation for the fMRI procedures and the CBV fMRI data acquisition itself were performed identical as described in the previous study (see paragraph 3.2.3.1), with the only difference fewer scans were acquired since only three different frequencies were evaluated (i.e. 10/20/40Hz). The set-up of the coil and the optical fiber is shown in Fig. 4.1A.

Similar to the DBS experiments described in the previous chapter, optic fiber placements above the GPe virus injection site were visualized using the anatomical MR image. Optic fiber placements within the GPe were confirmed for each rat. As opposed to the DBS-electrode, optic fibers are characterized by a smaller artifact on the fMRI images (see Fig. 4.2).

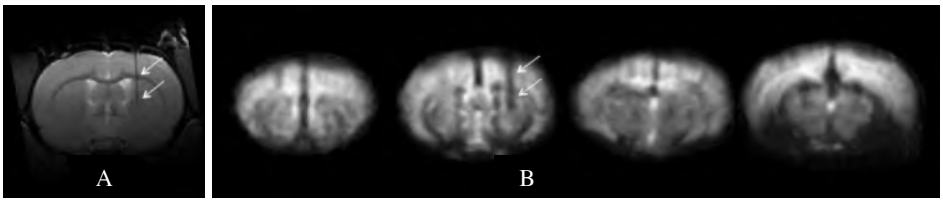

Figure 4.2: Representation of the fiber artifact on (A) an axial slice of an anatomical MR-image at height of the fiber and on (B) five axial slices of a functional MR-image (same rat as in (A)). The artifact is indicated with a white arrow.

4.2.6 Histology

Following scan procedures, rats were deeply anesthetized with 1-2ml Euthasol and transcardially perfused with saline followed by 10% formalin. Extracted brains were stored overnight in 10% formalin and transferred to a 30% sucrose solution (in DI water) for 2-3 days, until brains sunk to bottom of storage bottles. Brains were cut to 40 µm thick sections on a freezing microtome and mounted on glass slides for fluorescent imaging. Vectashield mounting medium with DAPI stain (Vector laboratories, Item # H-1200) was used to provide a cell body counterstain. Slides were imaged using a Zeiss 780 confocal microscope to verify the transfected area. A representative example of virally-mediated ChR2 expression in GPe neurons is provided in Fig. 4.1C. The expressions of tyrosine hydroxylase (TH) were examined by

immunofluorescence to verify the degree of induced hemiparkinsonism. A large number of cells estimated by TH-staining indicates successful induction of hemiparkinsonianism in all five rats. A representative example is shown in Fig. 4.3.

Figure 4.3: Representative image confirming dopamine loss in the striatum, ipsilateral to the injection site.

4.2.7 Data-analysis

Data-analysis was performed identically as described in the previous study (see paragraph 3.2.5.1).

4.3 Results

Our study was able to demonstrate circuit-level effects of neural modulation by optogenetic stimulation of the GPe in healthy and Parkinsonian rats. Optogenetic stimulation of the GPe with a 40Hz stimulation frequency produced a significant positive CBV response in the GPe and a negative CBV response in the striatum, only ipsilateral, in both healthy and Parkinsonian rats. The response maps for healthy and Parkinsonian rat are shown in Fig. 4.4A and Fig. 4.4B respectively. Response maps for other frequencies (i.e. 10 and 20Hz) are shown in Fig. 4.5 for both groups.

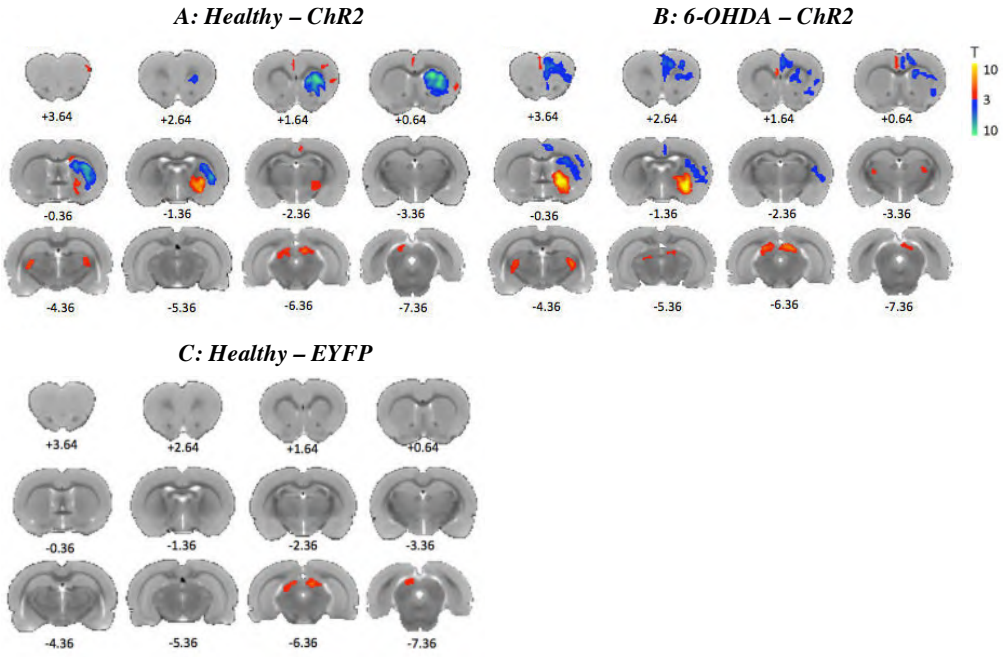

Figure 4.4: Mean functional response maps of CBV modulation by 40Hz GPe-opto in (A) healthy (n=5) and (B) Parkinsonian (n=5) rats expressing ChR2, and (C) control rats, expressing EYFP only (n=2). Coordinates (in mm) reflect approximate anteroposterior slice positioning relative to bregma.

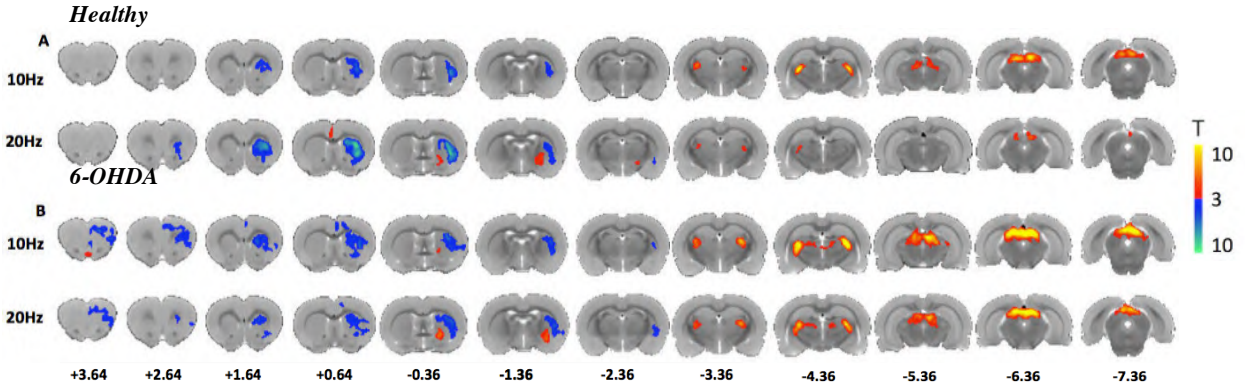

Figure 4.5: Mean functional response maps of CBV modulation by 10Hz and 20Hz GPe-opto in (A) healthy (n=5) and (B) Parkinsonian (n=5) rats. Coordinates (in mm) reflect approximate anteroposterior slice positioning relative to bregma.

Our data demonstrates distinct differences in the response maps between healthy and PD rats, we observe a (1) enhanced CBV-response in the GPe, (2) reduced CBV-response in the striatum, (3) a negative prefrontal response, in the PD rats compared to the healthy rats.

The temporal profile in the ipsilateral GPe shows an increase of 2.11±0.72% in the mean amplitude of the CBV-response at 40Hz in PD rats, and the temporal profile in the ipsilateral dorsolateral striatum shows a decrease of 2.08±0.23% in the mean amplitude of the CBV-response at 40Hz in PD rats, as opposed to healthy rats. Besides the differences in intensity of the CBV-response, we also observe distinct differences in the spatial extent of the CBV-responses in the GPe and the striatum, namely a wider and smaller CBV-response in the GPe and striatum, respectively, in the PD rats. Temporal profiles and complementing statistics of six regions of interest are displayed in Fig. 4.6. Note that, when comparing the temporal profile and the functional response map at the GPe, the temporal profile shown in Fig. 4.6 is most likely an underestimation of the actual CBV response at the GPe. This is probably because the actual response does not entirely overlap with the *a priori* drawn ROI, which was based on the location of the GPe in the rat brain atlas.

Since we did not intentionally close the eyes during the acquisition, responses to the light were observed in the rat superior colliculus and the lateral geniculate nucleus (LGN) in all groups. The responses in these relay nuclei of the visual system are located in the most posterior three slices of the shown response maps. This visual response is induced by the light-pulses that are sent during the optogenetic stimulation, and are therefore unrelated to the effect of optogenetic stimulation of the GPe. Note that the response in the superior colliculus and LGN increases with decreasing stimulation frequency (Fig. 4.5). Because the rodent visual system, like humans, cannot process high frequency inputs, responses are better at lower frequencies (<10Hz).

To exclude the possibility of a laser-induced heating artifact as the source of the observed optogenetic response, an identical stimulation paradigm was employed in rats expressing an inert EYFP fluorophore in the GPe. In these animals, no significant CBV modulation by optogenetic stimulation of the GPe was observed (Fig. 4.4C), except for in the superior colliculus. It is worth noting that our laser pulse duration was substantially shorter than that previously reported to induce heating artifacts, likely explaining the absence of such a response during laser stimulation in GPe-EYFP subjects. Thus, we can conclude that all CBV-responses observed in the healthy and PD groups are due to the optogenetic stimulation itself and not due to any laser heating effects.

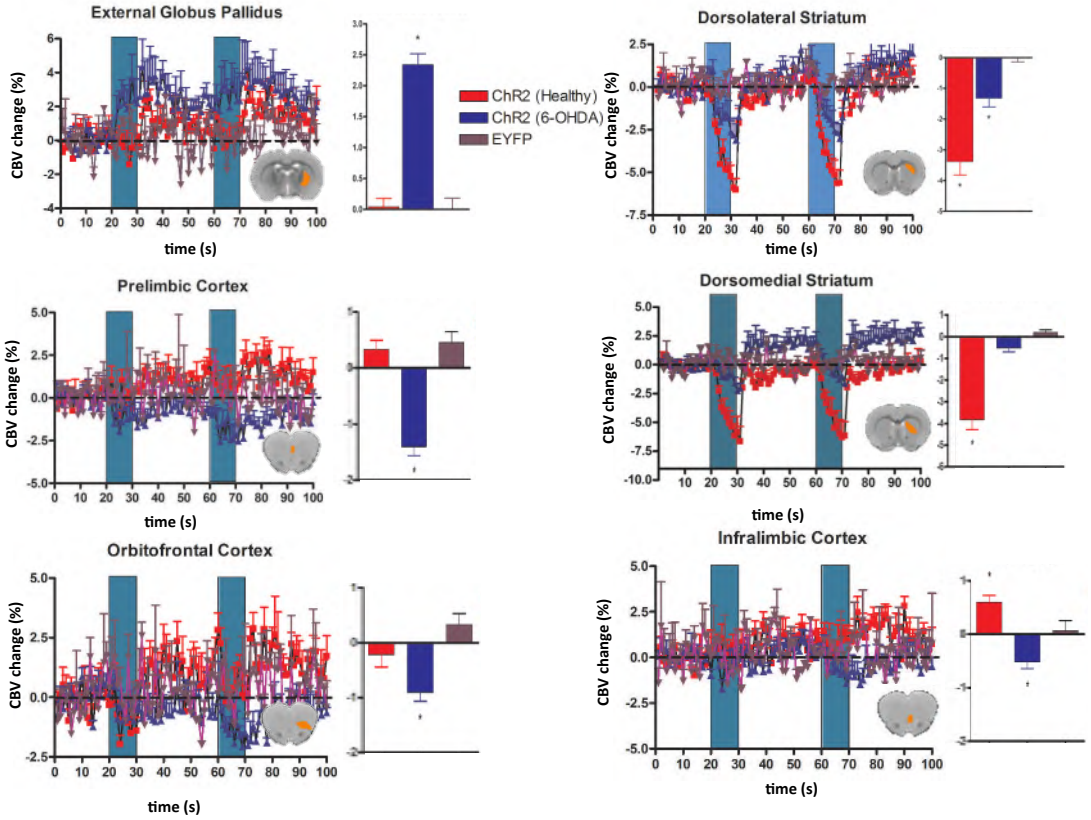

Figure 4.6: Temporal dynamics and amplitudes (bar graphs) of CBV responses by GPe-opto at 40Hz in healthy (red), Parkinsonian (blue) and control (brown) rats. All CBV responses are expressed as a percent change from pre-stimulation baseline values. Anatomically-defined ROIs are highlighted as figure inserts (single slice shown; note that many ROIs encompassed multiple slices). *$p \leq 0.05$ for controls compared to healthy and Parkinsonian rats (no other statistically significant comparisons).

For investigation of the frequency-dependency, timecourses (averaged across subjects) at 3 different stimulation frequencies were calculated (i.e. $\Delta R2^*$). Quantitative comparisons of frequency-dependent CBV modulation by optogenetic stimulation of the GPe are shown in Fig. 4.7 for healthy and PD rats, respectively. Frequency-dependency is similar between groups. Interestingly, the duration to peak CBV amplitude varied in a regions-specific manner. In general, optogenetics induced sharp decreases in CBV that returned to baseline values by the end of the stimulus ON period, and induced slow increases in CBV that returned to baseline values close to the end of the stimulus OFF period (i.e. 20s recovery period). Post-hoc testing revealed that 20 and 40Hz frequencies of optogenetic stimulation significantly altered CBV in the striatum, with a significant frequency-dependency in healthy rats. In PD rats, we did not observe a frequency-dependency in the striatum. CBV-responses in the GPe were frequency-insensitive for 20-40Hz, but significantly different from 10Hz, in both groups.

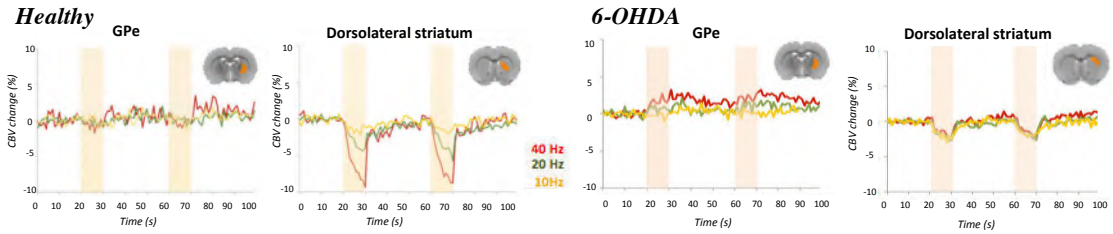

Figure 4.7: Temporal dynamics of CBV responses by GPe-opto in healthy (left) and Parkinsonian (right) for all frequencies. All CBV responses are expressed as a percent change from pre-stimulation baseline values. Anatomically-defined ROIs are highlighted as figure inserts (single slice shown; note that many ROIs encompassed multiple slices).

4.4 Discussion

In the previous study, we investigated the effect of electrical stimulation of the GPe, a potential target for DBS in PD. In this study, we performed opto-fMRI with selective stimulation of GPe neurons in healthy and Parkinsonian rats to investigate the downstream GPe-DBS response more in detail, since electrical stimulation is likely to have diffuse, off-target effects. Comparing electrical and optogenetic stimulation, we find distinct differences in the response maps, confirming fundamental differences between both stimulation approaches. Comparing healthy and Parkinsonian subjects, our data demonstrates: (1) enhanced CBV-response in the GPe, (2), reduced CBV-response in the striatum, and (3) negative prefrontal CBV-response, in PD rats, as opposed to healthy rats.

4.4.1 Optogenetics vs. electrical stimulation

In addition to electrical stimulation, optogenetic tools are being increasingly exploited for mapping functional connectivity among neural circuits. Several studies have also employed optogenetic stimulation to elucidate potential mechanisms of therapeutic DBS action at several targets (Gradinaru et al., 2009; Tye and Deisseroth, 2012; Luthi and Luscher, 2014; Creed et al., 2015). Thus, we were interested in qualitatively evaluating the functional circuit response profile obtained by optogenetic stimulation of the GPe.

Our comparison of evoked fMRI responses during electrical or optogenetic stimulation of the GPe revealed a greater capacity of electrical stimulation to modulate diverse and long-range neural circuits. In contrast, optogenetic stimulation of the GPe evoked CBV increases only within the local target region and the ipsilateral striatum. The comparison of both is shown in Fig. 4.8.

The main difference is the lack of a large positive CBV-response in prefrontal and motor cortices. The reason for these large differences in circuit modulation patterns between optogenetic and electrical stimulation is unclear, although several possibilities exist. First, it may simply be that GPe-opto was too weak to recruit detectable distal responses. However, we did get a large negative response in an extra-target area, namely the striatum. And, we observed CBV-responses in the prefrontal cortex in PD animals, confirming the ability of our optogenetics protocol to recruit downstream structures.

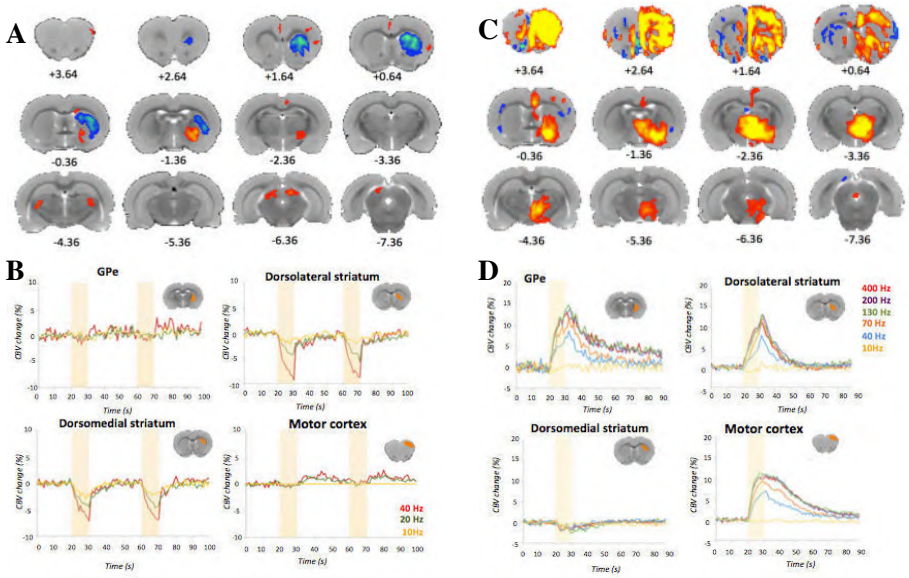

Figure 4.8: Above: Functional activation maps of CBV modulation by (A) 40Hz GPe-opto and (C) 40Hz GPe-DBS in healthy rats. Below: temporal dynamics of CBV responses by (B) GPe-opto and (D) GPe-DBS in healthy rats, across stimulation frequencies. All CBV responses are expressed as a percent change from pre-stimulation baseline values. Anatomically-defined ROIs are highlighted as figure inserts (single slice shown; note that many ROIs encompassed multiple slices).

A second possibility concerns more fundamental differences between these stimulation approaches. Specifically, while electrical stimulation may recruit all neural circuit elements within the target region (including afferent and passing fibers), optogenetic stimulation is generally confined to the opsin-expressing neurons and their efferent fibers. Thus, it is possible that extra-target areas modulated by DBS are downstream of passing fiber recruitment and antidromically-stimulated target afferents. However, such off-target effects might be important for therapeutic DBS. Gradinaru and colleagues compared the therapeutic efficacy of electrical and optogenetic high frequency stimulation of the STN in hemiparkinsonian rats (Gradinaru et al., 2009). They reported that optogenetic stimulation was unable to effectively reduce the motor symptoms, as opposed to electrical stimulation that was characterized by successful motor recovery. In addition, optical stimulation of motor cortical afferents to the STN, or motor cortex directly, has been shown to reduce pathological turning behavior in PD models. These findings support the hypothesis that antidromic stimulation effects may contribute to the therapeutic efficacy of DBS in motor disorders (Li et al., 2012; Dejean et al., 2009; Grill et al., 2008). Similarly, the GPe is the source of several non-reciprocal inputs that may be antidromically-driven by DBS, and modulation of these "upstream" areas may be therapeutically relevant.

Next, we explain why electrical stimulation of the GPe can influence upstream areas in addition to downstream areas. The GPe has two major reciprocal connections, namely with (1) the STN (and adjacent lateral hypothalamic area) (DeVito and Anderson, 1982; Harnois and Fillion, 1982; Kim et al., 1976; Kuo and Carpenter, 1973) and with (2) the striatum. Within the subthalamo-pallidal system, the GPe sends inhibitory input to the STN, and the STN sends in turn excitatory input to the GPe. Within the pallido-striatal system, the striatum sends inhibitory input to the GPe, and the GPe sends inhibitory input back to the striatum. Like in the pallido-striatal system, distinct regions of the STN may influence wider pallidal regions than it receives input from (Gittis et al., 2014; Parent and Hazrati, 1993; Smith et al., 1998). In other words,

while downstream projections from the various striatal regions are generally conducted via separate trajectories from the striatum to the GPe and from the GPe to the STN, such separation is apparently not strictly maintained in the upstream projections from the STN to the GPe and from the GPe to the striatum. Thus, separation of circuits is maintained downstream (i.e. the striato-pallido-subthalamic direction) but not upstream (i.e. the subthalamic-pallido-striatal direction). Consequently, a small substructure of the STN can influence greater parts of the striatum along upstream trajectories.

In addition, Mallet et al. recently discovered GABAergic projections from the GPe to striatal projection neurons and interneurons. This means there are two types of GABAergic neurons present in the GPe with distinct temporal, structural, physiological and molecular profiles. About two third of the GPe neurons are parvalbumin-expressing neurons that fire antiphase to the STN, and about one third of arkypallidal-expressing neurons fire in-phase with the STN, targeting the STN and the striatum, respectively. These recently identified arkypallidal-expressing neurons present the largest complement of external GABAergic projections to the striatum. The authors conclude that this newly identified bi-fold organization with distinct properties within GPe is fundamental to normal dopamine-intact GPe functioning. Further research is necessary to determine the therapeutic properties of these projection neurons in the context of GPe-DBS (Abdi et al., 2015; Mallet et al., 2012).

The attentive reader might have noticed the high degree of similarity between the activated networks induced by 40Hz of SNr-DBS (see Fig. 3.3 in chapter 3) and 40Hz of GPe-opto. The main similarity is the lack of the large positive prefrontal cortical response in the SNr-DBS group (and GPe-opto group) compared to the GPe-DBS group. This phenomenon might be explained by two mechanisms, namely the recently reported direct GABAergic GPe-FC projections (Saunders et al., 2015) and the passing fibers from the Internal Capsule (IC). The IC is a large white matter structure with fibers going to and coming from the cerebral cortex, and lies in close proximity to the targeted area within the GPe. In contrast, no direct SNr-FC projections have been reported and the passing fibers from the Cerebral Penduncle (CP), a white matter structure that lies next to the SNr, is much smaller than the IC and is further located form the area we targeted within the SNr. Taken, together this might explain the lack of prefrontal cortical response in the GPe-opto group as well as in the SNr-DBS group.

Note that optogenetics has a lower temporal spasticity compared to deep brain stimulation, meaning optogenetic stimulation is characterized by a much smaller volume of tissue activated (VTA). The irradiance in brain tissue during optogenetic stimulation can be calculated using Deisseroth's model for irradiance (Yizhar et al., 2009). The model is based on direct measurements in mammalian brain tissue and on a mathematical model of light propagation in brain tissue taking into account light absorption, scattering and geometric dispersion. For our experimental set-up (i.e. 473nm wavelength, 16mW power from fiber tip), 0.065mm fiber core radius, 0.22 fiber numerical aperture) the irradiance value is about 0.8mW/mm^2 at 0.125mm from the fiber tip and 0.2W/mm^2 at 0.5mm from the fiber tip. Thus, we could conclude that the optogenetic stimulation activates about 0.125mm^2 volume of tissue, as opposed to the estimated 1 mm^2 of VTA in the electrical stimulation (with 0mm distance between poles). Note that the heating effect (which can cause undesirable differences in membrane potential and spontaneous spiking) at 473nm might expand over a larger volume of tissue than the VTA, however we used a small pulse width with low duty cycle to reduce the risk. Moreover we did not observe any heating effects in the opsin-negative control animals.

4.4.2 Healthy vs. Parkinsonian subjects

As explained in section 1.2, it is well known that beta-oscillations under dopamine depletion become synchronized in the STN and GPe, which are strongly correlated to PD motor issues. In addition, studies have indicated that the direct and indirect pathways modify after dopamine depletion due to rewiring of the basal ganglia. Comparing healthy and Parkinsonian subjects, we find distinct differences in the response maps, confirming the rewiring of the basal ganglia associated with PD. As shown in Fig. 4.9, our data demonstrates: (1) enhanced CBV-response in the GPe, (2), reduced CBV-response in the striatum, and (3) negative prefrontal CBV-response, in PD rats, as opposed to healthy rats. These three effects are discussed below.

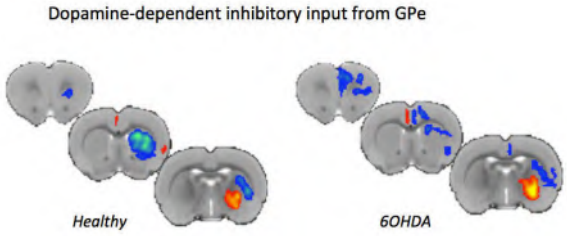

Figure 4.9: Comparison of mean functional response maps of CBV modulation by 40Hz GPe-opto in (A) healthy (n=5) and (B) Parkinsonian (n=5) rats, in three axial slices, demonstrating the three main differences in PD subjects: bottom slice: enhanced CBV in the GPe; middle slice: reduced CBV in the striatum; top slice: negative CBV in the prefrontal cortex.

4.4.2.1 Enhanced positive CBV-response in the GPe

Dopamine depletion has long been known to alter striatal circuit connectivity. One striking example of such a connectivity change reported, were the alterations in striatal feedforward inhibition (Gittis et al., 2011). Specifically, fast spiking interneurons (i.e. the major drivers of feedforward inhibition in the striatum) preferentially target direct pathway neurons under normal conditions. Following dopamine depletion, innervation patterns of these interneurons change dramatically, with enhanced, preferential input to indirect pathway neurons (see Fig. 4.10) (Kravitz et al., 2010; Albin et al., 1989; DeLong, 1990). This finding suggests the possibility that the indirect pathway is enhanced in response to dopamine lesioning, possibly as a compensatory mechanism for reduced direct striatonigral output, caused by the injection of 6-OHDA. Downstream of the striatum in the GPe, dopamine loss has also been shown to alter circuit connectivity (Mallet et al., 2012; Abdi et al., 2015). For example, pallido-subthalamic neurons show decreased firing rates, while pallido-striatal neurons show more tightly-coupled firing rates (Abdi et al., 2015). This data may similarly be explained by enhanced striato-pallidal output, although this remains to be tested.

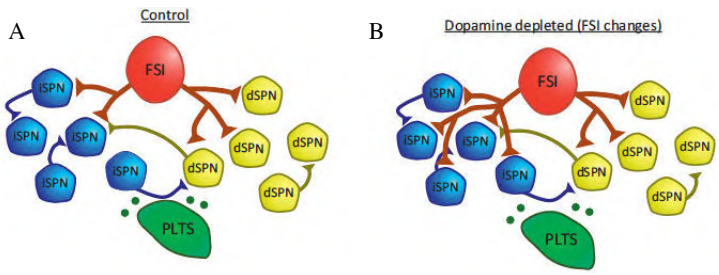

Figure 4.10: Innervation pattern of interneurons in (A) a normal situation (without dopamine depletion), and in (B) a PD situation (with dopamine depletion). Abbreviations: **FSI**: fast-spiking interneuron; **iSPN**: indirect pathway neurons; **dSPN**: direct pathway neurons; **PLTS**: persistent low-threshold spiking interneurons (Figure adopted from Gittis and Kreizer, 2012).

Our study confirms the above described circuit changes in the indirect pathway by dopamine loss. We hypothesize that striato-pallidal drive is enhanced in PD animals. Thus, the efficacy of the indirect pathway in the Parkinsonian state is enhanced, hereby "boosting" GABA-ergic projections to the GPe. Consequently, the reduced basal activity in the Parkinsonian state might lead to stronger CBV responses in PD rats.

4.4.2.2 Reduced negative striatal CBV-response

The origin of the negative fMRI signal remains to be elucidated, nonetheless, three theoretical mechanisms have been proposed to account for the fMRI signal decreases: (1) active neuronal suppression; (2) vascular steal; and (3) depleted local oxygen levels. See section 2.1.3.4 for a more detailed explanation. The active suppression hypothesis is supported by many showing that some cortical regions can exhibit a negative BOLD response linked to activation in the opposite hemisphere (Tootell et al., 1998, Shmuel et al., 2002). Although it may be intuitive to interpret our data as stimulus-induced striatal inhibition, the situation appears to be particularly muddled in the striatum, wherein dopaminergic neurotransmission has been hypothesized to induce vasoconstriction independent of direct activity changes within striatal neurons (Hsu et al., 2014). Since the injection of 6-OHDA causes dopamine depletion, this neurotransmitter-mediated vasoconstriction could be reduced in PD rats, consequently leading to a reduced negative striatal response in PD animals, as opposed to healthy animals. In addition, striatal CBV decreases have previously been correlated with heightened local neuronal activity (Shih et al., 2009) or uncorrelated with neuronal activity at all (Shih et al., 2014). In light of these complexities, further work will be necessary to determine the true source of striatal CBV decreases evoked during optogenetic stimulation, and to determine whether the differences between healthy and PD subjects are due to the loss of dopamine.

4.4.2.3 Negative prefrontal CBV-response

It has long been known that the basal ganglia interact closely with the frontal cortex (Alexander et al., 1986) and that damage to the basal ganglia can produce many of the same motor or cognitive impairments as damage to the frontal cortex (Brown et al., 1997; Middleton & Strick, 2000). It has been hypothesized that the basal ganglia modulates the prefrontal cortex indirectly through the thalamus, which is regulated by the inhibitory indirect and direct pathway of the striatum (Kravitz et al., 2010; Freeze et al., 2013). But recently, direct interactions between the GPe and the prefrontal cortex (PFC) have been demonstrated that this projection is made up of GABAergic and cholinergic neurons (based on electrophysiological recordings). Additionally the authors stated that inhibition of this GPe–PFC projection is sensitive to dopamine (D2) receptor signaling. Therefore, this pathway opens new possibilities for pharmacological treatment of neuropsychiatric disorders, where drugs target dopamine receptors in the basal ganglia in order to modulate frontal cortices (Saunders et al., 2015). Our GPe-opto data could be explained by the presence of this direct interaction between the GPe and the PFC. Alternatively, downstream effects of other circuits might also contribute to the GPe response. However, unexpectedly, our data demonstrates negative CBV-responses in all Parkinsonian rats, but no CBV-responses at all in all healthy rats. It is unclear why we only see a detectable response in PFC structures in Parkinsonian rats, and not in healthy rats. The strength of using fMRI as a measuring tool for the effect of optogenetic stimulation is the relatively unbiased nature of this imaging method, leading to discovery of unexpected responses. Complementing these findings

with, other techniques, such as electrophysiological recordings, are necessary to further explore the properties of this circuit.

Taken together, this study confirms rewiring of the basal ganglia in PD animals, since there are distinct differences in the measured connectivity profiles of healthy and Parkinsonian rats. Further research is necessary to evaluate whether the PD-induced alterations are due to the loss of dopamine depletion itself, or due to the indirect effect of it, such as changes in the indirect pathway.

4.4.3 Limitations

There are several limitations to the present study to consider. Firstly, there are limitations related to preclinical fMRI studies, namely: (1) the usage of anesthesia, which may alter the responsiveness of neural circuits to the effects of optogenetics, causing an underestimation or complete suppression of the CBV-response in certain brain structures; (2) the use of an acute stimulation paradigm, which was necessary in the context of our experimental MR setup. Similar OFF-ON-OFF paradigms are traditionally used in evoked fMRI studies (Knight et al., 2013; Lai et al. 2014), although they may provide a biased perspective on stimulus-evoked changes in functional connectivity. A recent report by Ewing and Grace highlights the importance of studying DBS network effects under chronic stimulation conditions over more translationally relevant timespans (i.e. days or weeks) (Ewing and Grace, 2013). Functional connectivity MRI, which does not require within-session baseline ("OFF") periods, provides an ideal experimental measure for future longitudinal examinations of effects of electrical or optogenetic stimulation across time and brain regions; (3) the artifact of the optical fiber affects the quality of the EPI around the fiber, potentially causing underestimation of the CBV response at the site of the fiber. Yet, compared to DBS-fMRI where a metal DBS-electrode is implanted in a brain structure, the artifact is much smaller with opto-fMRI. In addition, our data shows clear ipsilateral CBV responses, and therefore we can conclude the design of our opto-fMRI experiment minimizes the bias introduced by this artifact; (4) Deviations in the viral injection site and fiber placement, smaller than the spatial resolution of the MR images, may lead to large differences in response. However, our group-analysis indicates small inter-subject variability, indicating minimal bias due to the variation in viral injection or fiber placement; (5) optogenetic stimulation might cause temporary changes in cellular activity that might be overlooked with fMRI.

Besides limitations associated with preclinical fMRI studies, there are some limitations associated with the use of optogenetics, namely the reduced degree of specificity of the vector used, and the fact that translational research of optogenetics is highly challenging. Targeting specificity depends on multiple overlapping mechanisms, such as viral expression, the need for distinct viral tropisms for different cell types (Nathanson et al., 2009; Burger et al., 2004;), as well as on the use of cell-type-specific promoters to drive expression of the transgene (Nathanson et al., 2009; Dittgen et al., 2004; Jakobsson et al., 2003; Brenner et al., 1994). For example, when comparing expression of transgenes under the same promoter with AAV2 or LV, LV vectors were biased to transduction of excitatory neurons whereas AAV2 vectors expressed more in inhibitory neurons in the mice somatosensory cortex (Nathanson et al., 2009). And, AAV5 has shown to transduce larger volumes, i.e. a higher degree of viral spread, in both rodents (Burger et al., 2004; Paterna et al., 2004) and primates (Markakis et al., 2010). LV is characterized by a lower viral spread and thus can be used to target for example

hippocampal substructures. We chose to work with AAV5, which is among the most widely used AAV vectors, which transfect a larger volume of tissue, display low immunogenicity and are considered safer than LV (i.e. BSL1, compared with the BSL2+ for LV). However, some studies demonstrated selective retrograde transport of AAV5 along axon terminals, in addition to transducing cell bodies at the site of injection, thereby mediating gene expression in remote cell bodies having axons that terminate in the injected structure (Watakabe et al., 2015; Aschauer et al., 2013; Cearley and Wolfe, 2006; Burger et al., 2004). It is well known that optogenetics is characterized by a high spatial specificity because only *a priori* specified local neurons, and no incoming afferents, are transduced (e.g. Pama et al., 2013; LaLumiere, 2011; Lee et al., 2010). However, this possible axonal-transduction property (shared with rabies viruses, pseudotyped LVs, some other AAVs, and pseudorabies viruses (Miyamichi et al., 2011; Kato et al., 2011; Callaway, 2008; Kato et al., 2007; Burger et al., 2004; Kaspar et al., 2002) might diminish the expected specificity of the vector. But, it has to be noted that virus and promotor specificity, observed in a certain brain structure of a certain organism in one study, cannot readily be translated to other brain structure or organism of another study. Therefore, findings and promoter and tropism strategies of different studies cannot be generalized. Note, that this possible axonal transduction could be validated in our experimental set-up by using confocal images at the CPu to verify whether the EYFP signals arise from projection terminals or cell bodies.

The challenge of building an optogenetic system involves several steps, each presenting distinct translational challenges, such as inserting opsins into an *a priori* specified group of neurons, piping in sufficient light, and illuminating a volume of tissue with the proper pattern. Although the creation of a transgenic human application involving germline modification is not feasible, it is believed that the use of optogenetics through viral delivery in a gene therapy setting might be a potential clinical application in the long run (Chow et al., 2013). New delivery methods that improve gene therapy safety, such as self-regulating and self-inactivating vectors or nonviral genetic delivery packages, have been developed. In addition, some viral vectors, such as AAV, are now considered generally safe by regulatory bodies, so that the remaining safety issues concern the transgenes, rather than the viral delivery vectors themselves. Currently, there are several gene therapy trials on-going for the treatment of PD (Berry et al., 2011). And, optogenetic modulation using ChR2 in human neurons has been successfully demonstrated (Weick et al., 2010).

Management of energy in an optogenetic system is challenging because optogenetics is very inefficient at stimulating neuronal activity as opposed to electrical stimulation. The currently available opsins require a thousand times higher power investment to affect an equivalent volume of tissue. This created temperature fluctuations, the need for too large devices and shorter implant lifetimes. New and more sensitive opsins and opsins with lower duty cycles might provide a solution (Yizhar et al., 2011). Because the risk-benefit ratio of optogenetics is largely unknown, a lot of research is required to clear the clinical translational obstacles. Optogenetics as a neuromodulation therapy in humans is believed to be possible, but direct application is still far away (Bullmore, 2012; LaLumiere, 2011). However, using optogenetics as a complementary tool for a better understanding of the mechanisms underlying current clinical treatments is promising.

4.5 Conclusion

The ultimate goal of our research is to identify and investigate therapeutically effective DBS-targets within the circuit modulated by DBS. In this study, we aimed to explore the GPe as a non-canonical target for DBS in Parkinson's disease. Therefore, we performed opto-fMRI with selective stimulation of GPe neurons in healthy and Parkinsonian rats to investigate the downstream GPe-DBS response more in detail, since electrical stimulation is likely to have diffuse, off-target effects.

This study provides an in-depth characterization of the functional connectivity of the GPe, in both healthy and parkinsonian rodents. Our data clearly do not conform to the traditional model of the GPe as a straightforward relay nuclei; modulation of several noncanonical downstream circuits was observed, including prefrontal cortex and striatum. Our finding of reduced striatal vasoconstriction during GPe stimulation in parkinsonian animals is strongly suggestive of pallidostriatal circuit rewiring in the dopamine-depleted state. Future studies will address the electrophyiological correlates of this disease-altered striatal fMRI signal.

4.6 Original contributions

The work presented in this chapter resulted in an international conference contribution (see [13] in list of conference contributions). The results of this study are in preparation to submit to the peer-reviewed A1 journal *NeuroImage* (see [4] in list of publications) (shared first author). Dan Albaugh and the author of this section both equally contributed to this study.

Part III

Epilepsy:
Hippocampal DBS

Chapter 5

Investigation of the Effect of Hippocampal DBS on the Glucose Metabolism using PET

5.1 Introduction

As explained in chapter 1, deep brain stimulation (DBS) is a widely accepted treatment for advanced Parkinson's disease (PD) (Okun, 2012; Bronstein et al., 2011) and is a promising therapy for other neurological and psychiatric disorders, such as refractory epilepsy (Vonck et al., 2013; Fischer et al., 2010; Boon et al., 2009). Currently, hippocampal DBS (hDBS) is an experimental treatment for refractory epilepsy (Sprengers et al., 2014). It is strongly believed that the hippocampal formation is involved in seizure initiation in drug resistant epilepsy, and it has the lowest seizure threshold of all brain structures (Theodore and Fischer, 2007; Morrell, 2006; Spencer, 2002). Therefore, the hippocampus has been selected as an alternative DBS target to the anterior nucleus of thalamus (ANT), which is already FDA (Food and Drug Administration) approved for DBS-therapy of refractory epilepsy (Fischer et al., 2010). Velasco et al. discovered that unilateral hDBS decreased interictal and ictal epileptiform activity in refractory TLE patients (Velasco and Fischer, 2014; Velasco et al., 2007; Velasco et al., 2001). These findings were confirmed in other clinical trials (Cuckiert et al. 2014; Boon et al., 2007; Osorio et al., 2005; Vonck et al., 2002) and in animal experimental studies (Akman et al. 2011, Wyckhuys et al., 2009; Goodman et al., 2005). The refractory epilepsy center at Ghent's university hospital has over a decade of experience with hippocampal DBS as a treatment for refractory epilepsy. A seizure frequency reduction of at least 90% was reached in more than half of the patients treated (Vonck et al., 2013). Despite its remarkable clinical success, the precise mechanism of action of hDBS remains to be elucidated. A better understanding of the neuronal networks modulated by hDBS is therefore required to improve treatment efficacy. Since research in patients is restricted because of ethical and practical reasons, animal research becomes indispensable.

The preclinical investigation of hDBS is one of the main focuses of the Laboratory for Experimental and Clinical Neurophysiology, Neurobiology and Neuropsychology (LCEN3) of Ghent University. In 2010, a collaboration between the small animal imaging lab (INFINITY) and LCEN3 lead to the investigation of hippocampal DBS on the regional cerebral blood flow,

(rCBF) using small animal Single Photon Emission Computed Tomography (SPECT). Interestingly, this study revealed DBS-induced hypoperfusion in both hippocampi. Moreover a clear distinction in spatial extent and intensity of hypoperfusion was observed between stimulation parameters. A SPECT scan is primarily used to visualize cerebral blood flow and only provides an indirect measure of the brain's metabolism. Extra research is thus necessary to confirm that this hypoperfusion is caused by actual DBS-induced decreases in the brain's metabolism, as opposed to pure DBS-induced vasoconstriction. PET is the only imaging modality that allows the direct measurement of the glucose metabolism. Therefore, in this study, we aimed to employ 2-deoxy-2-[^{18}F]fluoro-D-glucose (^{18}F-FDG)-PET to investigate the effect of hippocampal DBS on the glucose metabolism, in the same experimental set-up as used in the SPECT-study.

We chose Poisson distributed stimulation over regular distributed high frequency stimulation because irregularity in interpulse intervals seems to induce more potent anti-seizure effects (Wyckhuys et al., 2010a; Wyckhuys et al., 2007). It has also been suggested that Poisson distributed DBS may cause disruption of the generation and propagation of synchronous epileptic activity (Cuellar-Herrera et al., 2006). Moreover, we decided to investigate the effect of DBS in the healthy brain in order to rule out the diseased brain as a confounder.

5.2 Materials & methods

5.2.1 Animals

Seven adult male Sprague-Dawley rats (200–250g body weight; Janvier, France) were used for this experiment. All rats were treated according to guidelines approved by the European Ethics Committee (decree 2010/63/EU). All experimental procedures were approved by the Animal Experimental Ethical Committee of Ghent University Hospital (ECD 13/14). The animals were kept under environmentally controlled conditions (12h normal light/dark cycles, 20-23°C and 40-60% relative humidity) with food and water *ad libitum*.

5.2.2 Surgery

The rats were anesthetized with an isoflurane mixture (2–5% isoflurane and medical O_2). After exposure of the skull, five small burr holes were drilled: four for the positioning of nylon anchor screws (Bilaney consultants GmbH, Germany) and one for insertion of the quadri-polar DBS-electrode. This DBS-electrode was inserted stereotactically in the right hippocampus (AP -5.6mm, ML 5.2mm, DV -7.4mm relative to bregma) (Paxinos and Watson, 2007), as illustrated in Fig. 4.1a.

Each DBS-electrode was custom-made by twisting together four polyimide coated stainless steel wires. The most ventral and dorsal electrode contact (Bilaney, Germany), with 125μm diameter, were used for stimulation purposes. The distance between the tips was 3mm. The two inner wires (California Fine Wire, CA, U.S.A.), with 70μm diameter, were used for electro-encephalographic (EEG) recording. The distance between these two tips was 0.5mm. The design of the electrodes is based on previous studies of DBS in rat models for TLE, where bipolar DBS with a 3mm gap between poles was shown to be therapeutically effective (Van Nieuwenhuyse et al., 2015; Wyckhuys et al., 2010a; Wyckhuys et al., 2007). The two inner wires were used for intracranial electro-encephalographic (iEEG) recording. The distance between these two tips was 0.5mm. The electrode and its placement are illustrated in Fig. 5.1.

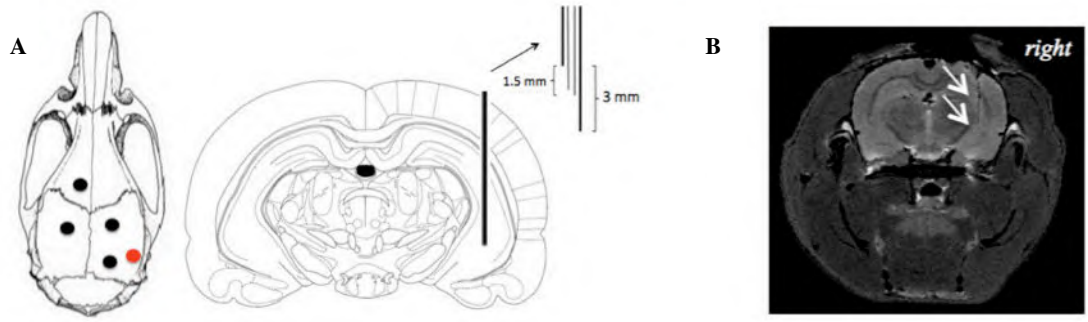

Figure 5.1: (A) The quadri-polar electrode was stereotactically implanted in the right hippocampus (AP -5.6, DV -7.4, ML +5.2 relative to Bregma (Paxinos & Watson, 2007)) together with four anchor screws. The outer two electrodes are used for stimulation and the inner two electrodes for EEG. The red dot represents the electrode insertion location on the skull. The black dots indicate anchor screw positions. (B) MR images, acquired after careful removal of the electrode, were used to verify the electrode track position. For all rats the electrode track was located in right the hippocampus.

For impedance optimization, all electrodes were electrolytically cleaned. The impedance was checked immediately before implantation and did not exceed 45kOhms (IMP-2, Bak electronics, Sanford Florida, USA). One additional polyimide coated stainless steel wire (Bilaney, Germany), with 125µm diameter, was inserted subcutaneously as a ground. The DBS-electrode and the ground-electrode were attached to a connector that was fixed to the screws and the skull with acrylic dental cement. Rats were allowed seven days of post-surgical recovery, during which they were handled.

5.2.3 Deep Brain Stimulation

All rats were subjected to the same DBS paradigm, namely a bipolar Poisson distributed unilateral hippocampal stimulation. The stimulation itself consisted of a series of biphasic, charge-balanced square-wave pulses with a pulse width of 100µs. The mean frequency of the stimulation paradigm was 130Hz and the inter-stimulus intervals were Poisson distributed with a mean and variance of 1/130s. Pulses were delivered to the outer two electrode contacts of the quadri-polar MR-compatible DBS-electrode using a constant current linear isolated stimulator, which was triggered by a data acquisition card (NI-DAQ USB-6343, National Instruments, Austin, TX, U.S.A.) that was connected to a standard PC.

The stimulation was applied continuously for 60 minutes. For each rat the stimulation intensity was determined individually (i.e. thresholding), one day after the post-surgical recovery period. The stimulation intensity was set at 60% of the stimulus intensity giving rise to an epileptic seizure. This seizure threshold was determined iteratively by applying 15s of stimulation, followed by 60s of rest, during which the iEEG was evaluated for epileptic discharges. For every stimulation episode, stimulation intensity was augmented with 25µA until an ictal discharge was observed on the iEEG. The EEG-signal was amplified using a custom made amplifier (gain 510) and connected to same data acquisition card used to trigger the current source. Ictal discharges were characterized on the iEEG by spiking activity with an amplitude exceeding at least three times the baseline amplitude and with a frequency exceeding 5Hz for at least 10 seconds (Wyckhuys et al., 2010b; Williams et al., 2009; White et al., 2006). Both the thresholding process and the DBS during the PET experiment itself were applied when the rat

was awake. Because the stimulation intensity causing the ictal discharge was subject-dependent, the length of stimulation is dependent on the subject during the thresholding step, preceding the actual imaging experiment. During the experiment the length of stimulation was the same for all subjects. Every rat received exactly one hour of DBS preceding the PET acquisition, from which 30 minutes were during tracer uptake.

5.2.4 Data acquisition

Each rat underwent three PET scans at three different time-points: one before surgery (i.e. baseline condition), one 9 days after surgery (i.e. surgery condition) and one after one hour of DBS (i.e. stimulation condition), 10 days after surgery. The general PET imaging was the following. All animals were food deprived for at least 18h prior to PET imaging. Rats were shortly anesthetized with an isoflurane mixture (2–5% isoflurane and medical O_2) to insert a catheter in one of the tail veins for tracer injection. This was done at least one hour before tracer administration in order to avoid the effects of anesthesia as a possible confounder for the experiment. Next, animals were, while awake, intravenously injected with 28.1±1.8MBq of ^{18}F-FDG (Ghent University Hospital, Belgium) dissolved in 200µl saline. Thirty minutes after tracer injection, the animals were placed under general anesthesia using an isoflurane mixture (2–5% isoflurane and medical O_2) and a 30-minutes PET scan was acquired in list-mode on a microPET scanner with a 75mm axial field-of-view and a 1.5mm spatial resolution (FLEX Triumph II, TriFoil Imaging®, Northridge CA). Animals were placed in the center of the field-of-view, in a prone position, receiving further anesthesia through a nose cone. The rat body temperature was maintained at ~37°C by a heated bed. The imaging protocol for the third PET scan (i.e. stimulation condition) required some additional actions on top of the general PET imaging protocol. The intravenous injection with 28.1±1.8MBq was done 30 minutes after starting hDBS and stimulation was not interrupted during injection of ^{18}F-FDG. Stimulation was delivered to the rat by means of a flexible cable and a commutator, allowing the rat to move freely. Continuous EEG recording was performed throughout the delivery of stimulation to evaluate for EEG abnormalities during DBS. Then, stimulation was interrupted, rats were anesthetized and moved to the PET scanner, after which a 30 minutes PET acquisition was initiated, followed by CT. After the last PET scan, rats were sacrificed, the DBS-electrode was removed with high caution and an MR-scan was acquired. Fig. 5.2 depicts the experimental imaging protocol.

The acquired PET images were reconstructed into a 200x200x50 matrix by a 2D Maximum Likelihood Expectation Maximization (MLEM) algorithm (LabPET Version 1.12.1, TriFoil Imaging®, Northridge CA) using 100 iterations and a voxel size of 0.5 x 0.5 x 1.175mm^3 (x, y, z). Each PET-scan was followed by a Computed Tomography (CT) scan, acquired for co-registration purposes, on the same scanner. CT projection data were acquired using the following parameters: 256 projections, detector pixel size 50μm, tube voltage 75kV, tube current 500μA and field-of-view 59.2mm. CT images were analytically reconstructed using the filtered back projection reconstruction software of the scanner into a 512x512x512 matrix with 100μm isotropic voxel size. Each resultant CT image is inherently co-registered with the corresponding PET scan.

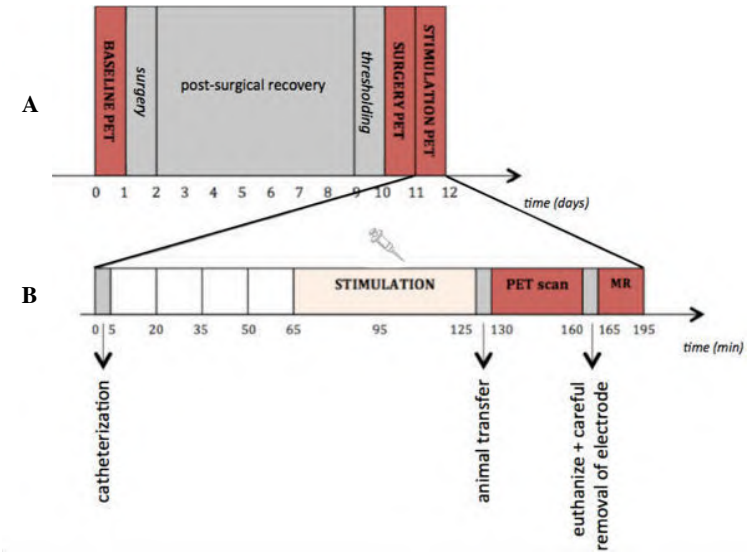

Figure 5.2: (A) Timeline of the experimental imaging protocol. (B) Sequence of actions of the last day of imaging. Before intravenous injection with 28.1±1.8MBq of ^{18}F-FDG rats received 30 minutes of hDBS. Stimulation was continued during and 30 minutes following tracer administration. Then, stimulation was interrupted, rats were anesthetized and moved to the PET scanner, after which a 30 minutes PET acquisition was initiated, followed by CT. Finally rats were sacrificed, the DBS-electrode was removed with high caution and an MR-scan was acquired.

After termination of all PET-CT scans, rats were sacrificed with pentobarbital (120mg/kg, i.v.) and the electrodes were carefully removed. Subsequently, rats underwent a magnetic resonance (MR) scan to obtain anatomical information and to verify electrode position. MR images were acquired on a 7 Tesla-system (PharmaScan 70/16, Bruker, Ettlingen, Germany) with a dedicated rat brain volume RF send/receive coil. Fixation of the head of the animal was achieved using the tooth and ear bars of the Bruker MR bed, before placement inside the magnet. In this way, the electrode is positioned as perpendicular as possible in comparison with the scanner bed. T2-weighted anatomical images, with a 100μm isotropic voxel size, were obtained using a RARE (Rapid Acquisition with Relaxation Enhancement) sequence. MR images were co-registered to CT, based on anatomical reference points, providing a registration between PET, MRI and CT. This way, an accurate anatomical correlation and electrode track position verification was possible.

5.2.5 Data-analysis

As each rat underwent three PET scans we divided the acquired PET data into three groups: (1) baseline condition-group, (2) surgery condition-group, (3) stimulation condition-group. Two rats were excluded from statistical group-analysis in group 2 and 3, meaning that only 5 datasets could be included in group 2 and 3. One of these animals was showing wet dog shakes and ictal activity on the EEG during administration of hDBS and tracer uptake, even though we took only 60% of the threshold for ictal activity. Wet dog shake behavior has been studied in different models of epilepsy in the rat and is associated with limbic seizures (Rondouin et al., 1987). We decided to exclude also a second animal since an irregular lesion was observed in the MR image of the animal, as indicated in Fig. 5.3. The electrode was not implanted perpendicular, since it is visible in three consecutive slices of the MR image. The implantation left a wider track compared to the other subjects.

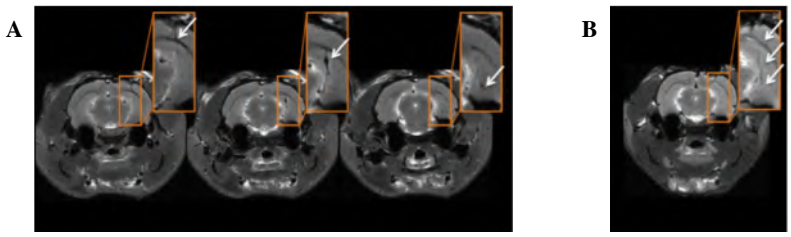

Figure 5.3: (A) Axial anatomical slices illustrating the big lesion caused by fault electrode implantation. Slices progress from most anterior at the left to most posterior at the right. The electrode track is indicated with white arrows. (B) One axial anatomical slice illustrating a typical electrode track. The electrode track is indicated with white arrows.

Further processing of the PET data was done in 4 steps. First, spatial smoothing was performed using a 3D Gaussian filter with FWHM of 1 mm. All datasets were then normalized to the global activity measured in a box drawn over the complete head of the animals to correct for physiological variations in tracer uptake. Third, all datasets from one group were co-registered onto the first animal scanned of that group using a mutual information (MI) algorithm with Powell's convergence optimization method (Press et al., 1992) implemented within PMOD (http://www.pmod.com). Fourth, a template was generated for each group, by calculating the mean value and the standard deviation in each voxel. The templates of group 2 and 3 were co-registered onto the template of group 1, also using the MI algorithm in PMOD. Finally, statistical analysis between groups was done using a voxelwise two-sample t-test, working in Matlab 2010.

To separate the effects of surgery from stimulation effects, data-analysis was undertaken three times: (1) comparison of the stimulation- and surgery condition-group (stimulation effect); (2) comparison of the surgery- and baseline condition-group (surgery effect); and (3) comparison of the stimulation- and baseline condition-group (combined effect). The p-value was determined for each voxel, indicating the significance of differences between groups and clusters (> 20 voxels) were accepted as significant if p-values were 0.01 or less after Bonferroni correction for multiple comparisons. Each resultant statistical map was co-registered onto the MR images for anatomical correlation. Additionally, all five rats from the group-analysis were analyzed individually using a voxelwise one-sample z-test to evaluate the impact of the stimulation intensity on the spatial extent and the intensity of the metabolic changes. Also, the two rats that were excluded from the statistical group-analysis were compared individually using this test-statistic.

5.3 Results

5.3.1 Template configuration

The three rat brain templates generated from the PET data, acquired in the three different conditions, are shown in Fig. 5.4. Each template is characterized by a mean image and a standard deviation image. In Fig. 5.4 only the mean images are depicted. Visual analysis of the three templates reveals hypometabolic changes in the ipsilateral hippocampus in template 2 and in both the ipsilateral and contralateral hippocampus in template 3, when comparing to template 1.

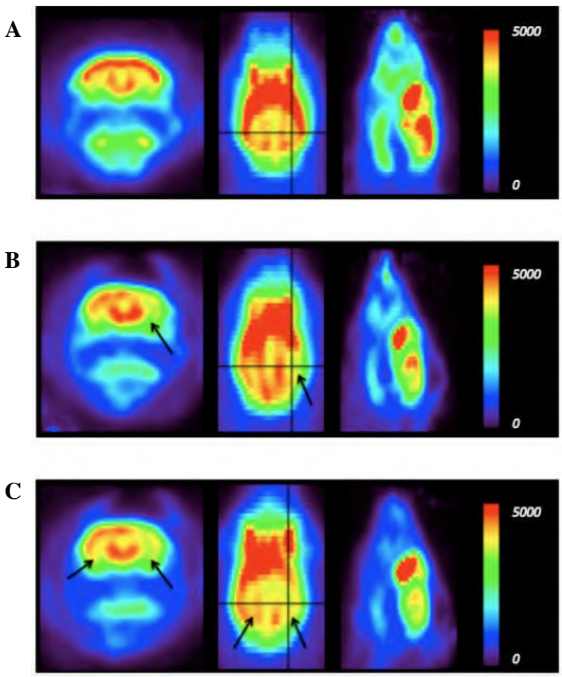

Figure 5.4: Three rat brain templates representing the mean data of their group. Axial, coronal and sagittal slices are shown on the left, middle and right, respectively. (A) Template from PET-data acquired one day before surgery. (B) Template from PET-data acquired nine days after electrode implantation and one day after determination of the stimulus intensity. Hypometabolic changes are observed in the ipsilateral hippocampus when comparing to A are indicated with a black arrow. (C) Template from PET-data acquired three days after post-surgical recovery. Unilateral hippocampal stimulation was initiated 30 minutes before tracer injection and continued during the tracer uptake for 30 minutes. Hypometabolic changes are observed in the ipsilateral and contralateral hippocampus when comparing to A and are indicated with black arrows.

5.3.2 Statistical analysis on group level

The results of the statistical group-analyses are displayed in Fig. 5.5: (1) statistical analysis between group 3 and 2, (2) statistical analysis between group 2 and 1, (3) statistical analysis between group 3 and 1, in order to investigate the 'stimulation' effect, the 'surgery' effect and the 'combined' effect, respectively.

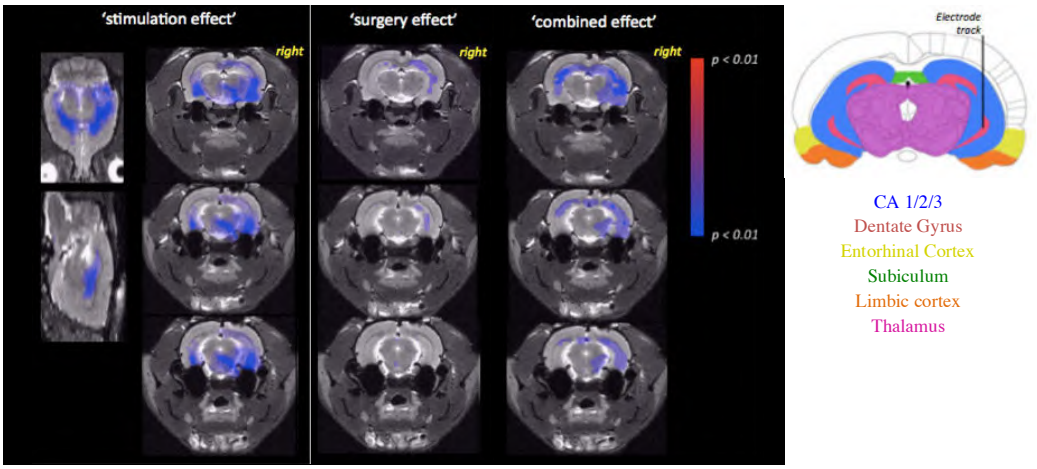

Figure 5.5: Hypometabolic t-maps resulting from statistical analysis. All t-values were converted to a corresponding p-value. (A) Hypometabolic t-map from statistical analysis between group 2 and 3. Coronal, sagittal and axial anatomical scans are co-registered with the t-map illustrating 'true' hypometabolic changes induced by hDBS, compared to the glucose metabolism one week after surgical intervention. Axial anatomical scans progress from most anterior to most posterior from top to bottom, respectively. (B) Hypometabolic t-map from statistical analysis between group 1 and 2. Axial anatomical scans are co-registered with the t-map illustrating the hypometabolic changes induced by stereotactical surgery. (C) Hypometabolic t-map from statistical analysis between group 1 and 3. Axial anatomical scans are co-registered with the t-map illustrating the 'summed' hypometabolic changes induced by hDBS and electrode implantation, compared to the glucose metabolism before surgical intervention. Axial anatomical scans progress from most anterior to most posterior from top to bottom, respectively. (D) Axial slice from rat brain atlas (Paxinos and Watson, 2007) at height of electrode. Hippocampal substructures and other limbic structures are marked in color.

Statistical group-analysis of group 3 and 2 (i.e. stimulation effect) revealed significant decreases in glucose uptake in the different structures of the hippocampal formation: the CA areas, the subiculum and the dentate gyrus; and in other limbic structures: entorhinal cortex, thalamic structures, the posteromedial part of amygdalohippocampal area, posterolateral cortical amygdaloid nucleus, amygdalopiriform cortex; from which the latter three substructures are part of the limbic cortex. Statistical group-analysis of group 2 and 1 (i.e. surgery effect) revealed very localized hypometabolic changes in the ipsilateral hippocampus due to electrode implantation. Statistical group-analysis of group 3 and 1 (i.e. combined effect) revealed hypometabolic changes in the ipsi- and contralateral hippocampus and other limbic structures. Taken together, this means DBS might have a similar effect on brain tissue as the electrode implantation itself, however the intensity and spatial extent of its effect is larger. No areas of significant hypermetabolism were detected.

5.3.3 Statistical analysis on subject level

All rats were also analyzed individually (i.e. compared to template 1) to evaluate the impact of the stimulation intensity on the spatial extent and the intensity of the metabolic changes. As mentioned before, the stimulation intensity was determined for each rat individually and was set at 60% of the stimulus intensity giving rise to ictal activity. We noticed a large variation among rats. Fig. 5.6 shows the relation between the administered stimulation intensity during hDBS and the spatial extent (Fig. 5.6A) and the intensity (Fig. 5.6B) of the hDBS induced hypometabolic changes in the ipsi- and contralateral hippocampal formation. The ipsilateral and contralateral hippocampal volumes were delineated based on an anatomical atlas of the rat brain (Paxinos and Watson, 2007). The spatial extent is characterized by the ratio of the significant (p_{corr}<0.05) hypometabolic volume in the ipsilateral and contralateral hippocampus, to the total ipsilateral and contralateral hippocampal volume, respectively. These results indicate higher stimulus intensity leads to more widespread hypometabolic changes in the ipsi- and contralateral hippocampus, although this relation is less clear in the contralateral hippocampus. The mean intensity of the DBS induced changes in the glucose uptake (i.e. mean z-score) was similar for all rats in both the ipsi- and contralateral hippocampus. These results only indicate a trend, further research is necessary in order to investigate the true relationship between the stimulation intensity and the level of hypometabolic changes.

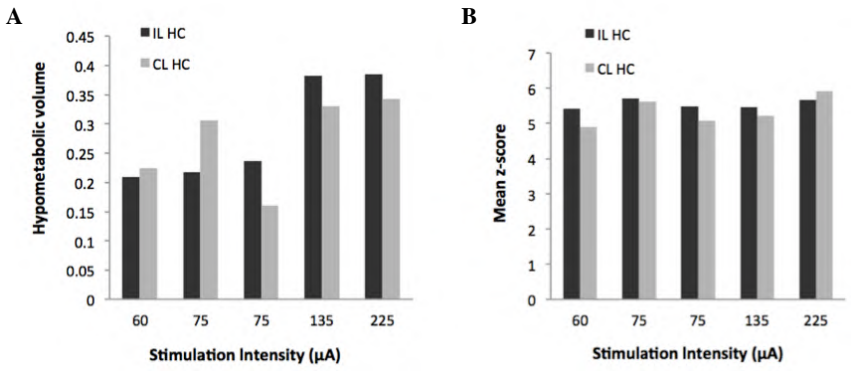

Figure 5.6: (A) Graph illustrating the relation between the stimulation intensity during hDBS and the spatial extent of the hDBS induced hypometabolic changes in the ipsi- and contralateral hippocampal formation. The spatial extent is characterized by the ratio of the significant (p_{corr} < 0.05) hypometabolic volume in the ipsilateral and contralateral hippocampus, to the total ipsilateral (ILHC) or contralateral hippocampal (CLHC) volume, respectively. (B) Graph illustrating the relation between the administered stimulation intensity during hDBS and the mean intensity of the hDBS induced hypometabolic changes in the ipsi- and contralateral hippocampal formation. The mean intensity is characterized by the mean z-score of the significant (p_{corr} < 0.05) hypometabolic volume in the ipsi- and contralateral hippocampus. Both graphs display results of individual subjects to the group1-template and subjects are sorted by increasing stimulation intensity.

5.4 Discussion

Statistical group-analysis of PET data revealed that unilateral Poisson distributed hDBS decreases the glucose metabolism in the different structures of the bilateral hippocampus, and also in thalamic and cortical limbic structures. With this study our aim was to understand how DBS affects the glucose metabolism throughout the entire healthy brain. Our experimental design allows to discriminate whether the observed changes in the glucose metabolism are due to DBS or due to the implantation of the DBS electrode or both, because scans were acquired

before and after surgical intervention. Furthermore, our study visualizes the true stimulation effect of DBS on the glucose metabolism in the brain, and is not biased by an interaction with brain pathology.

5.4.1 Whole-brain response of DBS

The current study revealed decreases in the glucose metabolism in the hippocampal formation and other anatomically connected limbic structures. This provides evidence for an interaction of hDBS with widespread limbic pathways in brain regions spatially remote from the targeted brain structure. It is well-known limbic structures and bilateral brain structures are connected. fMRI studies of the healthy rat brain have showed robust and reproducible autonomous circuits (Vedam-Mai et al., 2012; Beurrier et al., 2001). The observed bilateral synchrony of fMRI signals reflects these inter-hemispheric commissural connections, especially in brain regions with strong commissural connections such as the hippocampus (Vedam-Mai et al., 2012). This explains why we observed not only local hDBS induced changes in the cerebral glucose metabolism around the electrode tip but also remote changes in the contralateral hippocampus and anatomically connected limbic structures. Our findings suggest the hippocampus and other mesial and cortical limbic structures up- and downstream are affected by hippocampal DBS. However, it still remains to be elucidated if these structures are only temporarily affected. DBS induced changes in brain activity over time may lead to learning and plasticity in neural networks, leading to chronic changes located in the same and/or in another set of brain structures.

To our knowledge there is only one other PET imaging study of DBS in the healthy rat brain. Klein et al. investigated with ^{18}F-FDG-PET the neuronal network activity patterns in the healthy rat brain, affected by DBS of the subthalamic nucleus. They also concluded that unilateral DBS affects brain activity ipsi- as well as contralateral to the stimulation site, which implies a bilateral effectiveness (Klein et al., 2011). However, it has to be mentioned that the authors used an uncorrected p-value < 0.05 for statistical significance, meaning that they didn't correct for multiple comparisons. Since they used a Gaussian filter of 2mm FWHM for post-smoothing, the final spatial resolution of the images is limited for most of the brain structures they investigated.

A SPECT study in the healthy rat brain has been performed in our lab prior to this study, where they investigated the effect of unilateral Poisson distributed hDBS in the healthy rat on the rCBF, by means of ^{99m}Tc-hexamethylpropyl-eneamineoxime (^{99m}Tc-HMPAO)-SPECT (Wyckhuys et al., 2010b). The authors of that study observed hDBS induced hypoperfusion in the ispi- and contralateral hippocampal formation and found that the intensity of the hypoperfused region remained unaltered for all stimulation amplitudes, but that the total volume of hypoperfused tissue became more widespread and shifted contralaterally with higher stimulation intensities, meaning that higher stimulation intensities lead to larger volumes being stimulated. Our PET findings correspond with the SPECT study, since we find hDBS-induced decreases in the glucose metabolism. Moreover, we find that hypometabolic changes also become more widespread in the ipsi- and contralateral hippocampal formation with increasing stimulus intensity and that the intensity of the hypometabolic region and the stimulation intensity could not be correlated. Similar animal experimental studies have also observed a linear relationship between stimulus intensity and spatial extent of the DBS induced changes (Canals et al., 2008; McIntyre, 2004). More research needs to be done to investigate this relation between the intensity and spatial extent of hDBS induced hypometabolic changes and

the stimulation parameters used. If a correlation between DBS parameters, imaging result and seizure suppressive effect would exist, PET imaging could be used as a potential biomarker for responders to DBS.
Taken together, the earlier SPECT study and current PET study performed in our lab to investigate metabolic changes during hDBS, indicate that hDBS does cause decreases in the metabolism, suggesting an underlying functional inhibition mechanism of DBS.

5.4.2 Physiological meaning

Homeostatic downscaling mechanisms (i.e. downregulation of neuronal activity) might contribute to the explanation of the observed hypometabolic hDBS induced changes. By keeping the amplitude of stimulation below the threshold for seizure generation, no seizures are evoked, but neural circuits are subjected to a continuous and strong synaptic input. In order for these neural circuits not to become hyperactive, neurons decrease their intrinsic excitability and synaptic strength to keep their firing rates within the functional range (Turrigiano and Nelson, 2004), consequently leading to a reduced energy utilization of the synapses. It is well known the hippocampus is a highly plastic brain structure (Neves et al., 2008). Since unilateral Poisson distributed hDBS mimicks a continuous but irregular synaptic input towards the targeted area, we could expect homeostatic downscaling mechanisms are taking place, at a certain point in time during the stimulation, in the hippocampus to normalize the activity and bring the neuronal circuit to a less excitable state by reducing hippocampal excitatory glutamatergic output, consequently leading to a reduced PET signal. Importantly, these findings may explain the seizure-suppressive of DBS, since a seizure is characterized by excessive and hypersynchronous neural activity.

Our results indicate that unilateral hippocampal DBS causes significant hypometabolism in all limbic structures, ipsi- and contralateral to the stimulation side. These observations of a widespread involvement of limbic structures caused by hippocampal DBS are supported by the observed hypoperfusion in all limbic structures caused by unilateral hippocampal DBS (Wyckhuys et al., 2010b). Taken together the available cellular studies of DBS and our SPECT and PET study of DBS in the healthy rat brain, DBS likely exerts its effect not just locally but also using specific circuits, via complex modifications of the ongoing underlying molecular processes (Chang et al., 2012; Lyons et al., 2011). Besides commissural connections that connect both hemispheres, activated astrocytes might also contribute to the distal effects of inhibition induced by DBS. Astrocytes react to and communicate changes detected within their immediate external environment both locally and over networks (Vedam-Mai et al., 2012), through a complex calcium-wave induced regulation of glutamate levels in the extracellular environment of all the synapses they envelope. While astrocytic regulation might explain distal effects ipsilaterally, it is more likely the bilateral effect is explained by the commissural connections. It has to be noted that commissural fibers, especially those connecting the left and right hippocampus, are proportionally more pronounced in rats than in humans. Although connectivity studies in humans also show bilateral networks (van den Heuvel et al., 2009; Damoiseaux et al., 2006), it remains unclear whether bilateral effects of DBS will be observed in humans. Yet, bilateral DBS may hold superior efficacy to unilateral DBS in the treatment of mesial TLE (Vonck et al., 2013).

5.4.3 Limitations

The study has a number of limitations. First of all, ^{18}F-FDG-PET is limited by its spatial and metabolic resolution. Since the micro-PET scanner used in this study has a spatial resolution of 1.5mm we were able to retrieve signals from brain volumes such as the hippocampus, thalamus and limbic cortex. Considering the metabolic resolution, the hDBS induced metabolic changes should be large enough in order to distinguish them from noise. This is indeed the case, since significant metabolic changes were only present within the brain, and not in non-brain tissue in the FOV. Taking into account the spatial and metabolic resolution in the experimental set-up and data-analysis of our study, statistical group-analysis of PET data has provided us with a means to investigate hDBS induced changes in the glucose metabolism in the entire rat brain. Thus, we demonstrated that ^{18}F-FDG-PET neuroimaging studies have the potential to investigate how DBS affects the glucose metabolism throughout the entire brain, and may be a valuable tool to visualize and evaluate therapeutic effect of DBS, and the effect of various stimulation paradigms and target areas for DBS.

Secondly, the determination of the stimulation intensity, one day before the post-surgical scan, may act as a confounder of statistical analysis between PET data from before and after surgical intervention. The stimulation intensity was set at 60% of the stimulus intensity giving rise to ictal activity. Since we do not know what the impact of this short (order of seconds) ictal period might be on the post-surgical PET acquisition the next day, this process might also contribute to the hypometabolic changes observed in the group-analysis between template 1 and 2. However, comparison of the individual data of one rat, excluded from group-analysis due to an irregular lesion, to the group-data might indicate these changes are rather due to the surgical intervention or 'lesioning' than due to this thresholding process. Statistical analysis of this rat revealed more significant and more widespread hypometabolic changes in the ipsi- and additionally the contralateral hippocampus due to surgical intervention, compared to the observed changes in the group-analysis as shown in Fig. 5.7. These results coincide with literature findings (Schiffer et al., 2006). Since the thresholding process is exactly the same for all rats and the only difference in this is the larger lesion, we tend to believe it is in fact the lesioning that causes the hypometabolic changes when comparing data before and after surgical intervention.

Finally, a potential limitation of this study might be the length of stimulation, i.e. 30 min of DBS before tracer injection and 30 min of DBS during tracer uptake. There is a DBS study in epileptic patients that reports a succesful short term hippocampal stimulation in a closed loop system (van Luijtelaar and Huang, 2013), but in general hippocampal DBS in epileptic patients is administered continuously. However, this is not evidence based and it is through preclinal investigation in animals, e.g. by means of functional imaging techniques, that we should first explore both the short and long term effects, before any translation to clinical investigation is possible. Our study indicates significant short term (i.e. after 30 min) changes in brain structures relevant for epilepsy. However, certain plasticity mechanisms, such as habituation, sensitisation and homeostatic plasticity, etc., might cause additional effects. Further research needs to be done to evaluate those long term effects of DBS in healthy and epileptic subjects, both in a preclinical as well as in a clinical set-up.

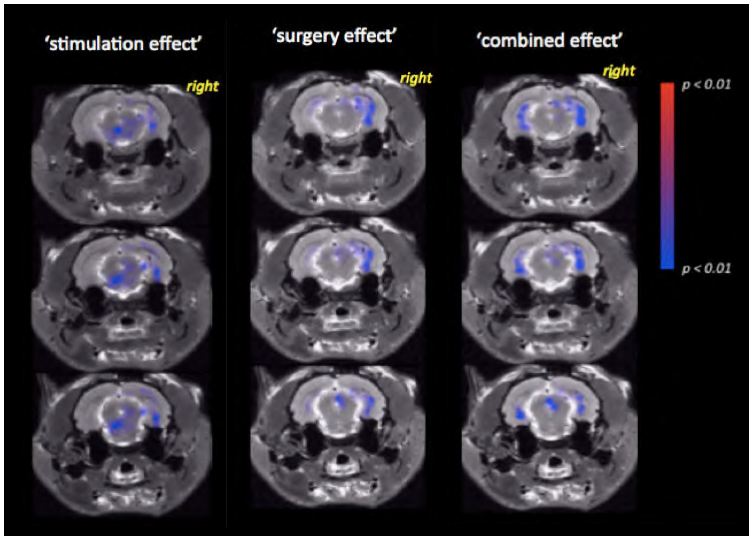

Figure 5.7: Hypometabolic t-maps resulting from statistical analysis of the rat with a bigger than regular lesion. The colors indicate the level of significance of the changes in the glucose metabolism induced by hDBS. Each time axial anatomical scans are co-registered with the t-map, and scans progress from most anterior to most posterior from top to bottom, respectively. (A) Hypometabolic t-map from statistical analysis between group 2 and this rat during hDBS. (B) Hypometabolic z-map from statistical analysis between group 1 and this rat after surgery. (C) Hypometabolic t-map from statistical analysis between group 1 and this rat during hDBS. No significant hypermetabolic changes were observed in the latter three cases.

5.5 Conclusion

Statistical group-analysis of PET-data revealed that unilateral Poisson distrubuted hDBS decreases the glucose metabolism, both in the ipsi- and contralateral hippocampus and other limbic structures. This means hDBS seems to interact with widespread limbic pathways in brain regions spatially remote from the targeted brain structure. The major contribution of this study to the investigation of DBS mechanisms, as opposed to studies on a cellular level, is that this study shows that DBS affects specific circuits, rather than just nearby tissue, due to neuroanatomical connections between limbic structures and interhemispheric commisures. This study demonstrates that hDBS causes immediate changes in the healthy rat brain and provides important additional evidence that hDBS exerts an effect on the entire circuit of the targeted structure, leading to a resultant functional inhibition of the affected areas, resulting in decreases in the glucose metabolism. Moreover, with this study we validated the results of an earlier SPECT study performed in our lab, where indirect measurements of the brain's metabolism already suggested a hypometabolic effect of DBS.

Thus, we demonstrated that ^{18}F-FDG-PET is a valuable tool to provide direct measures of metabolic responses to DBS throughout the entire brain. Consequently, ^{18}F-FDG-PET neuroimaging studies have the potential to provide better insight into the mechanism of action of DBS by simultaneously observing activity at multiple sites in the *in vivo* brain and may be a valuable tool to visualize the effect of various stimulation paradigms and target areas for DBS.

5.6 Original contributions

The work presented in this chapter resulted in two international conference contributions (see [2-3] in list of conference contributions). The results of this experiment were published in the peer-reviewed A1 journal *Molecular Imaging & Biology* (see [1] in list of publications) (first author). The surgeries discussed in section 5.2.2 were performed by Ine Dauwe. The design of the electrode, stimulation set-up, acquisition and data-analysis, were performed by the author of this chapter.

Chapter 6

Functional Circuit Mapping of the Hippocampus using Simultaneous DBS-fMRI

6.1 Introduction

DBS in the hippocampus has been proposed as an alternative treatment in case of drug resistant epilepsy. Clinical trials (Cuckiert et al. 2014; Vonck et al., 2013; Boon et al., 2007; Osorio et al., 2005) and animal experimental studies (Akman et al. 2011, Wyckhuys et al., 2007; Goodman et al., 2005) have shown promising results. More specifically, seizure frequency reduction of at least 90% was reached in more than half of the patients treated in Ghent's University hospital (Vonck et al., 2013). Despite its remarkable clinical success, the precise mechanism of action of hDBS remains to be elucidated. A better understanding of how hippocampal DBS and its stimulation parameters modulate neural circuitry, through animal research, is therefore necessary to ultimately improve treatment efficacy in patients. In our university, animal research has shown that electrical stimulation of the hippocampus results in reduced metabolism of several regions of the limbic system (chapter 5). In addition to the investigation of the glucose metabolism, it would be interesting to image whole-brain activation and functional connectivity changes during local hDBS.

fMRI allows the investigation of functional processes in the brain and is mainly used to image brain activation. This functional imaging technique can be used in both clinical and preclinical settings to evaluate the influence of brain region-specific activity upon neural circuits and networks. Stimulus-evoked fMRI detects hemodynamic changes across the entire brain that correlate with an experimental manipulation, such as electrical stimulation. Therefore, in this study, we aimed to visualize the brain network modulated by hippocampal DSB using fMRI.

In contrast to PET imaging, fMRI enables the investigation of the modulatory potential of electricity on a subcortical-cortical pathway, because stimulation parameters can easily be varied during a single fMRI scanning session (Lauritzen, 2005; Haslinger et al., 2003; Stefurak et al., 2003). Several PET scanning sessions would be needed to investigate the neuromodulatory effects of DBS, as a single PET scanning session does not allow the

acquisition of the physiological changes induced by making selective and reversible changes in the stimulation parameters.
Proper anesthetic use is crucial for successful fMRI experiments in rodents. It is known that the use of medetomidine, a selective alpha-2-adrenoreceptor agonist, as an anesthetic agent results in a reliable stimulus-induced hemodynamic response. Additionally, it can be used in longitudinal studies, since it is administered subcutaneously requiring no catheterization and no intubation, because the animal can be kept in a free breathing state (Chao et al., 2014; Pawela et al., 2009; Zhao et al., 2008, Weber et al., 2006). Another major benefit of the alpha-2-agonist is that its effect can be rapidly reversed by administration of alpha-2-antagonists and that it has a short *in vivo* half-life, which also favors the use of medetomidine to be used in chronic follow-up studies (Weber et al., 2006). Using the suggested dose of medetomidine, the animal is under sedation rather than full anesthesia, and a reliable fMRI signal can be detected.

6.2 Materials & Methods

6.2.1 Animals

Seven adult male Sprague-Dawley rats (200–250g body weight; Janvier, France) were used for this experiment. All rats were treated according to guidelines approved by the European Ethics Committee (decree 2010/63/EU). All experimental procedures were approved by the Animal Experimental Ethical Committee of Ghent University Hospital (ECD 13/14). The animals were kept under environmentally controlled conditions (12h normal light/dark cycles, 20-23°C and 40-60% relative humidity) with food and water *ad libitum*.

6.2.2 Surgery

The surgical procedures in this experiment were performed in the exact same way as in chapter 5 (see section 5.2.2), with the only difference that we implanted an MR-compatible electrode for the fMRI experiments. Each DBS-electrode was custom-made by twisting together four MR-compatible, PFA-coated, Platinum Iridium wires (A-M Systems, WA, USA), with 140µm diameter. Platimum Iridium was selected as the better MR-compatible material for our experimental set-up based on its MR-compatibility, conductivity, workability and bio-compatibility characteristics obtained in the *in vivo* pilot experiments described in chapter 2 (see section 2.1.6). Also in this case, the most ventral and dorsal electrode contacts were used for stimulation purposes, providing a bipolar stimulation, with a distance between the tips of 3mm. The electrode and its placement are illustrated in Fig. 6.1.

For impedance optimization, all electrodes were electrolytically cleaned. The impedance was checked immediately before implantation and did not exceed 70kOhms (IMP-2, Bak electronics, Sanford Florida, USA). The stimulator (DS4 Bi-phasic Stimulus Isolator, Digitimer Ltd, Hertfordshire, England) can generate up to 48V, meaning the impedance cannot be over approximately 74kOhms for a stimulation intensity of 650µA (i.e. the maximal administered intensity during threshold determination). Note, the impedance meter is designed for recording micro-electrodes, and does not provide accurate impedance measurements for stimulation electrodes, but is systematically overestimated due to non-linearity and frequency dependency. However, this overestimation does not imply practical consequences to this study.

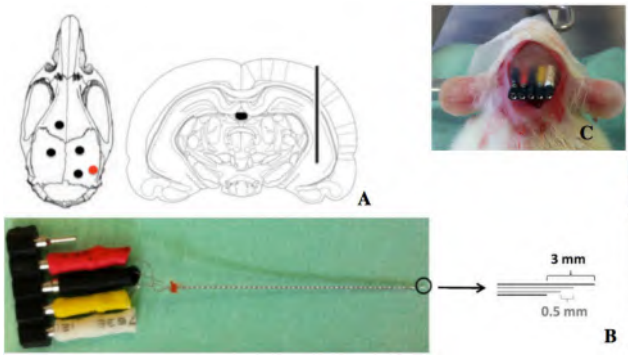

Figure 6.1: DBS-electrode specifications. (A) The quadri-polar DBS-electrode was stereotactically implanted in the right hippocampus (AP -5.6, DV -7.4, ML +5.2 relative to Bregma (Paxinos & Watson, 2007)) together with four anchor screws. The outer two electrodes are used for stimulation and the inner two electrodes for iEEG. The red dot represents the electrode insertion location on the skull. The black dots indicate anchor screw positions. (B) Illustration of the quadri-polar DBS-electrode. The DBS-electrode is custom made by twisting together four platina iridium wires (fMRI). The unused connection pin is reserved for connection to a ground-electrode, which is subcutaneously implanted in the neck. (C) Illustration of the DBS-electrode after fixation to the skull.

6.2.3 Deep Brain Stimulation

All rats received Poisson distributed unilateral hippocampal stimulation with the same parameters as used in the PET experiments (chapter 5), namely 100μs pulse width and 130Hz frequency. Yet the stimulation paradigm and intensity differ from those used in the PET experiments.

For the fMRI experiments, the stimulation paradigm was a five-minute-block-design paradigm with five cycles consisting of 40 seconds of rest (stimulation OFF) followed by 20 seconds of stimulation ON. For each rat the DBS paradigm was applied ten times using five different stimulation intensities, which were determined individually based on the subject's seizure threshold. The five different stimulation intensities were set at 10%, 30%, 50%, 70% and 90% of the minimal stimulus intensity that gives rise to an epileptic seizure. Every subject underwent fMRI on three different scandays, meaning that the DBS paradigm was applied thirty times (i.e. 30 minutes) in total. Note, in the PET study (chapter 5) only one stimulation intensity (i.e. 60% of the threshold determined in the awake rat) was used in the experiments, as a single PET scanning session does not allow for the investigation of several DBS-parameters within one PET scan.

Because DBS-fMRI was performed under medetomidine anesthesia, all rats were sedated with medetomidine during the thresholding process as well, and the stimulation itself started after at least one hour of continuous infusion of medetomidine.

The detection of ictal discharges was performed by recording the iEEG-signal using the inner two wires of the quadri-polar DBS-electrode. The iEEG-signal was amplified using an MRI-compatible amplifier (Brain Products, Gilching, Germany). The seizure threshold had a mean of 515μA, and a standard deviation of 130μA. The variation of seizure threshold between rats might be depending on three factors. First, the intrinsic biological variability causes differences in seizure susceptibility between rats. Second, small deviations in the electrode design (i.e. distance between poles) and electrode placement might generate variations in the volume of tissue activated (VTA). Since cells are activated at a given membrane current threshold, the VTA is dependent on the distance between the electrode and the individual target elements. Consequently, it could be that a certain volume of the initial target needs to be activated in order

for downstream structures to respond with a seizure. Third, the electrical stimulation can activate somata, axons or passing fibers. It is possible that one specific item must be stimulated to induce the final effect (i.e. modal recruitment). Therefore variations in electrode placement and design can cause variations in modal recruitment, which may lead to variations in the seizure threshold. The latter two factors are important to consider especially when working with a (rather large) 3mm distance between stimulation poles of the electrodes. However, the hippocampus is a large structure (less risk for off-target effects) and this 3mm-electrode design appears to work well in preclinical studies of hippocampal DBS (Van Nieuwenhuyse et al., 2015; Wyckhuys et al., 2010; Wyckhuys et al., 2007).
The variation in seizure threshold cannot be related to the impedance because the DS4 stimulus isolator is characterized by compliance voltage of 48V, which is large enough for our experimental purposes. As mentioned earlier, the measured impedances were kept under the upper limit and thus for every experiment enough voltage was available at the counter electrode to force current to flow while remaining control of the working electrode voltage.

6.2.4 Data acquisition

The timeline of the experimental protocol is shown in Fig. 6.2. Every subject underwent MR-acquisitions on three different timepoints. The first timepoint was one day after the threshold determination for all animals. Depending on scanner availability, the time between scanning days ranged from one day up to four days. Electrode impedance was checked at the start of each scanning day, by connecting an impedance meter (IMP-2, Bak electronics, Sanford Florida, USA) to the stimulation poles of the DBS-electrode using 1kHz sine wave testing stimuli. The currents used within the set-up are of magnitude < 30nA, meaning this set-up can be used in vivo. The impedance did not exceed 70kOhms in 4/7 subjects, and did not exceed 80kOhms in 3/7 subjects, which is still acceptable to administer up to 90% of the highest seizure threshold.

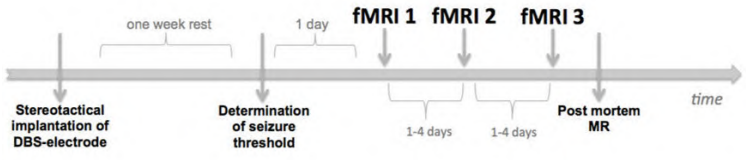

Figure 6.2: Timeline of the experimental imaging protocol. The animals were allowed one week of post-surgical recovery, after which the seizure threshold was determined. One day after threshold, the 1st series of fMRI datasets were acquired. The 2nd and 3rd series of fMRI datasets were acquired 1 to 4 days after the first set was acquired, depending on scanner availability. Finally rats were sacrificed, the DBS-electrode was removed with high caution and an MR-scan was acquired.

All acquisitions were performed under medetomidine anesthesia. All rats were initially anesthetized with a mixture of isoflurane (5% for induction and 2% for maintenance) and medical O_2. A bolus of 0.05mg/kg medetomidine was injected subcutaneously, and isoflurane was stopped 10 minutes afterwards. Continuous subcutaneous infusion of medetomidine (0.1mg/kg/hour) was started 15 minutes after the bolus injection to maintain sedation. At least 30 minutes was allowed for equilibration before the actual fMRI acquisition was started. After 2 hours the infusion rate was increased to 0.3mg/kg/hour. After stepping the infusion rate, a 30 minutes equilibration period was allowed before continuing fMRI acquisitions. Previous fMRI studies have shown that tripling the infusion rate after 2.5 hours resulted in a prolonged period of similar sedation level up to 6 hours, which could not be achieved with a constant infusion

rate (Pawela et al., 2009). After the acquisition atipamezole (0.03mg/kg) was administered to reverse the effects of the anesthesia.
In this study we employed fMRI with blood oxygenation level-dependent (BOLD) contrast, which is the most commonly used contrast in fMRI. MR images were acquired on a 7T system (Pharmascan 70/16, Bruker, Ettlingen, Germany) using a rat head volume coil in order to optimally acquire BOLD responses in deeper subcortical brain structures, such as the hippocampus. Fixation of the head of the animal was achieved using the tooth and ear bars of the Bruker MR bed, before placement inside the magnet. Rat body temperature was maintained at ~37°C by a water-circulated heating pad. Magnetic field homogeneity was optimized in two steps. First- and second-order shims were applied on the global volume, followed by local first-order shims on a volume of 4x6x12mm^3 using MAPSHIM. BOLD fMRI acquisitions were performed using a multi-slice single-shot gradient echo echo-planar imaging sequence (GE-EPI). Twelve interleaved slices were acquired with TE = 20ms, slice thickness = 1mm, matrix size = 80x80, FOV = 2.5x2.5cm^2 and voxel size = 0.312x0.312x1mm^3. Each fMRI run consisted of 150 repetitions with TR = 2s (total 5min), corresponding to the duration of the stimulation protocol. Ten GE-EPI runs (i.e. two times five stimulation intensities in randomized order) were acquired with a 5min rest period between scans for neurovascular recovery and to minimize bias from potential DBS induced heating and tissue damage. For anatomical reference, T2 weighted anatomical images were obtained using a Turbo RARE sequence with TR = 6345ms, TE = 37ms, slice thickness = 0.6mm, matrix size = 276x320, FOV = 3x3.5cm^2.

After completion of the experiment the animals were euthanized with an overdose of pentobarbital (150mg/kg, i.p.), and the electrode was removed cautiously. The electrode was inspected under the microscope to assess whether any tissue was removed together with the electrode, which was in our study never the case. Thereafter, a post-mortem structural MR was acquired for electrode path verification purposes and for potential tissue damage evaluation. T2 weighted anatomical images were obtained with a spatial resolution of 100μm x 100μm in the axial plane, i.e. smaller than the thickness of the electrode and thus the lesion. We made sure the positioning of one slice was at the level of the electrode. We believe this method is sufficiently accurate in assessing the correct electrode position, and thus that a post-mortem histological verification was not needed for this purpose. Our goal was to investigate the effect of DBS on hippocampal connectivity in general, rather than on the connectivity between hippocampal substructures.

The impact of the electrode artifact on the structural and functional MR image is illustrated in Fig. 6.3A and Fig. 6.3B/C, respectively. The electrode track obtained via a post-mortem MRI and after careful removal of the electrode, is shown in Fig. 6.3D. The electrode track was in the right hippocampus for all subjects.

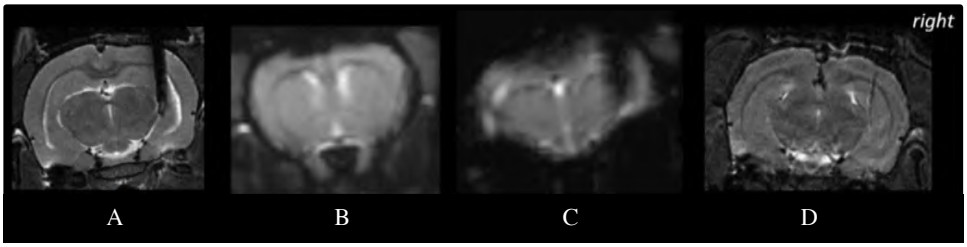

Figure 6.3: Illustration of electrode-artifact on MR-images. (A) structural MRI of axial slice at height of electrode. (B) functional MRI of axial slice through forebrain. (C) functional MRI of axial slice at height of electrode. (D) post-mortem structural MRI at height of the electrode path. The post-mortem MRI is used to verify the electrode track position. For all rats the electrode track was located in the right hippocampus.

6.2.5 Data-analysis

Preprocessing was done in SPM8 (http://www.fil.ion.ucl.ac.uk/) on a subject-by-subject basis. First, all images from all sessions were realigned to the first image of the first session, using a least squares approach and a 6 parameter rigid body spatial transformation. Second, all datasets were coregistered to the anatomical image using a normalized mutual information metric. Third, in-plane smoothing was done using a Gaussian kernel with Full Width at Half Maximum (FWHM) of (1x1)mm^2. Finally, a band pass filter (0.01Hz – 0.08Hz) was applied to reduce low frequency and physiological noise (e.g. breathing (~0.3Hz) and heartbeat (~1.0Hz)). No global signal regression was performed since detrending of the data did not appear to optimize the result. Probably, the filtering step did already suffice to remove low frequency baseline drift (e.g. MR scanner drift and aliasing of physiological pulsations), which is particularly important in brain regions that weakly activate (Tanabe et al., 2002). In order to prepare the preprocessed data for statistical analysis all datasets were normalized on a subject-by-subject basis to their mean, using SPM8.

Statistical data-analysis using the general linear model (GLM), which assumes a known haemodynamic response function (HRF) to a certain stimulus, is the standard way to identify correlated voxels in fMRI data. In this study, we employ a refined data-driven processing technique (Independent Component Analysis, ICA) to analyze our fMRI data. ICA has demonstrated successful extraction of a priori unknown independent components related to brain activations, without imposing constraints on the HRF. This technique divides the BOLD signal into different independent temporally correlated components. Therefore, ICA allows the detection of varying BOLD responses to a stimulus with varying delays and shapes, which could not be detected with GLM analysis that is restricted by HRF constraints. Additionally, also independent components related to both physiological and non-physiological noise are extracted using ICA (McKeown et al., 2003). ICA is frequently applied in neuroscience research to examine functional connectivity of the brain in the resting state, when no stimulus is present, and thus when no prior HRF-information can be included in the analysis (Becerra et al., 2011; Jonckers et al., 2011; Hutchison et al, 2010). However, limited prior information is included through the selection of the anatomically relevant components by the investigator during interpretation. ICA of the preprocessed fMRI data was performed using GIFT (Group ICA of fMRI toolbox (http://icatb.sourceforge.net/). We used 5 components, except in one subject that required 15 components for a clear separation of the actual activation for the ICA analysis. By choosing a balanced number of components, we prevent that components with similar temporal characteristics are not split up over different components, or that regions with

different temporal characteristics pile up into one component (Jonckers et al., 2011). Every activation or response map is an average across 6 fMRI-sessions, acquired at three different scanning days. Only voxels with a Bonferroni corrected p-value below 0.05 were considered active and used in further investigation and visualization. Bonferroni correction was done by dividing the significance level by the number of brain voxels, i.e. post-smoothing. The Bonferroni correction method corrects more strictly than is actually necessary, because it assumes that the data at neighbouring voxels are completely independent from each other. However, in reality, neighbouring voxels show similar activation patterns within functionally defined brain regions. In order to avoid type II errors, we made the correction less strict, by dividing by the number of brain voxels post-smoothing. This number was estimated to be around 10000, since the rat brain consists approximately of 30000 voxels with dimensions of $0.312 \times 0.312 mm^2$ and a smoothing kernel of 1 mm FWHM was used.
The response maps were overlaid on the structural MR. The response maps were not masked. The inter-subject reproducibility was evaluated based on the visual comparison of the mean response map of all subjects.

Prior to ICA analysis, response maps were compiled using standard GLM analysis, by calculating the correlation between the stimulation paradigm and the BOLD response over time for each voxel. A Bonferroni corrected p-value of 0.05 was used as the threshold for display. For the generation of the GLM-based response maps all fMRI sessions were grouped per subject, per stimulation intensity. For completeness, we compared the findings of ICA and GLM analyses.

6.3 Results

Bipolar Poisson distributed hippocampal DBS induces a reproducible positive stimulation intensity-dependent BOLD response in: ipsilateral hippocampal structures (il HC); contralateral hippocampal structures (cl HC); medial thalamic structures (mThal) such as the ventral posteromedial thalamic nucleus (VPM) and mediodorsal thalamic nucleï (MD); lateral thalamic structures (lThal), such as the ventral posterolateral thalamic nucleus (VPL), the reticular thalamic nucleus (Rt), the medial geniculate nucleus (MGN); septal nuclei; striatum; hypothalamus (hypoT); medial forebrain structures (mFB), including the nucleus Accumbens (NAc); and sensory cortex (SC). In some subjects a positive BOLD response was also observed in other structures, such as the mammillary bodies (MM) and the ventral tegmental area (VTA).

Table 6.1 shows the brain structures with a significant DBS-induced BOLD response per subject (S1/7). The most reproducible to least reproducible brain structures are listed from top to bottom. The response in the cl HC is reproducible throughout all subjects. mThal, septum, mFB and hypoT are present in 6/7 subjects and il HC, striatum, lThal and SC in 5/7 subjects. Mean whole-brain ICA- and GLM-based response maps are shown for one subject in Fig. 6.4A and Fig. 6.4B respectively. Supplementary figures are added in paragraph 10.7 at the end of this chapter, showing the ICA-based response maps for the six other subjects.

Furthermore, we can conclude that our results are reproducible within each subject (i.e. in-between sessions), since data-analysis of the grouped fMRI sessions (within one subject) results in a mean response map with significant activation in several brain structures, for all subjects.

Table 6.1: Inter-subject reproducibility.

Structure	S1	S2	S3	S4	S5	S6	S7
cl HC	x	x	x	x	x	x	x
mThal	-	x	x	x	x	x	x
septum	-	x	x	x	x	x	x
mFB	x	x	x	x	x	-	x
hypoT	x	x	x	x	x	-	x
il HC	x	x	x	x	-	x	-
striatum	-	x	x	x	x	-	x
lThal	-	-	x	x	x	x	x
SC	-	x	x	x	x	-	x
MM	x	x	-	-	-	-	-
VTA	-	x	-	-	-	-	-

The BOLD response became more widespread with a higher stimulation intensity for all subjects. A bilateral BOLD response was observed at 90% of the seizure threshold in all subjects, at 70% of the seizure threshold in 5/7 subjects, at 50% of the seizure threshold in 4/7 subjects, and in two subjects already at 30% of the seizure threshold. At 10% of the seizure threshold only a unilateral response was observed in all subjects. These results indicate the impact of the stimulation intensity to the spatial extent of the DBS-induced BOLD response. In each subject the response became more widespread with increasing stimulation intensity. There were no brain structures with a negative BOLD response (after Bonferroni correction) induced by DBS in any subject, at any stimulation intensity.

The unlabeled clusters in Fig. 6.4A, and in Supplementary Fig. 6.2-6.7, are considered to be fMRI-related artifacts. We observed an artifact in the lateral ventricles (e.g. the two clusters in the first two axial slices in Fig. 6.4A) and in the aqueduct, the small channel connecting the third and fourth ventricles of the rat brain (e.g. the cluster in the latter axial slice in Supplementary Fig. 6.5). These are probably artifacts because their cluster size is independent of the stimulation intensity, whilst it is hypothesized that DBS-related clusters become bigger with increasing stimulation intensity.

For completeness of the study, we compared the results from the standard GLM analysis to those from the ICA analysis. Mean whole-brain ICA- and GLM-based response maps are shown for one subject, for all stimulation intensities, in Fig. 6.4A and Fig. 6.4B respectively. Additional information on the GLM analysis can be found in Supplementary Fig. 6.1. As to be expected, GLM maps and ICA maps show significant correlation. However, GLM analysis reveals only unilateral BOLD responses in brain structures of the hippocampal formation, whereas ICA analysis also reveals bilateral and secondary BOLD responses in target areas of the hippocampus, more distant from the electrode tip. GLM analysis of the individual sessions shows significant activation in secondary brain structures in some sessions, but the response was not reproducible over sessions or within subject.

We were not able to correlate the stimulation intensity to the intensity or the significance of the BOLD response. This is illustrated in Fig. 6.5 for one subject. The graph depicts the mean timecourse of the cluster with the highest correlation to the stimulation paradigm per

stimulation intensity. This mean timecourse was calculated using GLM. The purpose of this graph is only to illustrate that the degree of correlation to the stimulation paradigm could not be correlated to the stimulation intensity. However, the size of the used clusters to calculate the mean timecourse increased with increasing stimulation intensity.

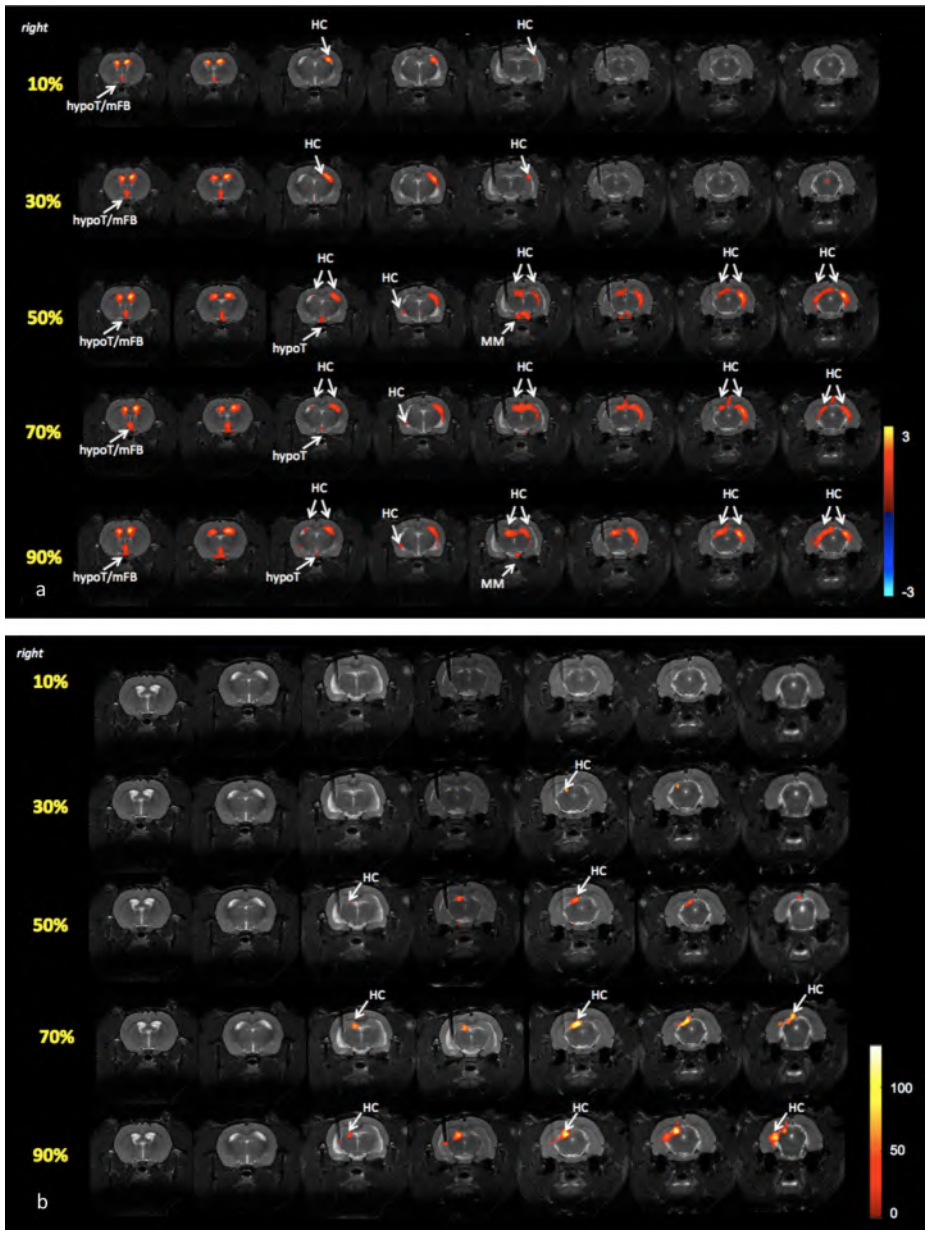

Figure 6.4: Representative whole-brain BOLD fRMI response-maps of one subject resulting from ICA and GLM analysis, listed separately in (A) and (B) respectively. All activation maps are thresholded with a Bonferroni corrected p-value < 0.05. Every response map displays the DBS-induced BOLD-response of 5 different stimulation intensities. Every row in the activation map represents a single intensity, listed from top to bottom, from 10% of the seizure threshold to 90% of the seizure threshold. Every row displays the mean of 6 fMRI-datasets for the specific stimulation intensity. Axial anatomical scans are co-registered with the corresponding activation maps. Slices progress from most anterior at the left to most posterior at the right. The hippocampal structures (**HC**), lateral thalamic structures (**lThal**), medial thalamic structures (**mThal**), septal nuclei (**septum**), striatum, hypothalamus (**hypoT**), medial forebrain (**mFB**), sensory cortex (**SC**), mammillary bodies (**MM**), and ventral tegmental area (**VTA**) are labeled with white arrows. (A) ICA-based response maps. The intensity of the color corresponds to the level of significance of the BOLD response, indicated by a z-score in the color bar on the right. (B) SPM-based response maps. The intensity of the color corresponds to the level of correlation of the voxel's timecourse to the stimulus, indicated by an F-value in the color bar on the right.

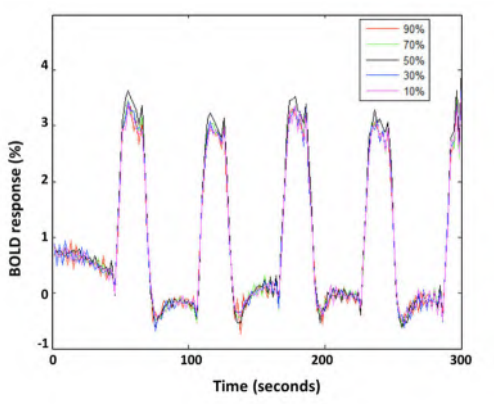

Figure 6.5: BOLD responses at different stimulation intensities in one subject. The graph depicts the mean timeseries per stimulation intensity in the volume of interest with the highest significance, per stimulation intensity, in one subject. The volume of interest increased with increasing stimulation intensity.

6.4 Discussion

6.4.1 Whole-brain response of DBS

With our simultaneous DBS-fMRI experiment we demonstrated that hippocampal DBS, with preclinically proven successful stimulation parameters to treat TLE (Vonck et al., 2013), significantly affects the BOLD signal in several brain structures of the limbic system. In some subjects, additional BOLD responses were observed in mesolimbic brain structures. Secondly, we were able to visualize not only global, but also bilateral responses to *in vivo* stimulation of the hippocampus. Moreover, this bilateral connectivity appears to increase with increasing intensity.

6.4.1.1 Limbic activation

The rat hippocampus is anatomically and physiologically well defined and is known as the key structure in the limbic system. Thus, it is not surprisingly that, in this study, local stimulation of the hippocampus induces distal responses in other structures of the limbic system, such as thalamic structures, the hypothalamus, septum and mammillary bodies.

6.4.1.2 Mesolimbic activation

In some subjects, we observed significant BOLD responses in brain structures of the mesolimbic pathway (VTA, mFB/NAc) as well. The mesolimbic pathway is a dopaminergic pathway in the brain, which begins in the VTA and connects to the NAc. However, neuroimaging studies have shown that the hippocampus and amygdala are also part of the mesolimbic network (Bunzeck et al., 2012; Koob and Volkow, 2010). This might explain why we find additional responses in the VTA and mesial forebrain structures. Moreover, previous fMRI studies of electrical stimulation of the rat hippocampus have also shown secondary fMRI responses in target regions of the hippocampus, such as the septum, striatum, NAc/mFB, substantia nigra, anterior cingulate cortex (ACC) and SC, indicating that stimulation of the hippocampal formation can activate the limbic and mesolimbic pathway (Alvarez-Salvado et

al., 2014; Helbing et al., 2013; Angenstein et al., 2013; Krautwald et al., 2013; Canals et al., 2009; Canals et al., 2008).
With regard to epilepsy, clinical and experimental studies have investigated the role of the dopaminergic system (Bozzi et al., 2011; Starr, 1996; Star, 1993), which is well known to regulate seizure activity. An fMRI study in unilateral mesial TLE (mTLE) patients has shown important decreases of functional connectivity in the ventromesial limbic forebrain regions and in the NAc (Pittau et al., 2012). These regions are involved in long-term memory for novel events and reward. The authors also observed reduced connectivity in the hippocampus, amygdala and default mode network (Pittau et al., 2012). An ictal iEEG study in TLE patients has suggested that the mFB is strongly affected by mesial temporal activity (Lieb et al., 1991), indicating a preferential seizure spread from mesial temporal lobes to mesial frontal lobes, consequently leading to reduced connectivity in all brain structures affected by seizure propagation. This reduced functional connectivity in the mesial temporal lobe structures may explain cognitive and psychiatric impairments often found in patients with mTLE. The therapeutic potential of DBS for mTLE patients, for seizure reduction purposes has been hypothesized in literature (Velasco and Fischer, 2014; Velasco et al., 2007; Vonck et al., 2013). Further research is necessary to investigate potential DBS-induced restoration of mTLE-induced loss of functional connectivity.

6.4.1.3 Bilateral activation

We observed increasing DBS-induced bilateral connectivity with increasing stimulation intensity. These findings are concordant with previous rodent fMRI research of direct stimulation of the perforant pathway of the rat hippocampus, which revealed a linear relationship between the intensity used to stimulate the hippocampal formation and the extension of the induced BOLD response. The higher the stimulation intensity, the more bilateral the response was (Canals et al., 2008; McIntyre et al. 2004).

6.4.1.4 Reproducibility

To our knowledge this is the first DBS-fMRI study with a chronically implanted MR-compatible electrode for hippocampal DBS. Previous fMRI studies of direct electrical stimulation of the hippocampus, are limited to acute stimulation and do not use a chronically implanted DBS-electrode, meaning their experimental protocol cannot be used for longitudinal studies (Alvarez-Salvado et al., 2014; Helbing et al., 2013; Angenstein et al., 2013; Krautwald et al., 2013; Canals et al., 2009; Canals et al., 2008). Other DBS-fMRI studies have used chronically implanted electrodes where they targeted thalamic structures and could reveal thalamic-cortical connectivity (Yang et al., 2014; Shyu et al., 2004). Besides longitudinal investigation of DBS, a chronically implanted electrode allows for a post-surgical recovery to minimize acute tissue inflammation and for electrode fixation with dental cement to minimize electrode movement during acquisition. With this study, we showed that our experimental protocol, for longitudinal DBS-fMRI studies, provides reproducible results.

6.4.2 GLM vs. ICA

Comparison of the results from the GLM analysis to those from the ICA analysis demonstrates that: (1) ICA analysis is able to replicate the results found with the standard GLM analysis; (2) ICA analysis returns additional information.
Since the GLM map indicates voxel regions that vary according to the a priori defined stimulus, a statistically independent source analysis should indeed include the brain activation found with GLM. With GLM we only found a unilateral brain response, whereas with ICA we were able to trace a bilateral brain response in structures remote from the stimulated area. With GLM, each voxel is independently evaluated for a statistical relationship between its timeseries and an *a priori* modeled stimulus response. ICA analysis is not restricted by the use of a specific modeled response, since it looks for functionally connected regions, which are indirectly dependent, or independent of the stimulus. This could explain why ICA analysis returns more information. Since with ICA, areas with a delayed HRF, remote from the stimulated area, can be traced as well. Our findings coincide with previous evoked fMRI studies where both data analysis techniques are compared. The authors found the regions of activation identified by ICA overlapped substantially with those identified by SPM and that ICA was able to separate additional structures. ICA is less sensitive to motion artifacts and therefore could provide better results in datasets corrupted with motion artifacts, e.g. due to changes in the level of sedation (Quigley et al., 2002; Simeral et al., 1999).

6.4.3 Comparison to other imaging modalities

In contradiction to the DBS induced increased BOLD responses, our PET study (chapter 5) shows a general trend toward hippocampal and limbic inhibition. Comparison between PET and fMRI findings is difficult, because each technique is based on different physiological processes and uses a different timescale. While BOLD fMRI uses a temporal resolution of seconds, ^{18}F-FDG-PET has a time window of 30-45 minutes. The contradiction between findings could be attributed to this difference in time course between both imaging modalities. We hypothesize that DBS might lead to initial (order of seconds) activation of the targeted structure and might lead to a decrease in baseline activity of the targeted structure after 30 minutes of continuous stimulation (due to homeostatic downscaling mechanisms).

On the other hand, the spatial extent of the response was similar between modalities. Similar to the PET (and SPECT study), we observed a response in the bilateral hippocampus and other limbic structures, and that the intensity of the response remained unaltered for all stimulation intensities, but that the spatial extent of the response became more widespread with higher stimulation intensities, meaning that higher stimulation intensities lead to larger volumes being stimulated. Another ^{18}F-FDG-PET study investigated the neuronal network activity patterns in the healthy rat brain, affected by DBS of the subthalamic nucleus. They also concluded that unilateral DBS affects brain activity ipsi- as well as contralateral to the stimulation site, which implies a bilateral effectiveness (Klein et al., 2011).

Taken together our functional imaging studies of DBS in the healthy rat brain indicate that DBS exerts its effect not just locally but globally through a combination of several mechanisms (not just activation or inhibition alone), resulting in a network effect (Chang et al., 2012; Lyons et al., 2011). Since the hippocampus is not only the presumed ictal focus in TLE but is also a

structure involved in networks regulating neuronal excitability, it is plausible that hippocampal DBS may subsequently affect the entire epileptogenic network (Boon et al. 2007).

6.4.4 Limitations

Simultaneous DBS-fMRI studies come with a few limitations: (1) Electrode artifact. The presence of metal in the MRI scanner causes the (f)MRI-signal to be distorted at and around the electrode, even with the use of an MR-compatible electrode (Lai et al., 2014; Younce et al., 2014). This might cause underestimation of the BOLD response at the site of the electrode, and could explain why we mainly observed a contralateral hippocampal response as opposed to an ipsilateral hippocampal response. PET imaging on the other hand does allow the visualization of DBS induced changes nearby the electrode. (2) Deviations in electrode placement, smaller than the spatial resolution of the MR images, may lead to large differences in response. This might explain the inter-subject variability of the affected brain structures, as shown in table 1. (3) DBS might cause temporary changes in cellular activity that might be overlooked with fMRI. (4) The BOLD response to a stimulus involves a complex interaction of the cerebral blood flow (CBF), cerebral blood volume (CBV) and cerebral metabolic rate of oxygen ($CMRO_2$) (Logothetis et al., 2001). This complex interaction within the fMRI signal makes it difficult to interpret BOLD fMRI data alone. Additional fMRI studies, such as CBV, CBF, and functional connectivity studies, and cellular studies might provide complementary information. (5) MRI is generally considered to be a safe imaging technique, as opposed to PET and SPECT, which are prone to the risk of exposure to ionizing radiation. However, the presence of intracerebral metal makes MRI a potentially dangerous technique in patients with subcutaneously DBS units. Safety risks include heating, local tissue damage due to high frequency currents and electrode displacement, induced by the MR gradient coils or/and radiofrequent pulses (Tagliati et al., 2009; Baker et al., 2005; Jech et al., 2003; Finelli et al., 2002). Despite the presence of intracerebral metal, neuronal function is unlikely to be affected by the high frequency of induced currents (Georgi et al., 2004). Provided a number of technical precautions are taken, MRI can be regarded as safe even in patients implanted with a DBS system (Zrinzo et al., 2011; Tagliati et al., 2009; Rezai et al., 2004). Carmichael et al. reported that temperature increases sufficiently low to suggest that thermal or electromagnetically mediated experimental confounds to fMRI with DBS are unlikely (Carmichael et al., 2007). Additionally, in patients with a DBS-system implanted, MRI is used routinely to control for correct implantation or more recently, for MR-guided implantation of the electrode (Carmicheal et al., 2007; Yelnik et al., 2003; Liu et al., 2001). However, further studies are required to rule out safety risks of MRI in patients implanted with a DBS system.

Due to an elaborate pre-experimental preparation we were able to establish an experimental protocol (i.e. the surgery, DBS and scan protocol) that minimized these limitations. Because we did not observe any signs of local tissue damage on the post-mortem structural MR images, and the BOLD response to DBS was found to be consistent, we can conclude we established a safe and robust experimental design.

As a final note to limitations of this study: inherent to electrical stimulation is the lack of specificity, which makes it difficult to evaluate the relevance of a specific brain structure to the network that is modulated by hDBS. In the future, opto-fMRI, which is characterized by an unprecedented spatial resolution, could be used to investigate the functional contribution of

separate brain structures of the limbic system to the epileptogenic network or the therapeutic efficacy of DBS-therapy.

6.5 Conclusion

With this study, we demonstrated that simultaneous DBS-fMRI is able to map distal and bilateral responses to local circuit activation on a large spatial scale, and that the brain volume affected by DBS increases with an increasing stimulation intensity. To our knowledge this is the first DBS-fMRI study with a chronically implanted MRI-compatible electrode for hippocampal DBS. We showed that our experimental protocol, for longitudinal DBS-fMRI studies, provides reproducible results. Our results demonstrate that hDBS robustly modulates the limbic and mesolimbic network. These findings may hold clinical relevance for hippocampal DBS therapy in epilepsy cases, as connectivity in these networks have previously been shown to be suppressed in mTLE. Further research is necessary to investigate potential DBS-induced restoration of mTLE-induced loss of functional connectivity in (meso)limbic brain structures. Clinical simultaneous DBS-fMRI studies could be complemented with behavioral and cognitive evaluation in order to achieve the visualization of therapeutic DBS circuits. In this way, translation to clinical investigation of existing as well as new parameters and targets for DBS might lead to the reduction of non-responders to the treatment.

6.6 Original contributions

The work presented in this chapter resulted in three international conference contributions (see [5, 8-10] in list of conference contributions). The results of this experiment were published in the peer-reviewed A1 journal *Plos One* (see [2] in list of publications) (first author). The surgeries discussed in section 6.2.3 were performed by Ine Dauwe or the author of this chapter. The design of the electrode, stimulation set-up, acquisition and data-analysis, were performed by the author of this chapter.

6.7 Supplementary figures

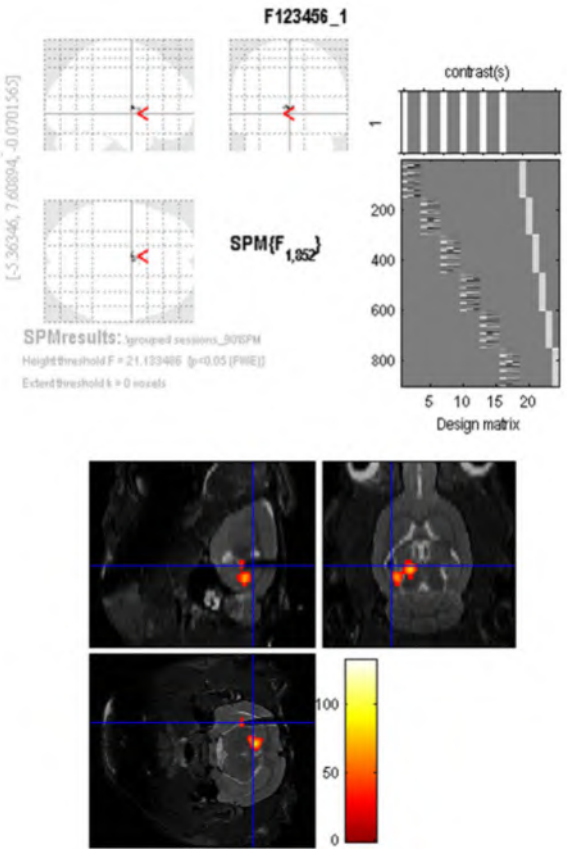

Supplementary figure 6.1: Representative DBS fMRI result of one subject, obtained with GLM analysis. The response map is the result of 6 sessions grouped together of one subject, at a stimulation intensity of 90% of the threshold. A positive BOLD response can be clearly observed in the ipsilateral hippocampus. The response map is thresholded at $p < 0.05$, after Bonferroni correction.

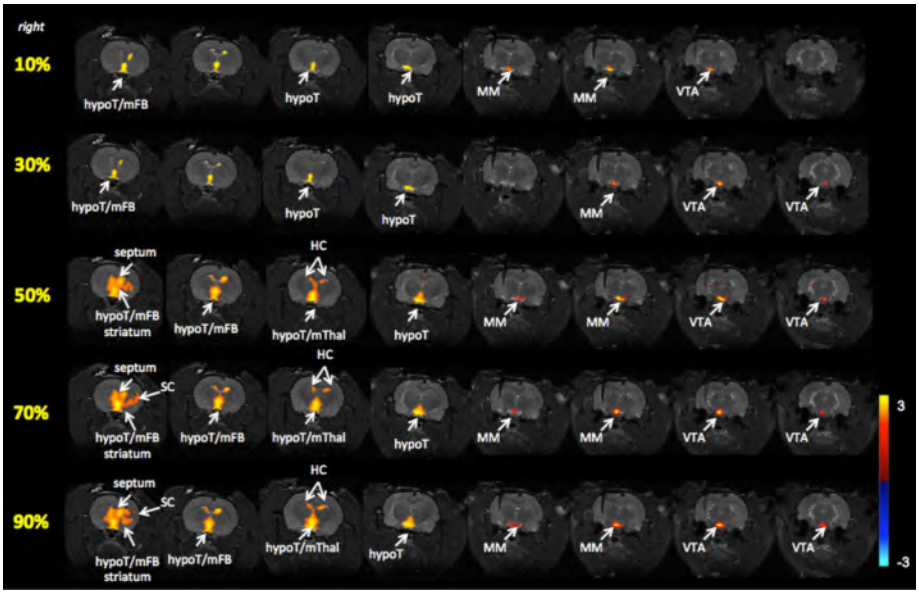

Supplementary figure 6.2: Individual whole-brain BOLD fRMI response map of **subject 2**, resulting from ICA analysis. The response map is thresholded with a Bonferroni corrected p-value < 0.05. The intensity of the color corresponds to the level of significance of the BOLD response, indicated by a z-score in the color bar on the right. The response map displays the DBS-induced BOLD-response of 5 different stimulation intensities. Every row in the response map represents a single intensity, listed from top to bottom, from 10% of the seizure threshold to 90% of the seizure threshold. Every row displays the mean of 6 fMRI-datasets for the specific stimulation intensity. Axial anatomical scans are co-registered with the corresponding activation maps. Slices progress from most anterior at the left to most posterior at the right. The hippocampal structures (**HC**), medial thalamic structures (**mThal**), septal nuclei (**septum**), striatum, hypothalamus (**hypoT**), medial forebrain (**mFB**), mammillary bodies (**MM**) and ventral tegmental area (**VTA**) are labeled with white arrows.

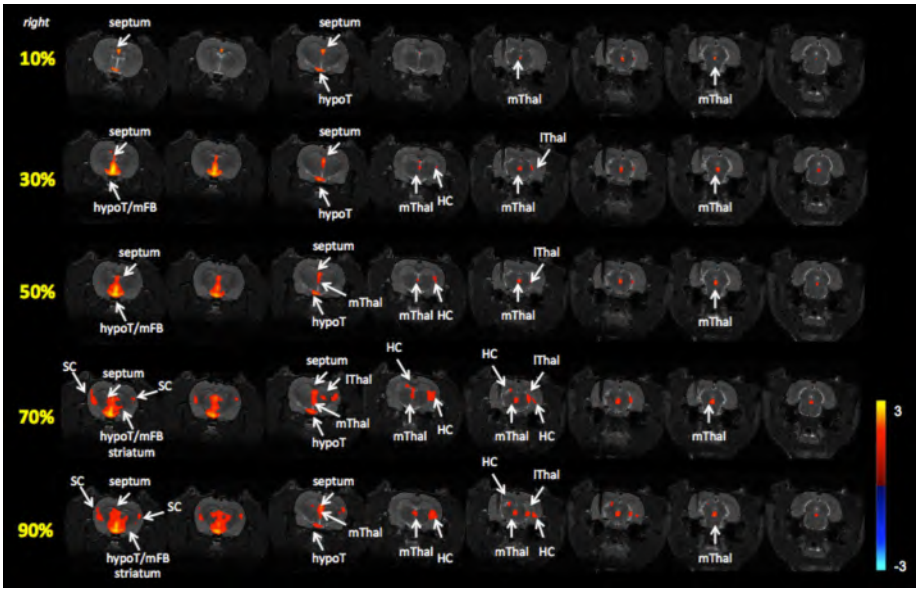

Supplementary figure 6.3: Individual whole-brain BOLD fRMI response map of **subject 3**, resulting from ICA analysis. The response map is thresholded with a Bonferroni corrected p-value < 0.05. The intensity of the color corresponds to the level of significance of the BOLD response, indicated by a z-score in the color bar on the right. The response map displays the DBS-induced BOLD-response of 5 different stimulation intensities. Every row in the response map represents a single intensity, listed from top to bottom, from 10% of the seizure threshold to 90% of the seizure threshold. Every row displays the mean of 6 fMRI-datasets for the specific stimulation intensity. Axial anatomical scans are co-registered with the corresponding activation maps. Slices progress from most anterior at the left to most posterior at the right. The hippocampal structures (**HC**), lateral thalamic structures (**lThal**), medial thalamic structures (**mThal**), septal nuclei (**septum**), striatum, hypothalamus (**hypoT**), medial forebrain (**mFB**) and sensory cortex (**SC**) are labeled with white arrows.

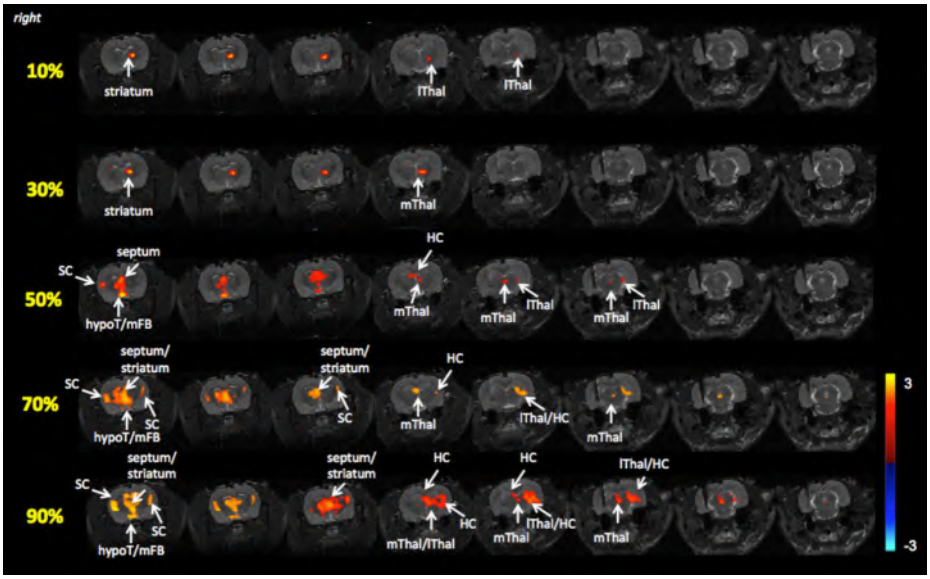

Supplementary figure 6.4: Individual whole-brain BOLD fRMI response map of **subject 4**, resulting from ICA analysis. The response map is thresholded with a Bonferroni corrected p-value < 0.05. The intensity of the color corresponds to the level of significance of the BOLD response, indicated by a z-score in the color bar on the right. The response map displays the DBS-induced BOLD-response of 5 different stimulation intensities. Every row in the response map represents a single intensity, listed from top to bottom, from 10% of the seizure threshold to 90% of the seizure threshold. Every row displays the mean of 6 fMRI-datasets for the specific stimulation intensity. Axial anatomical scans are co-registered with the corresponding activation maps. Slices progress from most anterior at the left to most posterior at the right. The hippocampal structures (**HC**), lateral thalamic structures (**lThal**), medial thalamic structures (**mThal**), septal nuclei (**septum**), striatum, hypothalamus (**hypoT**), medial forebrain (**mFB**) and sensory cortex (**SC**) are labeled with white arrows.

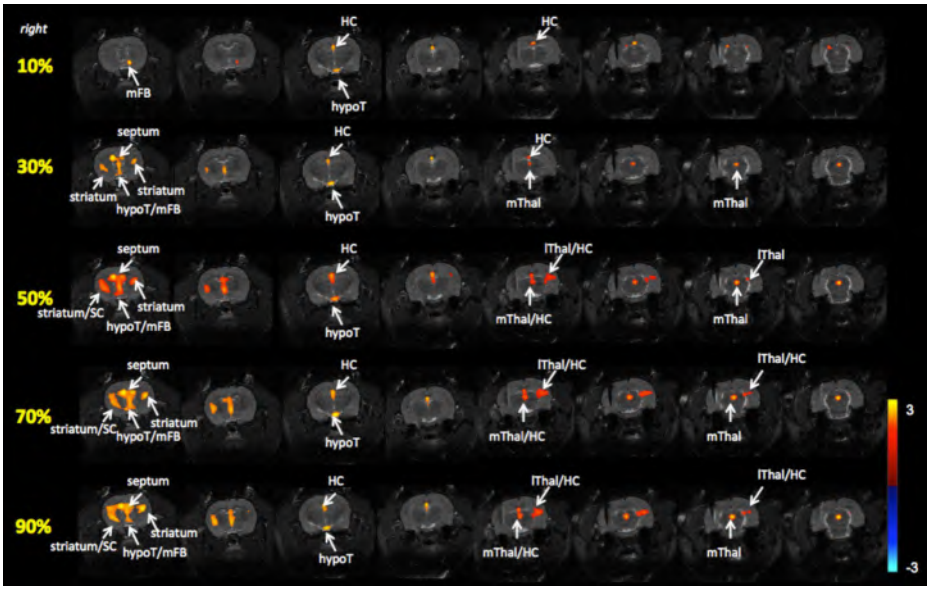

Supplementary figure 6.5: Individual whole-brain BOLD fRMI response map of **subject 5**, resulting from ICA analysis. The response map is thresholded with a Bonferroni corrected p-value < 0.05. The intensity of the color corresponds to the level of significance of the BOLD response, indicated by a z-score in the color bar on the right. The response map displays the DBS-induced BOLD-response of 5 different stimulation intensities. Every row in the response map represents a single intensity, listed from top to bottom, from 10% of the seizure threshold to 90% of the seizure threshold. Every row displays the mean of 6 fMRI-datasets for the specific stimulation intensity. Axial anatomical scans are co-registered with the corresponding activation maps. Slices progress from most anterior at the left to most posterior at the right. The hippocampal structures (**HC**), lateral thalamic structures (**lThal**), medial thalamic structures (**mThal**), septal nuclei (**septum**), striatum, hypothalamus (**hypoT**), medial forebrain (**mFB**), and sensory cortex (**SC**) are labeled with white arrows.

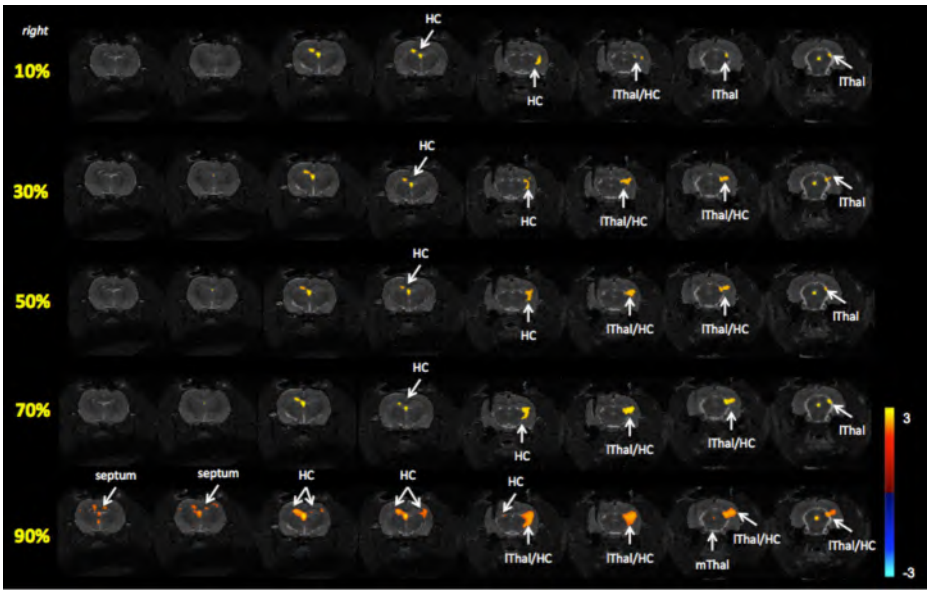

Supplementary figure 6.6: Individual whole-brain BOLD fRMI response map of **subject 6**, resulting from ICA analysis. The response map is thresholded with a Bonferroni corrected p-value < 0.05. The intensity of the color corresponds to the level of significance of the BOLD response, indicated by a z-score in the color bar on the right. The response map displays the DBS-induced BOLD-response of 5 different stimulation intensities. Every row in the response map represents a single intensity, listed from top to bottom, from 10% of the seizure threshold to 90% of the seizure threshold. Every row displays the mean of 6 fMRI-datasets for the specific stimulation intensity. Axial anatomical scans are co-registered with the corresponding activation maps. Slices progress from most anterior at the left to most posterior at the right. The hippocampal structures (**HC**), lateral thalamic structures (**lThal**), medial thalamic structures (**mThal**) and septal nuclei (**septum**) are labeled with white arrows.

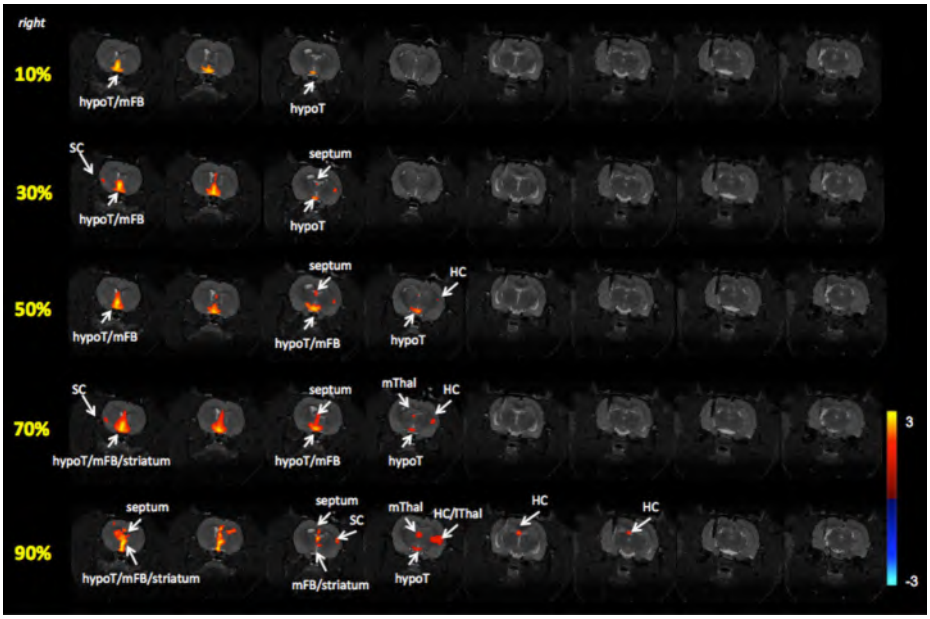

Supplementary figure 6.7: Individual whole-brain BOLD fRMI response map of **subject 7**, resulting from ICA analysis. The response map is thresholded with a Bonferroni corrected p-value < 0.05. The intensity of the color corresponds to the level of significance of the BOLD response, indicated by a z-score in the color bar on the right. The response map displays the DBS-induced BOLD-response of 5 different stimulation intensities. Every row in the response map represents a single intensity, listed from top to bottom, from 10% of the seizure threshold to 90% of the seizure threshold. Every row displays the mean of 6 fMRI-datasets for the specific stimulation intensity. Axial anatomical scans are co-registered with the corresponding activation maps. Slices progress from most anterior at the left to most posterior at the right. The hippocampal structures (**HC**), lateral thalamic structures (**lThal**), medial thalamic structures (**mThal**), septal nuclei (**septum**), striatum, hypothalamus (**hypoT**), medial forebrain (**mFB**) and sensory cortex (**SC**) are labeled with white arrows.

Part IV

Conclusions

Chapter 7

Conclusions and future perspectives

7.1 Significance

In the current work, we used functional neuroimaging techniques and optogenetics to explore experimental deep brain stimulation (DBS) targets for the treatment of Parkinson's disease (PD) and epilepsy. Currently, the *subthalamic nucleus (STN)* and the *anterior thalamic nucleus (ANT)* are standardly targeted in DBS-therapy for PD and epilepsy, respectively. Our investigation is significant because despite the well-reported clinical success of STN- and ANT-DBS, there are still non-responders to the treatment. In order to improve treatment efficacy, research is necessary to explore whether other brain structures might have therapeutic potential as well. More specifically, we aimed to investigate three experimental DBS targets associated with either PD or epilepsy, namely the substantia nigra pars reticulata, globus pallidus externa and hippocampus. Therefore, we defined three specific research goals in this thesis. In this chapter, a general overview of this work is presented, results and conclusions are summarised, and we will draw some general conclusions and provide some possible future research directions.

7.2 Research goals

Goal 1 - Functional circuit mapping of two striatal output nuclei using simultaneous DBS-fMRI

We employed DBS-fMRI to functionally and unbiasedly map the functional connectivity of *Substantia Nigra pars reticulata* (SNr) and the *Globus Pallidus externa* (GPe), and to investigate the influence of the stimulation frequency on the measured connectivity profiles. This set of experiments is described in chapter 3 of this thesis.

Previously, the SNr and GPe have been described as simple functionally antagonistic relay nuclei through the basal ganglia. However, recent anatomical studies have demonstrated newfound complexity in their connectivity, highlighting their potential role as far more than

relay nuclei alone. The functional roles of these novel circuit elements are likely complex and not easily predicted.Therefore, closer evaluation of the functional connectivity patterns among its constituent nuclei is necessary. Complementary to anatomical studies, functional Magnetic Resonance Imaging (fMRI) combined with neural stimulation approaches such as DBS, provide an ideal means for mapping the dynamic output patterns of target nuclei, including the directionality of downstream modulation (excitation or inhibition), and alterations in healthy vs. disease states. Moreover, the SNr and GPe are currently being explored as potential non-canonical DBS targets for high frequency DBS-therapy of PD.

Simultaneous DBS-fMRI with Cerebral Blood Volume (CBV) measurements revealed a number of surprising evoked responses, including unexpected CBV decreases within the striatum during DBS at either target, as well as GPe-DBS-evoked positive modulation of frontal cortex. Functional connectivity MRI provided evidence of robust, frequency-dependent global network modulation by electrical SNr- and GPe -stimulation, with more robust network changes observed with 130Hz compared to 40Hz stimulation. This work thus contributes to a growing literature demonstrating extensive and unanticipated functional connectivity among basal ganglia nuclei. Further, the inclusion of high frequency stimulation in our DBS experiments facilitates a translational perspective on our connectivity maps, as high frequency DBS at the SNr or GPe has demonstrated therapeutic benefits in Parkinson's disease.

Goal 2 - Functional circuit mapping of the Globus Pallidus externa using simultaneous opto-fMRI

We employed optogenetics with simultaneous fMRI measurements, also called "opto-fMRI", to investigate functional connectivity of the GPe in healthy and Parkinsonian rats. Optogenetics, or stimulation using light, is a state-of-the-art neuromodulation technique that has been proposed as a more selective alternative to electrical stimulation (DBS). This set of experiments is explained in chapter 4 of this thesis.

Electrical stimulation is well known to affect passing afferent fibers, in addition to cell bodies and efferent fibers, causing diffuse off-target effects. The presence of a metal electrode in the brain together with these diffuse off-target effects potentially confound the fMRI signal. In contrast, optogenetic stimulation has been confined to opsin gene transduction of local cell bodies without the confound of photosensitizing passing fibers. Furthermore, the size of the optic fiber artifact is substantially less as opposed to the DBS-electrode artifact. Consequently, opto-fMRI enables the visualization of downstream responses with increased specificity. However, little is known regarding the extent to which optogenetic stimulation mirrors the circuit-level responses achieved with electrical DBS.

As opposed to electrical stimulation, optogenetic stimulation resulted in only ipsilateral modulation, namely CBV increases in the GPe, and CBV decreases in the neighboring dorsal striatum. Furthermore, we were unable to achieve detectable circuit modulation in the prefrontal cortex, confirming the selectivity of the optogenetics technology.

Surprisingly, in Parkinsonian rats, we observed larger positive responses in the GPe, reduced striatal vasoconstriction and a unique prefrontal negative CBV signal during GPe stimulation. Our data clearly do not conform to the traditional model of the GPe as a "simple" relay nuclei, since modulation of several non-canonical downstream circuits was observed, including prefrontal cortex and striatum. Additionally, this study confirms GPe circuit remodeling following dopamine loss. Correlation of these findings to motor improvement in these rats could reveal the therapeutic role of the GPe neurons in DBS. With this study we exhibited the added

value of using opto-fMRI for a more detailed investigation of normal and pathological brain circuitry.

Goal 3 - Functional investigation of hippocampal DBS using simultaneous DBS-PET and DBS-fMRI

Our third goal is twofold. *Hippocampal* DBS has been proposed as an effective treatment in case of refractory temporal lobe epilepsy. Previous animal research has shown that electrical stimulation of the hippocampus results in reduced perfusion of several regions of the limbic system. Hence, we wanted to investigate whether hippocampal DBS also results in a reduced glucose metabolism using PET. Moreover, our progress in the development of fMRI procedures, to study DBS effects in rats, has created the opportunity to study additional experimental DBS-targets, such as the hippocampus. Thus secondly, we wanted to investigate how hippocampal DBS modulates brain circuitry because the results might contribute to the interpretation of the PET study. The DBS-PET experiments are explained in chapter 5, and the DBS-fMRI experiments are described in chapter 6.
In 2010, a SPECT-study in our lab revealed hippocampal DBS-induced hypoperfusion in the limbic system. Complementary to these findings, we observed significant decreases in the glucose metabolism in the ipsi- and contralateral hippocampus, as well as in other areas of the limbic network. Both studies suggest an underlying functional inhibition mechanism of DBS, i.e. downregulation of neuronal activity, and that this downregulation is not only local but appears also distal from the site of stimulation. Importantly, these findings may explain the seizure-suppressive of DBS, since a seizure is characterized by excessive and hypersynchronous neural activity.
In contradiction to the DBS induced metabolic signal drop in the limbic system, our DBS-fMRI study demonstrates DBS-induced activation of the limbic system. This may be attributed to the difference in length of stimulation in both experimental protocols, i.e. 60min of DBS (PET-study) vs. blocks of 20s of DBS (fMRI-study). Taken together, these studies suggest an initial acute DBS-evoked activation (characterized by fMRI signal increases), after which homeostatic downscaling mechanisms take place in response to more chronic stimulation (characterized by metabolic decreases). Moreover, this study highlights the importance of multi-modal imaging in the investigation of DBS and neurological disorders.

7.3 Future research possibilities

7.3.1 Preclinical applications

To our knowledge, these are the first preclinical DBS-fMRI studies to investigate the SNr, GPe and hippocampus *in vivo*; and the first opto-fMRI study to investigate GPe-circuitry in healthy and Parkinsonian rats. Our considerable progress in the development and application of fMRI procedures to study the effects of DBS and optogenetics in rats, tackling several of the major technical obstacles, can be seen as one of the major contributions of this research. The knowledge and experience obtained throughout these studies, enables further preclinical investigation using DBS- and opto-fMRI to explore neurological disorders and DBS-therapy.

One possible research direction involves the identification of therapeutically effective DBS-targets within the circuit modulated by DBS. When combining optogenetics with behavioral

testing in rat models for PD or epilepsy, therapeutic relevance of DBS-targets or other stimulation parameters could be determined. If preclinical *in vivo* studies using optogenetics reveal that there is an optimal target and stimulation paradigm that most effectively suppresses the symptoms of PD or epilepsy, then this would have an immediate impact on DBS-treatment in the clinical setting.

Besides the use of optogenetic techniques to help uncover the mechanisms of action of DBS, optogenetics, and more specifically opto-fMRI, could also be used as a complementary tool to investigate neurological disorders such as epilepsy. For instance, it would be highly interesting to investigate the role of a specific group of neurons in seizure initiation/propagation or seizure suppression in rodent models of epilepsy. It has already been demonstrated that optical inhibition of eNpHR-expressing hippocampal excitatory neurons delays seizure onset, and diminishes seizure evolution (Sukhotinsky et al., 2013). Moreover, seizure control has been achieved by activating parvalbumin-containing hippocampal interneurons with ChR2 or by inhibiting eNpHR-expressing hippocampal excitatory neurons (Armstrong et al., 2013). Nowadays, combinatorial opsins have become available, which enable the independent control of neuronal populations with blue and green light simultaneously (e.g. SFO: 546 nm deactivation; 470 nm activation). An interesting future experiment would be to simultaneously enhance the activity of inhibitory interneurons while reducing the activity of the excitatory cells in order to obtain a more effective seizure control in a rodent model of TLE (e.g. the viral injection of AAV5-CaMKIIa-SSFO-EYFP in transgenic mice with C1V1-mCherry expression in GABA-ergic PV neurons).

7.3.2 Translational research

Despite the promising progress in the development of closed-loop electrical neuromodulation devices, the use of optogenetic technology might improve the specificity of modulation and provide dynamic adjustments of stimulation on the basis of an individual patient's needs. Additionally, it is believed that optogenetics might even be used as a neuromodulation therapy in humans in the future because some viral delivery vectors such as AAV are considered to be safe. The remaining safety issues therefore mainly relate to the transgenes used itself. ChR2 has been proven to work successful in humans, and on-going gene therapy trials for the treatment of PD might open doors for using gene therapy for future opsin delivery in humans.

Although translational research of optogenetic neuromodulation therapies would be highly interesting, it is still highly challenging due to the high amount of translational obstacles (technical, practical and regulatory). Thus, rather than using optogenetics as a treatment, the use of optogenetics as a research tool (to investigate neurological disorders and treatments) will probably have a more direct impact of optogenetics on clinical care.

7.4 Final conclusion

In the current work we developed a robust fMRI protocol to investigate how DBS or optogenetics affects brain circuitry. We first employed DBS-fMRI to explore brain circuitry modulation by electrical stimulation of the SNr and GPe, and revealed new unanticipated connections between basal ganglia nuclei. Moreover, cortical responses (including motor cortex) to GPe-DBS peaked at a clinically relevant frequency (i.e. 130Hz), suggesting that the

GPe is functionally connected with motor cortex at therapeutic stimulation frequencies. To investigate these interesting findings more in detail, we next integrated fMRI and optogenetics for selective stimulation of GPe neurons in healthy and Parkinsonian rats, and confirmed the added specificity of using opto-fMRI. Finally, we aimed to further investigate hippocampal DBS, by performing a DBS-PET and DBS-fMRI study, and revealed opposing mechanisms between acute and long-term DBS. The experience gained through this set of experiments facilitates future investigation of epilepsy using opto-fMRI.

References

Abelson JL, Curtis GC, Sagher O, Albucher RC, Harrigan M, et al. (2005) Deep brain stimulation for refractory obsessive-compulsive disorder. Biol Psychiatry 75(5): 510-516

Abdi A, Mallet N, Mohamed FY, Sharott A, Dodson PD, et al. (2015) Prototypic and arkypallidal neurons in the dopamine-intact external globus pallidus. J Neurosci 35, 6667-6688

Adamantidis AR, Zhang F, Aravanis AM, Deisseroth K, de Lecea L (2007) Neural substrates of awakening probed with optogenetic control of hypocretin neurons. Nature 450: 420–424

Agid Y, Javoy F, Glowinski J, Bouvet D, Sotelo C (1973) Injection of 6-hydroxydopamine into the substantia nigra of the rat. II. Diffusion and specificity. Brain Res 58: 291–301

Aguirre GK (2006) Experimental design and data analysis for fMRI. In: Functional MRI. Ed. by Faro SH, Mohamed FB, 1st ed Springer-Verlag Chapter3: 59-74

Aguirre GK, Zarahn ZE, D'esposito M (1998) The variability of human BOLD hemodynamic responses. NeuroImage 8: 360-369

Airan RD, Thompson KR, Fenno LE, Bernstein H, Deisseroth K (2009) Temporally precise in vivo control of intracellular signalling. Nature 458: 1025-1029

Akman T, Erken H, Acar G, Bolat E, Kizilay Z, Acar F (2011) Effects of the hippocampal deep brain stimulation on cortical epileptic discharges in penicillin - induced epilepsy model in rats. Turk Neurosurg 21(1): 1-5

Albaugh DL, Shih YY (2014) Neural circuit modulation during deep brain stimulation at the subthalamic nucleus for Parkinson's disease: what have we learned from neuroimaging studies? Brain Connect 4, 1-14

Albin RL, Young AB, Penney JB (1989) The functional anatomy of basal ganglia disorders. Trends Neurosci 12: 366-375

Aldini J (1804) Essai théorique et expérimental sur le galvanisme, avec une série d'expériences faites devant des commissaires de l'Institut nationale de France, et en divers amphithéâtres anatomiques de Londres. Paris: Fournier Fils

Alexander GE, DeLong MR, Strick PL (1986) Parallel organization of functionally segregated circuits linking basal ganglia and cortex. Annu Rev Neurosci 9: 357-381

Alilain WJ, Li X, Horn KP, Dhingra R, Dick TE, Herlitze S, Silver J (2008) Light-induced rescue of breathing after spinal cord injury. J Neurosci 28: 11862-11870

Alvarez P, Zola-Morgan S, Squire LR. (1995) Damage limited to the hippocampal region produces long-lasting memory impairment in monkeys. J Neurosci 15: 3796-3807

Alvarez-Salvado E, Pallarés V, Moreno A, Canals S (2014) Functional MRI of long-term potentiation: imaging network plasticity. Philos Trans R Soc Lond B Biol Sci 369(1633): 20130152.

Angeli A, Akram H, Zacharia A, Limousin P, Hariz M, Zrinzo L, Foltynie T (2015) Varying time-course of effects of high frequency stimulation of sub-regions of the globus pallidus in patients with parkinson's disease. Parkinsonism Relat Disord 21(6): 597-602

Angenstein F, Krautwald K, Wetzel W, Scheich H (2013) Perforant pathway stimulation as a conditioned stimulus for active avoidance learning triggers BOLD responses in various target regions of the hippocampus: a combined fMRI and electrophysiological study. Neuroimage 75: 213-227

Arai N, Yokochi F, Ohnishi T, Momose T, Okiyama R, et al. (2008) Mechanisms of unilateral STN-DBS in patients with Parkinson's disease: a PET study. J Neurol 255: 1236-1243

Arantes PR, Cardoso EF, Barreiros MA, Teixeira MJ, Goncalves MR, et al. (2006) Performing functional magnetic resonance imaging in patients with Parkinson's disease treated with deep brain stimulation. Mov Disord 21:1154-1162

Aravanis AM, Wang LP, Zhang F, Meltzer LA, Mogri MZ, Schneider MB, Deisseroth K (2007) An optical neural interface: in vivo control of rodent motor cortex with integrated fiberoptic and optogenetic technology. J Neural Eng 4: S143–S156

Armstrong C, Krook-Magnuson E, Oijala M, Soltesz I (2013) Closed-loop optogenetic intervention in mice. Nat Protoc 8: 1475-1493

Arzimanoglou A, Hirsch E, Nehlig A, Castelnau P, Gressens P, Pereira dV (2002) Epilepsy and neuroprotection: an illustrated review. Epileptic Disord 4: 173-182

Asanuma K, Tang C, Ma Y, et al. (2006) Network modulation in the treatment of Parkinson's disease. Brain 129: 2667–2678

Aschauer DF, Kreuz S, Rumpel S (2013) Analysis of transduction efficiency, tropism and axonal transport of AAV serotypes 1, 2, 5, 6, 8 and 9 in the mouse brain. Plos one 8: e76310

Atasoy D, Aponte Y, Su HH, Sternson SM (2008) A FLEX switch targets Channelrhodopsin-2 to multiple cell types for imaging and long-range circuit mapping. J Neurosci 28: 7025-7030

Avanzini G, Franceschetti S. (2003) Cellular biology of epileptogenesis. Lancet Neurol 2(1): 33-42

Bandettini P (2012) 20 years of fMRI. NeuroImage 62(2): 575-1324

Bartholow R (1874) Experimental investigations into the functions of the human brain. Am J Med Sci 134: 305–313

Baker KB, Nyenhuis JA, Hrdlicka G, Rezai AR, Tkach JA, Shellock FG (2005) Neurostimulation systems: assessment of magnetic field interactions associated with 1.5- and 3- Tesla MR systems. J Magn Reson Imaging 21(1): 72-77

Banerjee PN, Filippi D, Hauser WA (2009) The descriptive epidemiology of epilepsy-a review. Epilepsy Res 85: 31–45

Beach TG, Adler CH, Sue LI, Vedders L, Lue L, et al. 2010. Multi-organ distribution of phosphorylated α-synuclein histopathology in subjects with Lewy body disorders. Acta Neuropathol 119: 689–702

Becerra L, Pendse G, Chang PC, Bishop J, Borsook D. (2011) Robust reproducible resting state networks in the awake rodent brain. PLoS One 6(10): e25701

Beckmann CF, Smith SM (2004) Probabilistic independent component analysis for functional magnetic resonance imaging. IEEE Trans Med Imaging 23: 137–152

Benabid AL, Chabardès S, Seigneuret E (2005) Deep-brain stimulation in Parkinson's disease: long-term efficacy and safety - What happened this year? Curr Opin Neurol 18(6): 623-630

Benabid AL (2003) Deep brain stimulation for Parkinson's disease. Current Opinion in Neurobiology 13: 696-706

Benabid AL, Pollak P, Gervason C, Hoffmann D, Gao DM, et al. (1991) Long-term suppression of tremor by chronic stimulation of the ventral intermediate thalamic nucleus. Lancet 337(8738): 403-436

Ben-Ari Y, Cossart R (2000) Kainate, a double agent that generates seizures: two decades of progress. Trends Neurosci 23(11): 580-587

Ben-Menachem E (2002) Vagus-nerve stimulation for the treatment of epilepsy. Lancet Neurol 1(8) :477-482

Berg AT, Berkovic SF, Brodie MJ, Buchhalter J, Cross JH, et al. (2010) Revised terminology and concepts for organization of seizures and epilepsies: report of the ILAE Commission on Classification and Terminology, 2005-2009. Epilepsia 51(4): 676-685

Berry AL, Foltynie T (2011) Gene therapy: A viable therapeutic strategy for Parkinson's disease? J Neurol 258: 179-188

Betchen SA, Kaplitt M (2003) Future and current surgical therapies in Parkinson's disease. Curr Opin Neurol 16(4): 487-493

Beurrier C, Bioulac B, Audin J, and Hammond C (2001) High-frequency stimulation produces a transient blockade of voltage-gated currents in subthalamic neurons. J Neurophysiol 85(4): 1351-1356

Bezard E, Przedborski S (2011) A tale on animal models of Parkinson's disease. Mov Disord 26(6): 993-1002

Birdno MJ, Grill WM (2008) Mechanisms of deep brain stimulation in movement disorders as revealed by changes in stimulus frequency. Neurotherapeutics 5: 14-25

Biswal BB, VanKylen J, Hyde JS (1997) Simultaneous assessment of flow and BOLD signals in resting-state functional connectivity maps. Nmr in Biomedicine 10(4-5): 165-170

Bloch A, Probst A, Bissig H, Adams H, Tolnay M (2006) Alpha-synuclein pathology of the spinal and peripheral autonomic nervous system in neurologically unimpaired elderly subjects. Neuropathol Appl Neurobiol 32: 284-295

Blumcke I, Thom M, Wiestler OD (2002) Ammon's horn sclerosis: a maldevelopmental disorder associated with temporal lobe epilepsy. Brain Pathol 12: 199-211

Boëx C, Vulliémoz S, Spinelli L, Pollo C, Seeck M (2007) High and low frequency electrical stimulation in non-lesional temporal lobe epilepsy. Seizure 16: 664-669

Boling W, Olivier A, Fabinyi G (2002) Historical contributions to the modern understanding of function in the central area. Neurosurgery 50: 1296–1310

Boon P, Raedt R, De Herdt V, Wyckhuys T, Vonck K. (2009) Electrical stimulation for the treatment of epilepsy. Neurotherapeutics 6: 218-277

Boon P, Vonck K, De Herdt V, Van Dycke A, Goethals M, Goossens L (2007) Deep brain stimulation in patients with refractory temporal lobe epilepsy. Epilepsia 48: 1551-1560

Bosetti M, Masse A, et al. (2002). Silver coated materials for external fixation devices; in vitro biocompatibility and genotoxicity. Biomaterials 23: 887–892

Boss A, Bisdas S, Kolb A, Hofmann M, Ernemann U, et al. (2010) Hybrid PET/MRI of Intracranial Masses: Initial Experiences and Comparison to PET/CT. J Nucl Med 51: 1198-1205

Bouilleret V, Valenti MP, Hirsch E, Semah F, Namer IJ (2002) Correlation between PET and SISCOM in temporal lobe epilepsy. J Nucl Med 43: 991-998

Bozzi Y, Dunleavy M, Henshall D (2011) Cell signaling underlying epileptic behavior. Front Behav. Neurosci 5: 45

Braak H, de Vos RA, Bohl J, Del Tredici K (2006) Gastric alpha-synuclein immunoreactive inclusions in Meissner's and Auerbach's plexuses in cases staged for Parkinson's disease-related brain pathology. Neurosci Lett 396: 67-72

Braak H, Del Tredici K, Rub U, de Vos RAI, Steur E, Braak E (2003) Staging of brain pathology related to sporadic Parkinson's disease. Neurobiol Aging 24: 197–211

Braak H, Braak E (2000) Pathoanatomy of Parkinson's disease. Journal of Neurology 247: 3-10

Brandt MD, Jessberger S, Steiner B, Kronenberg G, Reuter K, et al. (2003) Transient calretinin expression defines early postmitotic step of neuronal differentiation in adult hippocampal neurogenesis of mice. Mol Cell Neurosci 24: 603–613

Brenner M, Kisseberth WC, Su Y, Besnard F, Messing A (1994) GFAP promoter directs astrocyte-specific expression in transgenic mice. J Neurosci 14: 1030-1037

Bronstein JM, Tagliati M, Alterman RL, Lozano AM, Volkmann J, Stefanie A. et al. (2011) Deep brain stimulation for Parkinson disease: an expert consensus and review of key issues. Arch Neurol 68(2): 165-171

Bullmore E (2012).The future of functional MRI in clinical medicine. Neuroimage 62: 1267-1271

Bunzeck N, Doeller CF, Dolan RJ, Duzel E (2012) Contextual interaction between novelty and reward processing within the mesolimbic system. Hum Brain Mapp 33(6): 1309-1324

Burger C, Gorbatyuk OS, Velardo MJ, Peden CS, Williams P, et al. (2004). Recombinant AAV viral vectors pseudotyped with viral capsids from serotypes 1, 2, and 5 display differential efficiency and cell tropism after delivery to different regions of the central nervous system. Mol Ther 10: 302-317

Busskamp V, Duebel J, Balya D, Fradot M, Viney TJ, et al. (2010) Genetic reactivation of cone photoreceptors restores visual responses in retinitis pigmentosa. Science 329: 413-417

Buxton RB, Uludağ K, Dubowitz DJ, Liu TT (2004) Modeling the hemodynamic response to brain activation. Neuroimage 23(S1):S220-233

Buxton RB, Wong EC, Frank LR (1998) Dynamics of blood flow and oxygenation changes during brain activation: the balloon model. Magn Reson Med 39(6): 855-864

Calabresi P, Picconi B, Tozzi A, Ghiglieri V, Di Filippo M (2014) Direct and indirect pathways of basal ganglia: a critical reappraisal. Nat Neurosci 17, 1022-1030

Canals S, Beyerlein M, Merkle H, Logothetis NK (2009) Functional MRI evidence for LTP-induced neural network reorganization. Curr Biol 19: 398-403

Canals S, Beyerlein M, Murayama Y, and Logothetis NK (2008) Electric stimulation fMRI of the perforant pathway to the rat hippocampus. Mag Res Im 26: 978–986

Carmichael DW, Pinto S, Limousin-Dowsey P, Allen PJ, Lemieux L, Yousry T, et al. (2007) Functional MRI with active, fully implanted, deep brain stimulation systems: safety and experimental compounds. Neuroimage 37: 508-517

Castrioto A, Moro E (2013) New targets for deep brain stimulation treatment of Parkinson's disease. Expert Rev Neurother 13(12): 1319-1328

Cearley CN, Wolfe JH (2006) Transduction characteristics of adeno-associated virus vectors expressing cap serotypes 7, 8, 9, and Rh10 in the mouse brain. Mol Ther 13: 528-537

Chakravarthy VS, Joseph D, Bapi RS (2010) What do the basal ganglia do? A modeling perspective. Biol Cybern 103(3): 237-253

Chang SY, Kim I, and Marsh MP (2012) Wireless fast-scan cyclic voltammetry to monitor adenosine in patients with essential tremor during deep brain stimulation. Mayo Clin Proc 87(8): 760-5

Chao T-HH, Chen J-H, Yen C-T (2014) Repeated BOLD-fMRI Imaging of Deep Brain Stimulation Responses in Rats. PLoS One doi: 10.1371/journal.pone.0097305

Chastan N, Westby GW, Yelnik J, Bardinet E, Do MC, et al. (2009) Effects of nigral stimulation on locomotion and postural stability in patients with Parkinson's disease. Brain 132, 172-184

Chatziioannou A, Tai Y, Doshi N, Cherry S (2001) Detector development for microPET II: a 1 microl resolution PET scanner for small animal imaging Phys Med Biol 46: 2899-2910

Chavhan GB, Babyn PS, Thomas B, Shroff MM, Haacke EM (2009) Principles, Techniques, and Applications of T2*-based MR Imaging and Its Special Applications. Radiographics 29(5): 1433–1449

Chen MC, Ferrari L, Sacchet MD, Foland-Ross LC, Qiu MH, Gotlib IH, et al. (2015) Identification of a direct GABAergic pallidocortical pathway in rodents. Eur J Neurosci 41, 748-759

Chhabra V, Sung E, Mewes K, Bakay RA, Abosch A, Gross RE (2010) Safety of magnetic resonance imaging of deep brain stimulator systems: a serial imaging and clinical retrospective study. J Neurosurg 112: 497-502

Christie IN, Wells JA, Southern P, Marina N, Kasparov S, Gourine AV, et al. (2012) fMRI response to blue light delivery in the naive brain: Implications for combined optogenetic fMRI studies. Neuroimage. 66C: 634-641

Choi I, Gruetter R (2012) Neural metabolism in vivo. Springer, Kansas City

Chow BY, Han X, Dobry AS, Qian X, Chuong AS, et al. (2010). High- performance genetically targetable optical neural silencing by light-driven proton pumps. Nature 463: 98-102

Cigna Health Care (2005). Deep brain stimulation for Parkinson's disease (PD) and essential tremor (ET). www.cigna.com/ healthinfo/hw90970.html

Cole DM, Smith SM, Beckmann CF (2010) Advances and Pitfalls in the Analysis and Interpretation of Resting-State FMRI Data. Front Syst Neurosci 4: 8

Cooper IS, Amin I, Gilman S (1973) The effect of chronic cerebellar stimulation upon epilepsy in man. Trans Am Neurol Assoc 98:192–196

Coubes P, Vayssiere N, El Fertit H, Hemm S, Cif L, et al. (2002) Deep brain stimulation for dystonia. Surgical technique. Stereotact Funct Neurosurg 78(3-4): 183-191

Covington HE, Lobo MK, Maze I, Vialou V, Hyman JM, et al. (2010) Antidepressant effect of optogenetic stimulation of the medial prefrontal cortex. J Neurosci 30: 16082-16090

Creed M, Pascoli VJ, Lüscher C (2015) Refining deep brain stimulation to emulate optogenetic treatment of synaptic pathology. Science 347: 659-664

Crick FH (1979) Thinking about the brain. Sci Am 241: 219–232

Cuckiert A, Cuckiert CM, Burattini JA, and Lima AM (2014) Seizure outcome after hippocampal deep brain stimulation in a prospective cohort of patients with refractory temporal lobe epilepsy. Seizure 23(1): 6-9

Cuellar-Herrera M, Neri-Bazan L, Rocha LL (2006) Behavioral effects of high frequency electrical stimulation of the hippocampus on electrical kindling in rats. Epilepsy Res 72: 10–17

Cui G, Jun SB, Jin X, Pham MD, Vogel SS, et al. (2013) Concurrent activation of striatal direct and indirect pathways during action initiation. Nature 494, 238-242

Damoiseaux JS, Rombouts SA, Barkhof F, et al. (2006) Consistent resting-state networks across healthy subjects. Proc Natl Acad Sci (USA) 103: 13848–13853

de Hevesy G (1048) Radioactive indicators: their application in biochemistry, animal physiology and pathology. Interscience New York

Deichmann R, Noth U, Weiskopf N (2010) The basics of functional magnetic resonance imaging. In: EEG-fMRI: physiological basis, technique and applications. Ed. by Mulert C, Lemieux L, 1st ed Springer-Verlag Chapter 3: 39-62

Deisseroth K (2011) Optogenetics. Nat Methods 8: pp. 26–29

Deisseroth K, G. Feng G, A.K. Majewska AK, G. Miesenböck G, A. Ting A, M.J. Schnitzer MJ (2006) Next-generation optical technologies for illuminating genetically targeted brain circuits. J Neurosci 26: 10380-10386

Dejean C, Hyland B, Arbuthnott G (2009) Cortical effects of subthalamic stimulation correlate with behavioral recovery from dopamine antagonist induced akinesia. Cereb Cortex 19: 1055-1063

de Lanerolle NC, Lee TS (2005) New facets of the neuropathology and molecular profile of human temporal lobe epilepsy. Epilepsy Behav 7(2): 190-203

DeLong M, Wichmann T (2012) Deep brain stimulation for movement and other neurologic disorders. Ann N Y Acad Sci 1265, 1-8

DeLong MR (1990) Primate models of movement disorders of basal ganglia origin. Trends Neurosci 13, 281-285

Deniau JM, Degos B, Bosch C, Maurice N (2010) Deep brain stimulation mechanisms: beyond the concept of local functional inhibition. Eur J Neurosci 32: 1080-1091

Deniau JM, Mailly P, Maurice N, Charpier S (2007) The pars reticulata of the substantia nigra: a window to basal ganglia output. Prog Brain Res 160: 151-72

Desai M, Kahn I, Knoblich U, Bernstein J, Atallah H, Yang A, et al. (2011) Mapping brain networks in awake mice using combined optical neural control and fMRI. J Neurophysiol 105:1393-1405

DeVito JL, Anderson ME (1982) An autoradiographic study of the efferent connections of the globus pallidus in Macaca mullata. Brain Res 46: 107-117

Dickson DW, Fujishiro H, DelleDonne A, Menke J, Ahmed Z, et al. (2008) Evidence that incidental Lewy body disease is pre-symptomatic Parkinson's disease. Acta Neuropathol 115: 437-444

Dittgen T, Nimmerjahn A, Komai S, Licznerski P, Waters J, et al. (2004) Lentivirus- based genetic manipulations of cortical neurons and their optical and electro- physiological monitoring in vivo. Proc Natl Acad Sci USA 101: 18206–18211

Douglass AD, Kraves S, Deisseroth K, Schier AF, Engert F (2008) Escape behavior elicited by single, channelrhodopsin-2-evoked spikes in zebrafish somatosensory neurons. Curr Biol 18: 1133-1137

Drake PL, Hazelwood KJ (2005) Exposure-related health effects of silver and silver compounds: a review. Ann Occup Hyg 49(7): 575-585

Dreosti E, Lagnado L (2011) Optical reporters of synaptic activity in neural circuits. Exp Physiol 96: 4-12

Dreosti E, Odermatt B, Dorostkar MM, Lagnado L (2009) A genetically encoded reporter of synaptic activity in vivo. Nat Methods 6: 883-889

Dunn JF, Tuor UI, Kmech J, Young NA, Henderson AK, et al. (2009) Functional brain mapping at 9.4T using a new MRI-compatible electrode chronically implanted in rats. Magn Reson Med 61(1): 222-228

Duncan JS, Sagar HJ (1987) Seizure characteristics, pathology, and outcome after temporal lobectomy. Neurology 37: 405–409

Eckert T, Tang C, Eidelberg D (2007) Assessment of the progression of Parkinson's disease: a metabolic network approach. Lancet Neurol 6: 926 -932

El-Falougy H, Benuska J (2006) History, anatomical nomenclature, comparative anatomy and functions of the hippocampal formation. Bratisl Lek Listy. 107(4): 103-106

Engel J (2001) Mesial temporal lobe epilepsy: what have we learned? Neuroscientist 7(4): 340-352

Engel J (2006) Report of the ILAE Classification Core Group. Epilepsia 47: 1558-1568

Espinosa M, Jimenez B, Steinbach A, Wille A (2015) Radio IC for Quality Control in PET Diagnostics. http://www.sepscience.com/Sectors/Pharma/Articles/429-/

Ewing SG, Grace AA (2013) Long-term high frequency deep brain stimulation of the nucleus accumbens drives time-dependent changes in functional connectivity in the rodent limbic system. Brain Stimul 6: 274-285

Ewing SG, Witold JL, Grace AA, Wintera C (2013) An inexpensive, charge-balanced rodent deep brain stimulation device: a step-by-step guide to its procurement and construction. J Neurosci Methods 219(2): 10

Fahrner A, Kann G, Flubacher A, Heinrich C, Freiman TM, et al. (2007) Granule cell dispersion is not accompanied by enhanced neurogenesis in temporal lobe epilepsy patients. Exp Neurol 203(2): 320-332

Ferris CF, Febo M, Luo F, Schmidt K, Brevard M, et al. (2006) Functional magnetic resonance imaging in conscious animals: a new tool in behavioural neuroscience research. J Neuroendocrinol 18, 307-318

Fiala A, Suska A, Schluter OM (2010) Optogenetic approaches in neuroscience. Curr Biol 20: R897-903

Figee M, Luigjes J, Smolders R, Valencia-Alfonso CE, van Wingen G, et al. (2013) Deep brain stimulation restores frontostriatal network activity in obsessive-compulsive disorder. Nature Neuroscience 16: 386–387

Finelli DA, Rezai AR, Ruggieri PM, Tkach JA, Nyenhuis JA, Hrdlicka G, et al. (2002) MR imaging-related heating of deep brain stimulation electrodes: in vitro study. Am J Neuroradiol 23(10): 1795-1802.

Fischer R, Acevedo C, Arzimanoglou A, Bogacz A, Cross JH, et al. (2014) A practical clinical definition of epilepsy. Epilepsia 55(4): 475-482

Fischer R, Salanova V, and Witt T. SANTE Study Group (2010) Electrical stimulation of the anterior nucleus of thalamus for treatment of refractory epilepsy. Epilepsia 51(5): 899-908

Fischer RS, van Emde Boas W, Blume W, Elger C, Genton P, et al. (2005) Epileptic seizures and epilepsy: definitions proposed by the International League Against Epilepsy (ILAE) and the International Bureau for Epilepsy (IBE). Epilepsia 46(4): 470-472

Follett KA, Weaver FM, Stern M, Hur K, Harris CL, et al. CSP 468 Study Group (2014) Pallidal versus subthalamic deep-brain stimulation for Parkinson's disease. N Engl J Med 362(22): 2077-2091

Forsgren L, Beghi E, Oun A, Sillanpää M (2005) The epidemiology of epilepsy in Europe - a systematic review. Eur J Neurol 12(4): 245-253

Fox MD, Raichle ME (2007) Spontaneous fluctuations in brain activity observed with functional magnetic resonance imaging. Nat Rev Neurosci 8: 700–711

Franzini A, Ferroli P, Leone M, Broggi G (2003) Stimulation of the posterior hypothalamus for treatment of chronic intractable cluster headaches: first reported series. Neurosurgery 52: 1095–1099

Freeze BS, Kravitz AV, Hammack N, Berke JD, Kreitzer AC (2013) Control of Basal Ganglia output by direct and indirect pathway projection neurons. J Neurosci 33: 18531-18539

Freund TF (2003) Interneuron Diversity series: Rhythm and mood in perisomatic inhibition. Trends Neurosci 26: 489-495

Friend DM, Kravitz AV (2014) Working together: basal ganglia pathways in action selection. Trends Neurosci 37, 301-303

Frost B, Diamond MI (2010) Prion-like mechanisms in neurodegenerative diseases. Nature Reviews Neuroscience 11: 155-159

Fukuda M, Vazquez AL, Zong X, Kim SG (2013) Effects of the alpha(2)-adrenergic receptor agonist dexmedetomidine on neural, vascular and BOLD fMRI responses in the somatosensory cortex. Eur J Neurosci 37, 80-95

Galvan A, Devergnas A, Wichmann T (2015) Alterations in neuronal activity in basal ganglia-thalamocortical circuits in the parkinsonian state. Front Neuroanat 9: 5

Georgi JC, Stippich C, Tronnier VM, Heiland S (2004) Active deep brain stimulation during MRI: a feasibility study. Magn Reson Med 51(2): 380-388

Gittis AH, Berke JD, Bevan MD, Chan CS, Mallet N, et al. (2014) New roles for the external globus pallidus in basal ganglia circuits and behavior. J Neurosci 34, 15178-15183

Gittis AH, Kreitzer AC (2012) Striatal microcircuitry and movement disorders. Trends Neurosci 35(9): 557-64

Gjerløff T, Fedorova T, Knudsen K, Munk OL, Nahimi A, et al. (2015) Imaging acetylcholinesterase density in peripheral organs in Parkinson's disease with 11C-donepezil PET. Brain 138(Pt3): 653-363

Goerendt K, Lawrence AD, Mehta MA, et al. (2006) Distributed neural actions of anti-parkinsonian therapies as revealed by PET. J Neural Transm 113: 75–86

Goldberg JH, Farries MA, Fee MS (2013) Basal ganglia output to the thalamus: still a paradox. Trends Neurosci 36(12): 695-705

Goodman WK, Alterman RL (2012) Deep brain stimulation for intractable psychiatric disorders. Annu Rev Med 63, 511-524

Goodman JH, Berger RE, and Tcheng TK (2005) Preemptive low-frequency stimulation decreases the incidence of amygdala-kindled seizures. Epilepsia 46: 1-7

Gradinaru V, Mogri M, Thompson KR, Henderson JM, Deisseroth K (2009) Optical deconstruction of parkinsonian neural circuitry. Science 324: 354-359

Grafton ST, Turner RS, Desmurget M, Bakay R, DeLong M, et al. (2006) Normalizing motor-related brain activity: subthalamic nucleus stimulation in Parkinson disease. Neurology 66:1192-1199

Grealish S, Mattsson B, Draxler P, Björklund A (2010) Characterisation of behavioural and neurodegenerative changes induced by intranigral 6-hydroxydopamine lesions in a mouse model of Parkinson's disease. Eur J Neurosci. 31(12): 2266-2278

Greggio E, Civiero L, Bisaglia M, Bubacco L (2012) Parkinson's disease and immune system: is the culprit LRRKing in the periphery? J Neuroinflammation 9: 94

Grill WM and Snyder AN (2004) Miocinovic S. Deep brain stimulation creates an informational lesion of the stimulated nucleus. Neuroreport 15: 1137–1140

Groiss SJ, Wojtecki L, Siidmeyer M, Schnitzler A (2009) Deep Brain Stimulation in Parkinson's Disease. Ther Adv Neurol Disord 2(6): 20–28

Grüll H, Robillard M (2006) Molecular Agents for Targeted Imaging and Therapy. In Trends and Concepts in Agent Development. Springer, The Netherlands, 287-301

Guest WC, Silverman JM, Pokrishevsky E, O'Neill MA, Grad LI, Cashman NR (2011) Generalization of the prion hypothesis to other neurodegenerative diseases: an imperfect fit. J Toxicol Environ Health A 74(22-24):1433-1459

Guo Y, Duan W, Ma C, Jiang C, Xie Y, et al. (2015) Biocompatibility and magnetic resonance imaging characteristics of carbon nanotube yarn neural electrodes in a rat model. BioMed Eng 14: 118

Haensel JX, Spain A, Martin C (2015) A systematic review of physiological methods in rodent pharmacological MRI studies. Psychopharmacology (Berl) 232, 489-499.

Hamani C, Amorim BO, Wheeler AL, Diwan M, Driesslein K, Covolan L, et al. (2014) Deep brain stimulation in rats: different targets induce similar antidepressant-like effects but influence different circuits. Neurobiol Dis 71: 205-214

Hamani C, McAndrews MP, Cohn M, Oh M, Zumsteg D, et al. (2008) Memory enhancement induced by hypothalamic/fornix deep brain stimulation. Ann Neurol 63(1):119-123

Handwerker DA, Ollinger JM, D'Esposito M (2004) Variation of BOLD hemodynamic responses across subjects and brain regions and their effects on statistical analyses. Neuroimage 21(4): 1639-1651

Handforth A, DeGiorgio CM, Schachter SC, Uthman BM, Naritoku DK, et al. (1998) Vagus nerve stimulation therapy for partial-onset seizures: a randomized active-control trial. Neurology 51(1): 48-55

Harnois C, Filion M (1982) Pallidofugal projections to thalamus and midbrain: a quantitative antidromic activation study in monkeys and cats. Exp Brain Res 47: 277-285

Hashimoto M, Rockenstein E, Crews L, Masliah E (2003) Role of protein aggregation in mitochondrial dysfunction and neurodegeneration in Alzheimer's and Parkinson's diseases. Neuromolecular Med 4(1-2): 21-36

Haslinger B, Boecker H, Buchel C, Vesper J, Tronnier VM, Pfister F, et al. (2003) Differential modulation of subcortical target and cortex during deep brain stimulation. Neuroimage 18(2): 517–524

Hassler R, Riechert T (1955) A special method of stereotactic brain operation. Proc R Soc Med 48: 469-470

Hauser WA, Annegers JF, Rocca WA (1996) Descriptive epidemiology of epilepsy: contributions of population-based studies from Rochester, Minnesota. Mayo Clin Proc 71(6): 576-586

Heck CN, King-Stephens D, Massey AD, Nair DR, Jobst BC, et al. (2014) Two-year seizure reduction in adults with medically intractable partial onset epilepsy treated with responsive neurostimulation: Final results of the RNS System Pivotal trial. Epilepsia 55(3): 432-441

Helbing C, Werner G, Angenstein F (2013) Variations in the temporal pattern of perforant pathway stimulation control the activity in the mesolimbic pathway. Neuroimage 64: 43-60

Hershey T, Revilla FJ, Wernle AR, et al. (2003) Cortical and subcortical blood flow effects of subthalamic nucleus stimulation in PD. Neurology 61(6): 816-821

Hilker R, Voges J, Weber T, Kracht LW, Roggendorf J, et al. (2008) STN-DBS activates the target area in Parkinson disease: an FDG-PET study. Neurology 71: 708–713

Hilton D, Stephens M, Kirk L, Edwards P, Potter R, et al. (2014) Accumulation of α-synuclein in the bowel of patients in the pre-clinical phase of Parkinson's disease. Acta Neuropathol 127(2): 235-241

Histed MH, Bonin V, Reid RC (2009) Direct activation of sparse, distributed populations of cortical neurons by electrical microstimulation. Neuron, 63: 508–522

Ho SS, Berkovic SF, Berlangieri SU, Newton MR, Egan GF, Tochon-Danguy HJ, McKay WJ (1995) Comparison of ictal SPECT and interictal PET in the presurgical evaluation of temporal lobe epilepsy. Ann Neurol 37: 738-45

Hsu YH, Chang C, Chen CC (2014) Negative cerebral blood volume fMRI response coupled with Ca(2)(+)-dependent brain activity in a dopaminergic road map of nociception. Neuroimage 90: 43-51

Hu X, Le TH, Ugurbil K (1997) Evaluation of the early response in fMRI in individual subjects using short stimulus duration. Mag Res Med 37(6): 877-884

Huber D, Petreanu L, Ghitani N, Ranade S, Hromádka T, Mainen Z, Svoboda K (2008) Sparse optical microstimulation in barrel cortex drives learned behaviour in freely moving mice. Nature 451: 61-64

Huettel SA, Song AW, McCarthy G (2009a) BOLD fMRI: origin and properties. In: Functional Magnetic Resonance Imaging. Ed. by Huettel SA, Song AW, McCarthy G. 2nd ed. Sinauer Associates, In.c Chapter 7: 193-242

Huettel SA, Song AW, McCarthy G (2009b) From neuronal to hemodynamic activity. In: Functional Magnetic Resonance Imaging. Ed. by Huettel SA, Song AW, McCarthy G. 2nd ed. Sinauer Associates, In.c Chapter 6: 159-192

Huettel SA, Song AW, McCarthy G (2009c) MR contrast mechanisms and pulse sequences. In: Functional Magnetic Resonance Imaging. Ed. by Huettel SA, Song AW, McCarthy G. 2nd ed. Sinauer Associates, In.c Chapter 5: 121-157

Huettel SA, Song AW, McCarthy G (2009d) Experimental design. In: Functional Magnetic Resonance Imaging. Ed. by Huettel SA, Song AW, McCarthy G. 2nd ed. Sinauer Associates, In.c Chapter 9: 293-329

Huffman J, Kossoff EH (2006) State of the ketogenic diet(s) in epilepsy. Curr Neurol Neurosci Rep. 6(4): 332-340

Hung A, Goldberg IB, Judy JW, Zhou D, Greenbaum E (2010) Stimulation Electrode Materials and Electrochemical Testing Methods. In: Implantable Neural Prostheses. Springer New York Chapter 2: 191

Hutchison RM, Mirsattari SM, Jones CK, Gatl JS, Leung LS (2010) Functional networks in the anesthetized rat brain revealed by independent component analysis of resting-state fMRI. J Neurophysiol 103(6): 3398-3406

Hwang SI, Kim JH, Park SW, Han MH, Yu IK, et al. (2001) Comparative analysis of MR imaging, positron emission tomography, and ictal single-photon emission CT in patients with neocortical epilepsy. Am J Neuroradiol 22: 937-946

Hyde RA, Strowbridge BW (2012) Mnemonic representations of transient stimuli and temporal sequences in the rodent hippocampus in vitro. Nat Neurosci. 15(10): 1430-1438

Iancu R, Mohapel P, Brundin P, Paul G (2005) Behavioral characterization of a unilateral 6-OHDA-lesion model of Parkinson's disease in mice. Behav Brain Res 162: 1-10

Ito S, Takao M, Hatsuta H, Kanemaru K, Arai T, et al. (2011) Alpha-synuclein immunohistochemistry of gastrointestinal and biliary surgical specimens for diagnosis of Lewy body disease. Int J Clin Exp Pathol 7(4): 1714–1723

Jahfari S, Waldorp L, van den Wildenberg WP, Scholte HS, Ridderinkhof KR, Forstmann BU (2011) Effective connectivity reveals important roles for both the hyperdirect (fronto-subthalamic) and the indirect (fronto-striatal-pallidal) fronto-basal ganglia pathways during response inhibition. J Neurosci 31: 6891-6899

Jakobsson J, Ericson C, Jansson M, Bjork, E, Lundberg C (2003) Targeted transgene expression in rat brain using lentiviral vectors. J Neurosci Res 73: 876-885

James M, Gambhir S (2012) A Molecular Imaging Primer: Modalities, Imaging Agents and Applications. Physiol Rev: 897-965.

Jech R, Ruzicka E, Tintera J, Urgosik D (2003) Reply: fMRI during deep brain stimulation. Mov Disord 18(4): 461-462

Jech R, Urgosik D, Tintera J, Nebuzelsky A, Krasensky J, Liscak R, et al. (2001) Functional magnetic resonance imaging during deep brain stimulation: a pilot study in four patients with Parkinson's disease. Mov Disord 16: 1126-1132

Jonckers E, Van Audekerke J, De Visscher G, Van der Linden A, Verhoye M. (2011) Functional connectivity of the rodent brain: comparison of functional connectivity networks in rat and mouse. PLoS One 6(4): e18876

Jupp B, Williams JP, Tesiram YA, Vosmansky M, O'Brien TJ (2006) MRI compatible electrodes for the induction of amygdala kindling in rats. J Neurosci Methods 155(1): 72-76

Kahan J, Urner M, Moran R, Flandin G, Marreiros A (2014) Resting state functional MRI in Parkinson's disease: the impact of deep brain stimulation on 'effective' connectivity. Brain 137(Pt4): 1130-1144

Kalbe E, Voges J, Weber T, Haarer M, Baudrexel S, et al. (2009) Frontal FDG-PET activity correlates with cognitive outcome after STN-DBS in Parkinson disease. Neurology 72(1): 42-49

Kaneda K, Isa K, Yanagawa Y, Isa T (2008) Nigral inhibition of GABAergic neurons in mouse superior colliculus. J Neurosci 28: 11071-11078

Karimi M, Golchin N, Tabbal SD, et al. (2008) Subthalamic nucleus stimulation-induced regional blood flow responses correlate with improvement of motor signs in Parkinson disease. Brain 131, 2710–2719

Kaspar BK, Erickson D, Schaffer D, Hinh L, Gage FH, Peterson DA (2002). Targeted retrograde gene delivery for neuronal protection. Mol Ther 5: 50-56

Kato S, Inoue K, Kobayashi K, Yasoshima Y, Miyachi S, et al. (2007) Efficient gene transfer via retrograde transport in rodent and primate brains using a human immunodeficiency virus type 1-based vector pseudotyped with rabies virus glycoprotein. Hum Gene Ther 18: 1141-1151

Kato S, Kobayashi K, Inoue KI, Kuramochi M, Okada T et al. (2011). A lentiviral strategy for highly efficient retrograde gene transfer by pseudotyping with fusion envelope glycoprotein. Hum Gene Ther 22: 197-206

Kellaway P (1946) The part played by the electrical fish in the early history of bioelectricity and electrotherapy. Bull Hist Med 20: 112–137

Keilholz SD, Silva AC, Raman M, Merkle H, Koretsky AP (2006) BOLD and CBV-weighted functional magnetic resonance imaging of the rat somatosensory system. Magn Reson Med 55: 316-324.

Kim SG, Harel N, Jin T, Kim T, Lee P, Zhao F (2013) Cerebral blood volume MRI with intravascular superparamagnetic iron oxide nanoparticles. NMR Biomed 26: 949-962

Kim SG, Bandetti PA (2006) Principles of functional MRI. In: Functional MRI. Ed. by Faro SH, Mohamed FB, 1st ed Springer-Verlag Chapter 1: 3-23

Kim R, Nakano K, Jayaraman A, Carpenter MB (1976) Projections of the globus pallidus and adjacent structures: an autoradiographic study in the monkey. J Comp Neurol 169: 263-290

Kim S, Mountz JM (2011) SPECT imaging of epilepsy: an overview and comparison with F-18 FDG PET. Int J Mol Imaging (2011): 813028

King D, Spencer SS, Mccarthy G, Luby M, Spencer DD (1995) Bilateral Hippocampal Atrophy in Medical Temporal Lobe Epilepsy. Epilepsia 36: 905-910

Klapoetke NC, Murata Y, Kim SS, Pulver SR, Birdsey-Benson A, et al. (2014) Optical excitation of distinct neural populations. Nature Methods 11: 338-346

Klein J, Soto-Montenegro ML, Pascau J, Gu̇nther L, Kupschc A, Desco M, et al. (2011) A novel approach to investigate neuronal network activity patterns affected by deep brain stimulation in rats. Jour of Psych Res 45: 927-930

Knight EJ, Min HK, Hwang SC, Marsh MP, Paek S, et al. (2013) Nucleus accumbens deep brain stimulation results in insula and prefrontal activation: a large animal FMRI study. PLoS One 8, e56640

Koob GF, Volkow ND (2010) Neurocircuitry of addiction. Neuropsychopharmacology 35(1): 217–238

Kornak J. Hall DA, Haggard MP (2011) Spatially Extended fMRI Signal Response to Stimulus in Non-Functionally Relevant Regions of the Human Brain: Preliminary Results. Open Neuroimag J 5:24-32

Krautwald K, Min H-K, Lee HK, Angenstein F (2013) Synchronized electrical stimulation of the rat medial forebrain bundle and perforant pathway generates an additive BOLD response in the nucleus accumbens and prefrontal cortex. Neuroimage 77: 14-25.

Krautwald K, Angenstein F (2012) Low frequency stimulation of the perforant pathway generates anesthesia-specific variations in neural activity and BOLD responses in the rat dentate gyrus. J Cereb Blood Flow Metab 32, 291-305

Kravitz AV, Freeze BS, Parker PR, Kay K, Thwin MT, Deisseroth K, Kreitzer AC (2010) Regulation of parkinsonian motor behaviours by optogenetic control of basal ganglia circuitry. Nature 466: 622–626

Kringelbach ML, Jenkinson N, Owen SL, Aziz TZ (2007) Translational principles of deep brain stimulation. Nat Rev Neurosci 8(8): 623-635

Kuhlman SJ, Huang ZJ (2008) High-resolution labeling and functional manipulation of specific neuron types in mouse brain by Cre-activated viral gene expression. PLoS ONE 3: e2005

Kumar R, Simpson CV, Froelich CA, Baughman BC, Gienapp AJ, Sillay KA (2015) Obesity and deep brain stimulation: an overview. Ann Neurosci 22(3): 181–188

Kumar A, Semah F, Chugani HT, Theodore WH (2012) Epilepsy diagnosis: posi- tron emission tomography. Handb Clin Neurol 107: 409-424

Kuncel AM, Grill WM (2004) Selection of stimulus parameters for deep brain stimulation. Clin Neurophysiol. 115(11): 2431-2441

Kuntner C, Stout D (2014) Quantitative preclinical PET imaging: opportunities and challenges. Frontiers in Physics 2:1-12

Kuo JS, Carpenter MB (1973) Organization of pallidothalamic projections in the rhesus monkey. J Comp Neurol 151: 201-236

Laćan G, De Salles AA, Gorgulho AA, Krahl SE, Frighetto L, et al. (2008) Modulation of food intake following deep brain stimulation of the ventromedial hypothalamus in the vervet monkey. Laboratory investigation. J Neurosurg 108(2): 336-342

Lai HY, Albaugh DL, Kao YC, Younce JR, Shih YY (2015) Robust deep brain stimulation functional MRI procedures in rats and mice using an MR-compatible tungsten microwire electrode. Magn Reson Med 73, 1246-1251

Lai HY, Younce JR, Albaugh DL, Kao YC, Shih YY (2014) Functional MRI reveals frequency-dependent responses during deep brain stimulation at the subthalamic nucleus or internal globus pallidus. Neuroimage 84, 11-18

LaLumiere RT (2011) A new technique for controlling the brain: optogenetics and its potential for use in research and the clinic. Brain Stimul 4:1-6

Lang AE, Lozano AM (1998) Parkinson's disease. First of two parts. N Engl J Med 339(15): 1044-1053

Lanyi JK, Oesterhelt D (1982) Identification of the retinal-binding protein in halorhodopsin. J Biol Chem 257: 2674-2677

Lauritzen M (2005) Reading vascular changes in brain imaging: is dendritic calcium the key? Nat Rev Neurosci. 6: 77-85

Lee JH, Durand R, Gradinaru V, Zhang F, Goshen I, et al. (2010) Global and local fMRI signals driven by neurons defined optogenetically by type and wiring. Nature 465, 788-792

Leopold DA (2010) Neuroscience: fMRI under the spotlight. Nature 465: 700-701

Lewis DV (2005) Losing neurons: selective vulnerability and mesial temporal sclerosis. Epilepsia 46(S7): 39–44

Li N, Downey JE, Bar-Shir A, Gilad AA, Walczak P, et al. (2011) Optogenetic-guided cortical plasticity after nerve injury. Proc Natl Acad Sci USA 108: 8838-8843

Lieb JP, Dasheiff RM, Engel J (1991) Role of the frontal lobes in the propagation of mesial temporal lobe seizures. Epilepsia 32(6): 822–837

Ligot N, Krystkowiak P, Simonin C, Goldman S, Peigneux P, et al. (2011) External globus pallidus stimulation modulates brain connectivity in Huntington's disease. J Cereb Blood Flow Metab 31, 41-46

Lindauer U, Leithner C, Kaasch H, Rohrer B, Foddis M, et al. (2010). Neurovascular coupling in rat brain operates independent of hemoglobin deoxygenation. J Cereb Blood Flow Metab 30: 757–768

Liu HL, Chen HM, Wu YC, Lim SN, Huang CM, Hsu YY, Wai YY, Wu T (2008) False-positive analysis of functional MRI during simulated deep brain stimulation: A phantom study. Magn Reson Imaging 27(6): 1439-1442

Liu HL, Maxwell RE, Truwit CL (2001) Intraoperative MR-guided DBS implantation for treating PD and ET. Medical Imaging: Visualization, Display, and Image-Guided Procedures, Proc. SPIE 4319

Llewellyn ME, Thompson KR, Deisseroth K, Delp SL (2010) Orderly recruitment of motor units under optical control in vivo. Nat Med 16: 1161-1165

Logothetis NK, Pauls J, Augath M, Trinath T, Oeltermann A (2001) Neurophysiological investigation of the basis of the fMRI signal. Nature 412: 150-157

Lozano AM, Lipsman N (2013) Probing and regulating dysfunctional circuits using deep brain stimulation. Neuron 77(3): 406-424

Lozano AM, Hamani C (2004) The future of deep brain stimulation. J Clin Neurophysiol 21(1): 68-69

Lozano AM, Mahant N (2004) Deep brain stimulation surgery for Parkinson's disease: mechanisms and consequences. Parkinsonism Relat Disord 10:S49-57

Lozano AM, Dostrovsky J. Chen R, Ashby P (2002) Deep brain stimulation for Parkinson’s disease: disrupting the disruption. Lancet Neurol 1: 225-231

Lu H, Scholl CA, Zuo Y, Stein EA, Yang Y (2007) Quantifying the blood oxygenation level dependent effect in cerebral blood volume-weighted functional MRI at 9.4T. Magn Reson Med. 58(3): 616-21

Lundby A, Akemann W, Knöpfel T (2010) Biophysical characterization of the fluorescent protein voltage probe VSFP2.3 based on the voltage-sensing domain of Ci-VSP. Eur Biophys J 39: 1625-1635

Lüthi A, Lüscher C (2014) Pathological circuit function underlying addiction and anxiety disorders. Nature Neuroscience 17: 1635–1643

Luthman J, Fredriksson A, Sundström E, Jonsson G, Archer T (1989) Selective lesion of central dopamine or noradrenaline neuron systems in the neonatal rat: motor behavior and monoamine alterations at adult stage. Behav Brain Res 33(3): 267-277

Lyons MK (2011) Deep brain stimulation: current and future clinical applications. Mayo Clin Proc 86(7): 662-672

Magdaleno-Madrigal VM, Valdés-Cruz A, Martínez-Vargas D, Almazán-Alvarado S, Fernández-Mas R (2013) Effect of vagus nerve stimulation on electrical kindling in different stages of seizure severity in freely moving cats. Epilepsy Res 108(1): 81-89

Mallet N, Micklem BR, Henny P, Brown MT, Williams C, et al. (2012) Dichotomous organization of the external globus pallidus. Neuron 74, 1075-1086

Mandeville JB, Marota JJA, Kosofsky BE, Keltner JR, Weissleder R, Rosen BR, Weisskoff RM (1998) Dynamic Functional Imaging of Relative Cerebral Blood Volume During Rat Forepaw Stimulation. Magn Reson Med 39: 615–624

Markakis EA, Vives KP, Bober J, Leichtle S, Leranth C, et al. (2010) Comparative transduction efficiency of AAV vector serotypes 1-6 in the sub- stantia nigra and striatum of the primate brain. Mol Ther 18: 588-593

Marsden CD (1984) Origins of normal and pathological tremor. In: Movement Disorders: Tremor, eds Findley IJ, Capildeo R, London: Macmillan, 37-84

Martinez-Santiesteban FM, Swanson SD, Noll DC, AndersonDJ (2007) Magnetic field perturbation of neural recording and stimulating microelectrodes. Phys Med Biol 52: 2073–2088

Mathern GW, Babb TL, Leite JP, Pretorius K, Yeoman KM, Kuhlman PA (1999) The pathogenic and progressive features of chronic human hippocampal epilepsy. Epilepsy Res 26(1): 151-161

Mathern GW, Leite JP, Babb TL, Pretorius JK, Kuhlman PA (1996) Aberrant hippocampal mossy fiber sprouting correlates with greater NMDAR2 receptor staining. NeuroReport 7: 1029-1035

Matsuno-Yagi A, Mukohata Y (1977) Two possible roles of bacteriorhodopsin; a comparative study of strains of Halobacterium halobium differing in pigmentation. Biochem Biophys Res Commun: 237-243

Mattis J, Tye KM, Ferenczi EA, Ramakrishnan C, O'Shea DJ, et al. (2012) Principles for applying optogenetic tools derived from direct comparative analysis of microbial opsins. Nat Methods 9: 159-172

Mayberg HS, Lozano AM, Voom V, McNeely HE, Seminowicz D, Hamani C, Schwalb JM, Kennedy SH (2005) Deep brain stimulation for treatment-resistant depression. Neuron 45: 651–660

McConnel JC, So RQ, Hilliard JD, Lopomo P, Grill WM (2012) Effective deep brain stimulation suppresses low frequency network oscillations in the basal ganglia by regularizing neural firing patterns. J Neurosci 32(45): 15657-15668

McCracken CB, Grace AA (2007) High-frequency deep brain stimulation of the nucleus accumbens region suppresses neuronal activity and selectively modulates afferent drive in rat orbitofrontal cortex in vivo. J Neurosci 27: 12601-12610

McDevitt RA, Reed SJ, Britt JP (2014) Optogenetics in preclinical neuroscience and psychiatry research: recent insights and potential applications. Neuropsychiatr Dis Treat 10: 1369-1379

McIntyre CC, Savasta M, Kerkerian-Le Goff L, and Vitek JL (2004) Uncovering the mechanism(s) of action of deep brain stimulation: activation, inhivition, or both. Clinical Neurophysiology 115: 1239-1248

McKeown M, Hansen L, Sejnowsk T (2003) Independent component analysis of functional MRI: what is signal and what is noise? Curr Opin Neurobiol 13(5): 620–629

McLachlan RS, Pigott S, Tellez-Zenteno JF, Wiebe S, Parrent A (2010) Bilateral hippocampal stimulation for intractable temporal lobe epilepsy: impact on seizures and memory. Epilepsia 51(2): 304-307

Meltzer CC, Adelson PD, Brenner RP, Crumrine PK, Van Cott A, Schiff DP, Townsend DW, Scheuer ML (2000) Planned ictal FDG PET imaging for localization of extratemporal epileptic foci. Epilepsia 41: 193-200

Michaelides M, Anderson SA, Ananth M, Smirnov D, Thanos PK, et al. (2013) Whole-brain circuit dissection in free-moving animals reveals cell-specific mesocorticolimbic networks. J Clin Invest 123(12): 5342–5350

Middleton FA, Strick PL (2002) Basal-ganglia 'Projections' to the Prefrontal Cortex of the Primate. Cereb Cortex 12(9): 926-935

Min HK, Hwang SC, Marsh MP, Kim I, Knight E, Striemer B (2012) Deep brain stimulation induces BOLD activation in motor and non-motor networks: An fMRI comparison study of STN and EN/GPi DBS in large animals. Neuroimage 63(3): 1408-1420

Minguez-Castellanos A, Chamorro CE, Escamilla-Sevilla F, Ortega-Moreno A, Rebollo AC (2007) Do alpha-synuclein aggregates in autonomic plexuses predate Lewy body disorders?: a cohort study. Neurology 68(23): 2012-2018

Miyamichi K, Amat F, Moussavi F, Wang C, Wickersham I, et al. (2011) Cortical representations of olfactory input by trans-synaptic tracing. Nature 472: 191-196

Montgomery EB Jr, Baker KB (2000) Mechanisms of deep brain stimulation and future technical developments. Neurol Res 22(3): 259-266

Morrell M (2006) Brain stimulation for epilepsy: can scheduled or responsive neurostimulation stop seizures? Curr Opin Neurol 19: 164–168

Moses WW (2011) Fundamental Limits of Spatial Resolution in PET. Nucl Instrum Methods Phys Res A 648 (S1): S236–S240

Nagel G, Brauner M, Liewald JF, Adeishvili N, Bamberg E, Gottschalk A (2005) Light activation of channelrhodopsin-2 in excitable cells of Caenorhabditis elegans triggers rapid behavioral responses. Curr Biol 15: 2279-2284

Nagel G, Szellas T, Huhn W, Kateriya S, Adeishvili N, et al. (2003) Channelrhodopsin-2, a directly light-gated cation-selective membrane channel. Proc Natl Acad Sci USA 100: 13940-13945

Natale G, Ferrucci M, Lazzeri G, Paparelli A, Fornai F (2011a) Transmission of prions within the gut and towards the central nervous system. Prion. 5: 142-149

Natale G, Pasquali L, Paparelli A, Fornai F (2011b) Parallel manifestations of neuropathologies in the enteric and central nervous systems. Neurogastroenterol Motil 23: 1056-1065

Nathanson JL, Jappelli R, Scheeff ED, Manning G, Obata K et al. (2009) Short Promoters in Viral Vectors Drive Selec- tive Expression in Mammalian Inhibitory Neurons, but do not Restrict Activity to Specific Inhibitory Cell-Types. Front Neural Circuits 3: 19

Nazzaro JM, Lyons KE, Wetzel LH, Pahwa R (2010) Use of brain MRI after deep brain stimulation hardware implantation. Int J Neurosci 120: 176-183

Neves G, Cooke SF, and Bliss TV (2008) Synaptic plasticity, memory and the hippocampus: a neural network approach to causality. Nat Rev Neurosci 9(1): 65-75

Nooraine J, Iyer RB, Raghavendra S (2013) Ictal PET in presurgical workup of refractory extratemporal epilepsy. Ann Indian Acad Neurol 16: 676-67

Nuttin B, Cosyns P, Demeulemeester H, et al. (1999) Electrical stimulation in anterior limbs of internal capsules in patients with obsessive-compulsive disorder. Lancet 354: 1526

Nyenhuis J, Duan L (2009) An evaluation of MRI safety and compatibility of a silver-impregnated antimicrobial wound dressing. J Am Coll Radiol 6(7): 500–505

Okun MS. (2012) Deep-Brain Stimulation for Parkinson's Disease. N Engl J Med 367: 1529-1538

Oluigbo CO, Salma A, Rezai AR (2012) Deep brain stimulation for neurological disorders. IEEE Rev Biomed Eng 5: 88-99

Osorio I, Frei MG, Sunderam S, Sunderam S, Giftakis J, Bhavaraju NC, Schaffner SF, et al. (2005) Automated seizure abatement in humans using electrical stimulation. Ann Neurol 57: 258-268

Osorio I, Frei MG, Sunderam S, Giftakis J, Bhavaraju NC, et al. (2005) Automated seizure abatement in humans using electrical stimulation. Annals of neurology 57: 258-268

Paek SB, Min HK, Kim I, Knight EJ, Baek JJ, et al. (2015) Frequency-dependent functional neuromodulatory effects on the motor network by ventral lateral thalamic deep brain stimulation in swine. Neuroimage 105, 181-188

Palmowski K, Winz O, Rix A, Bzyl J, Behrendt F, et al. (2013) Accuracy of a clinical PET/CT vs. a preclinical μPET system for monitoring treatment effects in tumour xenografts. Eur J Rad 82: 1318-1324

Pama C, Colzato LS, Hommer B (2013) Optogenetics as a neuromodulation tool in cognitive neuroscience. Front Psychol 4: 610

Panayiotopoulos CP (2007) Principles of therapy in the epilepsies. A clinical guide to epileptic syndromes and their treatment. Ed. By Panayiotopoulos CP 2nd ed Vol1 Springer-Verlag Chap7: 155-179

Parent A (2004) Giovanni Aldini: from animal electricity to human brain stimulation. Can J Neurol Sci 31: 576–584

Parent JM, Lowenstein DH (2002) Seizure-induced neurogenesis: are more new neurons good for an adult brain? Prog Brain Res 135: 121–131

Parent JM, Tada E, Fike JR, Lowenstein DH (1999) Inhibition of Dentate Granule Cell Neurogenesis with Brain Irradiation Does Not Prevent Seizure-Induced Mossy Fiber Synaptic Reorganization in the Rat. J Neurosc, 19(11): 4508-4519

Parent A, Hazrati LN (1993) Anatomical aspects of information processing in primate basal ganglia. Trends Neurosci 16(3): 111-116

Parkkinen L, Kauppinen T, Pirttila T, Autere JM, Alafuzoff I (2005) α-Synuclein pathology does not predict extrapyramidal symptoms or dementia. Ann Neurol 57: 82-91

Paterna JC, Feldon J, Bueler H (2004) Transduction profiles of recombinant adeno-associated virus vectors derived from serotypes 2 and 5 in the nigrostriatal system of rats. J Virol 78: 6808-6817

Pawela CP, Biswal BB, Hudetz AG, Schule ML, Li R, Jones SR, et al. (2009) A protocol for use of medetomidine anesthesia in rats for extended studies using task-induced BOLD contrast and resting state functional connectivity. Neuroimage 46(4): 1137-1147

Paxinos G, and Watson C (2007) In: The rat brain in stereotactic coordinates, Academic Press 6th Ed

Penfield W, Rasmussen T (1950) The Cerebral Cortex of Man. A clinical Study of Localization of Function (New York: The MacMillan Company)

Petreanu L, Mao T, Sternson SM, Svoboda K(2009) The subcellular organization of neocortical excitatory connections. Nature 457: 1142-1145

Phillips MD, Baker KB, Lowe MJ, Tkach JA, Cooper SE, Kopell BH, Rezai AR (2006) Parkinson disease: pattern of functional MR imaging activation during deep brain stimulation of subthalamic nucleus--initial experience. Radiology 239: 209-216

Piedimonte F, Andreani JC, Piedimonte L, Graff P, Bacaro V (2013) Behavioral and motor improvement after deep brain stimulation of the globus pallidus externus in a case of Tourette's syndrome. Neuromodulation 16, 55-58; discussion 58

Pittau F, Grova C, Moeller F, Dubeau F, Gotman J (2012) Patterns of altered functional connectivity in mesial temporal lobe epilepsy. Epilepsia 53(6): 1013-1023

Press WH, Flannery BP, Teukolsky SA, and Vetterling WT (1992) Direction Set (Powell's) Methods in Multidimensions. In: Numerical Recipes in C, Cambridge University Press 2nd Ed: 412-420

Przedborski S, Tieu K (2006) Toxic animal models. In Neurodegenerative diseases, Eds. Beal MF, et al. Cambridge University Press, Cambridge, 196–221

Przedborski S, Levivier M, Jiang H, Ferreira M, Jackson-Lewis V, et al. (1995) Dose-dependent lesions of the dopaminergic nigrostriatal pathway induced by intrastriatal injection of 6-hydroxydopamine. Neuroscience 67(3): 631-647

Quigley MA, Haughton VM, Carew J, Cordes D, Moritz CH, Meyerand ME (2002) Comparison of independent component analysis and conventional hypothesis-driven analysis for clinical functional MR image processing. AJNR Am J Neuroradiol 23(1): 49-58

Rascol O, Payoux P, Ory F, Ferreira JJ, Brefel-Courban C, Montastruc JL (2003) Limitations of current Parkinson's disease therapy. Ann Neurol 53: S3-15

Recasens A, Dehay B (2014) Alpha-synuclein spreading in Parkinson's disease. Front Neuroanat 8: 159

Rezai AR, Philips M, Baker KB, Sharan AD, Nyenhuis J, Tkach J, et al. (2004) Neurostimulation system used for deep brain stimulation (DBS): MR safety issues and implications of failing to follow safety recommendations. Invest Radiol 39(5): 300-303

Romanelli P, Anschel DJ (2006) Radiosurgery for epilepsy. Lancet Neurol 5(7): 613-620

Rondouin G, Lerner-Natoli M, and Hashizume A (1987) Wet dog shakes in limbic versus generalized seizures. Exp Neurol 95(2): 500-505

Rorden C, Morgan P (2016) MRI Physics2: Contrasts and protocols. http://slideplayer.com/slide/3279600/

Ross EK, Kim JP, Settell ML, Han SR, Blaha CD, Min HK, Lee KH (2016) Fornix deep brain stimulation circuit effect is dependent on major excitatory transmission via the nucleus accumbens. Neuroimage 128: 138-148

Rossi U (2003) The history of electrical stimulation of the nervous system for the control of pain, in Electrical Stimulation and the Relief of Pain, ed. Simpson BA. Editor, Amsterdam: Elsevier BV: 5–16

Rothwell JC (2011) The motor functions of the basal ganglia. J Integr Neurosci 10(3): 303-315

Rosa MJ, Kilner J, Blankenburg F, Josephs O, Penny W (2010) Estimating the transfer function from neuronal activity to BOLD using simultaneous EEG-fMRI. Neuroimage 49(2): 1496–1509

Royer S, Zemelman BV, Barbic M, Losonczy A, Buzsáki G, Magee JC (2010) Multi-array silicon probes with integrated optical fibers: light-assisted perturbation and recording of local neural circuits in the behaving animal. Eur J Neurosci 31: 2279-2291

Ruge D, Cif L, Limousin P, Gonzalez V, Vasques X, et al. (2011) Shaping reversibility? Long-term deep brain stimulation in dystonia: the relationship between effects on electrophysiology and clinical symptoms. Brain 134(Pt 7): 2106-2115

Saha G (2010) Basics of PET Imaging: Physics, Chemistry and Regulationns, Springer

Sarre S, Yuan H, Jonkers N, Van HA, Ebinger G, Michotte Y (2004) In vivo characterization of somatodendritic dopamine release in the substantia nigra of 6-hydroxydopamine-lesioned rats. J Neurochem 90: 29-39

Sauer H, Oertel WH (1994) Progressive degeneration of nigrostriatal dopamine neurons following intrastriatal terminal lesions with 6-hydroxydopamine: a combined retrograde tracing and immunocytochemical study in the rat. Neuroscience 59(2): 401-415

Saunders A, Oldenburg IA, Berezovskii VK, Johnson CA, Kingery ND, et al. (2015) A direct GABAergic output from the basal ganglia to frontal cortex. Nature 521, 85-89

Savitt JM, Dawson VL, Dawson TM (2006) Diagnosis and treatment of Parkinson disease: molecules to medicine. J Clin Invest 116(7):1744-1754

Schiffer WK, Mirrione MM, Biegon A, et al. (2006) Serial microPET measures of the metabolic reaction to a microdialysis probe implant. J Neurosci Methods 155(2): 272-284

Scherzinger AL, Hendee WR (1985) Basic Principles of Magnetic Resonance Imaging—An Update. West J Med 143(6): 782–792

Schmidt R, Leventhal DK, Mallet N, Chen F, Berke JD (2013) Canceling actions involves a race between basal ganglia pathways. Nat Neurosc 16: 1118-1124

Schridde U, Khubchandani M, Motelow JE, Sanganahalli BG, Hyder F, Blumenfeld H (2008) Negative BOLD with Large Increases in Neuronal Activity. Cereb Cortex 18(8): 1814–1827

Schwalb JM, Hamani C (2008) The history and future of deep brain stimulation. Neurotherapeutics 5: 3–13

Scoville WB, Milner B (1957) Loss of recent memory after bilateral hippocampal lesions. J Neurol Neurosurg Psychiatry 20(1): 11-21

Seino M (2006) Classification criteria of epileptic seizures and syndromes. Epilepsy Res 70: S27-S33

Shannon KM, Keshavarzian A, Dodiya HB, Jakate S, Kordower JH (2012) Is alpha-synuclein in the colon a biomarker for premotor Parkinson's disease? Evidence from 3 cases. Mov Disord 27: 716–719

Shi LH, Luo F, Woodward D, Chang JY (2006) Deep brain stimulation of the substantia nigra pars reticulata exerts long lasting suppression of amygdala-kindled seizures. Brain Res 1090, 202-207

Shih YY, Huang S, Chen YY, Lai HY, Kao YC, et al. (2014) Imaging neurovascular function and functional recovery after stroke in the rat striatum using forepaw stimulation. J Cereb Blood Flow Metab 34: 1483-1492

Shih YYI, Yash TV, Rogers B, and Duong TQ (2013a) FMRI of deep brain stimulation at the rat ventral posteromedial thalamus. Brain Stimulation 7(2): 190-193

Shih YY, Wang L, De La Garza BH, Li G, Cull G, et al. (2013b) Quantitative retinal and choroidal blood flow during light, dark adaptation and flicker light stimulation in rats using fluorescent microspheres. Curr Eye Res 38, 292-298

Shih YY, Li G, Muir ER, De La Garza BH, Kiel JW, Duong TQ (2012) Pharmacological MRI of the choroid and retina: blood flow and BOLD responses during nitroprusside infusion. Magn Reson Med 68, 1273-1278

Shih YY I, Wey HY, Del La Garza BH, Duong TQ (2011) Striatal and cortical BOLD, blood flow, blood volume, oxygen consumption, and glucose consumption changes in noxious forepaw electrical stimulation. J Cereb Blood Flow Metab 31(3): 832–841

Shih YY I, Chen CC V, Shyu BC, Lin ZJ, Chiang YC, et al. (2009) A New Scenario for Negative Functional Magnetic Resonance Imaging Signals: Endogenous Neurotransmission. The Journal of Neuroscience 29(10): 3036-3044

Shmuel A (2010) Locally measured neuronal correlates of functional MRI signals. In: EEG-fMRI: Physiological basis, technique and applications. Ed. by Mulert C, Lemieux L. 1st ed Springer-Verlag Chapter 4: 63-82

Shmuel A, Augath M, Oeltermann A, Logothetis NK (2006) Negative functional MRI response correlates with decreases in neuronal activity in monkey visual area V1. Nat Neurosci 9: 569–577

Shmuel A, Yacoub E, Pfeuffer J, Van de Moortele PF, Adriany G, Hu X, Ugurbil K (2002) Sustained negative BOLD, blood flow and oxygen consumption response and its coupling to the positive response in the human brain. Neuron 36: 1195–1210

Shyu BC, Lin CY, Sun JJ, Chen SL, Chang C (2004) BOLD response to direct thalamic stimulation reveals a functional connection between the medial thalamus and the anterior cingulate cortex in the rat. Magn Reson Med. 52(1): 47-55

Siclari F, Prior JO, Rossetti AO (2013) Ictal cerebral positron emission tomography (PET) in focal status epilepticus. Epilepsy Res 105: 356-361

Siero JC, Petridou N, Hoogduin H, Luijten PR, Ramsey NF (2011) Cortical depth-dependent temporal dynamics of the BOLD response in the human brain. J Cereb Blood Flow Metab 31(10): 1999-2008

Silva AC, Koretsky AP, Duyn JH (2007) Functional MRI impulse response for BOLD and CBV contrast in rat somatosensory cortex. Magn Reson Med 57: 1110-1118

Simeral JD, Yen Y-F, Hernandez L, Pons TP, Hampson RE, Deadwyler SA (1999) Comparison of Independent Component Analysis (ICA) and Statistical Parametric Mapping (SPM) Procedures in an fMRI Visual Activation Study. Conf Proc ismrm 1716

Smith AT, Williams AL, Singh KD (2004) Negative BOLD in the Visual Cortex: Evidence Against Blood Stealing. Hum Brain Mapp 21: 213-220

Smith Y, Bevan MD, Shink E, Bolam JP (1998) Microcircuitry of the direct and indirect pathways of the basal ganglia. Neuroscience 86: 353-387

So RQ, McConnell GC, August AT, Grill WM (2012) Characterizing effects of subthalamic nucleus deep brain stimulation on methamphetamine-induced circling behavior in hemiparkinsonian rats. IEEE Trans Neural Syst Rehabil Eng

Sohal VS, Zhang F, Yizhar O, Deisseroth K (2009) Parvalbumin neurons and gamma rhythms enhance cortical circuit performance. Nature 459: 698–702

Spencer SS (2002) Neural networks in human epilepsy: evidence of and implications for treatment. Epilepsia 43: 219–227

Spencer SS, Spencer DD (1994) Entorhinal-Hippocampal Interactions in Medial Temporal-Lobe Epilepsy. Epilepsia 35: 721-727

Spencer SS (1994) The relative contributions of MRI SPECT and PET imaging in epilepsy. Epilepsia 35: S72-S89

Sprengers M, Vonck K, Carrette E, Marson AG, Boon P. (2014) Deep brain and cortical stimulation for epilepsy. Cochrane Database Syst Rev. 6:CD008497

Starr MS (1996) The role of dopamine in epilepsy. Synapse, 22; pp. 159–194

Starr MS (1993) Regulation of seizure threshold by D1 versus D2 receptors," in D1/D2 Dopamine Receptor Interactions. Academic Press, New York; pp. 235–269

Stefurak T, Mikulis D, Mayberg H, Lang AE, Hevenor S, Pahapill P, et al. (2003) Deep brain stimulation for Parkinson's disease dissociates mood and motor circuits: a functional MRI case study. Mov Disord 18(12): 1508–1516.

Sukhotinsky I, Chan AM, Ahmed OJ, Rao VR, Gradinaru V, Ramakrishnan C, Deisseroth K, Majewska AK, Cash SS (2013) Optogenetic delay of status epilepticus onset in an in vivo rodent epilepsy model. PLoS One 8: e62013

Sulzer D, Surmeier DJ (2013) Neuronal vulnerability, pathogenesis, and Parkinson's disease. Mov Disord 28: 715-724

Sutton AC, Yu W, Calos ME, Smith AB, Ramirez-Zamora A, et al. (2013) Deep brain stimulation of the substantia nigra pars reticulata improves forelimb akinesia in the hemiparkinsonian rat. J Neurophysiol 109, 363-374

Tagliati M, Jankovic J, Pagan F, Susatia F, Isaias IU, Okun MS (2009) National Parkinson Foundation DBS Working Group. Safety of MRI patients with implanted deep brain stimulation devices. Neuroimage 47(S2): T53-57.

Tagliati M, Jankovic J, Pagan F, Susatia F, Isaias IU, Okun MS, et al. (2009) Safety of MRI in patients with implanted deep brain stimulation devices. Neuroimage 47 (S2): T53-57

Tanabe J, Miller D, Tregellas J, Freedman R, Meyer FG (2002) Comparison of detrending methods for optical fMRI preprocessing. Neuroimage 15(4): 902-907

Tecuapetla F, Matias S, Dugue GP, Mainen ZF, Costa RM (2014) Balanced activity in basal ganglia projection pathways is critical for contraversive movements. Nat Commun 5, 4315

Tellez-Zenteno JF, McLachlan RS, Parrent A, Kubu CS, Wiebe S (2006) Hippocampal electrical stimulation in mesial temporal lobe epilepsy. Neurology 66(10):1490-1494

Temel Y, Cao C, Vlamings R, Blokland A, Ozen H, et al. (2006) Motor and cognitive improvement by deep brain stimulation in a transgenic rat model of Huntington's disease. Neurosci Lett 406, 138-141

Theodore WH, Fischer R (2007) Brain stimulation for epilepsy. Acta Neurochir Suppl 97: 261-272

Thobois S, Dominey P, Fraix V, Mertens P, Guenot M, et al. (2002) Effects of subthalamic nucleus stimulation on actual and imagined movement in Parkinson's disease: a PET study. J Neurol 249: 1689-1698

Tian L, Hires SA, Mao T, Huber D, Chiappe ME, et al. (2009) Imaging neural activity in worms, flies and mice with improved GCaMP calcium indicators. Nat Methods 6: 875–881

Tieu K (2011) A Guide to Neurotoxic Animal Models of Parkinson's Disease. Cold Spring Harb Perspect Med 1(1): a009316

Tootell RHB, Mendola JD, Hadjikhani NK, Liu AK, Dale AM (1998) The representation of the ipsilateral visual field in human cerebral cortex. Proc Natl Acad Sci USA: 818–824

Trost M, Su S, Su P, et al. (2006) Network modulation by the subthalamic nucleus in the treatment of Parkinson's disease. Neuroimage 31: 301–307

Tønnesen J, Sørensen AT, Deisseroth K, Lundberg C, Kokaia M (2009) Optogenetic control of epileptiform activity. Proc Natl Acad Sci USA 106: 12162-12167

Turrigiano GG, and Nelson SB (2004) Homeostatic plasticity in the developing nervous system. Nature Reviews Neuroscience 5: 97-107

Tye KM, Deisseroth K. (2012) Optogenetic investigation of neural circuits underlying brain disease in animal models. Nat Rev Neurosci 13(4): 251-266

Tye KM, Prakash R, Kim SY, Fenno LE, Grosenick L, et al. (2011) Amygdala circuitry mediating reversible and bidirectional control of anxiety. Nature 471: 358-362

Ungerstedt U (1968) 6-Hydroxydopamine induced degeneration of central monoamine neurons. Eur J Pharmacol 5(1): 107–110

Valdes-Hernandez PA, Sumiyoshi A, Nonaka H, Haga R, Aubert-Vasquez E, et al. (2011) An in vivo MRI Template Set for Morphometry, Tissue Segmentation, and fMRI Localization in Rats. Front Neuroinform 5, 26

Valente G, Esposito F, de Martino F, Goebel R, Formisano E (2010) Using ICA for the Analysis of fMRI Data. In Simultaneous EEG and fMRI: recording, analysis and application. Ed. by Ullsperger M, Debener S, Oxford University Press Chapter 3.2: 135-151

Van Den Berge N, Keereman V, Vanhove C, Van Nieuwenhuyse B, van Mierlo P, Raedt R, et al. (2015) Hippocampal deep brain stimulation reduces glucose utilization in the healthy rat brain. Mol Imaging Biol 17(3): 373-383

van den Heuvel P, Mandl RCW, Kahn RS, and Hulshoff Pol HE (2009) Functionally linked resting-state networks reflect the underlying structural connectivity architecture of the human brain. Hum Brain Mapp 30(10): 3127-3141

Vandewalle V, van der Linden C, Groenewegen HJ, Caemaert J (1999) Stereotactic treatment of Gilles de la Tourette syndrome by high frequency stimulation of thalamus. Lancet 353: 724

van Dijk A, Mason O, Klompmakers AA, Feenstra MG, Denys D (2011) Unilateral deep brain stimulation in the nucleus accumbens core does not affect local monoamine release. J Neurosci Methods 202: 113-118

van Houdt (2013) Simultaneous EEG and functional MRI. A noninvasive tool in the presurgical evaluation of focal epilepsy. Thesis, Vrije Universiteit Amsterdam.

van Luijtelaar G, and Huang L (2013) Brain Computer Interface for Epilepsy Treatment – Recent Progress and Future Prospects. In: InTech Open Science - Open Minds, DOI: 10.5772/55800

Van Nieuwenhuyse B, Raedt R, Delbeke J, Wadman WJ, Boon P, Vonck K (2015) In Search of Optimal DBS Paradigms to Treat Epilepsy: Bilateral Versus Unilateral Hippocampal Stimulation in a Rat Model for Temporal Lobe Epilepsy. Brain Stimul 8(2): 192-199

Van Roost D, Boon P, Vonck K, Caemaert J (2007) Neurosurgical aspects of temporal deep brain stimulation for epilepsy. Acta Neurochir S97: 333-336

Van Zijl P, Hua J, Lu H (2012) The BOLD post-stimulus undershoot, one of the most debated issues in fMRI. Neuroimage 62(2): 1092–1102

Vassoler FM, Schmidt HD, Gerard ME, Famous KR, Ciraulo DA, Kornetsky C, et al. (2008) Deep brain stimulation of the nucleus accumbens shell attenuates cocaine priming-induced reinstatement of drug seeking in rats. J Neurosci 28: 8735-8739

van Westen M, Rietveld E, Figee M, Denys D (2015) Clinical Outcome and Mechanisms of Deep Brain Stimulation for Obsessive-Compulsive Disorder. Curr Behav Neurosci Rep 2 :41-48

Vedam-Mai V, van Battum EY, Kamphuis W, et al. (2012) Deep brain stimulation and the role of astrocytes. Mol Psych 17: 124–131

Velasco AL, and Fischer RS (2014) Electrical brain stimulation for epilepsy. Nature Reviews Neurology 10: 261-270

Velasco AL, Velasco F, Velasco M, Trejo D, Castro G, Carrillo-Ruiz JD (2007) Electrical stimulation of the hippocampal epileptic foci for seizure control: a double-blind, long-term follow-up study. Epilepsia 48, 1895-1903

Velasco F, Velasco M, Velasco AL, Menez D, Rocha L (2001) Electrical stimulation for epilepsy: stimulation of hippocampal foci. Stereotactic and Functional Neurosurgery 77: 223–227

Velasco M, Velasco F, Velasco AL, Boleaga B, Jimenez F, et al. (2000) Subacute electrical stimulation of the hippocampus blocks intractable temporal lobe seizures and paroxysmal EEG activities. Epilepsia 41: 158-169

Velisek L, Veliskova J, Moshe SL (2002) Electrical stimulation of substantia nigra pars reticulata is anticonvulsant in adult and young male rats. Exp Neurol 173, 145-152

Vezzani A, Moneta D, Richichi C, Aliprandi M, Burrows SJ, et al. (2002) Functional role of inflammatory cytokines and antiinflammatory molecules in seizures and epileptogenesis. Epilepsia 43(S5): 30-35

Visanji NP, Brooks PL, Hazrati LN, Lang AE (1998) The prion hypothesis in Parkinson's disease: Braak to the future. Acta Neuropathol Commun 1: 2

Vitek JL, Zhang J, Hashimoto T, Russo GS, Baker KB (2012) External pallidal stimulation improves parkinsonian motor signs and modulates neuronal activity throughout the basal ganglia thalamic network. Exp Neurol 233, 581-586

Vitek JL (2002) Mechanisms of deep brain stimulation: excitation or inhibition. Mov Disord 17(S3): S69-S72

Vonck K, Sprengers M, Carrette E, Miatton M, Meurs A, Goossens L, et al. (2013) A decade of experience with deep brain stimulation for patients with refractory medial temporal lobe epilepsy. Int J of Neural Syst 23(1): 1-13

Vonck K, Boon P, Claeys P, Dedeurwaerdere S, Achten R, Van Roost D (2005) Long-term deep brain stimulation for refractory temporal lobe epilepsy. Epilepsia. 46 S5: 98-99

Vonck K, Boon P, Achten E, De Reuck J, Caemaert J (2002) Long-term amygdalohippocampal stimulation for refractory temporal lobe epilepsy. Annals of Neurology 52: 556-565

Wade AR (2002) Negative BOLD Signal Unmasked. Neuron 36(6): 993-995

Watakabe A, Ohtsuka M, Kinoshita M, Takaji M, Isa K, et al. (2015) Comparative analyses of adeno-associated viral vector serotypes 1, 2, 5, 8 and 9 in marmoset, mouse and macaque cerebral cortex. Neurosci Res 93: 144-157

Weber R, Ramos-Cabrer P, Weidermann D, van Camp N, Hoehn M (2006) A fully noninvasive and robust experimental protocol for longitudinal fMRI studies in the rat. Neuroimage 29(4): 1303-1310

Weick JP, Johnson MA, Skroch SP, Williams JC, Deisseroth K, Zhang SC (2010) Functional control of transplantable human ESC-derived neurons via optogenetic targeting. Stem Cells 28: 2008-2016

Weiner WJ, Lang AE (1989) Movement Disorders. A Comprehensive Survey. Future Press, Mount Kisco, NY

Weiss D, Walach M, Meisner C, Fritz M, Scholten M, et al. (2013) Nigral stimulation for resistant axial motor impairment in Parkinson's disease? A randomized controlled trial. Brain 136, 2098-2108

White AM, Williams PA, Ferraro DJ, Clark S, Kadam SD, Dudek FE, et al. (2006) Efficient unsupervised algorithms for the detection of seizures in continuous EEG recordings from rats after brain injury. J Neurosci Methods 152(1-2): 255-266

Wichmann T, Delong MR (2006) Deep brain stimulation for neurologic and neuropsychiatric disorders. Neuron 52(1):197-204

Wille C, Steinhoff BJ, Altenmuller DM, Staack AM, Bilic S, et al. (2011) Chronic high-frequency deep-brain stimulation in progressive myoclonic epilepsy in adulthood--report of five cases. Epilepsia 52, 489-496

Williams JC, Denison T (2013) From optogenetic technologies to neuromodulation therapies. Sci Transl Med 5: 177ps176

Williams PA, White AM, Clark S, Ferraro DJ, Swiercz J, Staley KJ, et al. (2009) Development of spontaneous recurrent seizures after kainate-induced status epilepticus. J Neurosci 29(7): 2103e12

Witten IB, Lin SC, Brodsky M, Prakash R, Diester I, et al. (2010) Cholinergic interneurons control local circuit activity and cocaine conditioning. Science 330: 1677-1681

Won HJ, Chang KH, Cheon JE, Kim HD Lee DS, et al. (1999) Comparison of MR imaging with PET and ictal SPECT in 118 patients with intractable epilepsy. AJNR Am J Neuroradiol 20(4): 593-599

Wu EX, Wong KK, Andrassy M, Tang H (2003) High-resolution in vivo CBV mapping with MRI in wild-type mice. Magn Reson Med 49: 765-770

Wyckhuys T, Boon P, Raedt R, Van Nieuwenhuyse B, Vonck K, Wadman W (2010a) Suppression of hippocampal epileptic seizures in the kainate rat by Poisson distributed stimulation. Epilepsia 51(11): 2297-2304

Wyckhuys T, Staelens S, Van Nieuwenhuyse B, Deleye S, Hallez H, Vonck K, et al. (2010b) Hippocampal deep brain stimulation induces decreased rCBF in the hippocampal formation of the rat. Neuroimage 52(1): 55-61

Wyckhuys T, Geerts PJ, Raedt R, Vonck K, Wadman W, Boon P (2009) Deep brain stimulation for epilepsy: knowledge gained from experimental animal models. Acta Neurol Belg. 109(2): 63-80

Wyckhuys T, De Smedt T, Claeys P, Raedt R, Waterschoot L, Vonck K. et al. (2007) High frequency deep brain stimulation in the hippocampus modifies seizure characteristics in kindled rats. Epilepsia 48: 1543-1550

Yang PF, Chen Y-Y, Chen D-Y, Hu JW, Chen J-H, Yen CT (2014) Comparison of fMRI BOLD Response Patterns by Electrical Stimulation of the Ventroposterior Complex and Medial Thalamus of the Rat. PLoS One doi: 10.1371/journal.pone.0066821

Yang Y, Tai Y, Siegel S, Newport D, Bai B, Li Q (2004) Optimization and performance evaluation of the microPET II scanner for in vivo small-animal imaging. Phys Med Biol 49: 2527-2545

Yelnik J, Damier P, Demerret S, Gervais D, Bardinet E, Bejjani BP, et al. (2003) Localization of stimulating electrodes in patients with Parkinson disease by using a three-dimensional atlas-magnetic resonance imaging coregistration method. J Neurosurg 99(1): 89-99

Yizhar O, Fenno LE, Davidson TJ, Mogri M, Deisseroth K (2011) Optogenetics in neural systems. Neuron 71(1): 9-34

Younce JR, Albaugh DL, and Shih Y-YL (2014) Deep brain stimulation with simultaneous fMRI in rodents. J Vis Exp 84: e51271

Yuan H, Sarre S, Ebinger G, Michotte Y (2005) Histological, behavioural and neurochemical evaluation of medial forebrain bundle and striatal 6-OHDA lesions as rat models of Parkinson's disease. J Neurosci Methods 144(1): 35-45

Zhang X, Cui SS, Wallace AE, Hannesson DK, Schmued LC, et al. (2002) Relations between brain pathology and temporal lobe epilepsy. J Neurosci 22(14): 6052-6061

Zhang F, Gradinaru V, Adamantidis AR, Durand R, Airan RD, de Lecea L, Deisseroth K (2010) Optogenetic interrogation of neural circuits: technology for probing mammalian brain structures. Nat Protoc 5: 439–456

Zhang F, Laiwalla JA, Kim H, Urabe R, Van Wagenen YK et al. (2009a) A microelectrode array incorporating an optical waveguide device for stimulation and spatiotemporal electrical recording of neural activity. Conf Proc IEEE Eng Med Biol Soc 2009: 2046–2049

Zhang F, Laiwalla JA, Kim H, Urabe R, Van Wagenen YK et al. (2009b) Integrated device for optical stimulation and spatiotemporal electrical recording of neural activity in light-sensitized brain tissue. J Neural Eng 6: 055007

Zhang F, Prigge M, Beyrière F, Tsunoda SP, Mattis J, Yizhar O, Hegemann P, Deisseroth K (2008) Red-shifted optogenetic excitation: a tool for fast neural control derived from Volvox carteri. Nat Neurosci 11: 631–633

Zhang F, Wang LP, Boyden ES, Deisseroth K (2006) Channelrhodopsin-2 and optical control of excitable cells. Nat Methods 3: 785-792

Zhao F, Williams M, Meng X, Welsh DC, Grachev ID, Hargreaves R, Williams DS (2009) Pain fMRI in rat cervical spinal cord: an echo planar imaging evaluation of sensitivity of BOLD and blood volume-weighted fMRI. Neuroimage 44: 349-362

Zhao F, Zhao T, Zhou L, Wu Q, Hu X (2008) BOLD Study of Stimulation-Induced Neural Activtiy and Resting-State Connectivity in Medetomidine-Sedated Rat. Neuroimage 39(1): 248-260

Zhao F, Wang P, Hendrich K, Ugurbil K, Kim SG (2006) Cortical layer-dependent BOLD and CBV responses measured by spin-echo and gradient-echo fMRI: insights into hemodynamic regulation. Neuroimage 30: 1149–1160

Zhao F, Wang P, Hendrich K, Kim SG (2005) Spatial specificity of cerebral blood volume-weighted fMRI responses at columnar resolution. Neuroimage 27(2): 416-24

Zemelman BV, Lee GA, Ng M, Miesenböck G (2002) Selective photostimulation of genetically charged neurons. Neuron 33: 15-22

Zifkin BG, Dravet C (2008) Generalized tonic-clonic seizures. In Epilepsy: A Comprehensive Textbook, 2nd ed. Ed by J Engel Jr and TA Pedley, Philadelphia: Lippincott Williams & Wilkins, 553-562

Zrinzo L, Yoshida F, Hariz MI, Thornton J, Foltynie T, Yousry TA, et al. (2011) Clinical safety of brain magnetic resonance imaging with implanted deep brain stimulation hardware: large case series and review of the literature. World Neurosurg 76(1-2): 164-172

List of figures

List of tables